Macrocyclic Tetraamido-*N* Ligands that Stabilize High Valent Complexes of Chromium, Manganese, Iron, Cobalt, Nickel, and Copper

Thesis by

Erich Stuart Uffelman

In Partial Fulfillment of the Requirements

for the Degree of

Doctor of Philosophy

California Institute of Technology

Pasadena, California

1992

(Submitted August 19, 1991)

Acknowledgements

My Ph.D. work has spanned two universities and almost seven years; as a result I have the pleasure of thanking several people for their assistance.

I should begin by thanking the Collins family for all of their help in this effort. Terry has been my advisor and he has constantly given me his unequivocal support. I am grateful that he allowed me to work on whatever I wanted, whenever I wanted, and never got upset with my frequent bouts of clandestine chemistry. I should emphasize that Terry gave me much of this scientific, creative, and personal freedom during times which were difficult for him. He made it financially possible for my wife and me to make the jump to Carnegie Mellon and prevented the CMU administration from reneging on their commitments to me. Caltech may indeed have so much talent that the institution does not miss him, but I think the institution erred in not retaining such a creative and dedicated scientist. I must thank Maureen for doing her best to make Louise and me surfeit on high-tech desserts. She's always been one of my good buddies. I'd like to thank Kelley and Gregory for providing hours of comic relief.

I'd like to thank Arnold George for being my big grown-up science friend since I was seven years old. I'll never forget the helium-in-the-kite trick.

I must thank my undergraduate advisor, Chuck Root, for teaching me so much inorganic chemistry, and for being so patient with me. I'd particularly like to thank him and his family for letting me stay with them several days after I first visited CMU. It was nice to see my Bucknell professors (Manning, Hans, Harold, et al.), talk science, and think about the decisions I had to make. Chuck will always be my good friend.

In speaking of good friends, I want to thank Martha Kanaskie for all of

her love and support over the years. The clock is still in the refrigerator.

There are several people at Caltech I would like to thank.

I'd like to thank all of the old Kiwis for their help and expertise, particularly Geoffrey Peake, John Keech, and Brian Treco. I would especially like to thank John Brewer for being my good friend and confidant during a trying year. He made the visit to CMU with me, and I think our 36 hour diagnosis was 90% on the mark. I've missed him, but I look forward to hearing his Canadian English at many ACS meetings in the future.

I must not forget to acknowledge the efforts that Sandra Potter, Beth Kerns, and Dian Buchness have exerted on my behalf. Any questions or problems I have had in the 46 months I've been at CMU have been handled with alacrity. Their cheerful friendliness and constant willingness to help have rescued me on several occasions.

My entering year of '84 classmates always were extremely supportive of me, and were a real blast to have around.

To conclude the Caltech acknowledgements section, I would like to thank the members of my committee. I'd like to thank Sunney for using the Kiwi group Mr. Coffee as much after the Spring of '86 as he did before the Spring of '86. I'd like to thank John for cogent advice in October of '84, May of '86, and April of '87. I'd like to thank Harry for asking me some incisive questions during my candidacy exam in March of '86. I had been thinking very carefully about several scientific points, and Harry's questions provided me with some useful new ways to consider those points. I would also like to thank him for his encouraging notes this past year. More than anything else, however, I would like to thank Harry for having the guts to call a Kiwi group meeting in the

Spring of '86. I appreciated his direct answers to our direct questions.

There are several people at Carnegie Mellon I would like to thank.

I'd like to thank all of the new Kiwis for adopting me so kindly. I'd like to thank Scott "Fortunately this is just a Riemann Zeta function" Gordon-Wylie for lots of fun late-night science chats, and for driving me to the hospital when Louise and Maureen were rear-ended. José Workman was the first new Kiwi, helped me rebuild the Kiwi lab, and was very useful in the aforementioned hospital escapade. I must also thank him for pertinent comments on chapters one and two of this thesis. Joe also merits our gratitude for forcing higher sartorial standards on Terry. Kim "Charlie, it's a chemical" Kostka became the second member of the exclusive MAC* club and has been my imine-busting buddy. I'd like to thank her for always letting me force-feed broccoli casserole down her throat via a plastic tube. Mike Bartos has been a wonderful addition to the group. I've enjoyed his company at my end of the lab and I've enjoyed, and been impressed by, his work. I'd like to thank Dr. L. James Wright for being my psychological guru during his sabbatical leave from Auckland. His science was always high-caliber, and any man who can stay calm, cool, and collected after chugging two gallons of heavy-duty coffee is a man to be valued.

Here are some utilitarian acknowledgements before I go any further: The NSF provided me with a Predoctoral Fellowship (1984–1987) and has funded much of the lab work. Dow funded the early stages of this work. Carnegie Mellon set-up funds supported some of this work, as did Terry's Sloan and Dreyfuss scholarships. Dr. David Bocian and Alexander Procyk provided the resonance Raman spectra, Dr. Kasi Somayajula (University of Pittsburgh) provided the negative ion FABS, Dr. Ryonosuke Shiono (University of Pittsburgh) and Dr.

Hugh Nicholas (CMU Supercomputing) provided access to the Cambridge Crystallographic Database, Dr. Eckard Münck and Dr. Brian Fox performed the Mössbasuer studies, Dr. Cynthia Day (Crystallytics Company) solved the crystal structures, Midwest Microlab did the combustion analyses, and Dr. James Whittaker gave *extensive* assistance with the EPR. My coauthors deserve special mention: Carla Slebodnick, Thomas Nichols, Kimberly Kostka, Dr. Eckard Münck, and Dr. Richard Powell. Louise Uffelman made a number of valuable editorial suggestions on my candidacy report, proposals, papers, and on this thesis.

I must thank Valerie Bridge and Mary-Beth Smith for preventing my CMU files from being sucked into the administrative black hole in Warner Hall.

I would like to thank the people who worked closest with me. Tim Parrott spent a summer with me doing some very useful work on my ill-fated first project. I was able to use his work as a smoke screen to conceal my initial efforts on macrocyclic tetraamides. Sonny Lee collaborated with me on the initial two months of this work. Sonny made a fabulous co-conspirator. It was really a great pleasure to hang out with him at the Washington ACS meeting and show him what had become of our efforts. I look forward to seeing him much more in the future. Carla Slebodnick worked with me for two years. She is one of the most devastatingly efficient lab machines I've ever met. In our first summer together I think only three or four reactions didn't work. I would like to thank Carla for all of her love and kindness, and I hope I can persuade her to hang out in sunny Stanford when the weather gets cold at Northwestern. Finally, I would like to thank my alter ego, Tom Nichols, for working with me for two years. Tom is CMU's Sonny Lee, and it was a pleasure watching him

rocket with the nickel chemistry. I'd like to thank Tom for the boomerang throwing sessions and the late night computer companionship. I look forward to seeing him up at Stanford when he's not punishing his work at Caltech.

Finally, the biggest thanks are reserved for Grandma, Grandpa, Mom, Dad, Jonathan, and especially for Louise. *Omnia vincit amor.*

For Louise

Abstract

High valent middle and later transition metal centers tend to oxidatively degrade their ligands. A series of ligand structural features that prevent discovered decomposition routes is presented. The result of the iterative design, synthesis, and testing process described are the macrocyclic tetraamides H_4MAC* and H_4DEMAMPA-DCB. H_4MAC* and H_4DEMAMPA-DCB are the parent acids of the macrocyclic tetraamido-*N* ligands $(\eta^4\text{-MAC*})^{4-}$ and $(\eta^4\text{-DEMAMPA-DCB})^{4-}$, which are shown to stabilize high valent middle and later transition metal complexes unavailable in other systems. The crystal structures of H_4MAC* and a copper complex of one of its synthetic precursors reveal intramolecular and intermolecular hydrogen-bonding patterns which are relevant to recent developments in the ordering effects of hydrogen-bonding on solution and solid state structures. The synthetic value of these ordering effects is discussed.

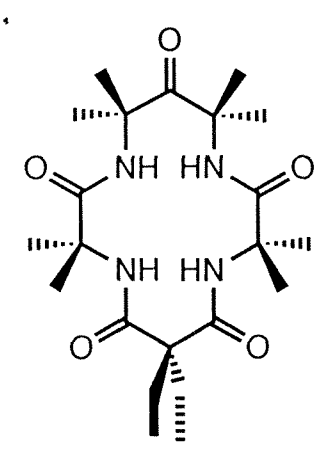

H_4MAC*

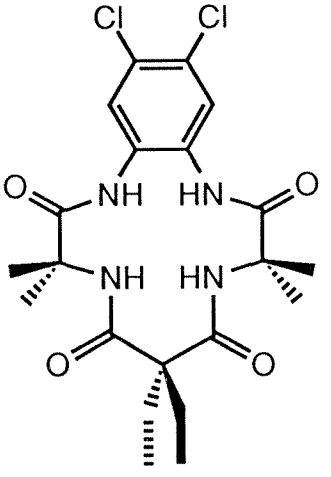

H_4DEMAMPA-DCB

Two chromium(V) oxo complexes, $[(CH_3)_4N][Cr(O)(\eta^4\text{-MAC*})]$ and $[(CH_3)_4N][Cr(O)(\eta^4\text{-DEMAMPA-DCB})]$, have been synthesized and character-

ized by X-ray crystallography and IR and EPR spectroscopies. Because exchange of the oxo ligand with water is slow, the easily synthesized, stable, crystalline ^{18}O-labeled diperoxide, $(CH_3)_2(H^{18}O^{18}O)CCH_2CH_2C(^{18}O^{18}OH)$-$(CH_3)_2$, was prepared and used to conveniently synthesize ^{18}O-labeled oxo complexes in high yields. The bonding of the two unique oxidation resistant macrocyclic tetraamides to chromium is compared. The structural and EPR properties are consistent with a chromium centered radical in each case and suggest that a chromium(V) oxidation state assignment is equally appropriate whether the ancillary ligand is the innocent $(\eta^4$-MAC*$)^{4-}$ or the potentially noninnocent $(\eta^4$-DEMAMPA-DCB$)^{4-}$. Both oxo complexes contain nonplanar amide groups. The distortions in $[Cr(O)(\eta^4$-MAC*$)]^-$ are more marked, and it is a unique species in containing four distinctly nonplanar amides.

The synthesis and characterization of the first water-stable Mn(V) monooxo complex is described. $[(C_2H_5)_4N][Mn(O)(\eta^4$-DEMAMPA-DCB$)]$ has been isolated as a green crystalline material and characterization includes ^1H NMR, IR, resonance Raman, and an X-ray crystal structure determination. The first definitive assignment of a $\nu_{Mn^V\equiv O}$ IR stretch (979 cm^{-1}) is made.

The first mononuclear five-coordinate Fe(IV) complex to be isolated as a crystalline compound and structurally characterized, $[Et_4N][FeCl(\eta^4$-MAC*$)]$, is described. The species has a square pyramidal structure. Cyclic voltammetry of $[Et_4N]_2[FeCl(\eta^4$-MAC*$)]$ shows a reversible $Fe^{IV/III}$ couple at E_f = -65 mV vs. Fc^+/Fc in CH_2Cl_2 with $[Bu_4N][ClO_4]$ (0.1 M) as supporting electrolyte. The Mössbauer spectrum of $[Et_4N][FeCl(\eta^4$-MAC*$)]$ obtained at 150 K has ΔE_Q = 0.87 mm s^{-1} and an isomer shift, δ_{Fe} = -0.03 mm s^{-1}, lending firm support to the iron(IV) oxidation state assignment. Data on $[FeCl(\eta^4$-

DEMAMPA-DCB)]$^-$ are provided for comparison

The synthesis and characterization of the first macrocyclic square planar Co(III) complex is described. [Co(η^4-MAC*)]$^-$ has been isolated as a red crystalline material and characterization includes a ^{1}H NMR spectrum of the lithium salt and an X-ray crystal structure determination of the [Me_4N]$^+$ salt. The cobalt complex contains one significantly nonplanar amido-*N* ligand where the source of the nonplanarity appears to be a simple mismatch between the geometrical features of the macrocycle and the structural requirements of the square planar metal center, a unique case of amide nonplanarity in inorganic chemistry.

The first crystallographically characterized neutral square planar complex of cobalt in an oxidation state higher than +II, Co(η^4-DEMAMPA-DCB), is reported. Structural data for this new class of compounds indicate that the macrocycle in Co(η^4-DEMAMPA-DCB) is noninnocent; however, EPR data in toluene at 5.9 K (S = 1/2; g_1=2.558, g_2=2.170, g_3=2.017; A_2 $\approx$15 G) show that the metal center is the primary residence site of the unpaired electron. Co(η^4-DEMAMPA-DCB) is a stable, yet potent, oxidant which is soluble in benzene and slightly soluble in pentane. The Co(η^4-DEMAMPA-DCB)/[Co^{III}(η^4-DEMAMPA-DCB)]$^-$ couple is reversible and found at 0.550 V vs. Fc^+/Fc in CH_2Cl_2 (ca. 1.26 V vs. NHE). Co(η^4-DEMAMPA-DCB) slowly oxidizes water, yielding H[Co^{III}(η^4-DEMAMPA-DCB)], which may also be prepared by the reaction of [Co^{III}(η^4-DEMAMPA-DCB)]$^-$ with HBF_4. Both the redox and the acid/base chemistries of [Co^{III}(η^4-DEMAMPA-DCB)]$^-$ are reversible. Electrochemical and EPR data are also presented for other derivatives.

The first square planar nickel(III) complex with an innocent ligand to be

structurally characterized, $[Et_4N][Ni(\eta^4\text{-MAC*})]$, is described: All four Ni(III)-N bond distances are significantly shorter (ca. 0.1 Å) than any known Ni(III)-N bond distance. The average Ni-N distance in $[Et_4N][Ni(\eta^4\text{-MAC*})]$ is 1.84 Å and the shortest of the four is 1.825(4) Å. EPR and UV-vis evidence are presented which indicate that the four-coordinate structure found for the solid state form is also present in solutions of non-coordinating solvents, and in noncoordinating glasses at 4 K. In CH_2Cl_2, five-coordinate species can be produced at 20 °C with cyanide ion ($K_{20°C} = 3.2(9) \times 10^3$ mol^{-1}), and at 77 K with pyridine, 2,6-lutidine, and $(CH_3)_3P$, but not with Et_3N, Ph_3P, THF (neat), 2,5-Me_2THF (neat), MeCN (neat), H_2O (neat), or acetone (neat) which do not coordinate. The EPR spectra of the four coordinate complex in glasses of CH_2Cl_2/toluene or CH_2Cl_2/2,5-Me_2THF are of significance to nickel bioinorganic chemistry since $g_\perp > g_\parallel$, the opposite to the usually accepted EPR signature for square planar nickel(III). The Ni(III/II) couple of $[Ni(\eta^4\text{-MAC*})]^-$ is reversible and occurs at -0.58 V vs. Fc^+/Fc (CH_2Cl_2, 0.1 M $[Bu_4N][ClO_4]$ supporting electrolyte, 0.13 V vs. NHE) showing that an abiological square planar ligand complement consisting of four deprotonated amides can produce a marked stabilization of four-coordinate nickel(III). Data on $[Ni(\eta^4\text{-DEMAMPA-DCB})]^-$ are provided for comparison.

The synthesis of copper(III) complexes with reversible cathodic and *anodic* waves is described. The low values for the Cu(III/II) couples (−0.815 V vs. Fc^+/Fc) and the high potentials for the $Cu^{0/-}$ couples (ca. +0.830 V vs. Fc^+/Fc) are presented.

The Dunitz amide nonplanarity analysis is applied to the crystal structures presented to illustrate the unique bonding that occurs in some of the

macrocyclic compounds.

Table of Contents

List of Figures

List of Figures (continued)

List of Figures (continued)

List of Figures (continued)

List of Figures (continued)

List of Figures (continued)

List of Figures (continued)

List of Figures (continued)

List of Figures (continued)

List of Figures (continued)

List of Tables

List of Tables (continued)

List of Schemes

Abbreviations Used

CHBA-DCB	1,2-bis(3,5-dichloro-2-hydroxybenzamido)-4,5-dichlorobenzene
CHBA-DMP	2,4-bis(3,5-dichloro-2-hydroxybenzamido)-2,4-dimethylpentanone
CHBA-Et	1,2-bis(3,5-dichloro-2-hydroxybenzamido)-ethane
CHBA-Pr	1,3-bis(3,5-dichloro-2-hydroxybenzamido)-propane
CHBA-TMEt	3,4-bis(3,5-dichloro-2-hydroxybenzamido)-3,4-dimethylbutane
cyclam	η^4-1,4,8,11-tetraazacyclotetradecane
H_4DEMAMPA-DXB	diethylmalonamidobis(methylpropanamido)-4,5-diXbenzene
H_4DEMAMPA-DCB	5,6:(4,5-dichlorobenzo)-3,8,11,13-tetraoxo-2,2,9,9-tetramethyl-12,12-diethyl-1,4,7,10-tetraazacyclotridecane
H_4DEMAMPA-B	5,6:(benzo)-3,8,11,13-tetraoxo-2,2,9,9-tetramethyl-12,12-diethyl-1,4,7,10-tetraazacyclotridecane
H_4DEMAMPA-DMB	5,6:(4,5-dimethylbenzo)-3,8,11,13-tetraoxo-2,2,9,9-tetramethyl-12,12-diethyl-1,4,7,10-tetraazacyclotridecane

Abbreviations Used (continued)

H_4DEMAMPA-DMOB	5,6:(4,5-dimethoxybenzo)-3,8,11,13-tetra-oxo-2,2,9,9-tetramethyl-12,12-diethyl-1,4,7,10-tetraazacyclotridecane
Fc	ferrocene
Fc^+	ferrocinium cation
HBA-B	1,2-bis(2-hydroxybenzamido)benzene
HMBuA-B	1,2-bis(3-hydroxy-3-methylbutamido)-benzene
HMBuA-DMP	2,4-bis(3-hydroxy-3-methylbutamido)-2,4-dimethylpentanone
HMPA-B	1,2-bis(2-hydroxy-methylpropanamido)-benzene
HMPA-DMP	2,4-bis(2-hydroxy-methylpropanamido)-2,4-dimethyl pentanone
H_4MAC* (mac-star)	peralkylated(*) macrocyclic polyanionic chelating ligand = 13,13-diethyl-2,2,-5,5,7,7,10,10- octamethyl-3,6,9,12,14-pentaoxo-1,4,8,11-tetraazacyclotetra-decane
Proton Sponge	N,N,N′,N′-tetramethyl-1,8-naph-thalenediamine
Salen	η^4-N,N′-ethylenebis(salicylideneimine) (doubly deprotonated)

Abbreviations Used (continued)

TAAB	η^4-tetrabenzo[b,f,j,n][1,5,9,13]-tetraaza-cyclohexadecine
TBHP	*tert*-butyl hydroperoxide
TMP	η^4-*meso*-tetramesitylporphyrin (doubly deprotonated)
TPP	η^4-*meso*-tetraphenylporphyrin (doubly deprotonated)

Other abbreviations are defined as needed in the text or correspond to abbreviations found in *The ACS Style Guide.*

Chapter 1

The Rationale for Macrocyclic Tetraamido-*N* Ligands in Oxidation Chemistry

Ligand design criteria for inorganic oxidation chemistry

High valent middle and later transition metal centers, particularly of the first row, tend to oxidatively degrade organic ligands. Although there are over 200,000 compounds of manganese and iron, most of the few (circa 20) stable high valent complexes of these two elements (Mn(V)–Mn(VII), Fe(V)–Fe(VI)) are halide and oxo systems. The consequence of ligand instability problems is that the areas of high valent structure and bonding and catalytic oxidation are underdeveloped compared to the wealth of data on low valent structure and bonding and the variety of efficacious catalytic reduction systems. The Collins group has sought to increase the number of high valent middle and later transition metal complexes by synthesizing organic ligands which possess the following features:

(i) high negative charge, to stabilize highly oxidized complexes and produce highly oxidizing complexes in higher oxidation states,

(ii) resistance to both oxidative and hydrolytic degradation, to permit the isolation of highly oxidizing intermediates in the absence of substrates,

(iii) resistance to decomposition with reduced forms of molecular oxygen, to permit long-lived catalysis with molecular oxygen,

(iv) multidentate binding, to control the coordination number of a complex, limit the metal center to one-electron or two-electron oxidations and reductions, and establish a superstructure upon which rational steric modification can be constructed,

(v) "innocence" for clean formal oxidation state assignments and "noninnocence" for tuning the reactivity of complexes.

This thesis will describe the chemistry associated with the tetradeprotonated

forms of the two ligand types shown in Figure 1.1. These ligands were carefully designed to satisfy the above criteria, and currently represent the best systems for producing stable high valent compounds of chromium, manganese, iron, cobalt, nickel, and copper. This chapter will describe the reasoning behind the development of these ligands.

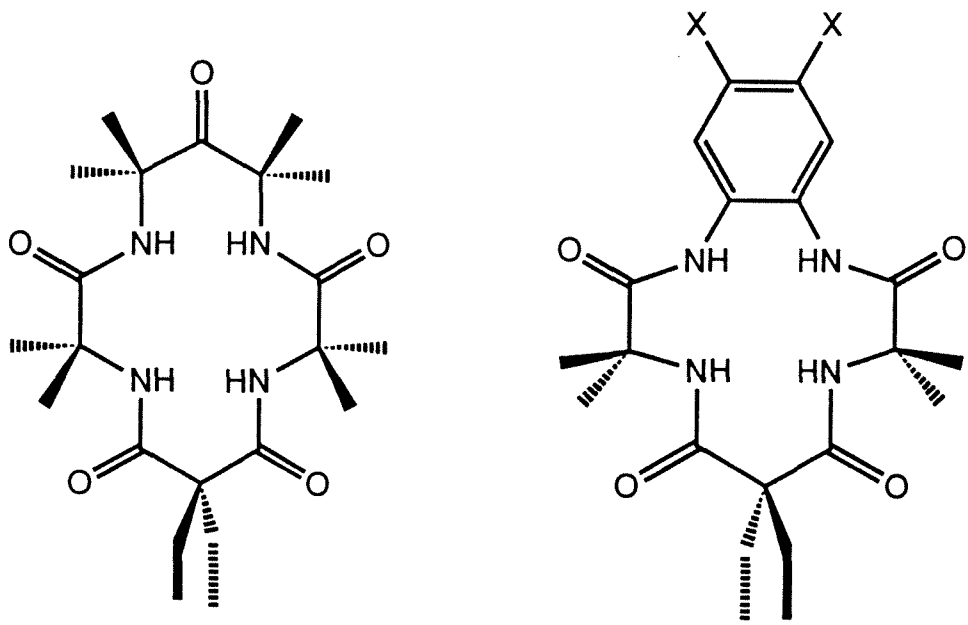

Figure 1.1. The macrocyclic tetraamides of this thesis. The macrocycle on the left is designated H_4MAC*; the macrocycle on the right is designated H_4DEMAMPA-DXB. To date, macrocycles with $X = Cl, H, Me, MeO$ have been synthesized (H_4DEMAMPA-DCB, H_4DEMAMPA-B, H_4DEMAMPA-DMB, and H_4DEMAMPA-DMOB, respectively).

The evolution of the Collins group's ligands prior to this thesis is summarized in Figure 1.2. Tetraanionic ligands stabilize highly oxidized complexes by quenching the formal positive charge of the central metal ion. The ligands were chosen to be tetradentate in order to both control the geometry and coordination number of a complex while leaving sites free to perform chemistry.

All of the ligands were readily synthesized and could be coordinated to several different metals in the presence of mild base (usually hydroxide). It will be useful to categorize the design lessons which arose from these earlier studies according to the five design features listed above.

Donor capacity (high negative charge)

The tetradeprotonated form of the macrocyclic ligands of this thesis contain four amido-*N* donors. Margerum demonstrated the strong donor properties of the amido-*N* ligand in early work.[1] Early efforts in the Collins group and results from other laboratories had established the impact of strong donor ligands on transition metal redox chemistry.

The first Collins group ligand used, the CHBA-Et ligand (Figure 1.2), was initially employed with osmium; metallation was achieved by reacting the free ligand with potassium osmate in MeOH. The strongly donating nature of the tetraanionic ligand was evident when the Os(III/II) couple of $[Os(\eta^4\text{-CHBA-Et})(py)_2]^-$ (-1.88 V vs. Fc^+/Fc) was compared to the Os(III/II) couple of $[Os(\eta^4\text{-OEP})(py)_2]^+$ (0.0 V vs. Fc^+/Fc) in the same medium.[2] This remarkable lowering of the osmium redox couples was consistent with well-known results from classic studies of the "Ni(III)/Ni(II)" couple with macrocyclic tetraazo systems (Figure 1.3).[3] In these Ni systems, the redox couple varied almost 2.0 V with different ligands.* The profound impact of ligands on thermodynamic reactivity makes it important to distinguish complexes which are highly oxidized from those which are highly oxidizing. Highly oxidized complexes are those in which the transition metal is in a high formal oxidation state.[4] Highly

* It is inappropriate to refer to all of these couples as Ni(III)/Ni(II) couples because of ligand noninnocence problems—vide infra.

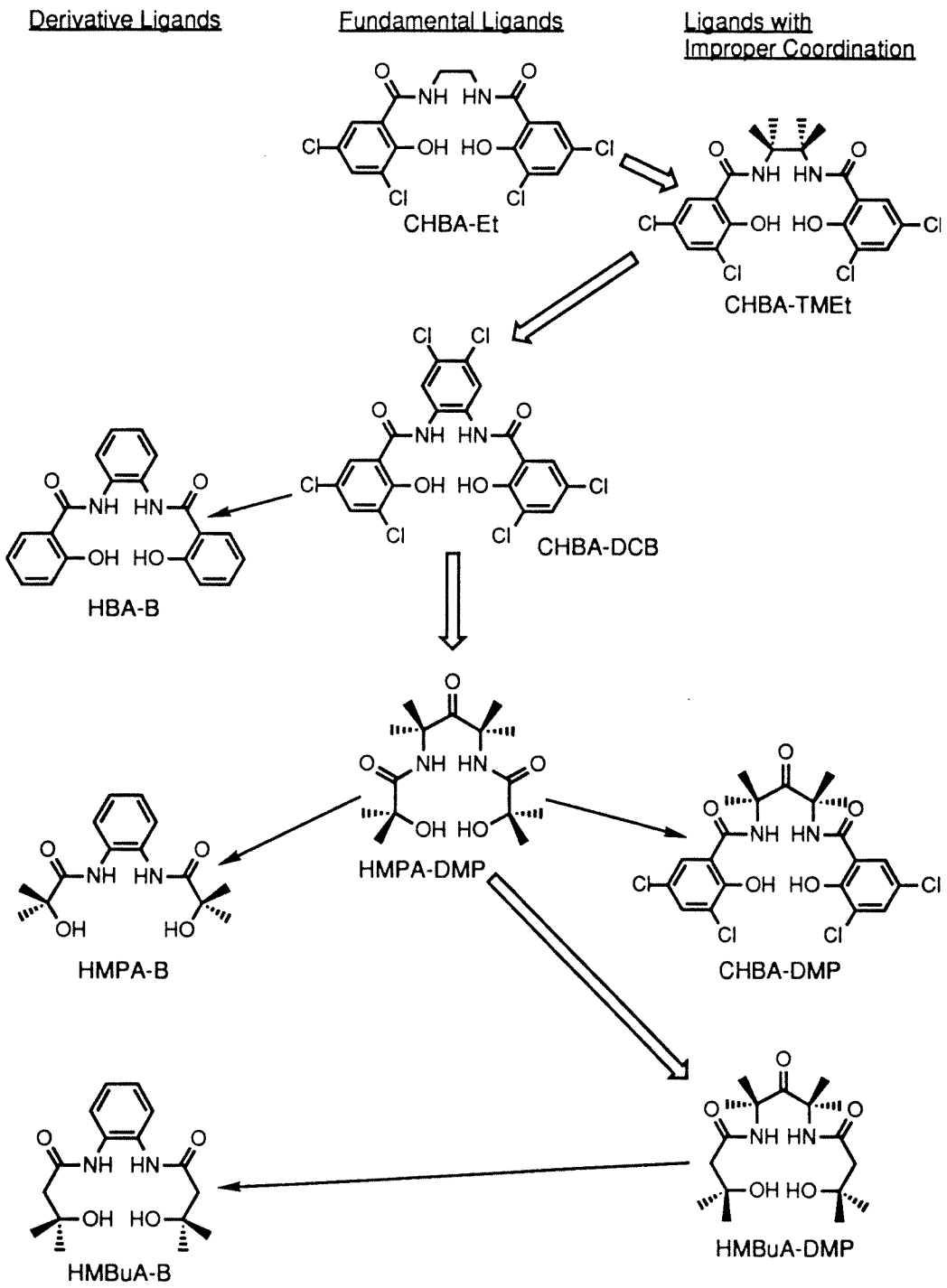

Figure 1.2. Ligand evolution in the Collins group prior to the macrocycles of this thesis (the coordinated ligands are tetradeprotonated). Conceptual alterations are indicated with broad arrows. Derivatizations are indicated with normal arrows.

oxidizing complexes are compounds which have a large driving force for electron transfer oxidations. Thus, for example, rhenium nonahydride dianion is a highly oxidized complex, since it contains formal Re(VII), but it is *not* highly oxidizing, since it is prepared from perrhenate in ethanol with excess sodium metal, a potent reductant.[5] Gold(I) in acetonitrile is highly oxidizing with a potential of ca. 1.39 V vs. NHE,[6] but the +I oxidation state for gold hardly classifies it as highly oxidized, since the +III state is also common. Obviously, many oxidants are both highly oxidized and highly oxidizing.[7]

For a given ligand type, the electron donor ability is roughly proportional to the pKa of the ligand. Each hydroxyl group in HMPA-DMP and HMPA-B has a pKa of approximately 18, while each dichlorophenol group in CHBA-DCB has a pKa of approximately 9. The Cu(III)/Cu(II) couples of these ligands reflect this difference.[8] The Cu(III)/Cu(II) couple is a particularly sensitive measure of the donor ability of a ligand complement, since the highest lying electron in Cu(II) is in an orbital directed at the ligand donor atoms (Figure 1.4, Table 1.1[9]). This higher donating ability is also seen in the formation of square planar Co(III) complexes with HMPA-B and HMPA-DMP,[10] rather than octahedral Co(III) complexes which are obtained with CHBA-DCB.[11] The formation of Os(VI) monooxos rather than Os(VI) *trans* dioxos also indicates the higher donor capacity of the aliphatic alcoxide donors (Figure 1.5).[9] It is interesting to note the strong inductive effect of the ketone carbonyl in DMP compared to Pr (Table 1.2[9]). Ultimately, the strong donor ability of HMPA-B led to the first crystallographically characterized Mn(V) monooxo complex.[12]

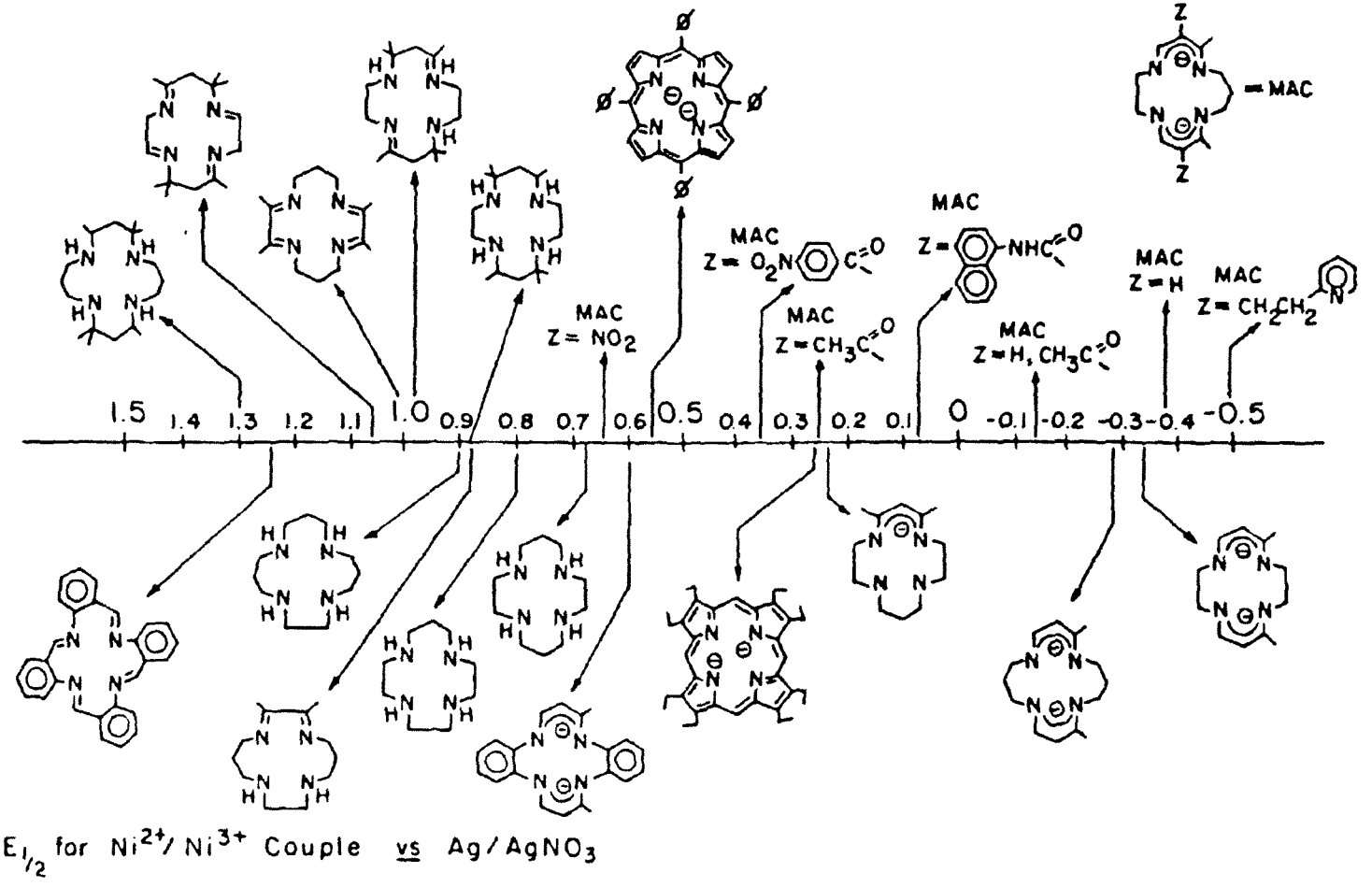

Figure 1.3. Ni(III)/Ni(II) couples with different ligands (noninnocence questions ignored here).

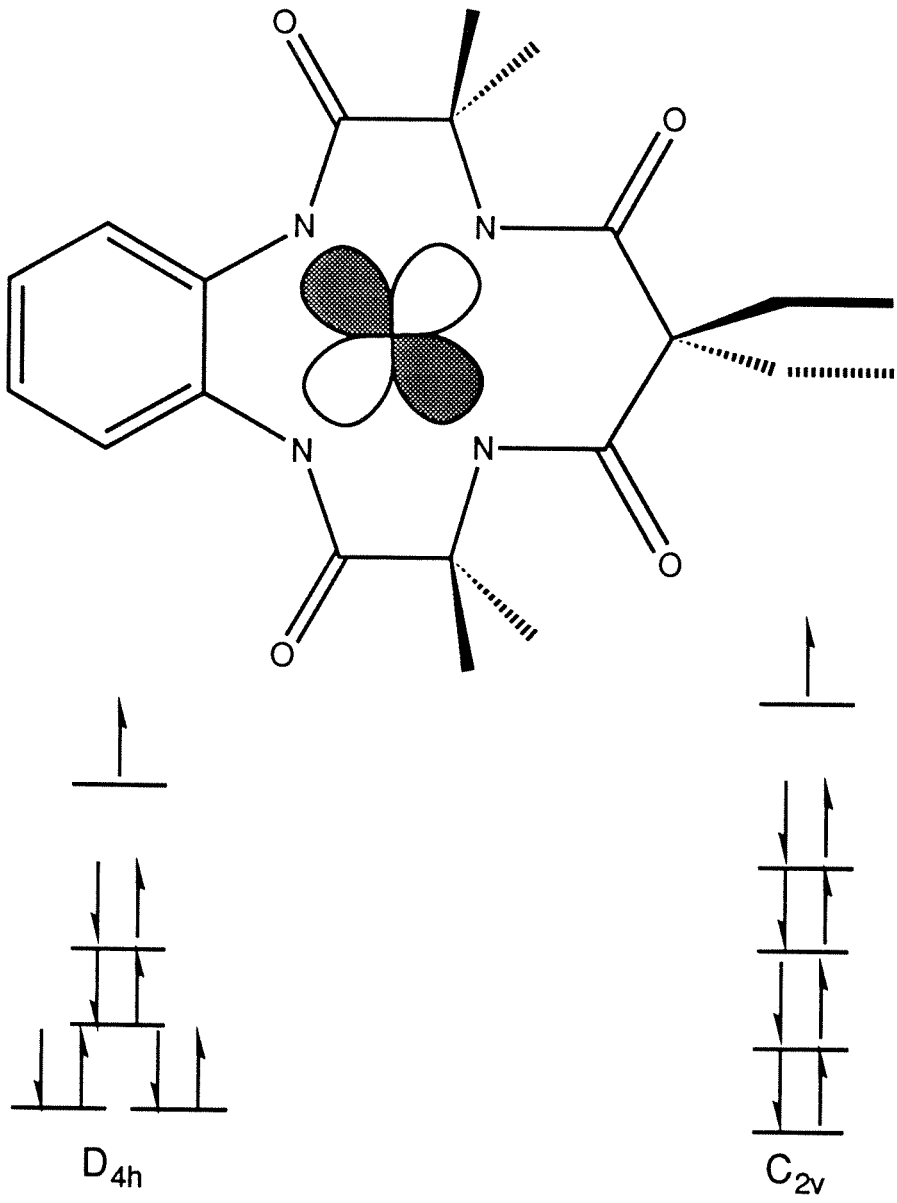

Figure 1.4. Rough sketch of the Cu(II) HOMO and the Cu(II) d-orbital electronic configuration.

Degradation resistance

The macrocyclic ligands of this thesis contain a series of protecting structural features which can be summarized as follows:[13] (i) The ligands are either *gem*-dimethylated or aromatized at the carbon atoms α to the nitrogens and β

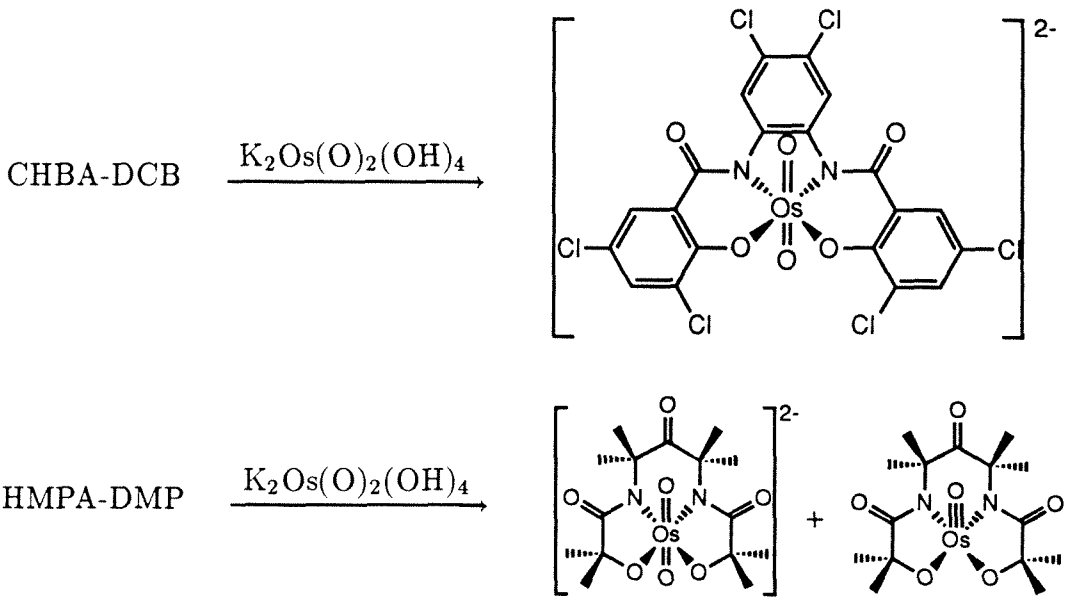

Figure 1.5. Reactions of CHBA-DCB and HMPA-DMP with potassium osmate.

Table 1.1. Formal Cu(III/II) Couples (V vs. Fc^+/Fc)[9]

Complex	E^f (CH_2Cl_2)	E^f (CH_3CN)	Δ (mV)
[Cu(η^4-CHBA-DCB)]$^-$	0.025	0.140	110(20)
[Cu(η^4-CHBA-Et)]$^-$	−0.140	−0.100	45(45)
[Cu(η^4-HMPA-B)]$^-$	−0.945	−0.835	110(20)
[Cu(η^4-HMPA-DCB)]$^-$	−0.920	−0.848	70(20)
[Cu(η^4-HMPA-DMP)]$^-$	−1.080	−1.000	80(20)

to the metal. H-substituents on the chelate backbones of earlier ligands were found to lead to two-electron reductions of the metal and ligand decomposition (Figure 1.6a).[14] *Gem*-dimethyl protection was first employed by Margerum with acyclic ligands.[15] The H-substituents can also be replaced by an aromatic group.[14a,16] (ii) Heteroatom donors in the chelate systems are all amido-*N* ligands. In contrast with alkoxide donors of the earlier systems, the nitrogen lone

Table 1.2. Formal (VI/V) Potentials for Os Monooxos[9]	
Complex	E^f (V vs. Fc^+/Fc)
Os(O)(η^4-HMBuA-DCB)	−0.57
Os(O)(η^4-HMBuA-B)	−0.68
Os(O)(η^4-HMPA-DMP)	−0.81
Os(O)(η^4-HMPA-Pr)	−1.10

pairs have minimal overlap with the σ^* orbitals of the C–C bond in the five-membered chelate rings, an arrangement believed to provide protection against heterolytic ligand oxidative decomposition (Figure 1.6b). (iii) The macrocyclic structure is believed to protect against homolytic ligand oxidative decomposition, another possible pathway for oxidative decomposition of earlier ligands (Figure 1.6c).[17] These design features were incorporated based on results from the earlier acyclic systems.

Electrochemistry of Os(CHBA-Et) complexes revealed that the ligand was vulnerable to oxidative degradation because of its α-hydrogens.[18] In the presence of benzyl alcohol the alcohol was oxidized in competition with ligand decomposition, and this led to an electrocatalytic system. The system produced benzaldehyde, and over one hundred turnovers were observed before catalysis terminated. It was initially assumed that the starting complex was the catalyst, but this was not correct. The redox cascade shown (Figure 1.7),[18] characterized by several crystal structures and high field NMR investigations, yielded what was *probably* the actual catalyst in the system. This study provided dramatic proof of the difficulty of identifying the catalyst in a decomposing catalyst system. The importance of the CHBA-Et decomposition story for

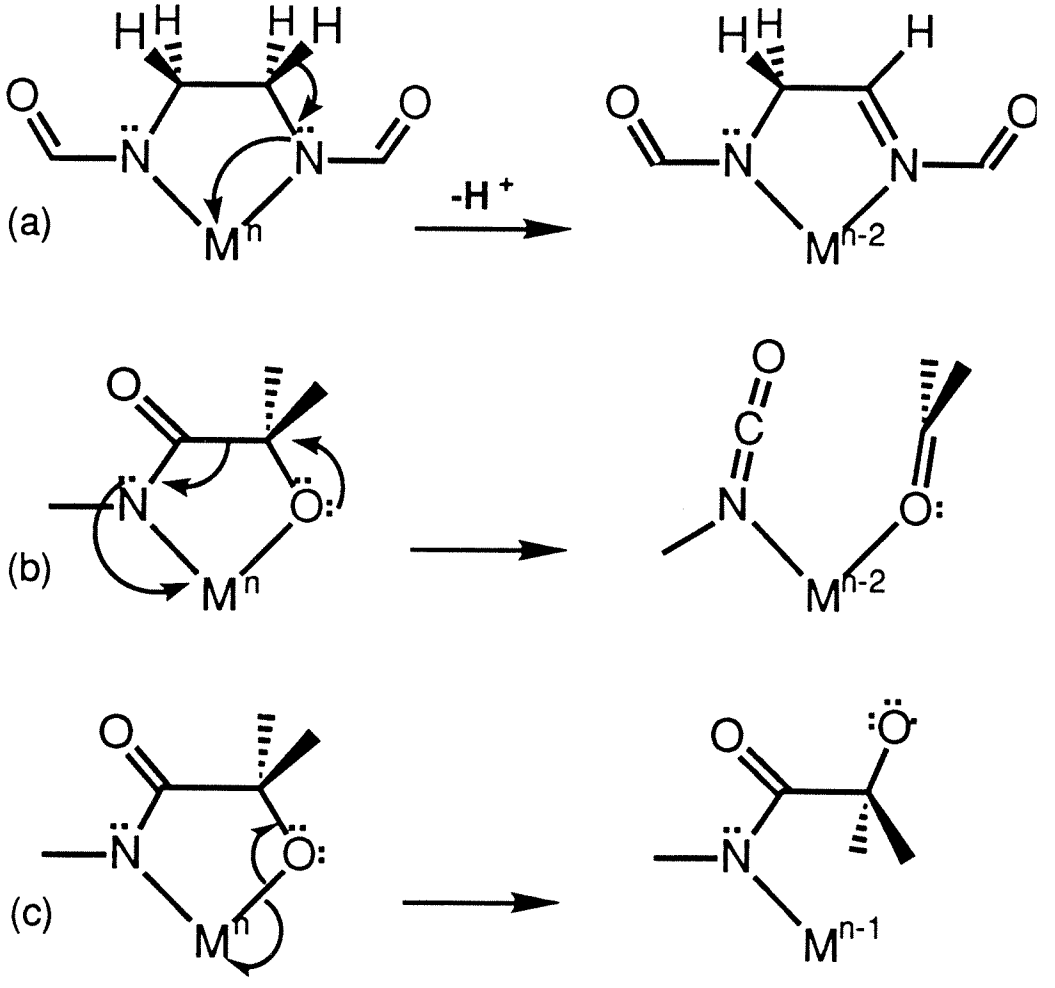

Figure 1.6. Destructive means of transferring electron density from a ligand to a metal. Subsequent homolytic steps not shown in (c) also lead to C–C bond scission.

this thesis was that it provided irrefutable evidence that hydrogen atoms alpha to nitrogen anions render ligands very susceptible to oxidative degradation.

The Os(CHBA-Et) results also illustrate that complexes with moderate reduction potentials can still be very susceptible to degradation; i.e., ligand donor capacity is distinct from ligand stability. Consider again the Ni complexes in Figure 1.3.[3] The stability of the complexes depends not only on the

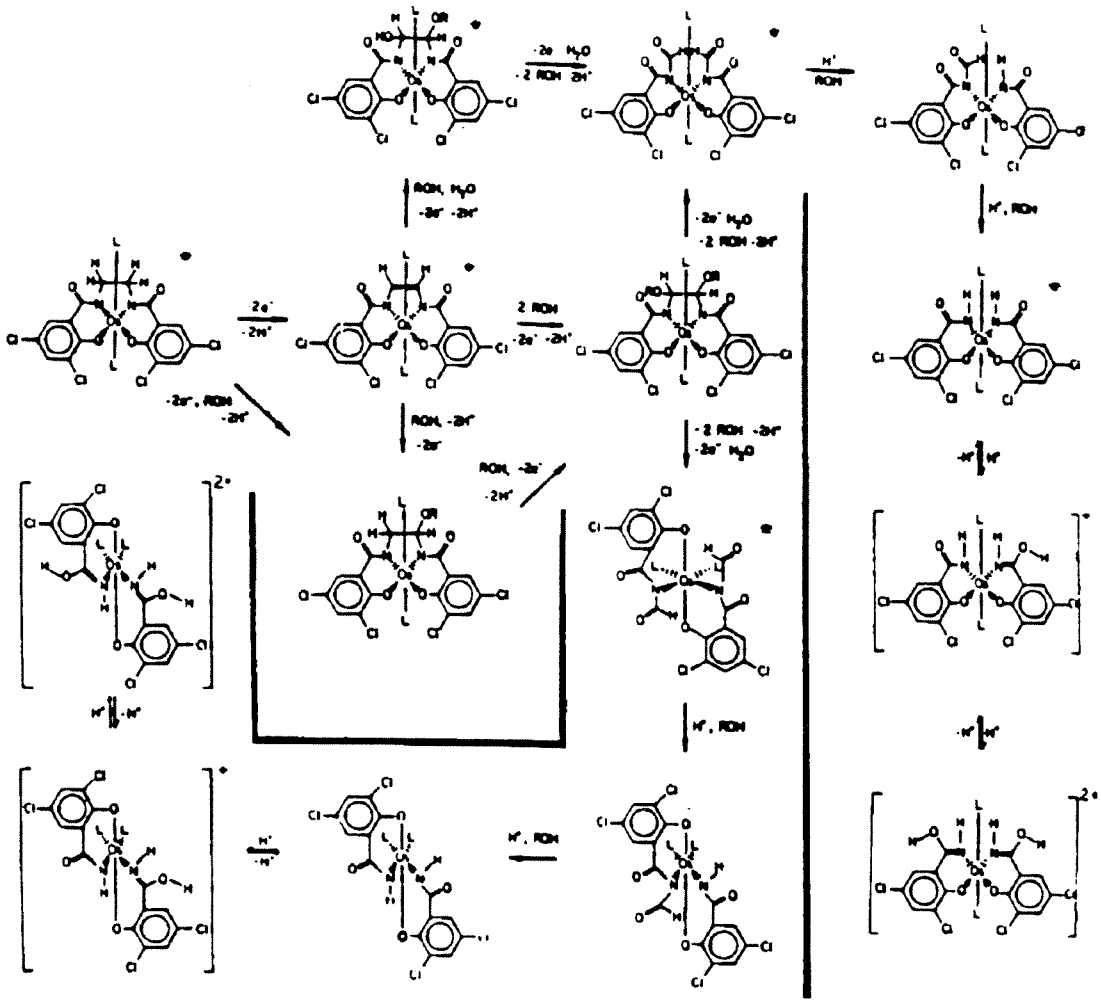

Figure 1.7. The electrocatalytic degradation of Os(IV) complexes of CHBA-Et in the presence of benzyl alcohol. Note that the initial step is oxidation followed by the loss of a proton α to the amide nitrogen.

Ni(III)/Ni(II) couple, but also on the resistance of the ligands to oxidative degradation. The complexes with potentials listed below 0 V (vs. $Ag/AgNO_3$, 0.60 V vs. NHE) all decompose rapidly in solution, while a few octahedral complexes of Ni(III) with cyclam ligands (here listed above 0.65 V vs. $Ag/AgNO_3$, 1.25 V vs. NHE) have been structurally characterized (see Chapter 7).[19] Thus, unless special steps have been taken to protect a strongly donating ligand, it

will often yield unstable species, even though they may have relatively low formal reduction potentials.

Two types of acyclic ligand systems were developed to eliminate the H-atom abstraction problem: CHBA-DCB and HMPA-DMP. In CHBA-DCB the solution involved aromatization of all of the relevant positions; in HMPA-DMP the solution involved permethylation of the relevant positions. Osmium complexes of the CHBA-DCB ligand proved to be extremely resistant to oxidative degradation, with some species exhibiting reversible cyclic voltammograms in liquid SO_2 above 2.0 V vs. NHE (Figure 1.8).[20]

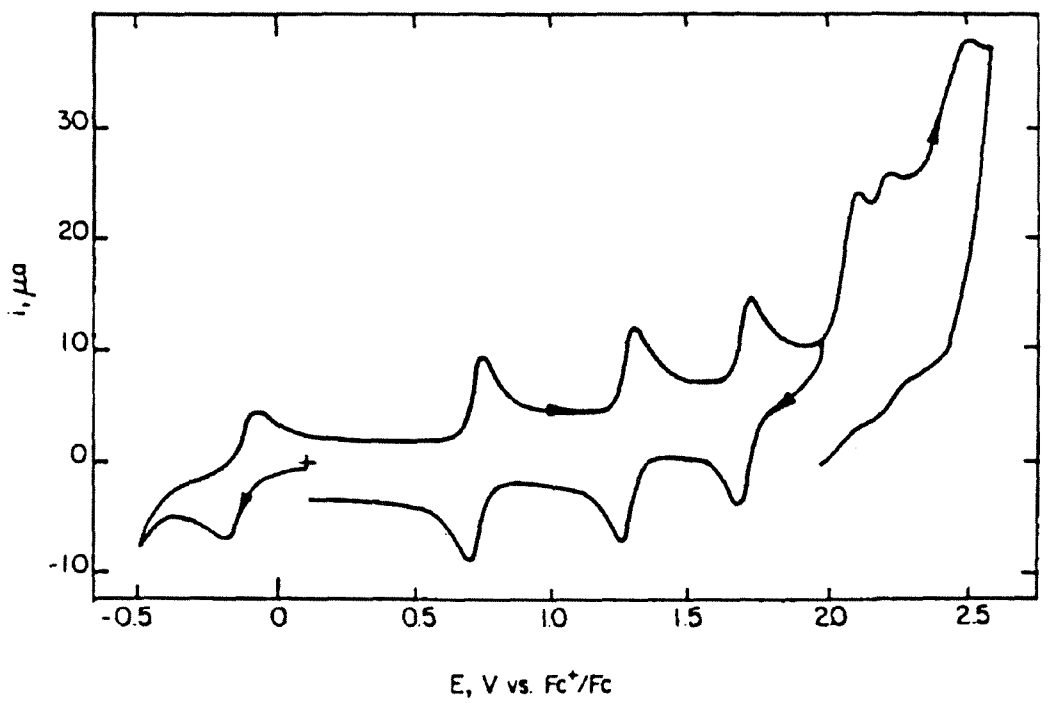

Figure 1.8. Cyclic voltammogram of *trans*-Os(CHBA-DCB)(PPh_3)$_2$ in liquid SO_2 at −60 °C (0.1 M [Bu_4N][BF_4]).

Unfortunately, although the ligands which contain hydroxymethyl-propanamido arms are more robust than systems with α-H-atoms, they seem

to be susceptible to an oxidative degradation pathway under moderately oxidizing conditions, namely a C–C bond scission between the amide carbonyl carbon and the quaternary carbon bearing the alkoxide group. This cleavage produces an isocyanate and acetone. Although the Collins group has not provided direct evidence for this mode of decomposition, it is reasonable considering similarities with other systems. For instance, Krumpolc, Deboer, and Roćek synthesized the first stable Cr(V) monooxo by reacting CrO_3 with 2-hydroxy-2-methylbutyric acid in aqueous $HClO_4$ (vide infra Chapter 3.).[17a]

$$2HCrO_4^- + 4C_2H_5(CH_3)C(OH)COOH + 4H^+ \longrightarrow$$
$$[(C_2H_5(CH_3)COCO_2)_2CrO]^- + Cr^{3+} + 2CH_3COC_2H_5 + 2CO_2 + 7H_2O$$

Furthermore, photochemical studies by the Schanz group on $[Co^{III}$(HMPA-B)$]^-$ have shown that irradiation of the complex produces acetone and other organic products.[17c]

The degradation resistance of a ligand to reduced forms of dioxygen is important for the following reason: The ultimate goal in catalytic oxidation chemistry is to have indefinitely lived catalysts which utilize molecular oxygen as the stoichiometric oxidant to selectively perform every oxidative transformation which can be thermodynamically driven by the four-electron reduction of dioxygen. In principle, virtually any oxidation (such as the conversion of alcohols to aldehydes and ketones) could be accomplished using molecular oxygen to drive the reaction. The feasibility of this approach has been demonstrated in synthetic systems at least in principle. Groves and Quinn discovered that dioxo(tetramesitylporphyrinato)ruthenium(VI) catalyzes the aerobic epoxida-

tion of olefins under ambient conditions.[21] Based on their findings, they proposed the reaction scheme shown in Figure 1.9. The initial Ru(VI) dioxo complex is reduced by olefin to a Ru(IV) monooxo which disproportionates to the Ru(VI) dioxo complex and an octahedral Ru(II) complex. This Ru(II) complex reacts with oxygen to produce more Ru(IV) monooxo. Many groups have carried out the catalytic oxidation of triphenylphosphine to triphenylphosphine oxide with molecular oxygen. In the Collins group, Brian Treco accomplished this catalytic transformation using the Os(HMPA-DMP) system.[9] The importance of ligand protection in these systems is clear; in recent work from Martell's group, a dioxygen complex of a Ni(dioxocyclam) decomposed by H-atom abstraction.[22]

The resistance of a complex to hydrolytic decomposition is useful for several reasons:

(i) Metal oxo isotope labeling may be accomplished with ^{17}O- and ^{18}O-labeled water.

(ii) Several useful oxidants such as H_2O_2 and NaOCl are conveniently used in water.

(iii) Many cation metathesis reactions run in water may be used to purify compounds.

(iv) Water is the ultimate solvent in terms of low cost and trivial waste disposal.

Unfortunately, a complication associated with the acyclic ligands is that their complexes with the first row metals are much less hydrolytically stable than the Os complexes. In particular, the Co complex of HMPA-DMP seems to be unstable in mildly acidic conditions, and the Cu complex is moderately

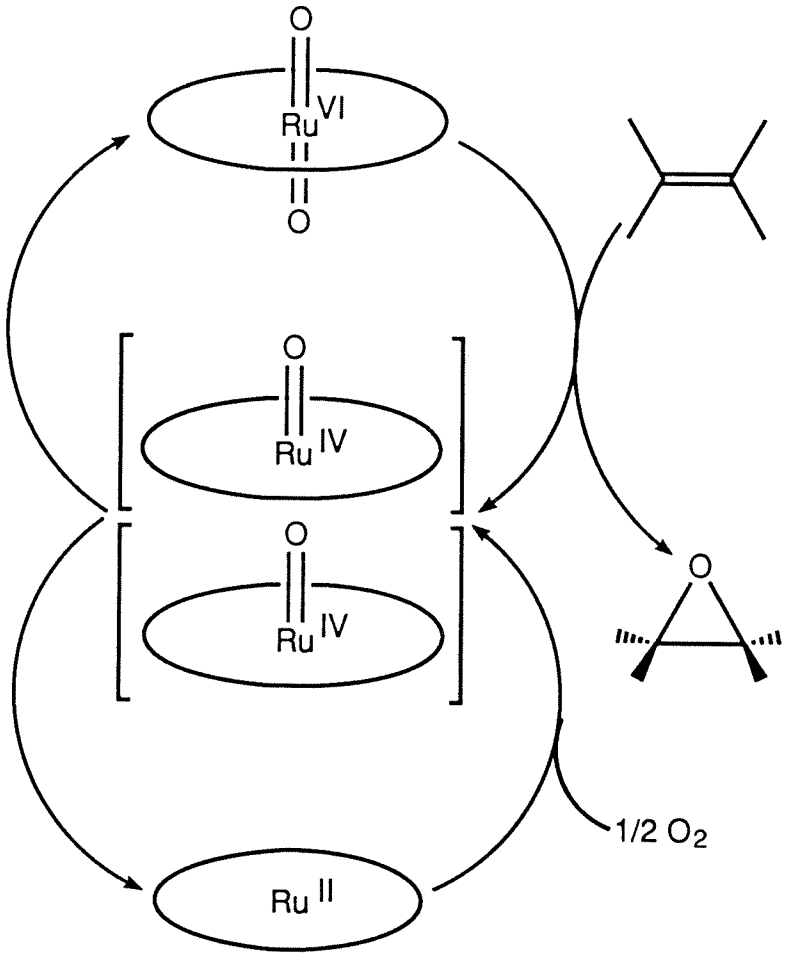

Figure 1.9. The proposed mechanism of Groves Ruthenium porphyrin olefin epoxidation catalyst. [The ligand is tetramesitylporphyrin.]

unstable in aqueous alcohol.[23] The metal exchange results shown in Figure 1.10 also indicate some protic solvent lability.[24] The basicity of the dialkoxide cleft has been seen in several crystal structures in which counter alkali metal cations invariably coordinate the dialkoxides—it is possible that demetallation/decomposition initiates from a small equilibrium percentage of an alkoxide-protonated arm dissociating from the metal. All of the transition metal compounds of the macrocycles presented in this thesis are water stable (If they are sufficiently oxidizing, they will be reduced, but not decomposed,

by water.). Most of the new complexes reported in this thesis are stable in water from pH 1–14.

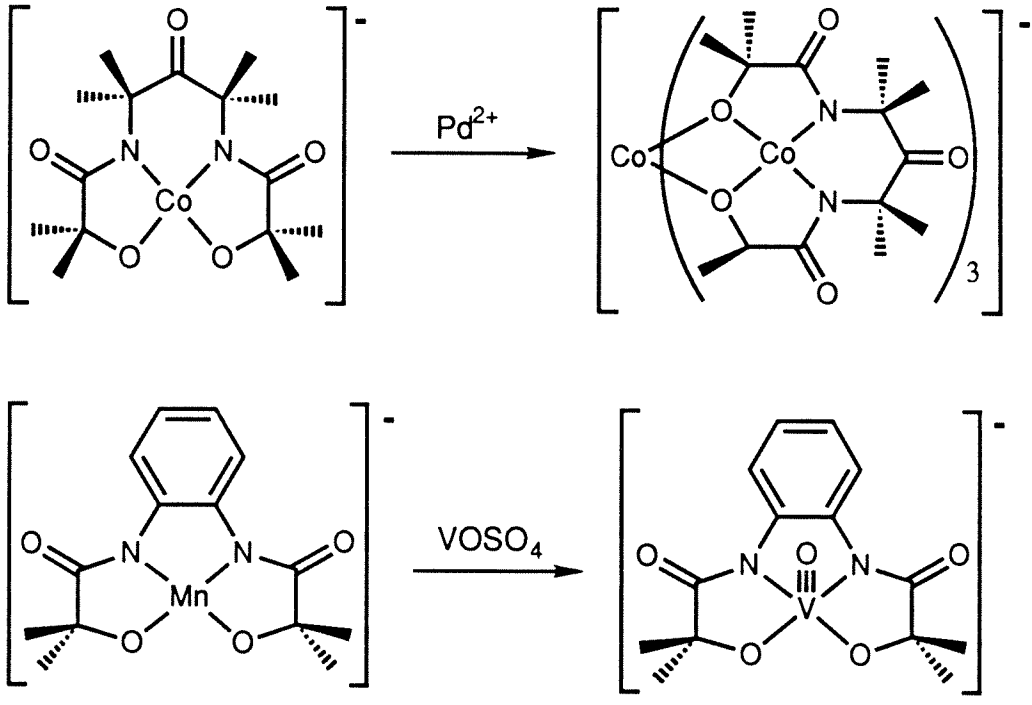

Figure 1.10. Metal metathesis reactions in the acyclic ligand systems. The absence of Pd in the product of the top reaction is not a typographical error.

Coordination geometry and steric bulk

One of the reasons for synthesizing the macrocycles of this thesis was to control coordination problems which had arisen in earlier Collins ligands.

Amides are ambidentate ligands, and the earlier metals can favor O-atom ligation. This was graphically illustrated with the group's early chromium work with CHBA-Et, in which two chromium cations are bridged by two ligands (Figure 1.11. see also Chapter 3).[25] Each ligand is tetradentate, binding one Cr with a phenolate oxygen and an amide nitrogen and binding the other Cr with a phenolate oxygen and an amide oxygen.

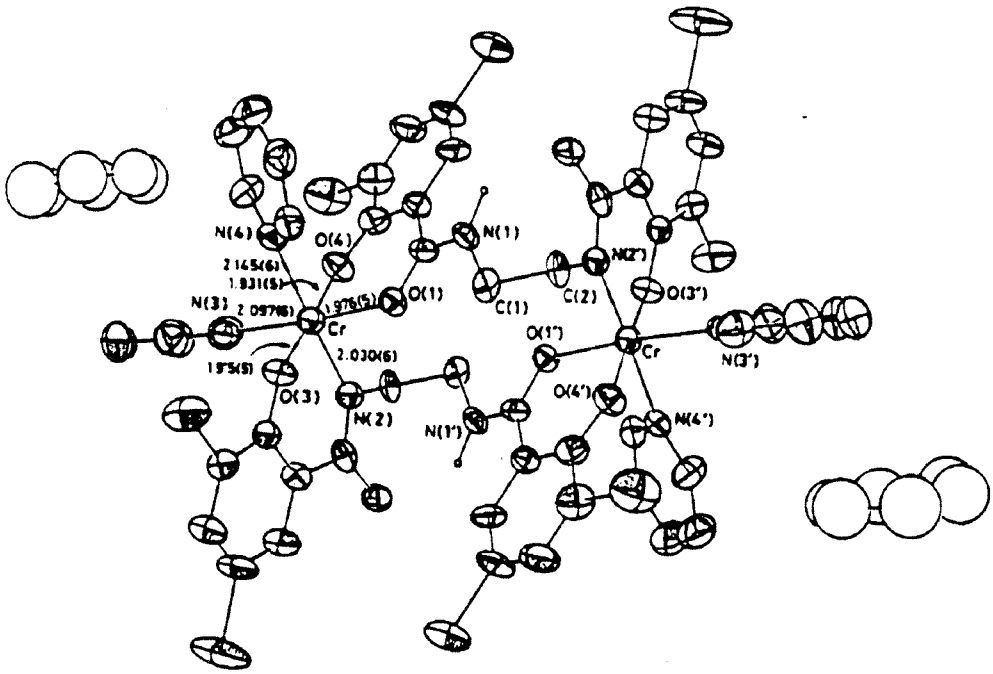

Figure 1.11. A Cr(III) crystal structure with the CHBA-Et ligand, where the ambidentate nature of the amide ligand results in a bridging structure having both N- and O-bound amides.

Similar coordination problems were encountered in the initial attempt to solve the α-hydrogen ligand degradation problem of CHBA-Et by replacing the ethylenediamine backbone with 1,1,2,2-tetramethylethylenediamine. CHBA-TMEt (Figure 1.2) was never properly coordinated to any of the metals tried by the Collins group. The geminal methyls in the backbone prevent simple monomeric tetradentate metal coordination in these systems. Kochi thought he had achieved tetradentate coordination of CHBA-TMEt with cobalt and interpreted a number of catalytic results based on such coordination, but his reasoning was severely flawed, because his compounds were air-stable as Co(II).[26] However, all studies performed with related ligand systems and systems of similar donor strength yielded air stable Co(III) (see Chapter 6).[10,11,27]

Indeed, a subsequent crystal structure performed by the Kochi group revealed that the potentially tetradentate CHBA-TMEt was bound as a bidentate ligand with one phenolate and one amide oxygen coordinating (Figure 1.12).[28] This result, of course, invalidated all of their prior mechanistic speculations.

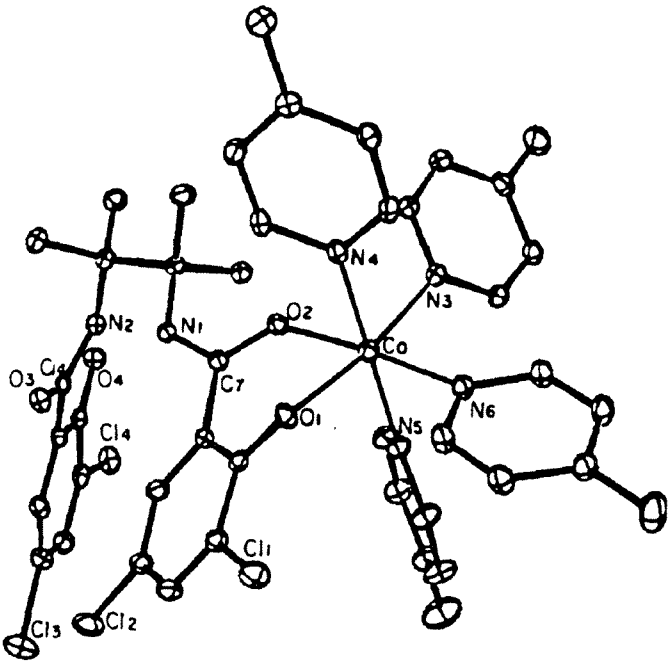

Figure 1.12. A cobalt complex of CHBA-TMEt in which the ligand is bidentate and the amide group is O-bound.

The reasons for the poor coordination properties of CHBA-TMEt may be understood by considering the crystal structure of bis-(perfluoropinacolato) nickel(II),[29] in which the steric clash of the perfluoro methyl groups forces them to adopt a staggered conformation. Because the alcoxide anion has three lone pairs with sp^3 hybridization, the ligand may still bind metals in a bidentate fashion by an appropriate rotation about the carbon-oxygen bond. In the amide system, however, the nitrogens are sp^2 hybridized and the staggered conformation causes the lone pairs to be localized in orbitals which

are separated by approximately 60°. In the crystal structure of the dioxygen adduct of N,N′-(1,1,2,2-tetramethyl)-ethylenebis(3-fluorosalicylaldiminato)-(1-methylimidazole)cobalt(II),[30] the ligand, which also has sp^2 hybridized nitrogen donors, accomplishes tetradentate planar coordination for a number of subtle reasons. The N-C-C-N torsion angle of 37° relieves some of the steric geminal dimethyl compression but is substantially less than 60°; small but distinct distortions of the imine double bond which involve pyramidalization at nitrogen and rotation about the C-N double bond help bring the imine lone pairs back into the ligand plane. Analysis of this structure using the Chem 3D program reveals another subtlety. Replacement of the imine functional group with an amide puts an oxygen atom in the place where the imine hydrogen was. This seems to result in steric compression as well (The amide oxygen-methyl distance estimated for this hypothetical complex is 0.35–0.50 Å closer than observed in the crystal structures of the complexes of the macrocyclic tetraamides in this thesis.). In other words, with the amide in place of the imine, fully staggered nitrogens with planar amides present no steric problems, but make coordination impossible. Eclipsed nitrogens make coordination possible but generate unacceptable steric clash between the methyl groups. Partially eclipsed nitrogens make coordination possible but generate two types of steric clash, methyl-methyl and methyl-O_{amide}, which taken together are unacceptable. Thus, use of 1,1,2,2-tetramethylethylenediamine in amide containing ligands designed to chelate would seem to be problematical in light of these considerations.

Another ligand which turned out to have poor coordination properties, HMBuA-DMP, was synthesized in an attempt to block the C–C bond scission

decomposition pathway available to HMPA-B and HMPA-DMP. Regrettably, it did not seem to coordinate Co, Cu, or Os, although the aromatic backbone derivatives did coordinate these metals.[9] In the Collins group's acyclic systems, ligands which contain exclusively 6-membered chelate rings do not seem to bind metals well. Analysis of models indicates that the arms simply wrap to the point of overlapping in a plane (Figure 1.13).

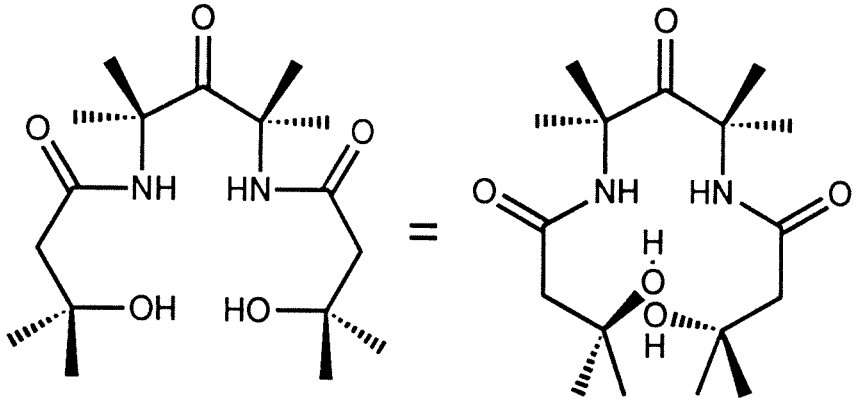

Figure 1.13. When models of HMBuA-DMP are placed flat on a table, the hydroxyl groups clash in front.

Coordination control problems were encountered with the CHBA-DCB and HBA-B ligands which involved isomerizations at the metal to form non-planar amides. A typical representation of bonding in an amide is represented in Figure 1.14.* In this normal picture, there are three significant resonance structures involving sp^2 hybridized C, N, and O atoms. The resonance structure with a double bond between the carbon and nitrogen atoms is the con-

* Although Wiberg, et al. have severely called this picture into question for simple organic amides, in the absence of theoretical study of transition metal bound amido-*N* ligands the classical resonance formulation will be used in this discussion.[31]

tributor used to explain the barrier to rotation about the C–N bond (10–35 kcal/mol) and the planarity of the amide group.[32] However, with the CHBA-DCB and HBA-B ligands metal oxidation or coordination of π-acids generated *cis*-α complexes, while ligand substitution by bidentate chelating ligands, such as 2,2′-bipyridyl, led to *cis*-β complexes (Figure 1.15).[33] The only way to achieve these geometries with ligands with such limited rotational degrees of freedom was to generate nonplanar amides by rotation of the C–N bonds and/or pyramidalization at N. Three distinct classes of inorganic nonplanar amides have been elucidated by the Collins' group to date:[34]

(i) amides nonplanar due to enhanced stability over the structurally accessible planar form (a class never before observed in chemistry),

(ii) amides nonplanar due to ring strain (a class previously of significance only in organic chemistry),

(iii) amides nonplanar due to steric clash (a class never documented before in chemistry).

The generality of these results has been broadened with the documented isomerization of a Co(HMPA-DMP) complex.[34e] [See Chapter 9 for a more detailed discussion of amide nonplanarity in the acyclic and macrocyclic Collins group ligands.]

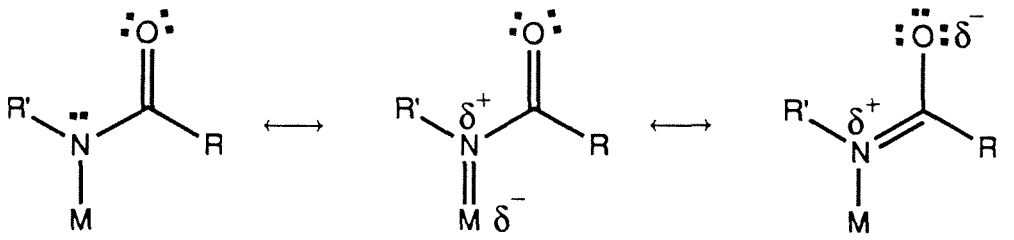

Figure 1.14. Amide resonance structures.

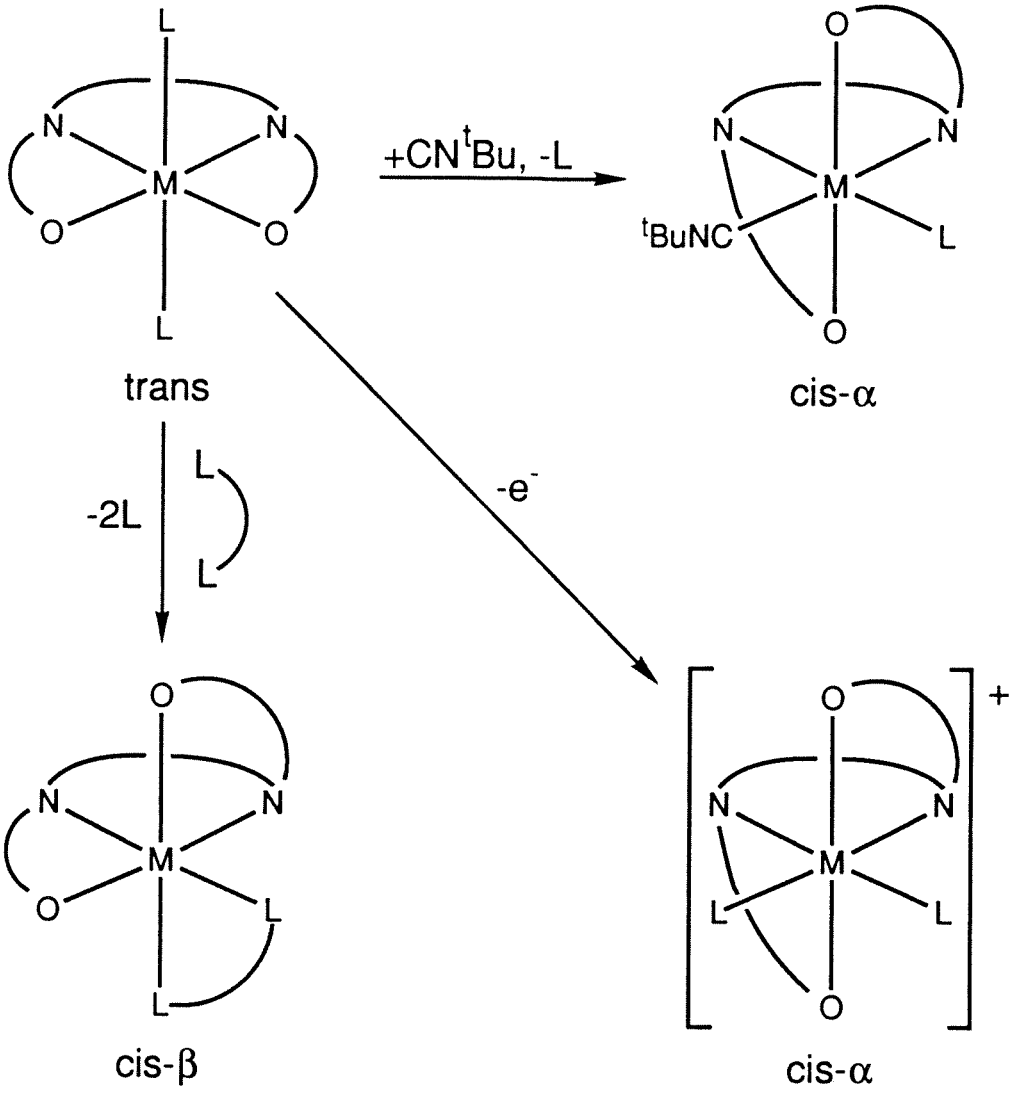

Figure 1.15. The three possible isomers of an octahedral complex with a tetradentate ligand as described by Sargeson.[33] In this specific example, the tetradentate ligand was CHBA-DCB, the metal was osmium, and the monodentate ligands were triphenylphosphines.

Although the nonplanar amide results are very significant to the understanding of the amide functional group and to general coordination chemistry, there are two difficulties associated with these isomerizations. First, three different isomers of these acyclic ligands can be obtained, and it is difficult to

know a priori which isomer(s) will be present under a given set of conditions. Thus, the rational design of oxidation catalysts with controlled selectivity becomes more difficult, because rational steric modification of the ligand aimed at controlling this selectivity becomes challenging. Second, the great difference in the redox couples (up to 500 mV[20]) between the *trans*, *cis*-α, and *cis*-β isomers (see Chapter 9), makes the thermodynamic reactivity of the complexes difficult to predict. Clearly, if both the reactivity and the spatial configuration of a complex may be drastically modified by isomerizations, predictable reactivity modification becomes impossible. Therefore, the ligand configuration must be controlled, and this has been achieved in the macrocyclic tetraamides introduced here.

Ligand innocence and noninnocence

The oxidation state assigned to the transition metal center of an inorganic complex is obtained by conceptually dissociating the ligands from the metal as closed shell species; i.e., for the charge at the metal to correspond to the oxidation state assigned, metal-ligand bonding would have to be perfectly ionic. Even though metal-ligand sigma-bonding is never perfectly ionic, and is often substantially or even predominantly covalent, the *formal* oxidation state at the metal still has utility as a means of indicating systems which will have unusual electronic configurations; i.e., the number of unpaired and paired non-bonding metal electrons may be reliably determined and spectroscopic data will be consistent with this assumption. Even the formal oxidation state assignment, however, is of little use when extended ligand π-systems may interact with metal d_π orbitals. In these situations, oxidation state assignments may be rendered ambiguous either by the existence of reasonable

resonance structures which put the metal in two or more different oxidation states (in molecular orbital terms, the existence of π orbitals which have significant contributions from a metal and several ligand atomic orbitals) or by the possiblity that oxidation (or reduction) will be ligand centered to give ligand radicals.[4c,35] The main point is that an electron deficient metal center will acquire electron density from its ligand either destructively (vide supra) or nondestructively. The nondestructive processes will either involve greater polarization of the metal-ligand σ-bonding electrons toward the metal or polarization of ligand π-electrons toward the metal via ligand-$\pi \rightarrow$metal-d_π overlap. These different processes are important and spectroscopically distinguishable. Innocent ligands will *not* have extended π-systems capable of interacting with the metal and noninnocent ligands will.[4c,35] The resistance of a ligand to oxidative degradation should not be confused with the resistance of a ligand to oxidation. A ligand may serve as the partial or entire site of a redox event, and this ligand oxidation may happen without decomposition and can be advantageous. Because many metal-centered redox processes are one-electron rather than the usually desirable (from the standpoint of organic transformations) two-electron processes, coupling the reactivity of the metal with the removal or addition of electrons from or to orbitals of pronounced ligand character can be a means of obtaining selective redox reactions; i.e., the ligand may act as a redox reservoir. As seen in Figure 1.16, the hydroxylation of alkanes mediated by cytochrome P-450 involves an O-atom transfer reaction which raises the formal oxidation state at carbon by two units and lowers the *formal* oxidation state at iron by two units (i.e., $+V \rightarrow +III$). However, all spectroscopic evidence indicates that the reactive iron oxo is best described as an iron(IV) oxo

porphyrin cation radical.[36] Thus, this selective two-electron O-atom transfer process can be viewed as involving redox at the porphyrin ligand as well as the metal. The role of cytochromes P-450 in sterol synthesis and metabolism has been reviewed.[37]

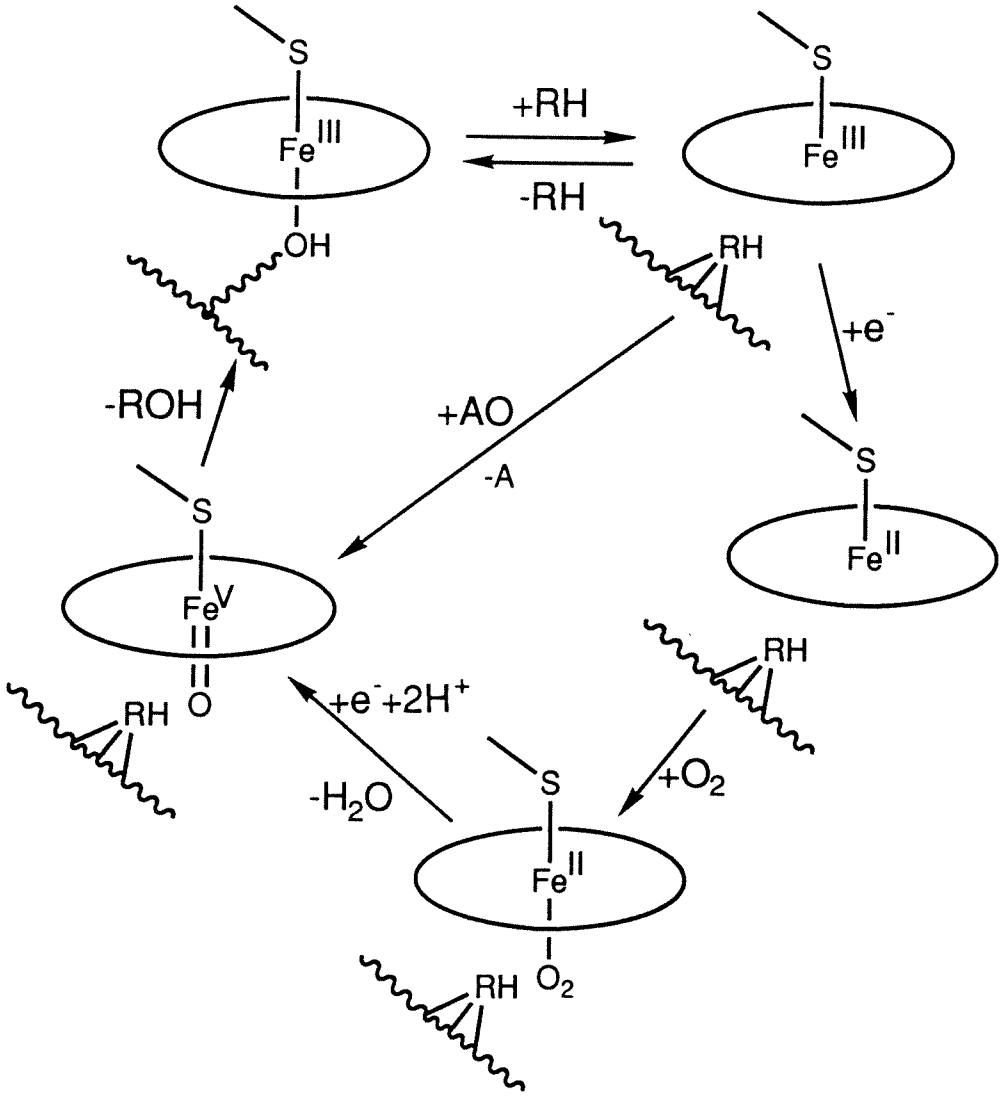

Figure 1.16. The generally accepted mechanism for hydroxylation of alkanes by cytochrome P-450. The coordinated OH group represents a hydroxyl residue from the protein. The reaction in the center of the Figure is commonly referred to as the peroxide shunt. The iron(V) species depicted is typically considered to be an iron(IV) oxo porphyrin cation radical.

In earlier Collins group work, the CHBA-DCB ligand yielded a number of interesting complexes, but a disadvantage of this ligand system was that it was noninnocent.[8] For instance, the oxidation state assignment of Co(IV) in

the complex shown in Figure 1.17 had to be supported by considerable EPR analysis and reference to literature complexes which had already been accepted as Co(IV).[11] For the Os system in Figure 1.8, the reversible couples above 0.72 V vs. Fc^+/Fc are primarily ligand centered.[20] Obviously, the noninnocence was not a disadvantage in terms of interesting reactivity, but it was an inherent weakness as far as assigning formal oxidation states. Thus, the HMPA-DMP ligand, although not as robust, was prepared in order to address oxidation state questions which could not be studied with CHBA-DCB or HMPA-B.

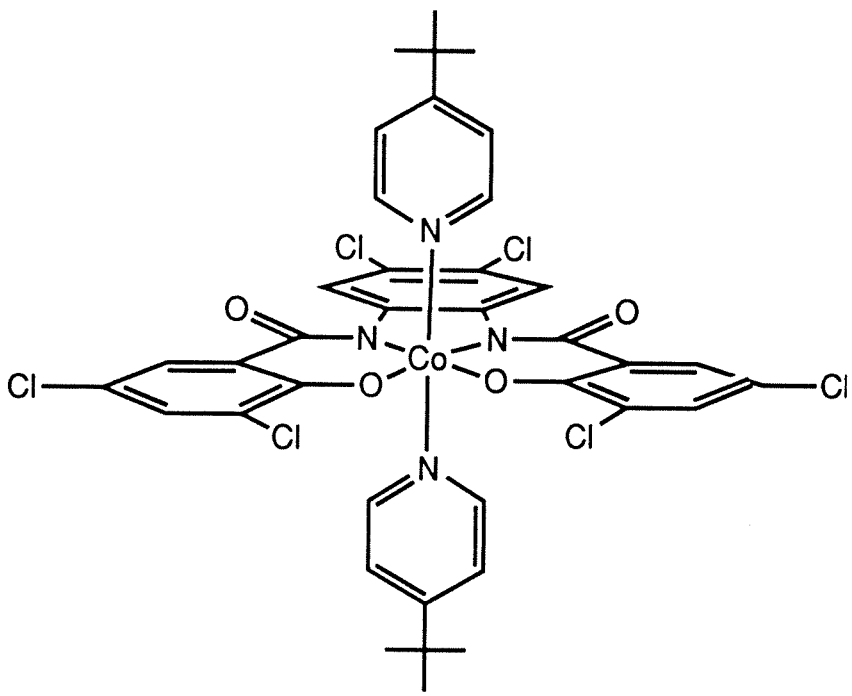

Figure 1.17. *Trans*-Co(η^4CHBA-DCB)(*tert*-butylpyridine)$_2$—a formally Co(IV) complex. The oxidation state assignment to Co is ambiguous in this complex because CHBA-DCB is a noninnocent ligand.

The two types of macrocyclic tetraamide ligands discussed in this thesis were deliberately prepared to study complementary problems. The H_4MAC*

ligand was synthesized to address questions of formal oxidation state assignments, while the system with the aromatic backbone was prepared to control and enhance available reactivity.

The accomplishments realized with the acyclic ligands were noteworthy. However, it seemed that a significantly different approach was needed to enlarge upon these achievements. Although there are many possible approaches given the design constraints discussed, the five macrocycles shown below were the targets which received attention (Figure 1.18). The deprotonated ligands would be tetraanions and thus, strong donor systems. The ligands would have no hydrogens α to nitrogen anions and thus, would not be susceptible to previously elucidated degradation pathways. Three of the ligands, although potentially vulnerable to the same C-C bond scission that is the weakness of some of the acyclic systems, might be expected to be less prone to this degradation pathway because the mechanisms depicted in Figure 1.6 (b and c) are unavailable in the macrocycles. The macrocyclic ligands would clearly be unable to isomerize to either the *cis*-α or *cis*-β geometries. The innocent ligands would provide the option of ready formal oxidation state assignment, while the noninnocent systems would provide the ability to tune reactivity through aromatic substitution chemistry and steric modification of the macrocyclic periphery. The macrocyclic effect (see Chapter 2) would be expected to increase the hydrolytic stability of first row complexes, while also effectively suppressing the ambidentate character of the amide group. The pyridine based ligand would offer the opportunity of switching the electron donor capacity of the ligand by protonation/deprotonation equilibria.

Prior to the efforts described in this thesis, only Margerum's group had

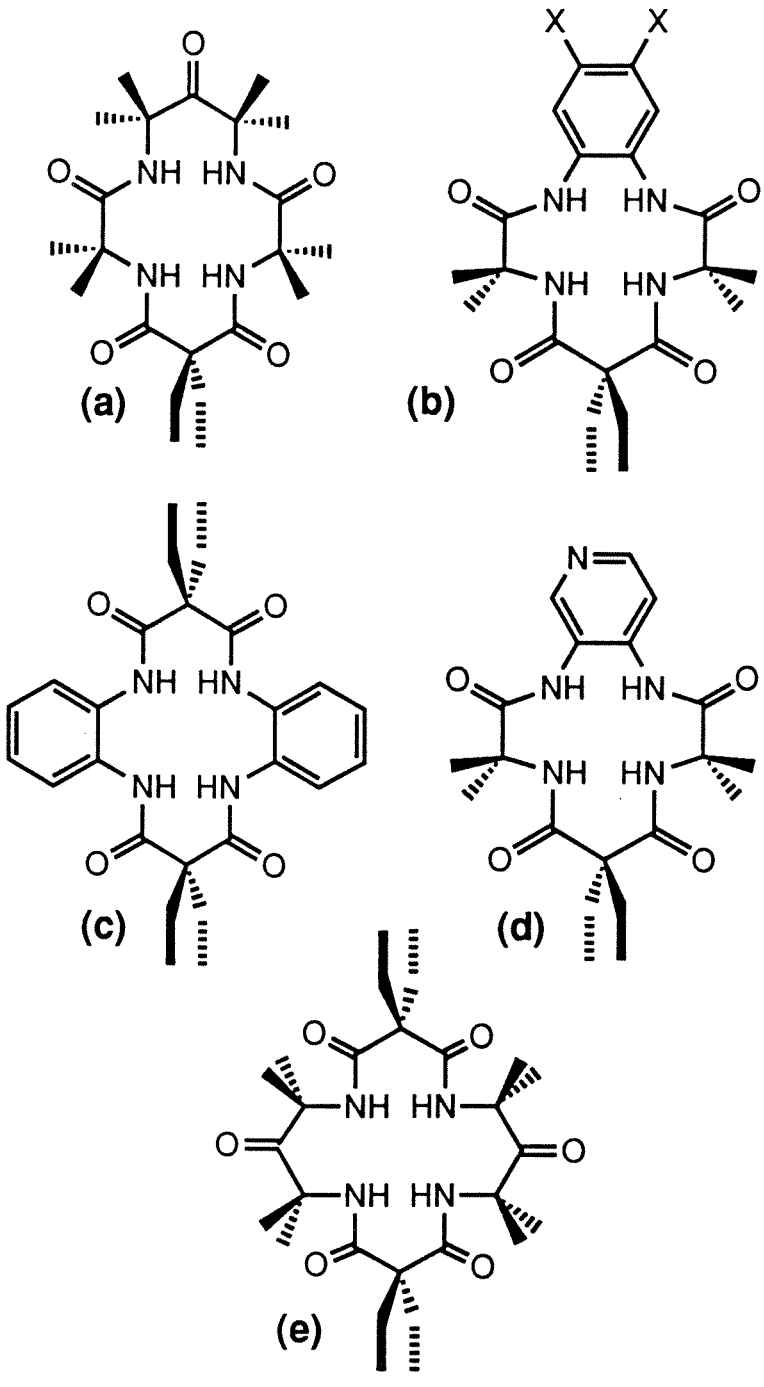

Figure 1.18. Macrocyclic tetraamide targets in this thesis which received synthetic attention. Systems (a) and (b) were successfully produced and constitute the subjects of subsequent chapters. Much has been learned about preparing systems (c) and (d), although they have not yet been produced (see Chapter 2). The synthesis of system (e) has received little effort to date.

done any work with a macrocyclic tetraamide (Figure 1.19) and this work had been limited to two papers on the Cu(III/II) chemistry.[38] Three fundamental points learned from this work were:

(i) Copper can be inserted into macrocyclic tetraamido-*N* ligands and the resultant complexes are water-stable.

(ii) Macrocyclic tetraamido-*N* ligands are very strong σ-donors (the Cu(III/II) couple was only 0.48 V vs. NHE, about 800 mV lower than the Cu(cyclam) Cu(III/II) couple).

(iii) Even though the tetrapeptide made the Cu(III) complex only a mild oxidant, the complex still slowly decomposed due to the α-hydrogens.

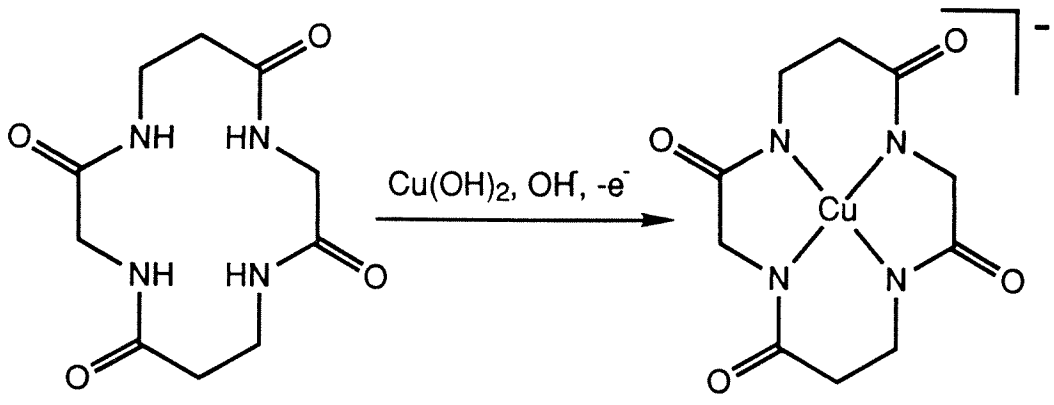

Figure 1.19. Margerum and Rybka's macrocyclic tetrapeptide. The tetradeprotonated form was characterized in both Cu(II) and Cu(III) complexes. The Cu(III) complex (E° = 0.48 V vs. NHE) slowly decomposed by processes involving H-atom abstraction β to the metal.

Considerable work with mono-, di-, and tri-oxocyclams has been done,[39] but all of these ligands, to date, have also had α-hydrogens and have been subject to facile degradation (Figure 1.20). Considerable work has been done with amine and Schiff base macrocycles, but these ligands are neutral and not as

donating as the anionic amide ligands (the amine and Schiff base macrocycles have also frequently been subject to oxidative decomposition). The porphyrins (which are subject to oxidative decomposition in the absence of several protecting schemes[16]) and phthalocyanines are only dianionic, as are several other highly conjugated systems. We thus had reason to believe that we could expand the coordination chemistry of macrocyclic tetraamido-*N* ligands beyond copper, and that doing so with ligands protected against oxidative degradation would enable us to stabilize a number of species previously unobtained.

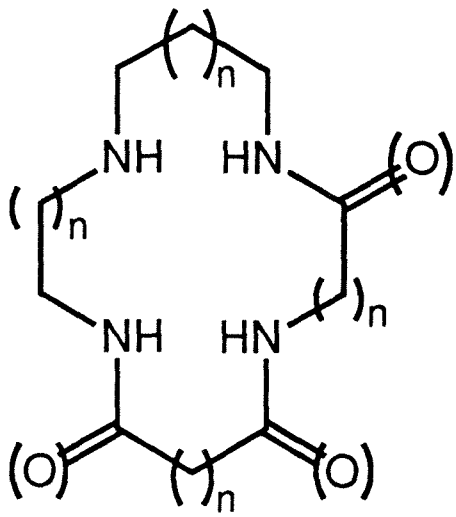

Figure 1.20. Cyclam derivatives. With no amide oxygens and $n = 1$ for all of the incipient chelate rings, the molecule is cyclam. Ligands of this type with 12-, 13-, 14-, 15-, and 16-membered rings have been prepared with 0, 1, 2, or 3 amide oxygens. Many of these molecules have been prepared with tertiary amine donors and with various substituents on the carbon atoms. Prior to the macrocyclic tetraamides described in this thesis, **all** molecules of this general class have had hydrogens in oxidatively vulnerable positions.

References

1. For the elucidation of the strong σ-donor strength of amido-*N* ligands see, for example: (a) Margerum, D. W. *Pure Appl. Chem.* **1983**, *55*, 23–34. (b) Margerum, D. W. *Oxidases Relat. Redox Syst., Proc. Int. Symp., 3rd., 1979* **1982**, 193–206.

2. Krafft, T. E. Ph.D. Thesis, California Institute of Technology, 1985.

3. Busch, D. H. *Acc. Chem. Res.* **1978**, *11*, 392–400.

4. (a) Collman, J. P.; Hegedus, L. S.; Norton, J. R.; Finke, R. G. *Principles and Applications of Organotransition Metal Chemistry*, 2nd ed.; University Science Books: Mill Valley, CA, 1987; Chapter 2. (b) Willemse, J.; Cras, J. A.; Steggerda, J. J.; Keijzers, C. P. *Struct. Bonding* **1976**, *28*, 83–126. (c) Jørgensen, C. K. *Oxidation Numbers and Oxidation States*; Springer: New York, 1969.

5. Cotton, F. A.; Wilkinson, G. *Advanced Inorganic Chemistry*, 5th ed.; Wiley-Interscience: New York, 1988; p. 864.

6. Goolsby, A. D.; Sawyer, D. T. *Anal. Chem.* **1968**, *40*, 1978–1983.

7. It is important to distinguish between atom transfer and electron transfer reactivity. For instance, permanganate ion and osmium tetroxide, which are considered highly oxidizing in an atom transfer sense, are only moderate one-electron transfer oxidants. Discussing atom transfer oxidants is also often complicated by kinetic issues.

8. Anson, F. C.; Collins, T. J.; Richmond, T. G.; Santarsiero, B. D.; Toth, J. E.; Treco, B. G. R. T. *J. Am. Chem. Soc.* **1987**, *109*, 2974–2979.

9. Treco, B. G. R. T. Ph.D. Thesis, California Institute of Technology, 1988.

10. (a) Collins, T. J.; Richmond, T. G.; Santarsiero, B. D.; Treco, B. G. R. T. *J. Am. Chem. Soc.* **1986**, *108*, 2088–2090. (b) Brewer, J. C.; Collins, T. J.; Smith, M. R.; Santarsiero, B. D. *J. Am. Chem. Soc.* **1988**, *110*, 423–428. (c) Collins, T. J.; Ozaki, S.; Richmond, T. G. *J. Chem. Soc., Chem. Commun.* **1987**, 803–804.

11. Anson, F. C.; Collins, T. J.; Coots, R. J.; Gipson, S. L.; Richmond, T. G. *J. Am. Chem. Soc.* **1984**, *106*, 5037.

12. Collins, T. J.; Gordon-Wylie, S. W. *J. Am. Chem. Soc.* **1989**, *111*, 4511–4513.

13. Collins, T. J.; Kostka, K. L.; Uffelman, E. S. *Inorg. Chem.* in press.

14. See for example: (a) Anson, F. C.; Christie, J. A.; Collins, T. J.; Coots, R. J.; Furutani, J. J.; Gipson, S. L.; Keech, J. T.; Krafft, T. E.; Santarsiero, B. D.; Spies, G. H. *J. Am. Chem. Soc.* **1984**, *106*, 4460–4472. (b) Anson, F. C.; Collins, T. J.; Coots, R. J.; Gipson, S. L.; Keech, J. T.; Krafft, T. E.; Santarsiero, B. D.; Spies, G. H. *Inorg. Chem.* **1987**, *26*, 1161–1168. (c) Anson, F. C.; Collins, T. J.; Gipson, S. L.; Keech, J. T.; Krafft, T. E. *Inorg. Chem.* **1987**, *26*, 731–736.

15. Diaddario, L. L.; Robinson, W. R.; Margerum, D. W. *Inorg. Chem.* **1983**, *22*, 1021–1025.

16. For examples of porphyrin protection, see: (a) Tsuchiya, S.; Seno, M. *Chem. Lett.* **1989**, 263-266. (b) Traylor, P. S.; Dolphin, D.; Traylor, T. G. *J. Chem. Soc., Chem. Commun.* **1984**, 279. (c) Groves, J. T.; Neuman, R. J. *J. Am. Chem. Soc.* **1987**, *109*, 5045. (d) Chang, C. K.; Kuo, M. S. *J. Am. Chem. Soc.* **1979**, *101*, 3413. (e) Hill, C. L.; Schardt, B. C. *J. Am. Chem. Soc.* **1980**, *102*, 6374. (f) Traylor, T. G.; Tsuchiya, S. *Inorg. Chem.* **1987**,

26, 1338. (g) Cook, B. R.; Reinart, T. J.; Suslick, K. S. *J. Am. Chem. Soc.* **1986**, *108*, 7281. (h) Chang, C. K.; Ebina, F. *J. Chem. Soc., Chem. Commun.* **1981**, 778.

17. (a) Krumpolc, M.; Deboer, B. G.; Roćek, J. *J. Am. Chem. Soc.* **1978**, *100*, 145–153. (b) Collins, T. J.; Ozaki, S.; Richmond, T. G. *J. Chem. Soc., Chem. Commun.* **1987**, 803–804. (c) Schanze, K. S. personal communication to T. J. Collins.

18. (a) Anson, F. C.; Collins, T. J.; Coots, R. J.; Gipson, S. L.; Keech, J. T.; Krafft, T. E.; Santarsiero, B. D.; Spies, G. H. *Inorg. Chem.* **1987**, *26*, 1161–1168. (b) Anson, F. C.; Collins, T. J.; Gipson, S. L.; Keech, J. T.; Krafft, T. E.; *Inorg. Chem.* **1987**, *26*, 731–736.

19. Ito, T.; Sugimoto, M.; Toriumi, K.; Ito, H. *Chem. Lett.* **1981**, 1477–1478. (b) Zeigerson, E.; Bar, I.; Bernstein, J.; Kirschenbaum, L. J.; Meyerstein, D. *Inorg. Chem.* **1982**, *21*, 73–80.

20. Keech, J. T. Ph.D. Thesis, California Institute of Technology, 1987.

21. Groves, J. T.; Quinn, R. *J. Am. Chem. Soc.* **1985**, *107*, 5790–5792.

22. (a) Chen, D.; Motekaitis, R. J.; Martell, A. E. *Inorg. Chem.* **1991**, *30*, 1396–1402. (b) Chen, D.; Martell, A. E. *J. Am. Chem. Soc.* **1990**, *112*, 9411–9412.

23. Brewer, J. C.; Lee, S. C. personal communications to E. S. Uffelman

24. Workman, J. M.; Gordon-Wylie, S. W. unpublished results.

25. Collins, T. J.; Santarsiero, B. D.; Spies, G. H. *J. Chem. Soc., Chem. Commun.* **1983**, 681.

26. Koola, J. D.; Kochi, J. K. *J. Org. Chem.* **1987**, *52*, 4545–4553.

27. (a) Eisenberg, R.; Dori, Z.; Gray, H. B.; Ibers, J. A. *Inorg. Chem.*

1968, *7*, 741. (b) Baker-Hawkes, M. J.; Billig, E.; Gray, H. B. *J. Am. Chem. Soc.* **1966**, *88*, 4870. (c) Dorfman, J. R.; Rao, Ch. P.; Holm, R. H. *Inorg. Chem.* **1985**, *24*, 453. (d) Fikar, R.; Koch, S. A.; Millar, M. M. *Inorg. Chem.* **1985**, *24*, 3311. (e) Rao, Ch. P.; Dorfman, J. R.; Holm, R. H. *Inorg. Chem.* **1986**, *25*, 428. (f) van der Put, P. J.; Schilperoord, A. A. *Inorg. Chem.* **1974**, *13*, 2476. (g) Bour, J. J.; Beurskins, P. T.; Steggerda, J. J. *J. Chem. Soc., Chem. Commun.* **1972**, 221. (h) Birker, P. J. M. W. L.; Bour, J. J.; Steggerda *Inorg. Chem.* **1973**, *12*, 1254. (i) Birker, P. J. M. W. L.; Beurskins, P. T. *J. R. Neth. Chem. Soc.* **1974**, *93* 218. (j) Brewer, J. C.; Collins, T. J.; Smith, M. R.; Santarsiero, B. D. *J. Am. Chem. Soc.* **1988**, *110*, 423–428. (k) Collins, T. J.; Richmond, T. G.; Santarsiero, B. D.; Treco, B. G. R. T. *J. Am. Chem. Soc.* **1986**, *108*, 2088–2090. References a–f concern aliphatic and aromatic thiolate ligands. References g–i concern biuret ligands.

28. Koola, J. D.; Kochi, J. K. *Inorg. Chim. Acta* **1987**, *133*, 119–127.

29. (a) Barnhart, D. M.; Lingafelter, E. C. *Cryst. Struct. Comm.* **1982**, *11*, 733–739. Christopher J. Willis' group has published more than a dozen papers on this and related ligand systems. See for example (b) Willis, C. J. *J. Chem. Soc., Chem. Commun.* **1972**, 944–945. (c) Loeb, S. J.; Martin, J. W. L.; Willis, C. J. *Can. J. Chem.* **1978**, *56*, 2369–2373. (d) Boeré, R. T.; Willis, C. J. *Inorg. Chem.* **1985**, *24*, 1059–1065.

30. Avdeef, A.; Schaefer, W. P. *J. Am. Chem. Soc.* **1976**, *98*, 5153–5159.

31. Wiberg, K. B.; Laidig, K. E. *J. Am. Chem. Soc.* **1987**, *109*, 5935–5943.

32. Stewart, W. E.; Siddall, T. H., III *Chem. Rev.* **1970**, *70*, 517–551.

33. The *trans*, *cis*-α, and *cis*-β nomenclature was coined by Sargeson

to describe the three possible isomers for octahedral complexes of cobalt(III) with triethylaminetetraamine ($[Co(trien)X_2]^+$). This nomenclature has since been generally applied to octahedral complexes of many tetradentate ligands. (a) Sargeson, A. M.; Searle, G. H. *Nature* **1963**, *200*, 356–357. (b) Sargeson, A. M.; Searle, G. H. *Inorg. Chem.* **1965**, *4*, 45–52.

34. (a) Collins, T. J.; Coots, R. J.; Furutani, T. T.; Keech, J. T.; Peake, G. T.; Santarsiero, B. D. *J. Am. Chem. Soc.* **1986**, *108*, 5333–5339. (b) Anson, F. C.; Collins, T. J.; Gipson, S. L.; Keech, J. T.; Krafft, T. E.; Peake, G. T. *J. Am. Chem. Soc.*, **1986**, *108*, 6593–6605. (c) Collins, T. J.; Lai, T.; Peake, G. T. *Inorg. Chem.* **1987**, *26*, 1674–1677. (d) Collins, T. J.; Lee, S. C.; Keech, J. T. *J. Am. Chem. Soc. 110*, **1988**, 1162–1167. (e) Collins T. J.; Workman, J. M. *Angew. Chem. Int. Edn. Engl.* **1989**, *28*, 912–914. (f) Collins, T. J.; Uffelman, E. S. *Angew. Chem. Int. Ed. Engl.* **1989**, *28*, 1509–1511. (g) Collins, T. J.; Powell, R. D.; Slebodnick, C.; Uffelman, E. S. *J. Am. Chem. Soc.* **1990**, *112*, 899–901. (h) Collins, T. J.; Kostka, K. L.; Münck, E.; Uffelman, E. S. *J. Am. Chem. Soc.* **1990**, *112*, 5637–5639. (i) Collins, T. J.; Slebodnick, C.; Uffelman, E. S. *Inorg. Chem.* **1990**, *29*, 3432–3436. (j) Collins, T. J.; Nichols, T. R.; Uffelman, E. S. *J. Am. Chem. Soc.* **1991**, *113*, 4708–4709. (k) Collins, T. J.; Kostka, K. L.; Uffelman, E. S. *Inorg. Chem.* in press.

35. Pierpont, C. G.; Buchanan, R. M. *Coord. Chem. Rev.* **1981**, *38*, 45–87.

36. (a) *Cytochrome P-450; Structure, Mechanism, and Biochemistry*; Ortiz de Montellano, P. R., Ed.; Plenum: New York, 1986. (b) *Activation and Functionalization of Alkanes*, Hill, C. L., Ed; Wiley Interscience: New York,

1989. (c) Dawson, J. H.; Sono, M. *Chem. Rev.* **1987**, *87*, 1255–1276.

37. Jefcoate, C. B. In *Cytochrome P-450; Structure, Mechanism, and Biochemistry*; Ortiz de Montellano, P. R., Ed.; Plenum: New York, 1986; pp 387–428.

38. (a) Margerum, D. W.; Rybka, J. S. *Inorg. Chem.* **1980**, *19*, 2784-2790. (b) Rybka, J. S.; Margerum, D. W. *Inorg. Chem.* **1981**, *20*, 1453-1458.

39. Kimura, E. *J. Coord. Chem.* **1986**, *15*, 1–28.

Chapter 2

Synthetic Methodologies for Macrocyclic Tetraamido-*N* Ligands and their Low Valent Complexes

The classic objective in macrocycle synthesis is to enhance the desired intramolecular ring-forming reaction at the expense of competing intermolecular reactions (Figure 2.1). This objective is usually achieved by employing one or more of the following principles:[1]

(i) template effects,

(ii) rigid group effects,

(iii) high dilution effects.

In this chapter, the ligand syntheses will be discussed, along with the reasoning behind the methodology employed. These discussions will be organized around the effects listed above. It will be shown that, contrary to the usual problem of controlling undesired *inter*molecular reactions, the more demanding challenge in preparing the macrocycles of this thesis involves controlling undesired *intra*molecular reactions (Figure 2.2). The chapter will conclude with a discussion of the methods required to metallate the ligands.

Template effect

The template effect is well documented in macrocyclic chemistry and has many manifestations.[1] Reactions may be templated by alkalai metal/alkaline earth ions,[2] transition metal ions, hydrogen-bonds, and organic donor-acceptor interactions.[3] Only the transition metal and hydrogen-bond templates will be discussed here.

Transition metal templates may be classified according to whether or not any of the ligated atoms participate in the bond-forming reactions. Lindoy has summarized both types of reactions without this distinction,[1h] and Table 2.1 has been constructed from his summary, but has been reorganized to emphasize the two template types. In the work of this thesis, macrocycles are

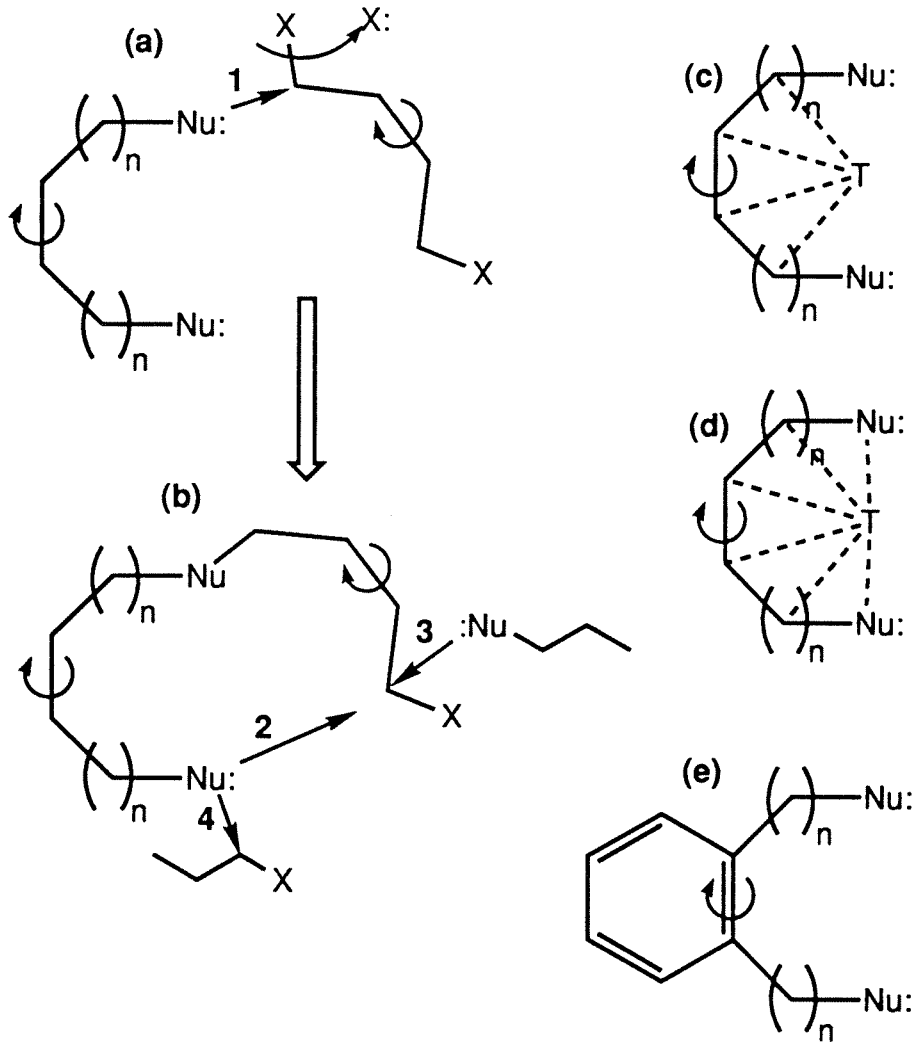

Figure 2.1. The classic macrocycle synthesis problem. In (a) the reactivity and concentration of the nucleophilic fragment (Nu:) with the electrophilic fragment (X) must be arranged so that the intermolecular reaction, **1**, occurs at a reasonable rate. In (b), the desired reaction is the intramolecular reaction, **2**, but the rotation arrows indicate that unprofitable rotational degrees of freedom in the intermediate will enable other intermolecular reactions (**3, 4**) to minimize the macrocyclic yield. In (c), a template eliminates many degrees of rotational freedom. Template (d) is similar to (c), except that the template may also bind the nucleophilic group. In (e), rigid groups prevent rotation from occurring. A reaction run at high dilution allows reaction **2** to compete with reactions **3** and **4**, but also unfortunately slows reaction **1** too.

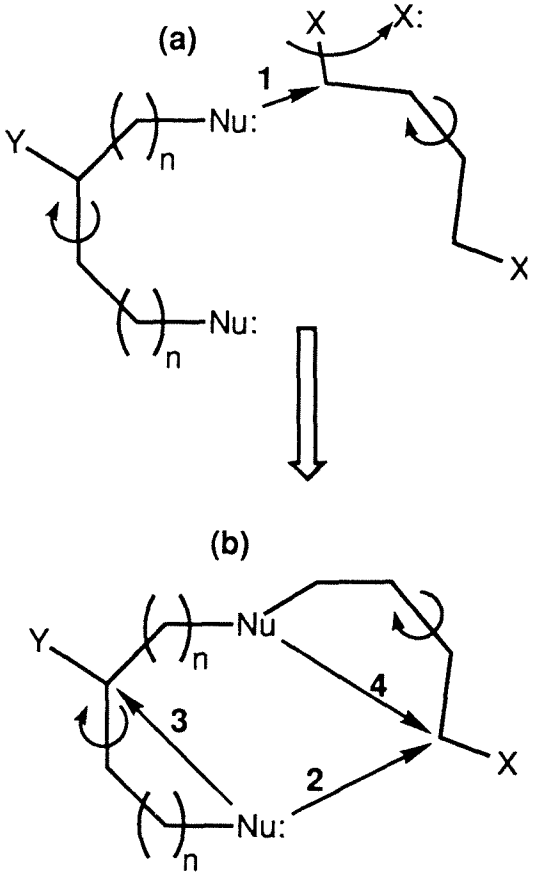

Figure 2.2. The predominant synthetic problems affecting the macrocycles in this thesis involve intramolecular side reactions. In (a), the intermolecular reaction **1** leads to the intermediate (b). In (b), intramolecular reaction **2** is desired for all systems, but the possible intramolecular side reactions vary according to the ligand being synthesized. For H_4MAC*, reaction **3** involves the primary amine attacking the backbone ketone to form an imine, and reaction **4** involves reaction of the secondary amide with the acyl chloride to form an imide. For H_4DEMAMPA-DXB systems, reaction **3** can not occur, but imide formation, **4**, can still transpire. Since the significant side reactions are intramolecular, the high dilution effect can not be utilized.

prepared by amide-forming reactions. It is significant to note that no metal templated macrocyclizations involving amide formation have been discussed in the literature where a coordinated amine has been acylated. Until Raymond's group published their iron carcerand synthesis (Figure 2.3),[4] there was also no example of a templated macrocycle-forming amide synthesis with an uncoordinated amine. It is not clear if this gap in the literature arose from the historical development of the field or from inherent chemical problems associated with acylating a coordinated amine. It should be noted that some ligands can not be synthesized in the absence of a metal template and, once formed, can not be isolated after demetallation. Busch's TAAB ligand is a classic example (Figure 2.4).[5]

Table 2.1. Transition metal template reactions.

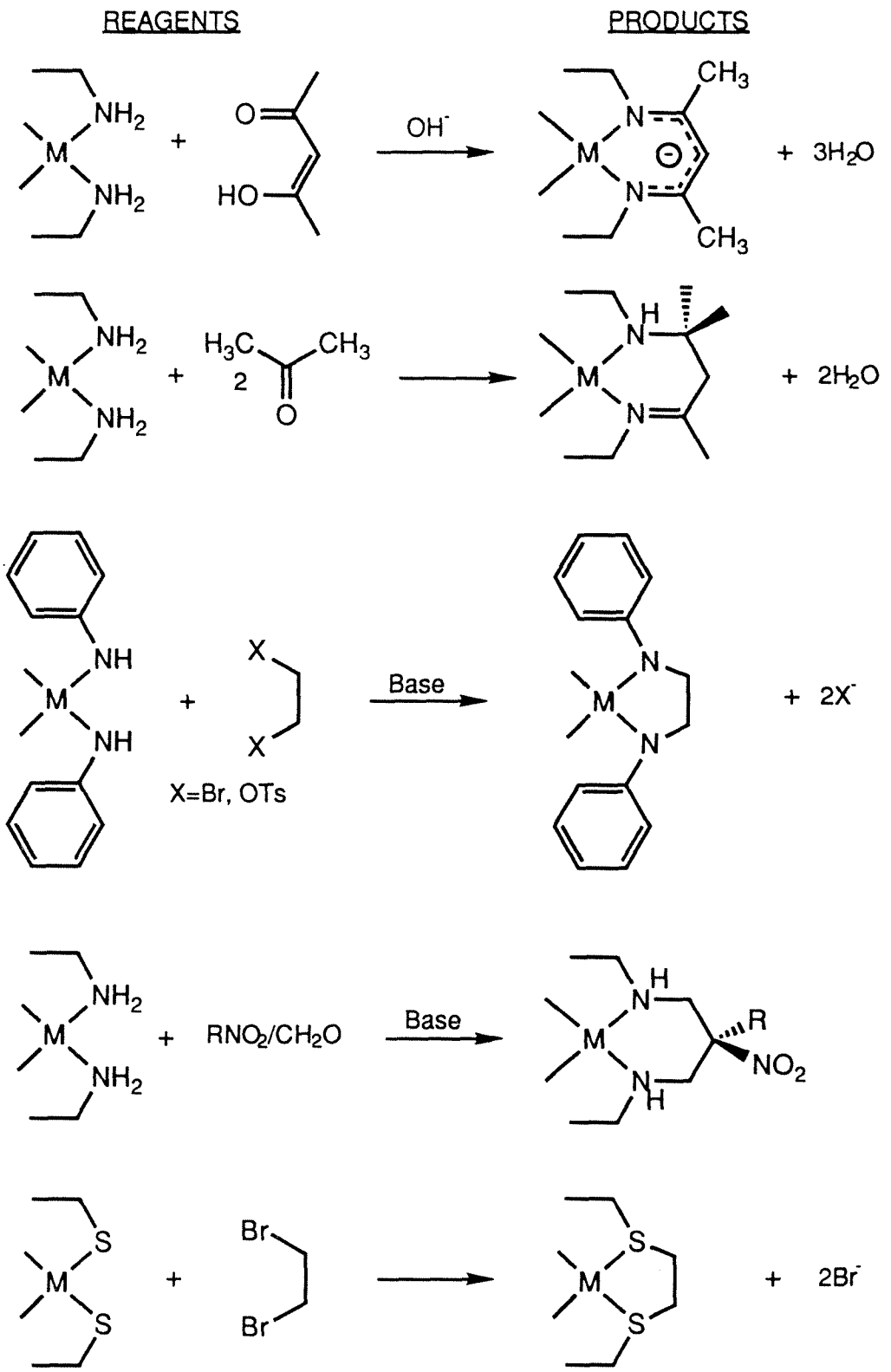

Table 2.1. Transition metal template reactions (continued).

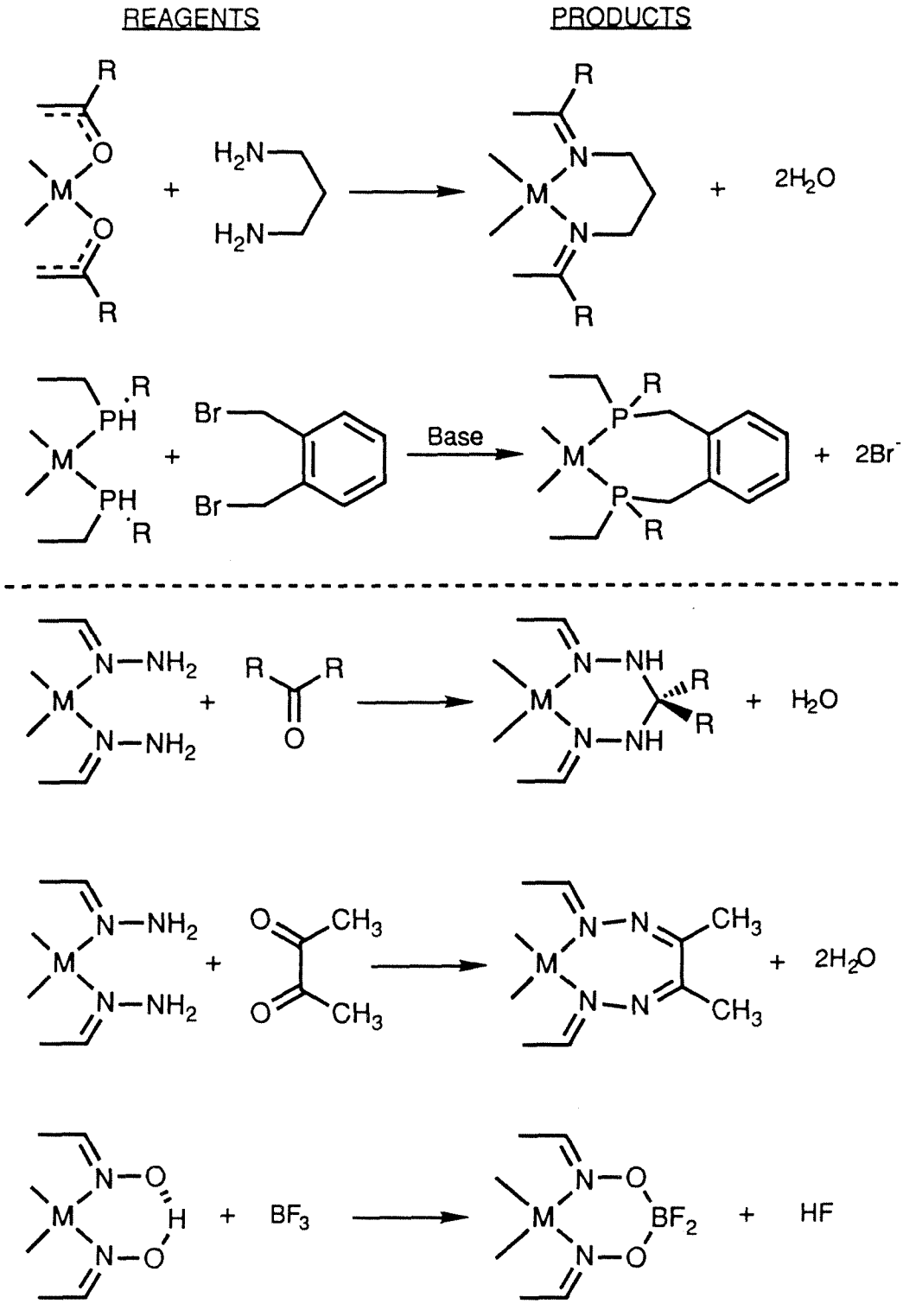

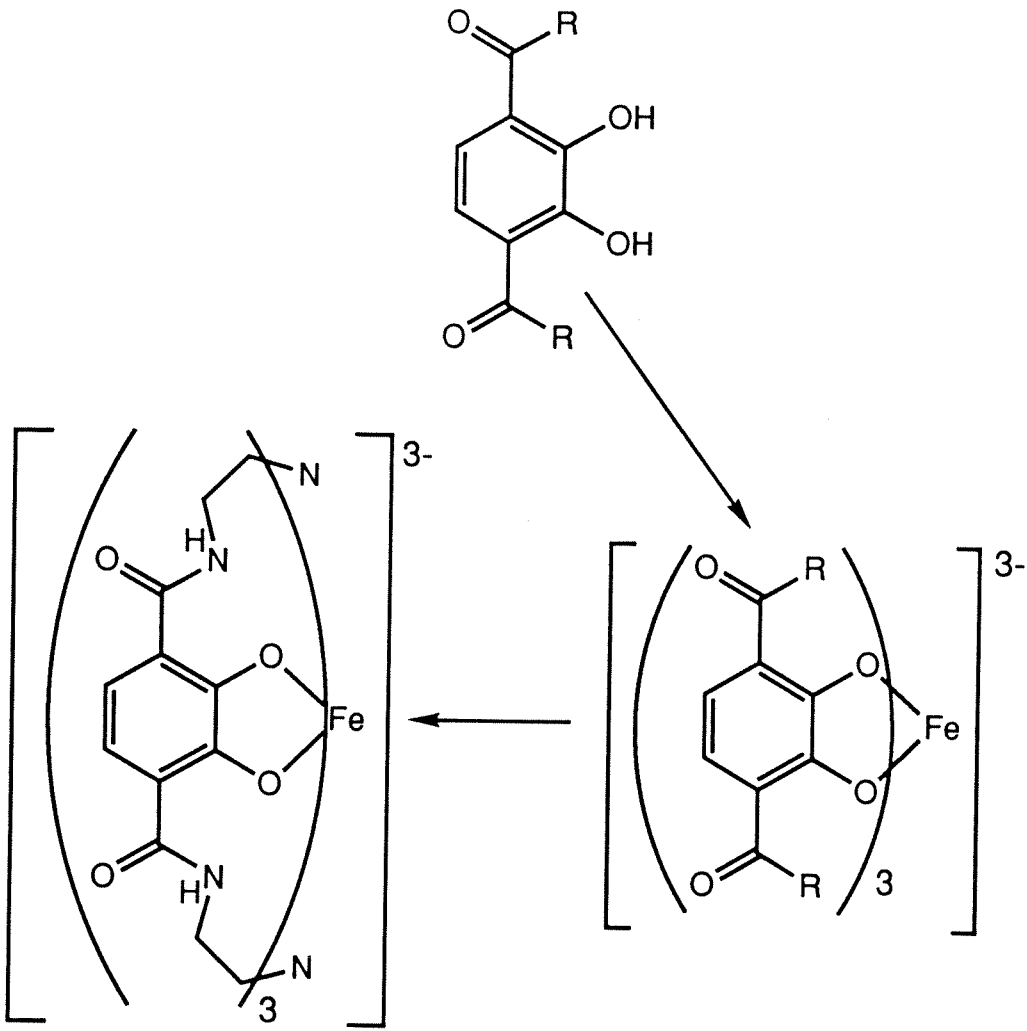

Figure 2.3. Metal templated iron carcerand synthesis.

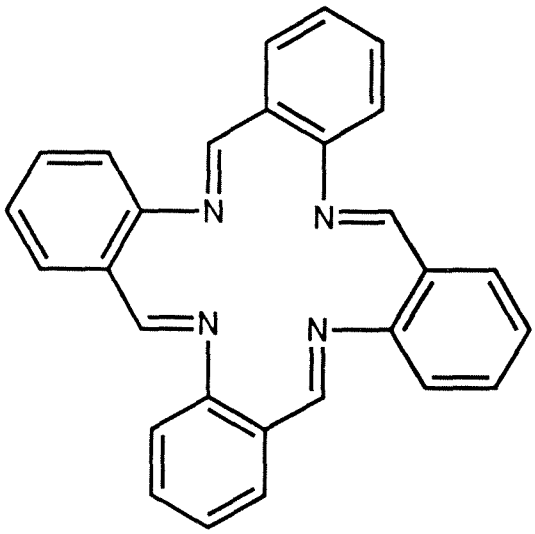

Figure 2.4. Busch's TAAB ligand. The molecule may only be synthesized by condensing *o*-aminobenzaldehyde in the presence of a transition metal. The molecule may not be isolated in the absence of a coordinated metal cation.

Macrocyclizations templated by intramolecular hydrogen-bonds are much less documented, but have been noted (Figures 2.5 and 2.6).[6] The most pertinent example for this discussion is an intramolecular hydrogen-bond template claimed by Kemp and Vellaccio in the one pot reaction of 1,3-diaminodimethylpropane with dimethylmalonyldichloride to form the 16-membered ring (Figure 2.7).[7] They claimed that formation of the eight-membered ring was sterically blocked, and that analysis of molecular models indicated that the macrocycle was templated by a 10-membered ring hydrogen-bond related to the β-turn of polypeptide chemistry (Figure 2.7). The relatively high yield of macrocycle they obtained (28%) under non-high dilution conditions supported this claim.

Rigid group effects

Rigid group effects are also well documented in macrocyclic literature.[1g] Every bond in the acyclic precursor which is locked into the conformation of the

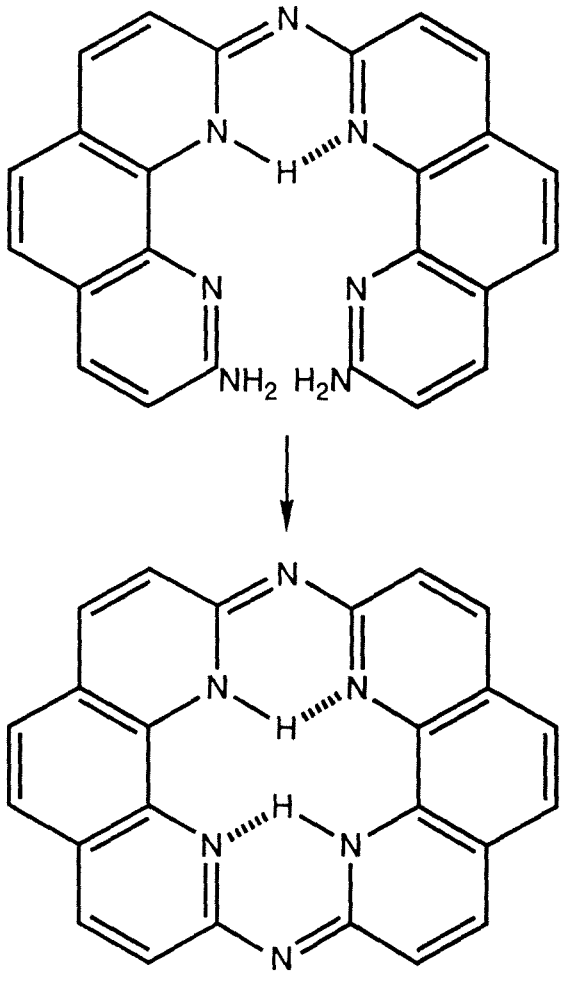

Figure 2.5. Ogawa's intramolecular hydrogen-bond template.

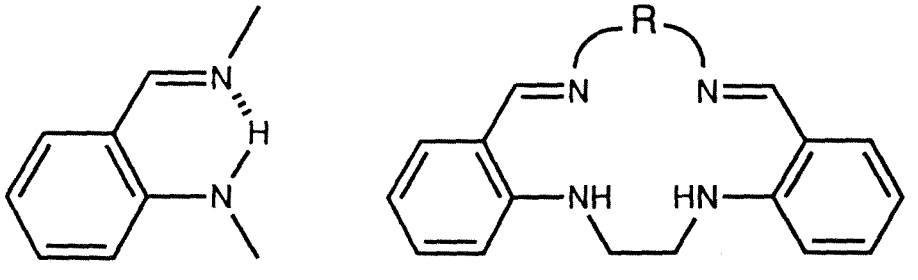

Figure 2.6. Owston, et al.'s intramolecular hydrogen-bond template.

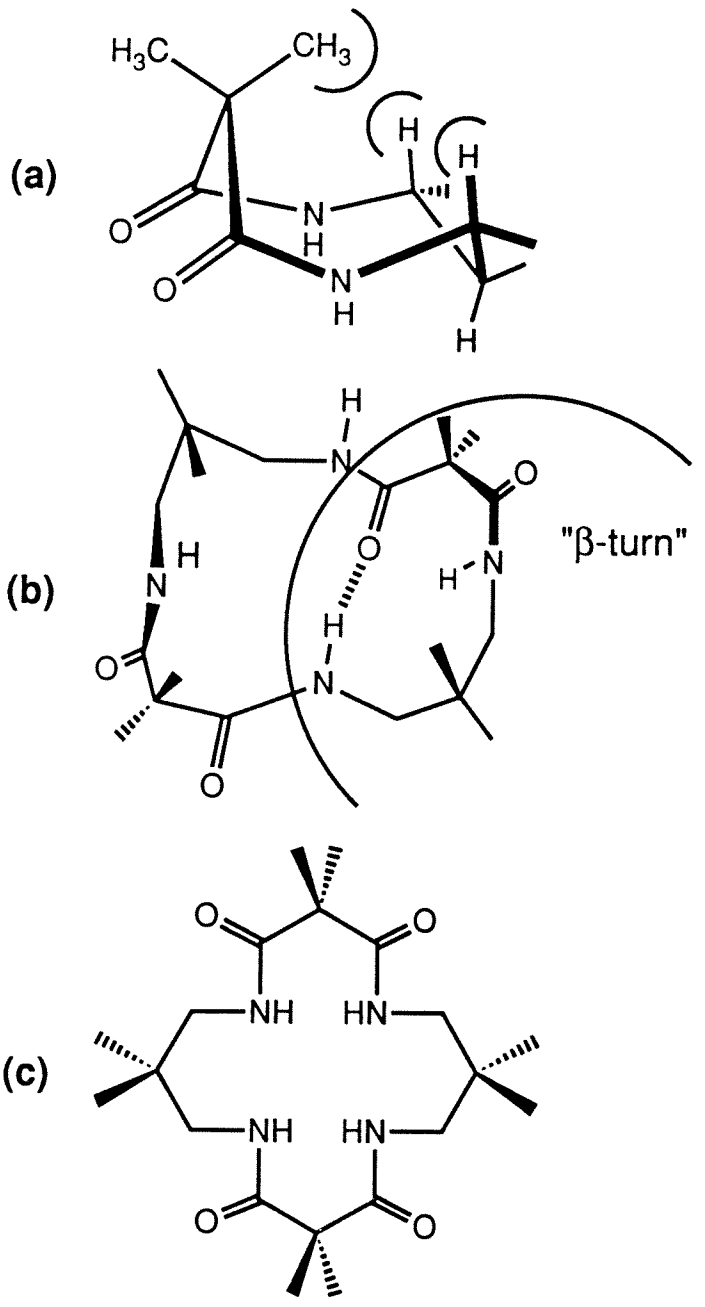

Figure 2.7. The macrocyclic tetraamide (b = c) synthesized by Vellacio, Punzar, and Kemp. The authors claimed that steric interactions prevented the eight-membered ring (a) from forming. Representation "b" is the actual structure they proposed for the macrocycle, based on inspection of models. The hydrogen-bond they postulated is indicated, and its relationship to the β-turn is indicated.

final product will help increase the yield of macrocycle by eliminating unprofitable degrees of rotational freedom in the precursor. This has been elegantly demonstrated by Stoddart, et al.[3] Thus, *o*-disubstituted aromatic rings, *cis*-double bonds, fused ring systems, etc. incorporated into the acyclic precursor will diminish the proportion of polymer to macrocycle. In the macrocyclic tetraamides of this thesis, two critical points should be noted. First, the *trans*-conformation of amides is favored, for steric reasons, over the *cis*-conformation. The *trans*-conformation favors macrocyclization, since all of the amides in the free ligands (and their complexes) are *trans* amides. Second, the amide rotation barrier is approximately 20 kCal/mol. In effect, the amide can behave like a rigid group.

High dilution effects

High dilution effects have received considerable attention in the literature of macrocyclic synthesis.[1] The simple idea behind the high dilution principle is that once the acyclic precursor to the macrocycle has formed, dilute conditions will favor intramolecular cyclization over intermolecular polymerization. Because polymer formation is not the primary problem in the syntheses to be described, high dilution effects will not be discussed further.

Macrocycle syntheses

The retrosynthetic analyses and syntheses of the ligand systems may now be considered. Capitalizing on the C_{2v} symmetry of the molecules should lower the number of steps in the syntheses, and since acylation of amines is synthetically easier than primary amide *N*-alkylation or carbon-carbon bond formation, there are two retrosynthetic cuts more promising than the others (Figures 2.8 and 2.9). There are potential advantages to breaking the molecules

in either fashion. Since it was felt, however, that a transition metal template in the macrocyclization seemed more feasible with the diamide diamines rather than the diamide dicarboxylates (Figures 2.10 and 2.11), and since it was felt such a template reaction might be critical to the success of the final step, these retrosynthetic pathways will be discussed. Since Aldrich sells the acid chloride of diethylmalonic acid rather than dimethylmalonic acid, it was chosen for the final acylating agent.

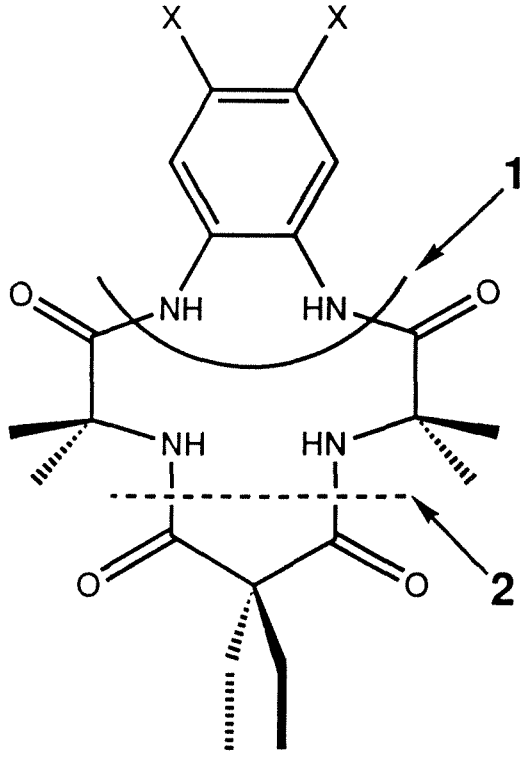

Figure 2.8. The two straightforward options for making the first retrosynthetic "cut" in the H_4DEMAMPA-DXB macrocycles.

Synthesis of the diamide diamines could have been achieved by acylating phenylenediamine or DMP with an aminoisobutyric acid derivative. However, these reactions were ineffective. Because the Collins group had experience reducing azides to amines in the synthesis of one of their acyclic ligands,[8]

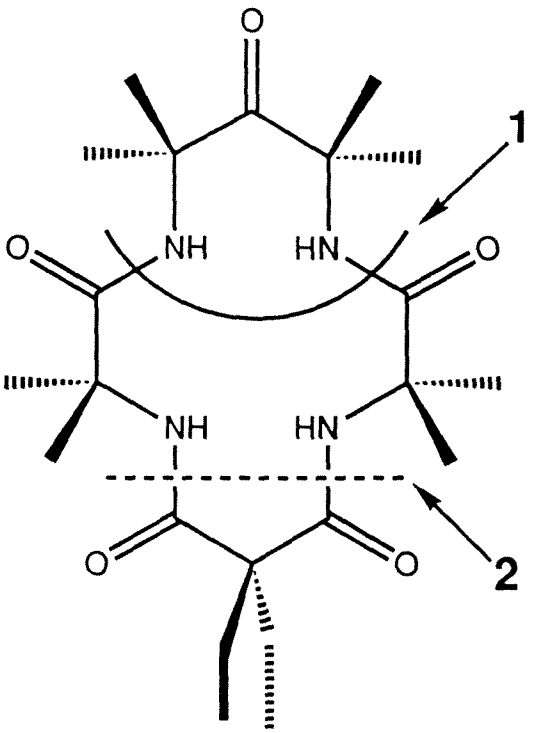

Figure 2.9. The two straightforward options for making the first retrosynthetic "cut" in H_4MAC*.

the diamide diamines could be prepared by reduction of the diamide diazide. Experience had earlier shown that nucleophilic displacement of bromide from a tertiary alkyl bromide by azide was a highly successful reaction. Thus all that remained was to find a route to the diamide dibromides, and this may be done by acylation with 2-bromoisobutyryl bromide (which may be purchased from Aldrich). The actual syntheses proceed along these paths.

The syntheses of the H_4DEMAMPA-DXB macrocycles are depicted in Scheme 2.1. The 2-bromoisobutyryl bromide is, as expected, considerably more reactive than the acid chlorides used in previous Collins group syntheses, and this enhanced reactivity conveys a special advantage. In the synthesis of CHBA-DCB, a major byproduct (and sometimes the major product) was the benzimidazole (Figure 2.12).[9] The synthetic problem was that the diamine was

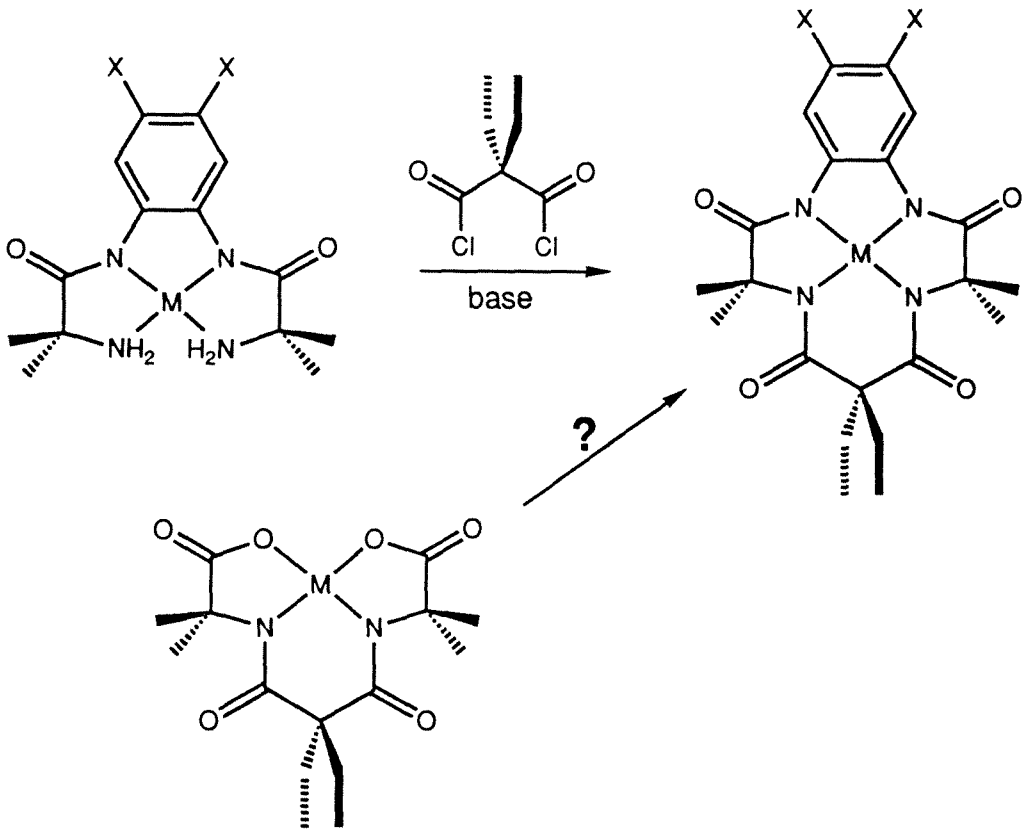

Figure 2.10. Feasible and dubious template molecules for synthesizing the H_4DEMAMPA-DXB macrocycles.

a weak nucleophile. Thus, cooling the reaction in an ice bath to suppress the intramolecular benzimidazole condensation also suppressed the necessary second intermolecular acylation. However, 2-bromoisobutyryl bromide is so reactive that the second intermolecular acylation occurs rapidly at 0 °C. With highly pure phenylenediamines the acylation is nearly quantitative. The displacement of bromide by azide occurs straightforwardly due to azide's low basicity and excellent nucleophilicity. Although the organic diazide has been tested for shock and thermal instability, it is regarded cautiously,[10] and only small quantities (less than 20 mg) have been isolated. The azide reduction may be

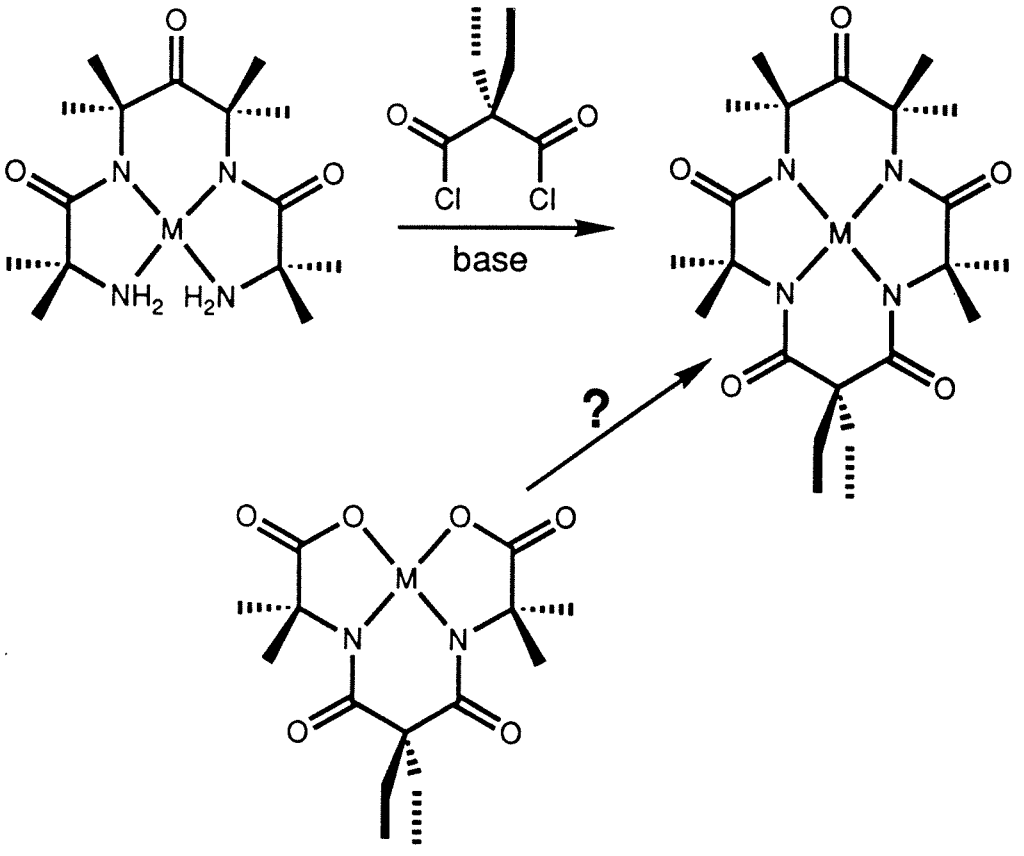

Figure 2.11. Feasible and dubious template molecules for synthesizing H_4MAC*.

accomplished with 10% Pd/C and H_2, or with $(NH_4)_2S$ for the dichloro derivative (Pd/C and H_2 can hydrogenolize aromatic chloro groups[11]). The resultant diamide diamine may be cyclized with diethylmalonyl dichloride. Even though the reaction is not run at high dilution, polymer formation is inconsequential; the major byproducts are the mono and diimides. The 25% yield for the last step is excellent for non-dilute conditions, seeming to imply the existence of either rigid group effects or intramolecular hydrogen-bond templating, or both. The macrocycles are readily isolated in pure form by recrystallization, and their variable temperature NMR's indicate the presence of at least two differ-

ent slowly interconverted conformers on the NMR timescale. One is tempted to speculate that the broadening in the room temperature NMR spectrum in $CDCl_3$ is caused by some sort of intramolecular hydrogen-bonding, as seen in the structure of H_4MAC^* (vide infra). Room temperature NMR spectra of the *complexed* ligand (i.e., lacking the possibility to hydrogen-bond) in $CDCl_3$ reveal sharp quartets (see Chapters 4, 6, 7, and 8).

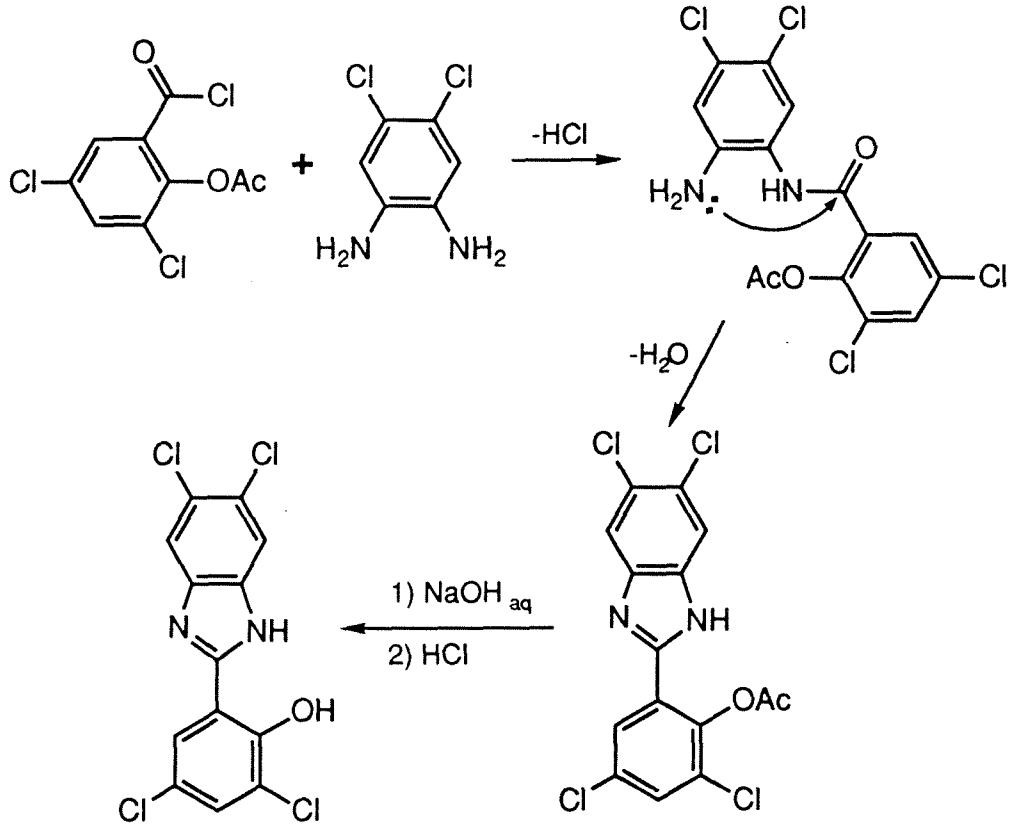

Figure 2.12. Mechanism of imidazole formation.

The synthesis of H_4MAC^* is simple until the reduction of the diamide diazide (Scheme 2.2). The dimethylpentanone may be dibrominated in high yield to give the dibromide. Conversion to the diazide (which is never isolated in quantities greater than 20 mg) and reduction yields the diamine.[8] Although

Scheme 2.1. Synthesis of the H_4DEMAMPA-DXB macrocycles. Ligands with X=Cl, H, Me, and OMe have been prepared. When X=Cl, $(NH_4)_2S$ was used as the reductant; $(NH_4)_2S$ or $H_2/Pd/C$ may be used as the reductant for the other derivatives.

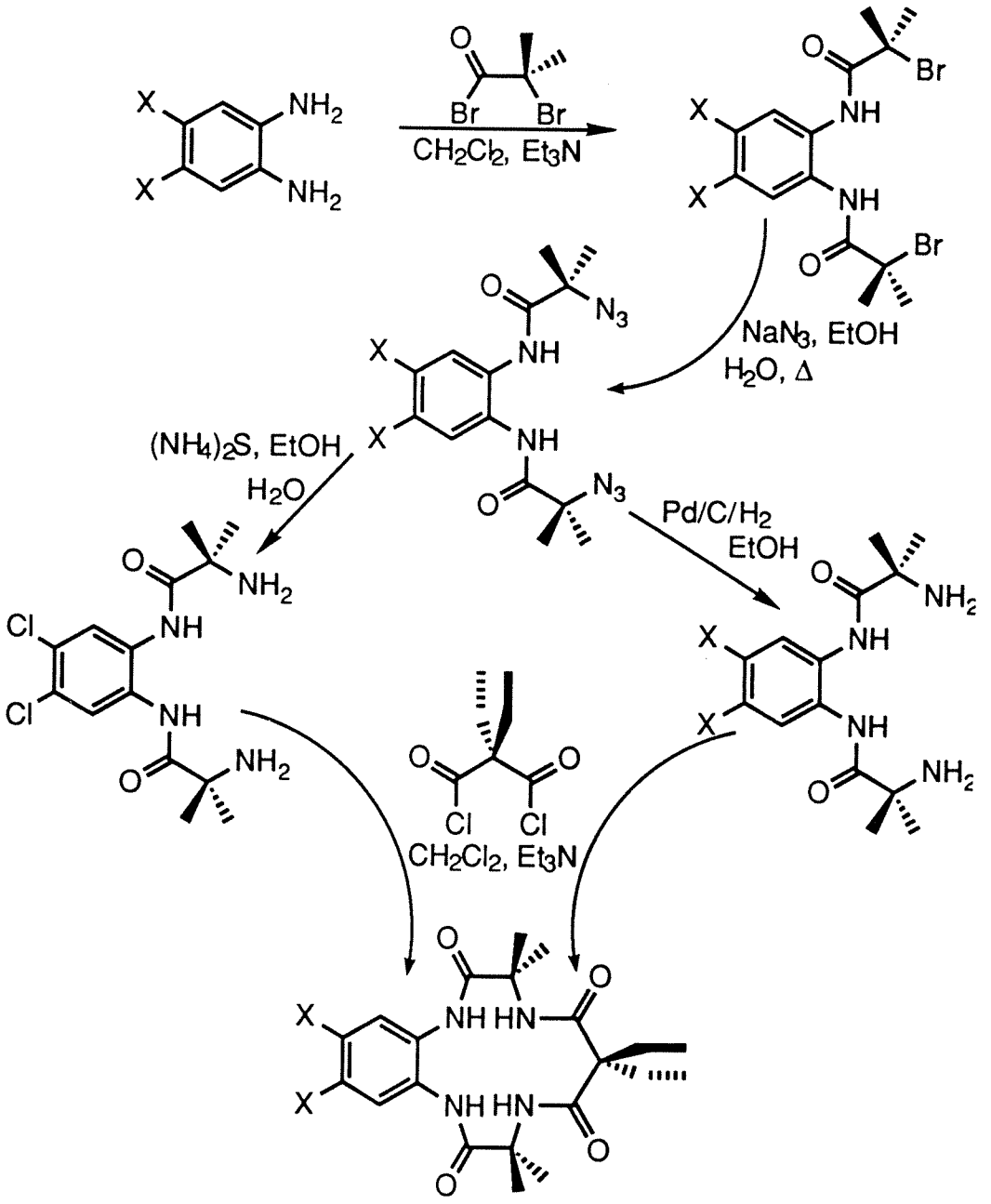

this diamine may be produced in large quantities, it must be stored as its hydrohalide salt. Acylation of the diamine with 2-bromoisobutyryl bromide proceeds nearly quantitatively to give the diamide dibromide, which may be readily converted to the diamide diazide (which is again handled cautiously). Reduction of the diazide with $(NH_4)_2S$, or catalytic hydrogenolysis with neutral ethanolic Pd/C, acidic ethanolic Pd/C, or basic ethanolic Pd/C yields not the diamide diamine, but the Schiff base (Scheme 2.3).

Scheme 2.2. Synthesis of the H_4MAC* diamide diazide.

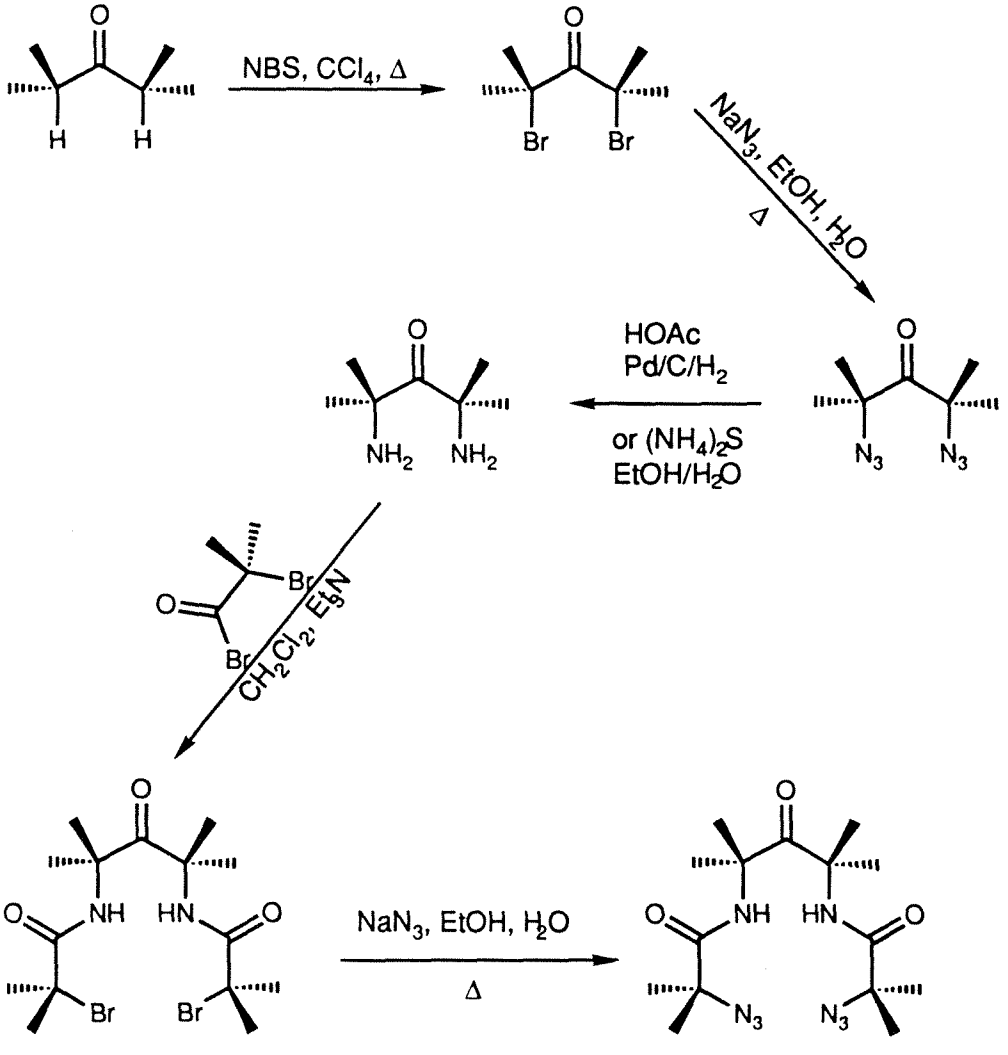

Scheme 2.3. Schiff base and H_4MAC^* synthesis.

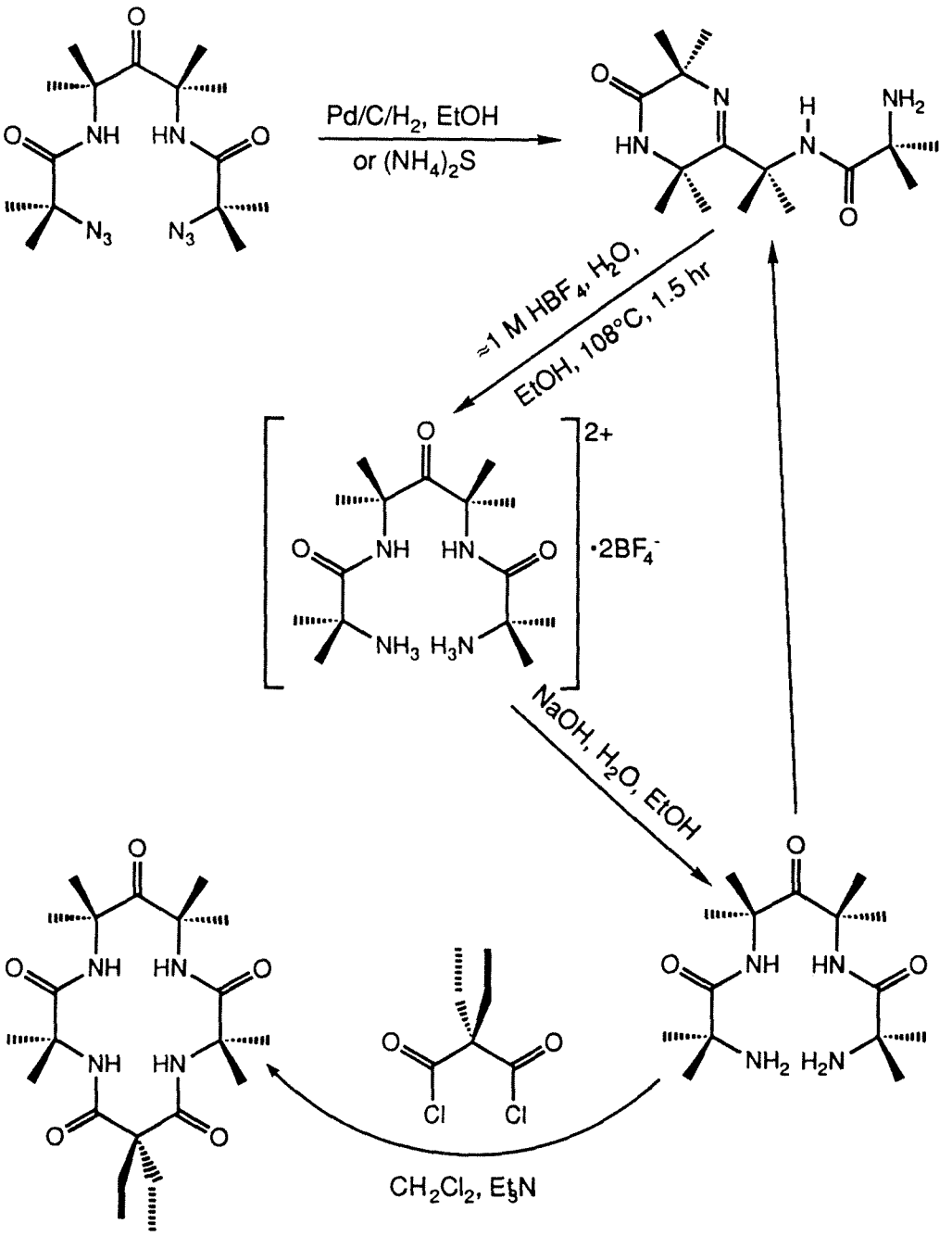

The Schiff base formation was a surprise. Based on a knowledge of general aliphatic imine behavior, an appreciation for the steric bulk of the hindered ketone (which does not react with 2,4-dinitrophenylhydrazine to give dinitro-

phenylhydrazone derivatives) and the hindered amine, and the knowledge that the six-membered ring formed had to contain a *cis*-amide rather than the more usual *trans*-amide, Schiff base formation was considered unlikely. Even if the Schiff base did form, it was thought it would readily hydrolize, since most aliphatic non-conjugated imines must be synthesized with a Dean-Stark trap to azeotropically remove water and drive the equilibrium to imine formation. However, the Schiff base forms, and it is unusually difficult to re-open. The best method to date of opening the Schiff base is to heat it at 104–108 °C in a bomb in an aqueous ethanolic solution of HBF_4 (pH = 1) for three hours. Fortunately, no amide hydrolysis is observed under these conditions. Once opened, the system will not recyclize in aqueous acid. However, with the free base, the amine/imine equilibrium favors the imine such that cyclization of the diamine, AMPA-DMP, proceeds to completion. AMPA-DMP has an approximate half-life of 12 hours in CH_2Cl_2, and the base used to produce AMPA-DMP prior to macrocyclization is important. When an aqueous solution of AMPA-DMP·2HBF_4 is neutralized with $[Me_4N][OH]$, the Schiff base is obtained quantitatively upon workup. However, aqueous NaOH yields exclusively the diamine, AMPA-DMP. Both the Schiff base and AMPA-DMP have high solubility in water and CH_2Cl_2. Thus, extraction of the free base from dilute aqueous solutions with CH_2Cl_2 is ineffective. If the neutral aqueous solution is pumped to dryness and CH_2Cl_2 is added, the yield of extracted AMPA-DMP is low (AMPA-DMP probably binds sodium). If the aqueous solution is pumped to a low volume and then extracted with CH_2Cl_2, AMPA-DMP can be obtained in quantitative yield. Small amounts of water probably prevent AMPA-DMP from binding sodium tightly.

In the hope of preparing H_4MAC* via a template reaction on copper, AMPA-DMP was reacted with copper acetate in ethanolic NaOH. The resultant blue solid was reacted with diethylmalonyl dichloride and this blue product was structurally characterized (Figure 2.13). The complex is square planar, with the Schiff base acting as a tridentate ligand, binding through the imine nitrogen, a deprotonated amide, and the remaining primary amine. The largest deviation from the mean plane defined by the copper atom, the coordinated nitrogen atoms, and the chlorine atom is 0.09 Å for the copper atom. As expected from its high σ-donor capacity, the shortest bond to copper is made by the deprotonated amide (1.884(4) Å), followed by the bond to the amine (2.012(4) Å), the bond to the imine (2.049(4) Å), and the bond to chloride (2.236(2) Å). The average amide C-N bond length (1.33 Å) is longer than the imine C-N bond (1.286(6) Å). The copper complex has no nonplanar amides (see Chapter 9).

Once the diamide diamine is obtained, synthesis of the macrocycle is trivial. Addition of diethylmalonyl dichloride to the diamide diamine followed by extraction of the CH_2Cl_2 with aqueous acid and base yields a solution which is taken to dryness. This solid, when dissolved in a minimum of CH_2Cl_2 and treated with warm CCl_4, gives, upon further evaporation and cooling, the product in 32% yield as floating white crystals. It is likely that the majority of side products contain 4-membered ring imides, based on results from the H_4DEMAMPA-DXB systems.

The crystal structure of H_4MAC* is shown in Figure 2.14. The amide C-O bonds are indistinguishable at the 3σ confidence level (average 1.22 Å). At the 3σ confidence level, the C-O bond of the ketone is the same length as the

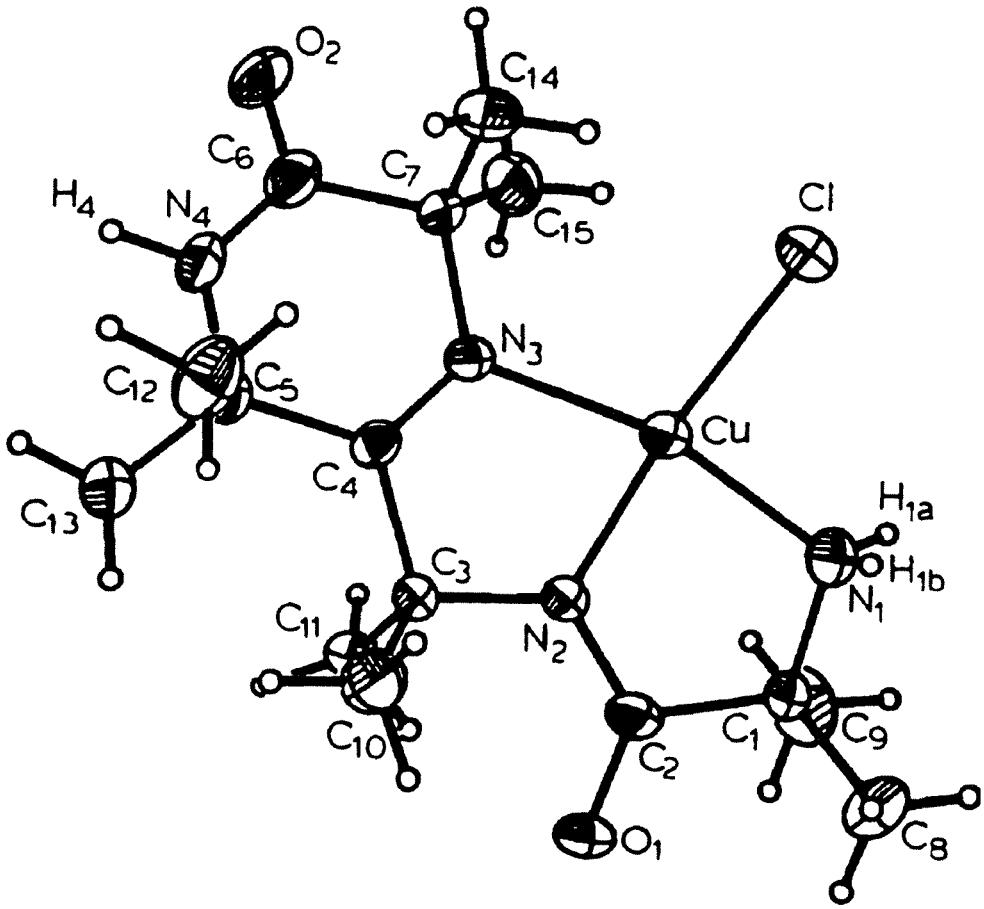

Figure 2.13. ORTEP of the Cu(II) complex of the Schiff base, CuCl(η^3-Imine).

Table 2.2. Bond Lengths in CuCl(η^3-Imine)			
Atoms	Length (Å)	Atoms	Length (Å)
CuCl	2.236(2)	CuN1	2.012(4)
CuN2	1.884(4)	CuN3	2.049(4)
O1C2	1.248(6)	O2C6	1.227(6)
N1C1	1.484(6)	N2C3	1.467(6)
N3C7	1.489(5)	N4C5	1.458(6)
N2C2	1.340(6)	N3C4	1.286(6)

Table 2.2. Bond Lengths in CuCl(η^3-Imine) (continued)			
Atoms	Length (Å)	Atoms	Length (Å)
N4C6	1.324(6)	N1H1a	0.72(4)
N1H1b	0.97(5)	N4H4	0.89(5)
C1C2	1.530(6)	C3C4	1.550(6)
C4C5	1.532(6)	C6C7	1.531(7)
C1C8	1.519(8)	C1C9	1.514(9)
C3C10	1.531(7)	C3C11	1.545(7)
C5C12	1.523(7)	C5C13	1.522(7)
C7C14	1.529(8)	C7C15	1.525(8)

Table 2.3. Bond Angles in CuCl(η^3-Imine)			
Atoms	Angle (°)	Atoms	Angle (°)
ClCuN1	89.6(1)	ClCuN2	168.4(1)
ClCuN3	105.6(1)	N1CuN2	83.3(2)
N1CuN3	164.1(1)	N2CuN3	81.0(1)
CuN1C1	109.3(3)	CuN2C2	118.4(3)
CuN2C3	120.0(3)	CuN3C4	114.2(3)
CuN3C7	122.4(3)	CuN1H1a	114(3)
CuN1H1b	108(3)	C4N3C7	123.0(4)
C5N4C6	127.8(4)	N1C1C2	108.7(3)
N1C1C8	109.7(5)	N1C1C9	109.0(4)
C2C1C8	110.3(4)	C2C1C9	108.4(5)
C8C1C9	110.6(5)	N2C3C4	105.7(3)

Table 2.3. Bond Angles in CuCl(η^3-Imine) (continued)			
Atoms	Angle (°)	Atoms	Angle (°)
N2C3C10	108.5(4)	N2C3C11	109.6(4)
C4C3C10	112.9(4)	C4C3C11	107.0(4)
C10C3C11	113.0(4)	C4C5N4	109.9(4)
C4C5C12	108.1(4)	C4C5C13	116.7(4)
N4C5C12	108.6(4)	N4C5C13	104.4(4)
C12C5C13	108.9(4)	C6C7N3	113.6(4)
C1C2O1	118.1(4)	N2C2O1	127.5(4)
C1C2N2	114.3(4)	N3C4C3	117.1(4)
N3C4C5	121.8(4)	C3C4C5	121.1(4)
N4C6O2	123.0(5)	C7C6O2	120.4(4)
N4C6C7	116.5(4)	C1N1H1a	113(3)
H1aN1H1b	105(5)	C1N1H1b	106(3)
C5N4H4	119(3)	C6N4H4	113(3)
C6C7C14	106.1(4)	C6C7C15	108.0(4)
N3C7C14	110.1(4)	N3C7C15	107.1(4)
C14C7C15	112.2(4)		

amide C-O bonds (1.21 Å). The amide C-N bonds are also indistinguishable at the 3σ confidence level (average 1.34 Å). The molecule has a nonplanar amide (see Chapter 9).

The directing effects of hydrogen-bonding in the solid state and the solution state have long been a subject of interest and have recently come under considerable study.[12,13] CuCl(η^3-Imine) has three potential hydrogen donors, H_{1a}, H_{1b}, and H_4, and all three are involved in intermolecular hydrogen-bond-

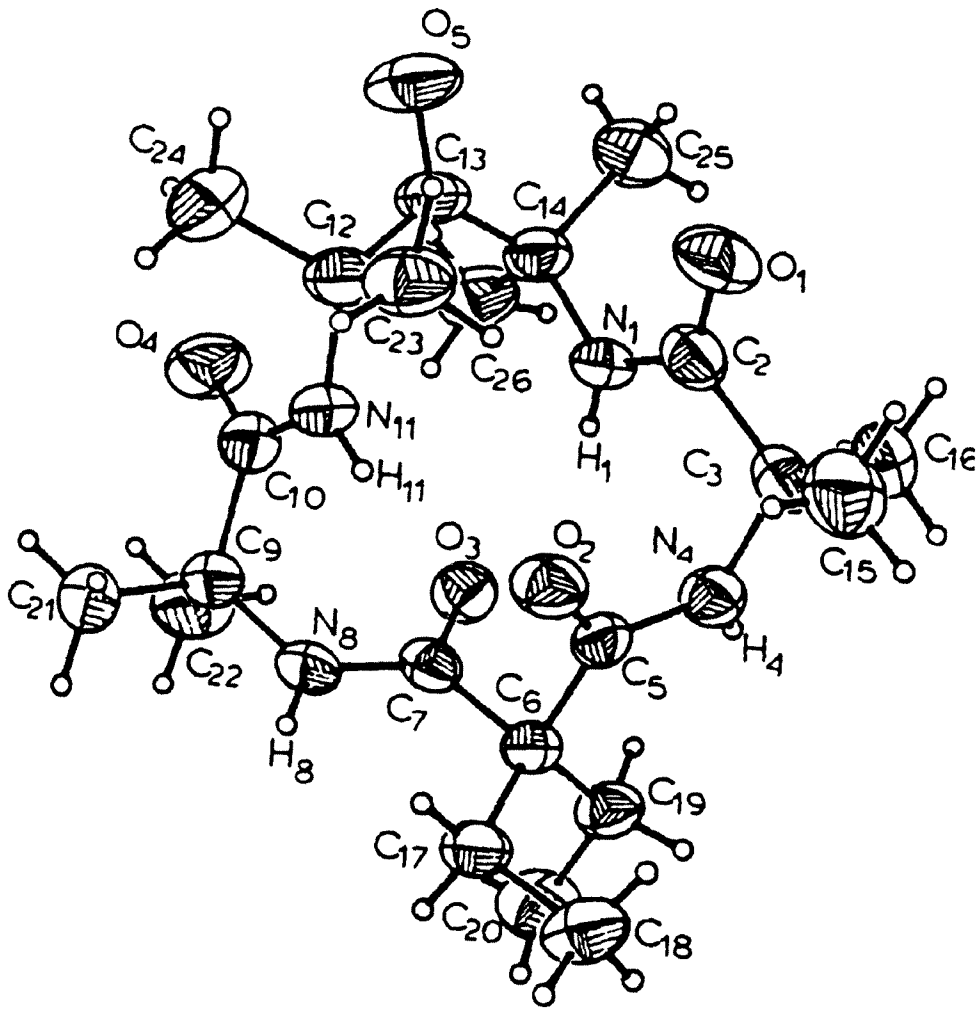

Figure 2.14. ORTEP of H_4MAC*.

Table 2.4. Bond Lengths in H_4MAC*			
Atoms	Length (Å)	Atoms	Length (Å)
O1C2	1.211(5)	O2C5	1.219(5)
O3C7	1.233(5)	O4C10	1.224(6)
O5C13	1.211(5)	N1C2	1.342(5)
N4C5	1.341(6)	N8C7	1.331(5)
N11C10	1.349(5)	N1C14	1.470(6)

Table 2.4. Bond Lengths in H_4MAC* (continued)			
Atoms	Length (Å)	Atoms	Length (Å)
N4C3	1.471(5)	N8C9	1.475(5)
N11C12	1.465(5)	N1H1	0.78(3)
N4H4	0.73(3)	N8H8	0.80(3)
N11H11	0.86(4)	C2C3	1.554(6)
C5C6	1.539(5)	C6C7	1.541(6)
C9C10	1.532(6)	C12C13	1.553(6)
C13C14	1.541(6)	C3C15	1.514(6)
C3C16	1.535(6)	C9C21	1.525(6)
C9C22	1.516(6)	C12C23	1.535(6)
C12C24	1.537(7)	C14C25	1.550(6)
C14C26	1.530(6)	C6C17	1.540(6)
C17C18	1.518(6)	C6C19	1.550(5)
C19C20	1.519(5)		

Table 2.5. Bond Angles in H_4Mac*			
Atoms	Angle (°)	Atoms	Angle (°)
C2N1C14	123.6(3)	C3N4C5	124.4(4)
C7N8C9	124.1(3)	C10N11C12	125.1(4)
O1C2N1	124.2(4)	O1C2C3	119.5(3)
N1C2C3	116.1(3)	O2C5N4	121.5(3)
O2C5C6	119.9(3)	N4C5C6	118.3(4)
N4C5C6	118.3(4)	O3C7C6	119.5(3)
O3C7N8	121.0(4)	C6C7N8	119.1(4)

Table 2.5. Bond Angles in H_4Mac* (continued)			
Atoms	Angle (°)	Atoms	Angle (°)
O4C10C9	118.8(3)	O4C10N11	122.5(4)
C9C10N11	118.4(4)	O5C13C12	116.8(4)
O5C13C14	117.6(4)	C12C13C14	125.6(4)
C6C17C18	113.2(3)	C6C19C20	113.6(3)
C2C3N4	111.6(3)	C2C3C15	110.7(4)
C2C3C16	106.1(4)	N4C3C15	110.8(4)
N4C3C16	106.9(3)	C15C3C16	110.5(3)
C5C6C7	98.5(3)	C5C6C17	107.5(3)
C5C6C19	115.1(3)	C7C6C17	114.7(3)
C7C6C19	107.9(3)	C17C6C19	112.5(3)
N8C9C10	111.0(3)	N8C9C21	107.7(3)
N8C9C22	111.0(3)	C10C9C21	105.5(3)
C10C9C22	111.3(4)	C21C9C22	10.1(3)
N11C12C13	113.6(3)	N11C12C23	107.1(4)
N11C12C24	110.5(3)	C13C12C23	107.7(3)
C13C12C24	109.3(4)	C23C12C24	108.4(4)
C2N1H1	120(2)	C14N1H1	116(2)
C3N4H4	119(2)	C5N4H4	116(2)
C7N8H8	117(2)	C9N8H8	119(2)
C10N11H11	120(2)	C12N11H11	115(2)
C13C14N1	113.1(3)	C13C14C25	109.8(3)
C13C14C26	108.7(3)	N1C14C25	109.6(3)
N1C14C26	107.7(3)	C25C14C26	107.8(4)

ing. H_{1a} hydrogen-bonds to the oxygen atom of the THF molecule of crystallization (H-A: 2.31(4) Å; DH-A: 174(3)°). H_{1b} hydrogen-bonds to the oxygen atom of the uncoordinated amide (H-A: 2.08(5) Å; DH-A: 166(3)°). H_4 hydrogen-bonds to the oxygen atom of the coordinated amide (H-A: 2.10(5) Å; DH-A: 150(3)°). These data are consistent with Etter's empirical general rule of hydrogen-bonding which states that a molecule will use all good proton donors and acceptors in hydrogen-bonding.[12a] Crystalline H_4MAC* forms intramolecular hydrogen-bonds diagonally across the ring with H_1 bonded to O_3 (H-A: 2.39(3) Å; DH-A: 155(2)°, with an additional close contact with N_4, H-A: 2.43(3) Å; DH-A: 108(2)°), and H_{11} bonded to O_2 (H-A: 2.36(3) Å; DH-A: 156(2)°), with an additional close contact with N_8 (H-A: 2.42(3) Å; DH-A: 106(2)°). A third hydrogen-bond is formed intermolecularly with H_8 bonded to O_5 (H-A: 2.47(3) Å; DH-A: 142(2)°). These hydrogen-bonds are long, but within the accepted range of 1.7–2.5 Å found for amide NH···O_{amide} hydrogen-bonds in globular proteins.[12b] In a recent structural paper, Gellman and coworkers have noted the tendency of linear malonamide-containing triamides to form nine-membered ring intramolecular hydrogen-bonds and have discussed the relationship of this bonding to the ten-membered ring β-turn conformation observed in proteins.[13] It is interesting that the intramolecular H-O hydrogen-bonds of H_4MAC*, which also contains the malonamide fragment, are each part of nine-membered rings. The H-O bond distances and the N-H-O bond angles are comparable to those found by Gellman and coworkers. Of the four potential hydrogen-bond donors of H_4MAC*, only one is unused.

Under the non-dilute macrocyclization conditions employed in the synthesis of H_4MAC*, a lower yield of macrocycle than observed and a higher yield

of polymer might be expected. The structure of H_4MAC* indicates that the relatively high yield obtained (32%) might be attributable to a template effect arising from one or more internal hydrogen-bonds in monoacylated AMPA-DMP, the immediate precursor to the macrocycle. It is likely that manipulating solvent polarity to encourage hydrogen-bond templates, or to break up undesirable hydrogen-bonds, is an under-utilized technique in the synthesis of amide-containing macrocycles.

The good yield of H_4MAC* might also be favored by the rigid group effects of the amide bonds. In organic amides, the *trans* conformation is favored, for steric reasons, over the *cis* conformation. The *trans* conformation favors macrocyclization, since all of the amides in H_4MAC* are *trans*. The barrier to rotation about the carbonyl carbon-nitrogen bond of an amide is approximately 20 kcal mol^{-1}, so the macrocyclic geometry of the amide bonds of the precursor is held more or less in place. It is useful to note that the Schiff base contains a *cis* amide, and that the approximate 12 hour half-life of AMPA-DMP might be attributable to the steric *trans*-amide preference and the hindered C-N amide bond rotation.

A few attempts were made to synthesize the aromatic D_{2h} ligand (Figure 1.18c), but success has not yet been realized. Synthesis by straightforward means such as reaction of *o*-nitroaminobenzene (with subsequent reduction of the nitro groups to the amines planned) with diethylmalonyl dichloride gave four-membered cyclic imides (Figure 2.15). Attempts at ring opening these imides proved to be impractical. An alternative route to the diamide dinitro compound was found in the early German literature. By reacting diethylmalonamide,[14] an excess of *o*-chloronitrobenzene, K_2CO_3, and CuI at

160 °C in the absence of solvent, one obtains a 50% yield of diamide dinitro (this reaction is essentially a "double" Goldberg reaction[15]). This compound is readily reduced to the diamide diamine. However, reaction of this compound with diethylmalonyl dichloride at room temperature or reduced temperatures (as low as −40 °C) gives exclusively mono and diimides (Figure 2.16). Because the H_4MAC* and H_4DEMAMPA-DXB reactions work (the H_4DEMAMPA-DXB reactions have also been shown to yield significant amounts of imides), control of the imide versus amide pathways must be subtle. A modest number of attempts at macrocyclization have been tried with other coupling methods, so far without success.

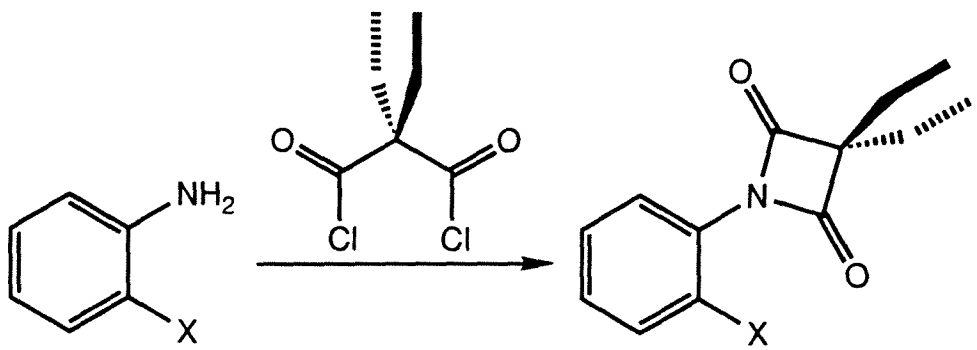

Figure 2.15. Aniline and its derivatives form four-membered cyclic imides with diethylmalonyl dichloride.

The pyridine-based macrocycle (Figure 1.18d) has not been completed. The synthesis proceeds identically to that for the H_4DEMAMPA-DXB systems up to and including production of the diamide diazide (Figure 2.17). Reducing the diazide in the presence of the pyridine ring has caused complications, but a procedure from the Knowles group[16] involving the use of 1,3-propanedithiol as the reductant appears promising.

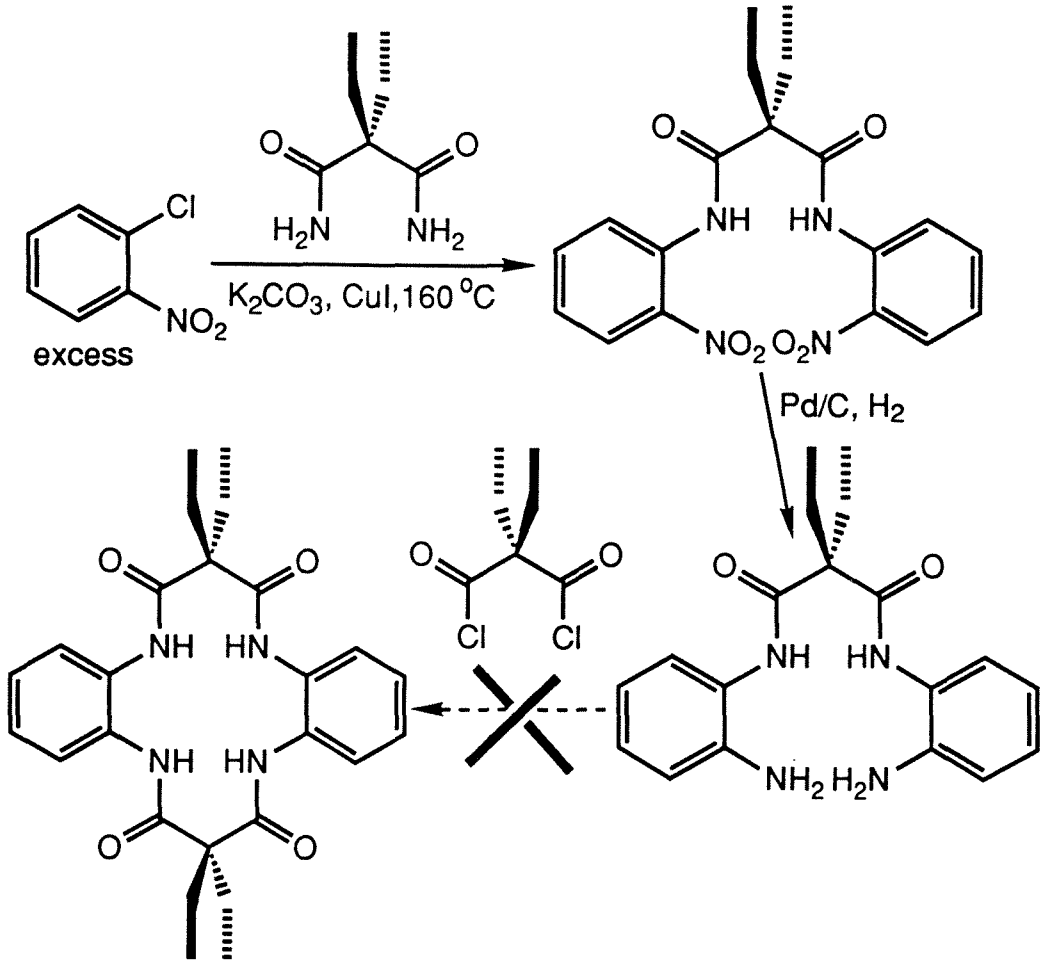

Figure 2.16. A variation of the Goldberg reaction followed by catalytic reduction yields the diamide diamine in 40% total yield. Unfortunately, reaction of the diamide diamine with diethylmalonyl dichloride gives exclusively a statistical mixture of starting material, diamide amine monoimide, and diamide diimide; no macrocycle is obtained.

The differences between the macrocyclic tetraamides of this thesis and other macrocyclic ligands used in inorganic chemistry are numerous, as the rest of this thesis will demonstrate. The differences begin with the methods by which transition metals are inserted into the ligands. Porphyrins are frequently heated to reflux with an anhydrous divalent metal salt in dimethylformamide.[17]

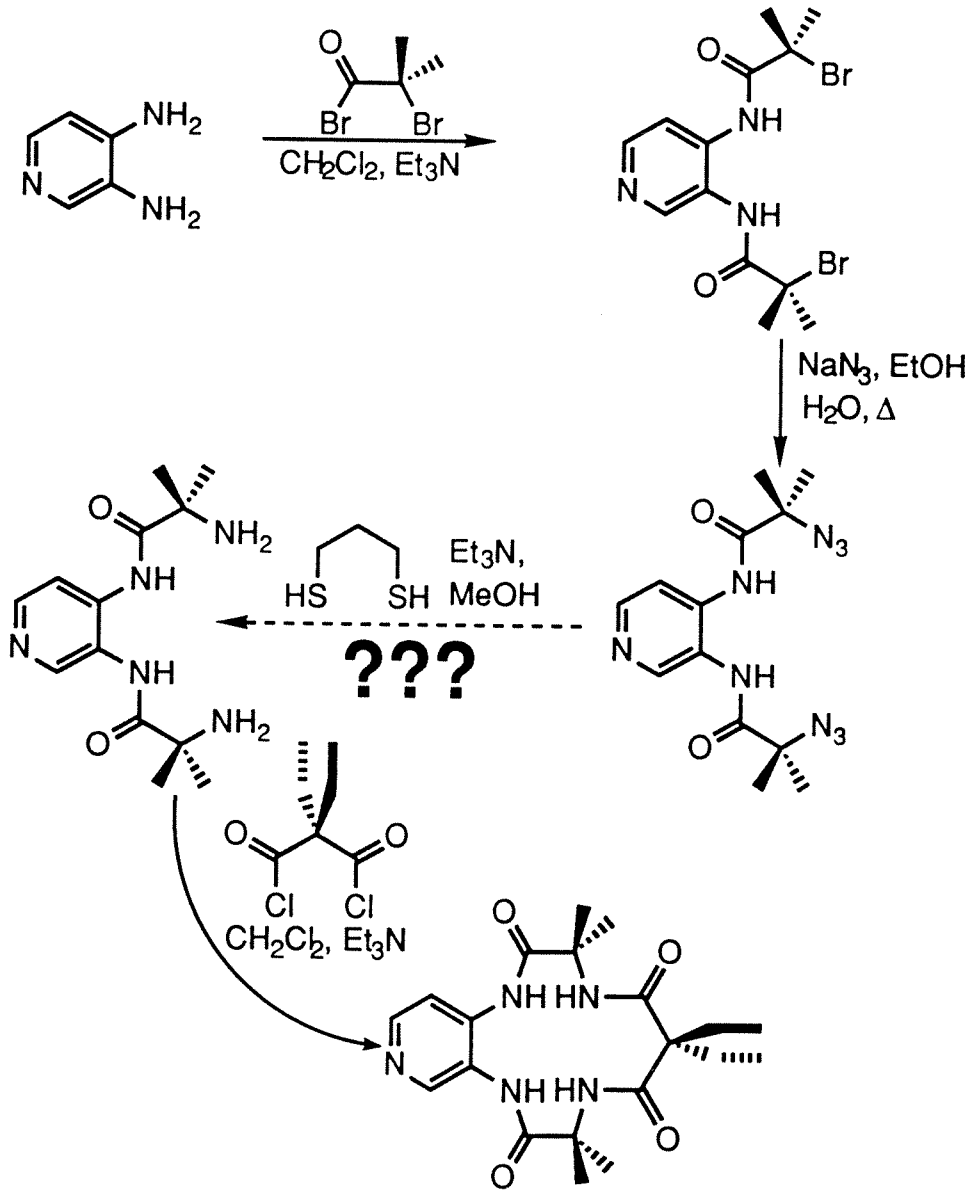

Figure 2.17. The synthesis of the pyridine-based macrocycle has been complicated by the reduction step. Test reactions indicate that 1,3-propanedithiol is a promising reducing agent.

Cyclams may be metallated simply by refluxing the ligand with a soluble metal salt. Many macrocycles do not need to be metallated, since template reactions which lead to their synthesis also yield the complex. A number of research

groups have studied the chemistry of macrocyclic transition metal complexes with one, two, or three amido-*N* ligands since Kimura and Kodama's first report of such a complex in 1979.[18] In all these cases, the amide unit is part of a macrocyle in which one or more neutral Lewis base ligands, such as amines, are also present. It is reasonable to assume that metal insertion proceeds first by coordination to these accessible or unmasked donor atoms (the protonated amide does not contain a σ-donating lone pair to lead the coordination process). Subsequent amide deprotonation/coordination gives the macrocyclic complexes. The technical challenge of effecting metal insertions into polyamide macrocycles free of unmasked donor groups has been one of the primary obstacles hindering the development of this area. In Margerum's system, metal insertion was performed in the presence of aqueous sodium hydroxide and freshly precipitated $Cu(OH)_2$.[19] However, none of the above methods works for the macrocycles of this thesis. The pKa 1 of the macrocycles is too high to make the syntheses amenable to mild bases, and the ligands are rigid enough and sterically hindered enough that the relatively small equilibrium concentration of monodeprotonated ligand that is generated with hydroxide can not react before the metal salts are all precipitated as inert hydroxide/oxide polymers. Thus, a means of coordinating a hindered, high pKa macrocycle was needed. A side benefit of the peralkylation and aromatization of the ligands was that the amide protons clearly had a pKa lower than any other protons in the molecules by about 20 orders of magnitude (i.e., there were no enolizable protons). Thus, as shown (Figure 2.18), dissolving the ligands in anhydrous deoxygenated THF, adding strong hindered base, and adding a THF soluble (or partially soluble) divalent neutral metal complex yields the divalent macro-

cyclic complexes in yields typically of 80%.[20] This method does not work with trivalent transition metal starting materials such as anhydrous $FeCl_3$, $CoCl_3$, or $CrCl_3$. One can speculate that this is due either to the greatly reduced kinetic lability of these compounds relative to the divalent compounds or to the mild oxidizing power of these complexes being sufficient to create problems given the strongly reducing nature of the very basic reaction mixture. The synthetic method shown in Figure 2.18 does not work with copper. For copper, refluxing the H_4DEMAMPA-DXB macrocycles with anhydrous copper acetate in a dry MeCN solution of Proton Sponge in air yields the Cu(III) complexes (Figure 2.19). This synthetic method does not work for the other metals, and it does not work for H_4MAC* with copper. One can speculate that the strong base approach for these ligands is successful not only due to the high pKa of the ligands, but also because one would anticipate that multiple deprotonation should increase the fraction of molecules in the proper conformation for complexation. Since lithium will ion pair with oxygen rather than nitrogen whenever it can, coulombic repulsion in a multiply deprotonated ligand could result in the solution structure depicted (Figure 2.20), which may be contrasted with the solid state structure of the neutral molecule (Figure 2.14). A study which has not yet been performed which might give insight into synthetic strategies for other metals is to determine pKa 1, pKa 2, pKa 3, and pKa 4 for the different macrocycles.

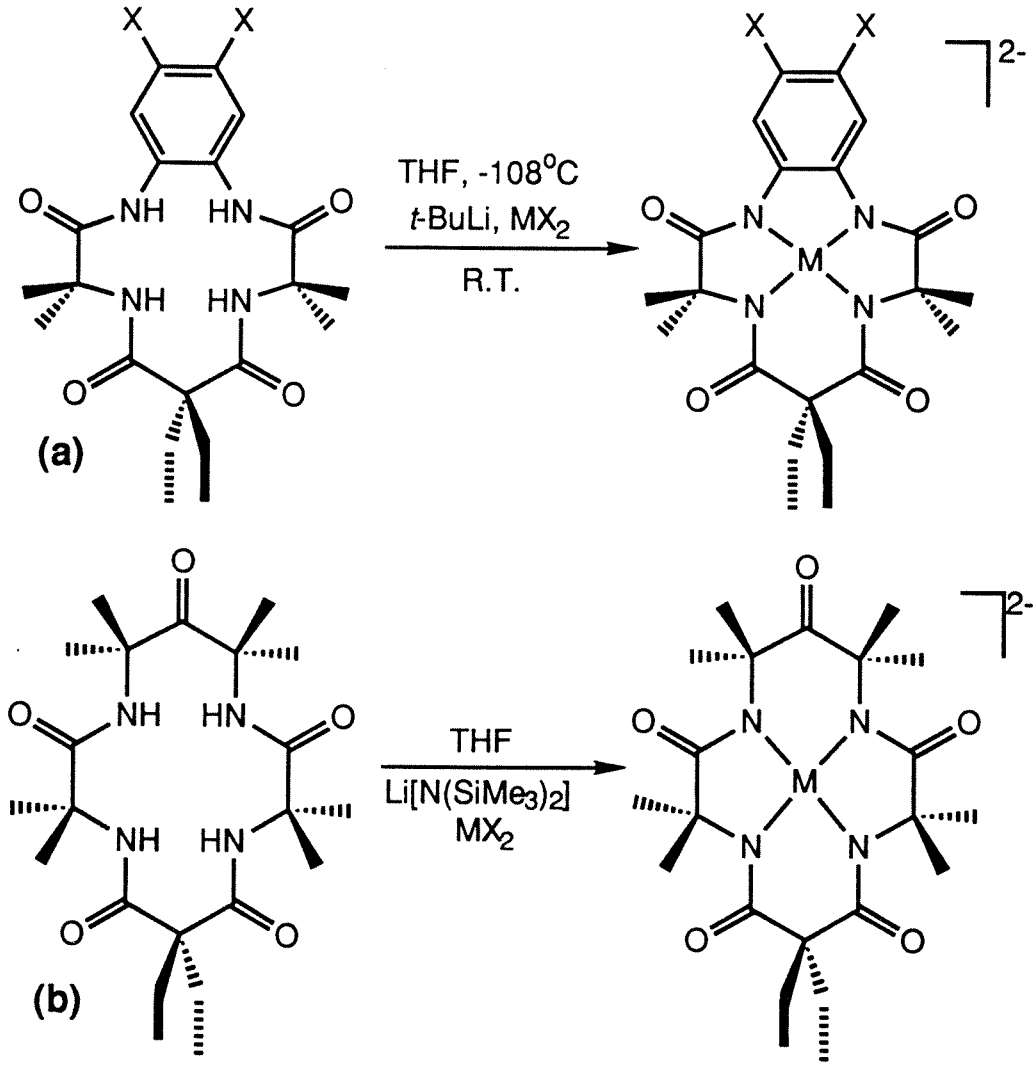

Figure 2.18. The base, solvent, and temperature conditions indicated in (a) and (b) work for either ligand system with $CrCl_2$, $MnCl_2$, $FeCl_2$, $CoCl_2$, and $((C_6H_5)_3P)_2NiBr_2$. Low temperature conditions are used in (a), because THF is well known to decompose with alkyl lithiums at room temperature.

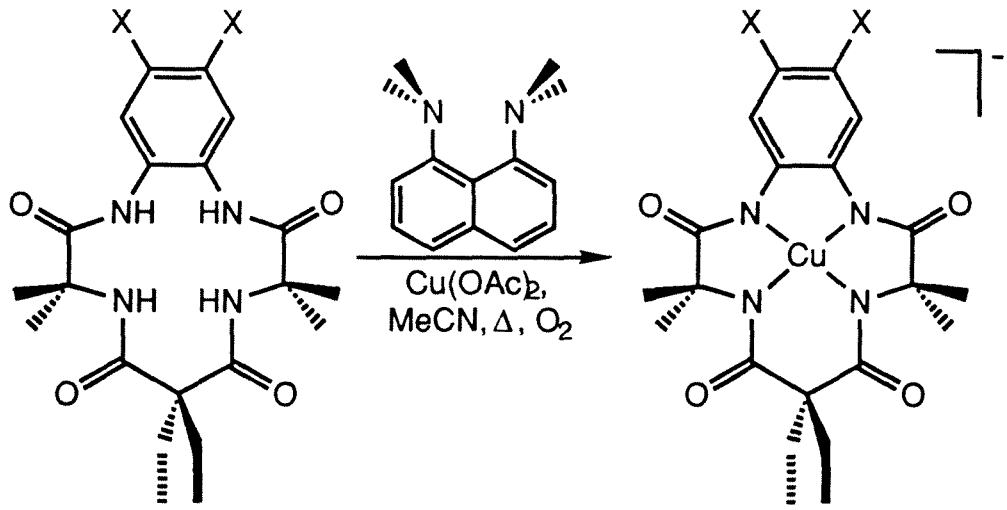

Figure 2.19. The insertion method depicted here apparently works only with Cu and the H_4DEMAMPA-DXB systems. It does not appear to work with other metals, nor does it appear to work with Cu and H_4MAC*.

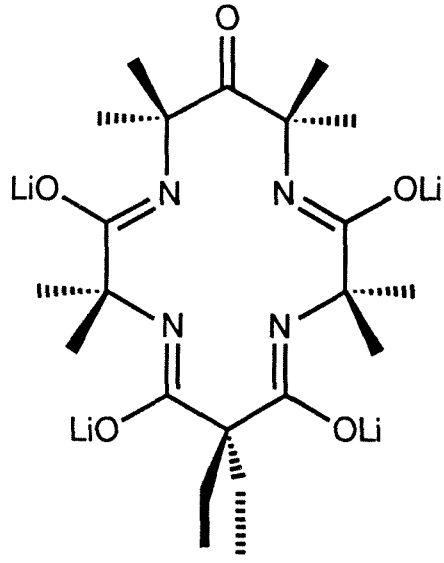

Figure 2.20. Possible role of deprotonation in generating favorable conformations of $[MAC^*]^{4-}$.

Experimental

SAFETY NOTE. The organic azides produced in the following syntheses are never isolated in concentrated form as oils or as solids in quantities greater than 20 mg. Appropriate care should be exercised when handling organic azides.[10] Organic azides are potentially explosive. Keep away from contact with metals and/or high heat. NaN_3 is toxic and an explosion hazard with metals. HN_3 is very toxic and can be violently explosive and very shock sensitive. Keep the azide reactions and work ups away from strong acid!

Materials. All solvents and reagents were reagent grade (Aldrich) except for CH_2Cl_2, conc HCl, glacial acetic acid, fuming nitric acid, EtOH, and CCl_4 (Fisher, reagent grade) and were used as received.

Physical Measurements. ^1H and ^{13}C NMR were measured at 300 and 75.45 MHz, respectively, on an IBM NR/300 FT-NMR Spectrometer. ^1H NMR spectra were also measured at 90 MHz on a Varian EM-390 Spectrometer. ^1H and ^{13}C NMR data are reported in δ vs. $(CH_3)_4Si$ with the solvent as internal standard. Infrared data were obtained on a Beckman IR 4240 Spectrophotometer or on a Nicolet 5DXB FT-IR Spectrophotometer. Crystal structures were solved by Crystalytics Co. of Lincoln, Nebraska.

Synthetic Note. Compounds 2,4-dibromo-2,4-dimethylpentanone,[8] 2,4-diazido-2,4-dimethylpentanone,[8] 2,4-diamino-2,4-dimethylpentanone,[8] 1,2-dimethoxy-4,5-dinitrobenzene,[21] and 4,5-dimethoxy-1,2-diaminobenzene[21] have been previously prepared.[21] The procedures for making these compounds have been modified as discussed below. It should be noted that the syntheses re-

ported here are currently in press in *J. Am. Chem. Soc.*[22a] and *Inorg. Chem.*[22b] in substantially similar form. The synthesis of H_4MAC* published in the supplementary materials of reference 23 is inferior to that published here, because $AgNO_3$ is critical to removing sulfur contaminants from the Schiff base, and lowers the isolated yield. Scott Gordon-Wylie and Steve Paterno at Carnegie Mellon University are currently developing procedures for the synthesis of the aromatic-bridged macrocycles which do not involve organic azides.[24] Their results should be sought following optimization and subsequent publication.

2,4-Dibromo-2,4-dimethylpentanone. *This free-radical chain reaction is potentially very hazardous on this scale. There have been a few reported incidents of explosions of NBS reactions.* To 2,4-dimethylpentanone (85 mL, 68.5 g, 0.60 mol) in CCl_4 (1000 mL) was added *N*-bromosuccinimide (NBS) (240 g, 1.35 mol, 2.26 equiv.). The mixture was heated under reflux, and benzoyl peroxide (20 mg) was added to the solution. While the solution was heated under reflux (24 h), a pale orange solid (succinimide) floated to the surface of the CCl_4, while unreacted NBS remained on the bottom. Benzoyl peroxide was added to the refluxing mixture (20 mg, 12–24 h intervals) until no NBS was visible; usually the reaction was complete after 24 h. When the reaction was complete, the solids were collected by filtration and discarded, and the CCl_4 was removed from the mother liquor under reduced pressure, leaving a pale yellow oil. To remove residual CCl_4, 95% EtOH (100 mL) was added, and the solvents were removed under reduced pressure to leave a pale yellow oil (159.99 g, 0.59 mol, 98%). ^{1}H NMR ($CDCl_3$): 2.1 (s).

2,4-Diazido-2,4-dimethylpentanone. A solution of 2,4-dibromo-2,4-dimethylpentanone (89.8 g, 0.33 mol) in EtOH (1200 mL, 95%) was added to a

solution of NaN_3 (*CAUTION!*) (47.2 g, 0.726 mol, 2.2 equiv) in water (600 mL). The solution was heated under reflux (16 h) to give a pale orange solution. The EtOH was removed under reduced pressure until the solution became cloudy. The cloudy aqueous solution was extracted with pentane (500 mL) three times, and the combined extracts were dried over Na_2SO_4 and concentrated to 300 mL under reduced pressure. Glacial acetic acid (100 mL) was then added, and the remaining pentane was removed under reduced pressure. It is important to execute this procedure to remove the NaN_3, since the product is exposed to Pd/C in the next step and care should be taken to avoid the formation of a heavy metal azide. The pentane was removed from a small sample under reduced pressure to give a neat oil (< 20 mg) for spectroscopic characterization: ^{1}H NMR ($CDCl_3$): 1.54 (s). IR (neat): $\bar{\nu}[cm^{-1}]$ = 2115 ($\nu(N_3)$), 1720 ($\nu(CO)_{ketone}$).

2,4-Diamino-2,4-dimethylpentanone (DMP). Glacial acetic acid (50 mL) was added to the HOAc solution from the previous step, and this solution was added to 10% Pd/C (2.7 g). The mixture was hydrogenated at 50 psi (1 week) in a Parr hydrogenator. Because the reaction evolves one N_2 molecule for every H_2 molecule absorbed, the bomb was evacuated and refilled with H_2 10 times. [H_2 from the high pressure reservoir is not efficiently consumed.] The charcoal was removed by filtration. The HOAc was removed under reduced pressure. After adding HBr (48%, 76 mL), the mixture was dissolved in EtOH. The volatiles were removed under reduced pressure to yield a tan solid which was washed with a mixture (200 mL) of THF (50%), EtOH (45%), and 48% HBr (5%). The white powdery product was the dihydrobromide salt of DMP (56.2 g, 48% from the dibromide). ^{1}H NMR

($CDCl_3$/DMSO-d_6) of DMP·2HBr: 8.62 (s, 6H, br, NH_3), 1.77 (s, 12H, Me). IR (free base, nujol):$\bar{\nu}[cm^{-1}]$ = 3460–3160 ($\nu(NH_2)$), 1690 ($\nu(CO)_{ketone}$). The product must be stored as the dihydrochloride or dihydrobromide salt. Note that earlier syntheses have employed $(NH_4)_2S$ as the reducing agent. Although $(NH_4)_2S$ cuts the reduction time considerably, sulfur contamination prevents Pd/C reduction of the second diazide in the synthetic sequence. Furthermore, sulfur contamination of the Schiff base appears to drastically decrease the efficiency of isolating ring-opened diamide diamine. Although treatment of these intermediates with aqueous $AgNO_3$ removes both elemental sulfur and polysulfide contaminants, the yield of the organic products from such treatment is very low. Therefore, the catalytic hydrogenation procedure described above is strongly recommended.

Bis-2,4-(2-bromo-2-methylpropanamido)-2,4-dimethylpentanone (BrMPA-DMP). The compound DMP·2HBr (24.25 g, 0.073 mol) and Et_3N (40 mL) were added to CH_2Cl_2 (500 mL). The mixture was dried over Na_2SO_4 (1 h) and then filtered into a three-neck round-bottom flask (1 L) equipped with a reflux condenser and a pressure-equalizing addition funnel. Under a N_2 atmosphere, 2-bromoisobutyryl bromide (20 mL, 0.162 mol) was carefully added to the solution from the addition funnel to avoid boiling the solvent. (*The reaction is VERY exothermic.*) The solution became cloudy upon production of $[Et_3NH]Br$. After stirring (1 h), the reaction mixture was washed twice with dilute aqueous HCl and twice with dilute aqueous Na_2CO_3. The resultant CH_2Cl_2 solution was dried over Na_2SO_4 to give a clear, pale yellow solution. The CH_2Cl_2 was removed under reduced pressure yielding the white solid product (32.3 g, 100% yield). Anal. Calcd for BrMPA-DMP: C,

40.74; H, 5.93; N, 6.34. Found: C, 40.54; H, 5.88; N, 6.24. ^{1}H NMR ($CDCl_3$): 7.42 (s, 2H, NH), 1.90 (s, 12H, Me), 1.65 (s, 12H, Me). IR (Nujol): $\bar{\nu}[cm^{-1}]$ = 3327 (ν(NH)), 1724 ($\nu(CO)_{ketone}$), 1652 ($\nu(CO)_{amide}$).

Bis-2,4-(2-azido-2-methylpropanamido)-2,4-dimethylpentanone (AzMPA-DMP). NaN_3 (*CAUTION!*) (40 g, 0.55 mol, 2.5 equiv.) was dissolved in water (500 mL) and the solution was added to a solution of BrMPA-DMP (95 g, 0.22 mol) in EtOH (800 mL, 95%). The mixture was heated under reflux (30 h). The EtOH was removed under reduced pressure until the solution became cloudy. The aqueous solution was extracted twice with CH_2Cl_2 and the extract was dried over anhydrous Na_2SO_4. It is important to execute this procedure to remove the NaN_3, since the product is exposed to Pd/C in the next step and care should be taken to avoid the formation of a heavy metal azide. The solution was concentrated carefully under reduced pressure so the procedure could be halted before the oil or solid separated. EtOH (ca. 250 mL) was added, and the solution was again concentrated under reduced pressure. A small sample was isolated as a solid for spectroscopic characterization. ^{1}H NMR ($CDCl_3$): 7.28 (s, 2H, NH), 1.62 (s, 12 H, Me), 1.50 (s, 12 H, Me). IR (Nujol): $\bar{\nu}[cm^{-1}]$ = 3440–3260 (ν(NH)), 2110 ($\nu(N_3)$), 1713 ($\nu(CO)_{ketone}$), 1675 ($\nu(CO)_{amide}$).

HImine. About 26 g of AzMPA-DMP were dissolved in EtOH (100 mL) and H_2O (9 mL) and hydrogenated with 10% Pd/C (1.51 g) at 50 psi (4 days) with 5 purgings (See synthesis of DMP.). The dihydrobromide salt (32.77 g, 82% from BrMPA-DMP) was obtained after a workup similar to that used for DMP. ^{1}H NMR (after isolation of the free base of HImine) ($CDCl_3$): 8.63 (s, 1H, amide NH), 7.60 (s, 1H, amide NH), 1.52 (s, 6H, Me), 1.42 (s, 6H,

Me), 1.27 (s, 6H, Me), 1.18 (s, 6H, Me), amine proton resonance broad and underneath methyl singlets. IR (Nujol): $\bar{\nu}[cm^{-1}]$ = 3260–3180 (ν(NH, weak)), 1679 ($\nu(CN)_{imine}$), 1648 ($\nu(CO)_{amide}$).

Bis-2,4-(2-amino-2-methylpropanamido)-2,4-dimethylpentanone (AMPA-DMP). *The bomb procedure used here will generate pressures above 1 atm. Appropriate shielding and caution must be employed.* The Schiff base HImine (4.60 g) was dissolved in EtOH (35 mL, 95%) and HBF_4 (5.5 mL, 48%, diluted with 7 mL water) was added. The solution was added to a glass bomb (125 mL volume) which was placed in a silicone oil bath and heated (104–108 °C, 3 h) [**CAUTION—Pressure!**]. The solution was chilled in an ice bath and a chilled aqueous syrupy slurry of NaOH was added until the pH was $\approx$ 12. The mixture was immediately taken to a viscous, but still freely stirring, sludge without heat under reduced pressure. CH_2Cl_2 was added (150 mL) and the mixture was stirred (5 min). Na_2SO_4 was added rapidly with swirling (10 s) to dry the mixture and was filtered away immediately. The sodium salts were washed several times with CH_2Cl_2, and the combined CH_2Cl_2 solutions were taken to dryness in a weighed round bottom flask at room temperature under reduced pressure to yield the solid product (4.44 g, 97%). The compound is stored as a solid; it recyclizes in solution. Whenever more than 20% HImine impurity was found in AMPA-DMP, the above procedure was repeated until AMPA-DMP was at least 80% pure before proceding to the next step. ^{1}H NMR ($CDCl_3/CCl_4$) of the free base: 8.19 (s, 2H, amide NH), 1.61 (s, 12H, Me), 1.48 (s, 4H, amine NH_2), 1.34 (s, 12H, Me); (D_2O): 1.52 (s, 12H, Me), 1.27 (s, 12H, Me). ^{1}H NMR (D_2O) AMPA-DMP·2HBF_4: 1.24 (s, 12H, Me), 1.21 (s, 12H, Me). IR (Nujol, free base): $\bar{\nu}[cm^{-1}]$ = 3390–3290 (ν(NH—amide/amine,

strong)), 1703 ($\nu(CO)_{ketone}$), 1650 ($\nu(CO)_{amide}$).

H_4MAC*. AMPA-DMP (4.44 g) was dissolved in CH_2Cl_2 (800 mL) and Et_3N (9.9 mL) was added. After adding diethylmalonyl dichloride (2.45 mL) the reaction was stirred under N_2 (10 h). The reaction was washed three times with dilute aqueous HCl and three times with dilute aqueous Na_2CO_3. After drying over Na_2SO_4, the solution was concentrated to a pale yellow oil under reduced pressure. Several small portions of boiling CH_2Cl_2 were used to wash the oil into a 150 mL beaker (60 mL total). CCl_4 (40 mL) was added and the solvent volume was reduced to 50 mL by boiling. Upon cooling, white microcrystalline H_4MAC* floated to the surface of the solution. The crystals were filtered, washed twice with CH_2Cl_2 (3 mL) and then twice with pentane (10 mL). The crystalline product was pure (2.06 g, 32.3%, 12.1% from 2,4-dimethylpentanone). Anal. Calcd for H_4MAC*·CH_2Cl_2: C, 52.77; H, 7.70; N, 10.70. Found: C, 52.67; H, 7.61; N, 10.63 (the presence of one CH_2Cl_2 per molecule of H_4MAC* was quantified by ^{1}H NMR). Mp. 273–276 °C. ^{1}H NMR ($CDCl_3$): 6.58 (s, 2H, amide NH, broad), 6.22 (s, 2H, amide NH, broad), 2.0 (4H, broad, methylene), 1.52 (s, 12H, Me), 1.47 (s, 12H, Me), 0.89 (t, 6H, Me–ethyl, 7.5 Hz). IR (Nujol): $\bar{\nu}[cm^{-1}]$ = 3500 (ν(NH—amide, weak)), 3450 (ν(NH—amide, medium)), 3405 (ν(NH—amide, strong)), 3377 (ν(NH—amide, very strong)) (all amide-NH stretches are very sharp for H_4MAC*), 1702 ($\nu(CO)_{ketone}$), 1680 ($\nu(CO)_{amide}$), 1645 ($\nu(CO)_{amide}$). Crystals suitable for diffraction were grown by vapor diffusion of pentane into a 1,2-dichloroethane solution.

CuCl(η^3-Imine). AMPA-DMP (0.92 g) was dissolved in EtOH (100%, 20 mL) and $Cu(OAc)_2·2H_2O$ (0.673 g) was added. NaOH pellets (0.25 g) were

added to the solution and dissolved with stirring, while the solution turned dark blue. Removing the EtOH under reduced pressure yielded a dark blue solid (1.43 g). A portion of this solid (0.107 g) was added to dry THF (20 mL), excess NaH was added, then diethylmalonyl dichloride (0.10 g) was added. A pale blue solid (0.056 g) was isolated from the THF and crystals suitable for diffraction were grown from THF. A compound with identical properties was prepared by reacting $CuCl_2 \cdot 2H_2O$ (0.400 g) with AMPA-DMP (0.745 g) and NaOH (0.105 g) in absolute EtOH (20 mL). The compound was purified by removing the EtOH under reduced pressure, dissolving the residue in MeCN, filtering, and adding Et_2O to precipitate the product (0.576 g, 62.1%). IR (Nujol): $\bar{\nu}[cm^{-1}]$ = 3500–3100 (ν(NH—amide and amine, weak)), 1682 ($\nu(CN)_{imine}$), 1620 ($\nu(CO)_{amide}$), 1590 ($\nu(CO)_{amide}$).

X-ray Data Collection and Structure Refinement of H_4MAC*·$C_2H_4Cl_2$ and CuCl(η^3-Imine)·THF. Crystal Data: Single crystals of $H_4MAC^* \cdot C_2H_4Cl_2$, at 20±1°C, are monoclinic, space group $P2_1/C\text{-}C_{2h}^5$ (No. 14), with a = 14.193(4) Å, b = 11.700(3) Å, c = 18.328(5) Å, β = 105.03(1)°, V = 2940(1) Å^3 and Z = 4 formula units (d_{calcd} = 1.215 g cm^{-3}). A total of 4053 independent reflections having $2\theta(MoK\bar{\alpha}) < 45.8°$ (the equivalent of 0.60 limiting $CuK\bar{\alpha}$ spheres) were collected on a computer-controlled Nicolet autodiffractometer using full (0.90°-wide) ω scans and graphite-monochromated $MoK\bar{\alpha}$ radiation. The dichloroethane solvent molecule of crystallization is disordered, with its nonhydrogen atoms occupying 4 of 6 sites in the lattice at any given time. Single crystals of CuCl(η^3-Imine)·THF are orthorhombic (space group $Pna2_1\text{-}C_{2v}^9$ (No. 33) at 20±1°C), with a = 15.953(3) Å, b = 13.711(2) Å, c = 10.229(2) Å, V = 2237(1) Å^3, and Z = 4 formula

units (d_{calcd} = 1.385 g cm^{-3}). A total of 2723 independent reflections having $2\theta(MoK\bar{\alpha}) < 55°$ (the equivalent of 1.0 limiting $CuK\bar{\alpha}$ spheres) were collected on a computer-controlled Nicolet autodiffractometer using full (0.90°-wide) ω scans and graphite-monochromated $MoK\bar{\alpha}$ radiation. The structures were solved using Direct Methods techniques with the Nicolet SHELXTL software package as modified at Crystalytics Company. The resulting structural parameters have been refined to convergence R_1(unweighted, based on F) = 0.037 for 1983 independent reflections having $2\theta_{MoK\bar{\alpha}} < 45.8°$ and $I > 3\sigma(I)$ for $H_4MAC^*{\cdot}C_2H_4Cl_2$ and R_1(unweighted, based on F) = 0.035 for 1917 independent reflections having $2\theta_{MoK\bar{\alpha}} < 55.0°$ and $I > 3\sigma(I)$ for $CuCl(\eta^3\text{-Imine}){\cdot}THF$ using counter-weighted cascade block-diagonal least-squares techniques and a structural model which incorporated anisotropic thermal parameters for non-hydrogen atoms and isotropic thermal parameters for all hydrogen atoms. The methyl groups were included in the refinements as idealized sp^3-rigid rotors.

Bis-1,2-(2-bromo-2-methylpropanamido)-4,5-dichlorobenzene. 4,5-Dichloro-1,2-phenylenediamine (38.45 g) was dissolved in CH_2Cl_2 (550 mL), Et_3N (80 mL) was added, and then 2-bromoisobutyryl bromide (100.0 g) was added via a constant pressure addition funnel (45 min), and the reaction was stirred (6 h) under N_2. Water and CH_2Cl_2 were added until all the solids dissolved. The layers were then separated, and the CH_2Cl_2 layer was extracted four times with dilute aqueous HBr and three times with dilute aqueous Na_2CO_3. Evaporating the CH_2Cl_2 solution to dryness yielded a black solid which was washed on a sintered glass crucible with pentane until the eluents were nearly colorless and the solid turned pale brown. Drying in vacuo yielded the product (76.21 g, 73.9%). ^1H NMR ($CDCl_3$): 8.68 (s, 2H,

amide NH), 7.70 (s, 2H), 2.05 (s, 12H). Anal. Calcd: C, 35.40; H, 3.40; N, 5.90. Found: C, 35.37; H, 3.38; N, 5.88. IR (Nujol): $\bar{\nu}[cm^{-1}] = 3290$ (amide NH); 1676 (amide).

Bis-1,2-(2-amino-2-methylpropanamido)-4,5-dichlorobenzene. The above product (76.2 g) was suspended in EtOH (1.5 L), NaN_3 (*CAUTION!*) (60 g) dissolved in H_2O (900 mL) was added and the solid dissolved as the reaction was heated to reflux. The mixture was heated under reflux (12 h), was allowed to cool, and was then extracted with CH_2Cl_2 (5.0 L). The CH_2Cl_2 solution was concentrated to 1.5 L, EtOH was added (1.5 L), the solution was concentrated to 2.0 L, and more EtOH was added (2.0 L). *CAUTION! NMR analysis was performed on 3 mg of isolated material. The bulk diazide product was not isolated.* [^{1}H NMR ($CDCl_3$): 8.61 (s, 2H, amide NH), 7.67 (s, 2H), 1.65 (s, 12H).] $(NH_4)_2S$ (125 mL, 23% aqueous solution) was added to the EtOH solution under N_2, and the reaction was stirred overnight. After a fraction of the solvent had been removed under reduced pressure, sulfur and insoluble polysulfides were filtered away. The filtrate was taken to dryness under reduced pressure and the solid was dissolved in CH_2Cl_2 and extracted with ice cold aqueous NaOH (21 g in 700 mL H_2O). The CH_2Cl_2 layer was separated and dried over Na_2SO_4. The CH_2Cl_2 was removed under reduced pressure and the resultant dark brown solid was treated with CH_2Cl_2 (150 mL) and transferred to a sintered glass crucible. The dark brown solid was washed twice with small quantities of CH_2Cl_2 and then washed with Et_2O until a pale, sulfur-contaminated (10–20%), tan solid remained (10.73 g). The dark brown filtrates were combined, taken to dryness under reduced pressure, and the resultant brown solid was washed with Et_2O until most of the color had

been removed, giving a sulfur-contaminated (10–20%) tan solid (16.15 g). The combined solids (total yield 26.88 g, 48% from diamide dibromide) were used in the macrocyclization without further purification. The compound may be purified on a preparative TLC plate (0.360 g compound, 20×20 cm 2000 micron silica gel plate, THF developing solvent, 0.225 g purified compound isolated). ^{1}H NMR ($CDCl_3$): 9.85 (br, 2H, amide NH), 7.88 (s, 2H), 1.69 (br, 4H, amine NH), 1.45 (s, 12H). Anal. Calcd: C, 48.43; H, 5.81; N, 16.13. Found: C, 48.38; H, 5.76; N, 16.00. IR (Nujol): $\bar{\nu}[cm^{-1}]$ = 3401, 3349, 3302, 3288, 3215 (amide and amine NH); 1646 (amide).

5,6:(4,5-dichlorobenzo)-3,8,11,13-tetraoxo-2,2,9,9-tetramethyl-12,12-diethyl-1,4,7,10-tetraazacyclotridecane: H_4DEMAMPA-DCB. The diamine (9.00 g), Et_3N (7.5 mL), and diethylmalonyl dichloride (2.4 mL) were added to CH_2Cl_2 (5.0 L) under N_2. Additions of identical quantities of the three reactants were repeated twice at seven hour intervals. [Totals: diamine, 27.00 g; Et_3N, 22.5 mL; diethylmalonyl dichloride, 7.2 mL.] The reaction mixture was stirred (7 h) and then extracted three times with dilute aqueous HBr and three times with dilute aqueous $NaHCO_3$. The CH_2Cl_2 layer was taken to dryness under reduced pressure. CH_2Cl_2 was added, and the solid (mostly macrocycle) (10.6 g) was filtered away. The solid was boiled as a suspension in a mixture of dichloroethane (75 mL) and CH_2Cl_2 (75 mL) and after cooling, pure H_4DEMAMPA-DCB (8.023 g, 21.99%) was filtered away from the pale yellow solution. ^{1}H NMR ($CDCl_3$): 7.65 (s, 2H), 7.46 (s, 2H, amide NH), 6.40 (s, 2H, amide NH), 2.06 (br, 4H), 1.57 (s, 12H), 0.88 (t, 6H, 7.0 Hz). ^{1}H NMR (DMSO-d6, 295 K): 8.33 (s, 2H, amide NH), 7.75 (s, 2H, amide NH), 7.65 (s, 2H, aromatic), 1.98 (q/br, 4H), 1.45 (s, 12H), 0.76 (t, 6H, 7.5 Hz). ^{1}H NMR

(DMSO-d6, 337 K): 8.24 (s, 2H, amide NH), 7.67 (s, 2H, aromatic), 7.55 (s, 2H, amide NH), 2.02 (q, 4H, 7.5 Hz), 1.48 (s, 12H), 0.78 (t, 6H, 7.5 Hz). Anal. Calcd for H_4DEMAMPA-DCB·0.5H_2O: C, 52.51; H, 6.08; N, 11.66. Found: C, 52.65; H, 5.86; N, 11.66 (H_2O found in NMR in addition to solvent background H_2O). IR (Nujol): $\bar{\nu}[cm^{-1}]$ = 3454, 3346 (amide NH); 1706, 1688, 1645 (amide).

Bis-1,2-(2-bromo-2-methylpropanamido)benzene. 1,2-Phenylenediamine (23.52 g) was dissolved in CH_2Cl_2 (550 mL), Et_3N (80 mL) was added, and then 2-bromoisobutyryl bromide (100.0 g) was added via a constant pressure addition funnel (2 h), and the reaction mixture was stirred (6 h) under N_2. The CH_2Cl_2 reaction solution was extracted twice with dilute aqueous HBr and twice with dilute aqueous Na_2CO_3. Upon removal of the solvent under reduced pressure, a tan powder was obtained which was washed with pentane and collected (77.18 g, 87.4%). ^{1}H NMR ($CDCl_3$): 8.75 (s, 2H, amide NH), 7.51 (m, 2H), 7.27 (m, 2H), 2.06 (s, 12H). Anal. Calcd: C, 41.41; H, 4.47; N, 6.90. Found: C, 41.37; H, 4.37; N, 6.81. IR (Nujol): $\bar{\nu}[cm^{-1}]$ = 3342, 3252 (amide NH); 1665 (amide).

Bis-1,2-(2-amino-2-methylpropanamido)benzene. The above product (77.18 g) was dissolved in EtOH (1.8 L), an aqueous solution of NaN_3 (*CAUTION!*) (30.56 g in 1.0 L) was added, and the mixture was heated under reflux (12 h). Solvent was removed under reduced pressure until precipitation was initiated. CH_2Cl_2 was immediately added to redissolve the trace precipitate. The CH_2Cl_2 layer was separated, the aqueous layer was washed with more CH_2Cl_2, and the combined CH_2Cl_2 extracts were dried over Na_2SO_4. The CH_2Cl_2 was again removed under reduced pressure until precipitation was

initiated, and EtOH was immediately added to redissolve the trace quantity of precipitate. The solution was again concentrated until precipitation initiated, and more EtOH was again immediately added to redissolve the trace quantity of precipitate. *CAUTION! NMR analysis was performed on 3 mg of isolated material. The bulk diazide product was not isolated.* [^{1}H NMR ($CDCl_3$): 8.65 (s, 2H, amide NH), 7.45 (m, 2H), 7.20 (m, 2H), 1.61 (s, 12H).] This solution was reduced in portions with H_2 in a bomb (50 psi) with 10% Pd/C. Because the reaction evolves one N_2 molecule for every H_2 molecule absorbed, frequent evacuation of the bomb and refilling with H_2 is advantageous (i.e., H_2 from the high pressure reservoir is not efficiently consumed). The mixture was filtered to remove the catalyst, the filtrate was taken to dryness, the resultant white solid was washed with pentane and then dried (30.145 g, 57.0% yield from dibromide). ^{1}H NMR ($CDCl_3$): 9.78 (br, 2H, amide NH), 7.61 (m, 2H), 7.19 (m, 2H), 1.88 (br, 4H, amine NH), 1.45 (s, 12H). Anal. Calcd: C, 60.41; H, 7.97; N, 20.13. Found: C, 60.40; H, 8.01; N, 19.86. IR (Nujol): $\bar{\nu}[cm^{-1}]$ = 3389, 3360, 3309, 3245, 3190 (amide and amine NH); 1665 (amide).

5,6:(Benzo)-3,8,11,13-tetraoxo-2,2,9,9-tetramethyl-12,12-diethyl -1,4,7,10-tetraazacyclotridecane: H_4DEMAMPA-B. Diamine (4.135 g) was split into four equal portions. The first portion was added to CH_2Cl_2 (700 mL), followed by Et_3N (2.0 mL) and diethylmalonyl dichloride (0.63 mL), and the reaction mixture was stirred (3 h). The remaining three portions were added sequentially with the equivalent portions of Et_3N and diethylmalonyl dichloride, waiting (3 h) between each addition. The reaction mixture was stirred (12 h) and then extracted twice with dilute aqueous HBr and twice with dilute aqueous Na_2CO_3. The CH_2Cl_2 solution was taken to

dryness under reduced pressure, and the solid was redissolved in a minimum of CH_2Cl_2 and applied to the top of a UV-transparent dry nylon column (3 cm diameter) packed to a 45 cm height with fluorescent silica gel (60 Å pore size, 75–150 micron mesh, 4% UV 254 indicator). TLC (developed with Et_2O) of the solution before it was applied to the column showed four spots with RF's of 0.42 (macrocycle), 0.54, 0.64, and 0.71 (diimide). The column was eluted with a 9:1 mixture of CH_2Cl_2/Et_2O until 400 mL had run through the bottom of the column. The first 200 mL contained nothing, the second 200 mL contained the diimide byproduct resulting from the addition of two molecules of diethylmalonyl dichloride to the diamine. [^{1}H NMR ($CDCl_3$): 8.55 (s, 2H, amide NH), 7.33 (m, 2H), 7.23 (m, 2H), 1.78 (s, 12H), 1.77 (q, 8H, 7.4 Hz), 1.05 (t, 12H, 7.4 Hz).] At this point, examination of the column with UV irradiation indicated that the macrocycle had separated from the other two byproducts. Elution was stopped, the column was turned on its side, and the macrocycle was separated by slicing the column 85 mm and 225 mm from the top. The silica gel in this 140 mm length of column was washed four times with boiling EtOH. The combined filtrates were taken to dryness under reduced pressure, yielding pure macrocycle as a white crystalline solid (1.451 g, 24.3%). ^{1}H NMR ($CDCl_3$): 7.55 (m, 2H), 7.48 (br, 2H, amide NH), 7.17 (m, 2H), 6.46 (br, 2H, amide NH), 2.07 (br, 4H), 1.60 (s, 12H), 0.89 (t, 6H, 7.1 Hz). ^{1}H NMR (CD_3OD): 7.42 (m, 2H), 7.22 (m, 2H), 2.12 (q, 4H, 7.3 Hz), 1.55 (s, 12H), 0.87 (t, 6H, 7.3 Hz). Anal. Calcd for H_4DEMAMPA-B·H_2O: C, 59.98; H, 7.67; N, 13.36. Found: C, 60.36; H, 7.24; N, 13.01 (H_2O found in NMR in addition to solvent background H_2O.). IR (Nujol): $\bar{\nu}[cm^{-1}]$ = 3395, 3363 (amide NH); 1702, 1680, 1652, 1635 (amide).

1,2-Dimethoxy-4,5-dinitrobenzene. *CAUTION: The nitration reaction must not be allowed to overheat; use a thermometer to ensure that the temperature does not rise above 30–40 °C.* 1,2-Dimethoxybenzene (24.2 g) and glacial acetic acid (73 mL) were placed in a 500 mL flask and cooled with an ice bath to 0°C. Using a dropping funnel, concentrated (70%) nitric acid (5.0 mL) was added dropwise; a dark yellow precipitate developed (1,2-dimethoxy-4-nitrobenzene). Fuming nitric acid (sp gr 1.50: 107 mL) was added dropwise (1–2 h). The precipitate slowly dissolved to give a yellow-orange solution, which was stirred (2 h). This solution was poured over 1.5 L of ice/water in a large beaker, mixed thoroughly, and allowed to stand until the ice had melted. The yellow solid was filtered off, washed with distilled water (until the pH of the washings was 4 or greater), and then dissolved in the minimum quantity of hot EtOH (about 750 mL) and left to crystallize overnight. The large yellow needles were filtered off and washed with small amounts of cold EtOH (32.4 g, 81%). Melting point: 129.5–130.5°C.

Bis-1,2-(2-bromo-2-methylpropanamido)-4,5-dimethoxybenzene. *The intermediate, 1,2-diamino-4,5-dimethoxybenzene, is sensitive to air oxidation; it keeps best if it is stored as the acid chloride, under N_2, at −20°C. Do not isolate—acylate immediately using the acid salt in solution.* 1,2-Dimethoxy-4,5-dinitrobenzene (10 g), MeOH (100 mL), and Pd/C catalyst (10% Pd, 0.3 g, slurried in MeOH) were placed in a bomb, and concentrated HCl (18 mL) was added. The mixture was hydrogenated (50 psi) until the pressure in the bomb stopped decreasing. The Pd/C was then filtered away, and the 1,2-diamino-4,5-dimethoxybenzene dihydrochloride solution was evaporated to dryness, dissolved in Et_3N (100 mL) and CH_2Cl_2 (400 mL), and

poured quickly into a 1 L flask equipped with a pressure-equalizing addition funnel, a reflux condenser, and a $CaCl_2$ drying tube. N_2 was blown through the flask to minimize air oxidation of the free diamine. The solution was dark greenish-brown. The flask was cooled using an ice bath, then 2-bromoisobutyryl bromide (35 mL) was added dropwise with stirring (2 h). The mixture was stirred overnight. The resulting solution was extracted three times with dilute HBr, then three times with aqueous Na_2CO_3. The organic layer was dried with Na_2SO_4, then filtered and evaporated to dryness. This gave a sticky, dark brown solid, which was stirred (8 h) with a 1:2 Et_2O/pentane mixture (600 mL), filtered, and air-dried to give a pale brown powder (11.3 g, 54% from 1,2-dimethoxy-4,5-dinitrobenzene). ^{1}H NMR ($CDCl_3$): 8.57 (s, 2H, amide NH), 7.00 (s, 2H), 3.84 (s, 6H), 2.03 (s, 12H). Anal. Calcd: C, 41.22; H, 4.76; N, 6.01. Found: C, 41.35; H, 4.75; N, 5.99. IR (Nujol): $\bar{\nu}[cm^{-1}] = 3301$ (amide NH); 1668 (amide).

Bis-1,2-(2-amino-2-methylpropanamido)-4,5-dimethoxybenzene. Bis-1,2-(2-bromo-2-methylpropanamido)-4,5-dimethoxybenzene (6.0 g) was stirred with EtOH (135 mL) in a 500 mL flask. A solution of NaN_3 (*CAUTION!*) (2.4 g, 0.037 mol) in distilled water (80 mL) was added, and the solution was heated under reflux overnight. The solution was evaporated under reduced pressure until precipitation initiated, then extracted with CH_2Cl_2. The organic layer was dried over Na_2SO_4 and filtered. EtOH (50 mL) was added and the CH_2Cl_2 removed under reduced pressure. More EtOH (80 mL) was added and evaporation continued to ensure all the CH_2Cl_2 had been removed. *CAUTION! NMR analysis was performed on 3 mg of isolated material. The bulk diazide product was not isolated.* [^{1}H NMR ($CDCl_3$): 8.62 (s, 2H,

amide NH), 7.05 (s, 2H), 3.87 (s, 6H), 1.67 (s, 12H).] The solution was diluted to 350 mL with EtOH, then aqueous 23% $(NH_4)_2S$ solution was added (11.2 mL) under N_2. The mixture was stirred (36 h). The reaction solution was evaporated to dryness and CH_2Cl_2 (160 mL) was added. This solution was cooled to 0–5 °C (ice/water bath), then extracted twice with ice-cold 1 M aqueous NaOH. The organic phase was separated, dried with Na_2SO_4, filtered, and evaporated to dryness. The product was stirred for several hours in a mixture of CH_2Cl_2 (20 mL) and Et_2O (100 mL), then the pale brown solid was filtered off and washed with a small amount of CH_2Cl_2 (1.9 g, 44% from diamide dibromide). ^{1}H NMR ($CDCl_3$): 9.62 (s, 2H, amide NH), 7.15 (s, 2H), 3.82 (s, 6H), 1.94 (s, 4H, amine NH), 1.40 (s, 12H). A sample uncontaminated with sulfur suitable for analysis was prepared by hydrogenating the diazide with Pd/C (10%) at 50 psi in EtOH. Anal. Calcd: C, 56.79; H, 7.74; N, 16.56. Found: C, 57.04; H, 7.80; N, 15.92. IR (Nujol): $\bar{\nu}[cm^{-1}]$ = 3396, 3362, 3265 (amide and amine NH); 1651 (amide).

5,6:(4,5-dimethoxybenzo)-3,8,11,13-tetraoxo-2,2,9,9-tetramethyl-12,12-diethyl-1,4,7,10-tetraazacyclotridecane: H_4DEMAMPA-DMOB. CH_2Cl_2 (400 mL) was placed in the reaction vessel. The reagents were added in four portions, separated by four-hour intervals. At each addition, bis-1,2-(2-amino-2-methylpropanamido)- 4,5-dimethoxybenzene (0.48 g), Et_3N (0.78 mL), and diethylmalonyl dichloride (0.26 mL) were added. After the last addition, stirring was continued overnight. The solution was extracted three times with dilute HBr and three times with aqueous Na_2CO_3, then the organic layer was dried with Na_2SO_4, filtered, and evaporated to dryness. The pure compound was isolated by repeated recrystallization from

CH_2Cl_2/pentane. The product was an off-white microcrystalline solid (0.605 g, 23.1%). ^1H NMR (CD_2Cl_2): 7.26 (s, 2H, amide NH), 7.01 (s, 2H), 6.41 (s, 2H, amide NH), 3.80 (s, 6H), 2.07 (br, 4H), 1.54 (s, 12H), 0.90 (t, 6H). Anal. Calcd for H_4DEMAMPA-DMOB·1/3H_2O: C, 58.96; H, 7.46; N, 11.96. Found: C, 58.90; H, 7.26; N, 11.76 (1/3H_2O found in NMR in addition to solvent background H_2O.). IR (Nujol): $\bar{\nu}[cm^{-1}]$ = 3451, 3391, 3347 (amide NH); 1695, 1670, 1655 (amide).

References

1. Macrocyclic chemistry is one of the most mature subdivisions of the general area of host-guest chemistry. For comprehensive treatises, see: (a) Gokel; Korzeniowski "Macrocyclic Polyether Syntheses"; Springer- Verlag: New York, 1982. (b) Izatt, R. M.; Christensen, J. J. (Eds.) "Synthetic Multidentate Macrocyclic Compounds"; Academic Press: New York, 1978. (c) Izatt, R. M.; Christensen, J. J. (Eds.) "Progress in Macrocyclic Chemistry", vol. 1; Wiley-Interscience: New York, 1979. (d) Izatt, R. M.; Christensen, J. J. (Eds.) "Progress in Macrocyclic Chemistry", vol. 2; Wiley-Interscience: New York, 1981. (e) Izatt, R. M.; Christensen, J. J. (Eds.) "Progress in Macrocyclic Chemistry", vol. 3; Wiley-Interscience: New York, 1987. (f) Keehn, P. M.; Rosenfeld, S. M. (Eds.) "Cyclophanes", vols. I and II; Academic Press: New York, 1983. (g) Lehn, J. M. In "Structure and Bonding", vol. 16; Springer-Verlag: New York, 1973. (h) Lindoy, L. F. "The Chemistry of Macrocyclic Ligand Complexes"; Cambridge University Press: New York, 1989. (i) Melson, G. A. (ed.) "Coordination Chemistry of Macrocyclic Compounds" Plenum Press: New York, 1979. (j) Patai, S. (Ed.) "The Chemistry of Ethers, Crown Ethers, Hydroxyl Groups, and their Sulfur Analogues"; Wiley: New York, 1980. (k) Vögtle, F.; Weber, E. (Eds.) "Host Guest Complex Chemistry Macrocycles"; Springer-Verlag: New York, 1985. (l) Vögtle, F. (Ed.) "Topics in Current Chemistry: Host Guest Complex Chemistry II", vol. 101; Springer-Verlag: New York, 1982. (m) Vögtle, F. (Ed.) "Topics in Current Chemistry: Cyclophanes I", vol. 113; Springer-Verlag: New York, 1983. (n) Vögtle, F. (Ed.) "Topics in Current Chemistry: Cyclophanes II", vol. 115; Springer-Verlag: New York, 1983.

2. The alkali metal/alkaline earth templates are based primarily on electrostatic attractions between the cation and the negative ends of ligand donor atom dipoles. These template cations are typically used to synthesize polyether hosts. See reference 1 and: (a) Mandolini, L.; Masci, B. *J. Am. Chem. Soc.* **1977**, *99*, 7709. (b) Greene, R. N. *Tetrahedron Lett.* **1972**, 1793.

3. For Stoddart's recent work with donor-acceptor catenanes and molecular belts, see: (a) Ashton, P. R.; Isaacs, N. S.; Kohnke, F. H.; Mathias, J. P.; Stoddart, J. F. *Angew. Chem. Int. Ed. Engl.* **1989**, *28*, 1258–1261. (b) Ashton, P. R.; Isaacs, N. S.; Kohnke, F. H.; Stagno D' Alcontres, G.; Stoddart, J. F. *Angew. Chem. Int. Ed. Engl.* **1989**, *28*, 1261–1263. (c) Kohnke, F. H.; Mathias, J. P.; Stoddart, J. F. *Angew. Chem. Int. Ed. Engl.* **1989**, *28*, 1103–1110. (d) Ortholand, J.-Y.; Slawin, A. M. Z.; Spencer, N.; Stoddart, J. F.; Williams, D. J. *Angew. Chem. Int. Ed. Engl.* **1989**, *28*, 1394–1395. (e) Ashton, P. R.; Goodnow, T. T.; Kaifer, A. E.; Reddington, M. V.; Slawin, A. M. Z.; Spencer, N.; Stoddart, J. F.; Vicent, C.; Williams, D. J. *Angew. Chem. Int. Ed. Engl.* **1989**, *28*, 1396–1399.

4. McMurry, T. J.; Rodgers, S. J.; Raymond, K. N. *J. Am. Chem. Soc.* **1987**, *109*, 3451–3453.

5. Melson, G. A.; Busch, D. H. *J. Am. Chem. Soc.* **1964**, *86*, 4834–4837.

6. (a) Ogawa, S. *J. Chem. Soc., Perkin Trans. 1* **1977**, 214–216. (b) Ogawa, S.; Yamaguchi, T.; Gotoh, N. *J. Chem. Soc., Perkin Trans. 1* **1974**, 976–978. (c) Owston, P. G.; Peters, R.; Ramsammy, E.; Tasker, P. A.; Trotter, J. *J. Chem. Soc., Chem. Commun.* **1980**, 1218–1220.

7. Vellacio, F. Jr.; Punzar, R. V.; Kemp, D. S. *Tetrahedron Lett.* **1977**, 547–550.

8. (a) Mock, W. L. Ph. D. Thesis, Harvard University, 1964. (b) Collins, T. J.; Richmond, T. G.; Santarsiero, B. D.; Treco, B. G. R. T. *J. Am. Chem. Soc.* **1986**, *108*, 2088–2090. (c) Treco, B. G. R. T. Ph.D. Thesis, California Institute of Technology, 1988.

9. Keech, J. T. Ph. D. Thesis, California Institute of Technology, Aug. 1986.

10. For documentation of a recent violent explosion involving the distillation of an organic azide, see reference (a). For more documentation on azide hazards, see reference (b). (a) Tobias, B. I. *Chem. Eng. News* **1991**, March 11, 2. (b) *Bretherick's Handbook of Reactive Chemical Hazards*, 4th ed.; Butterworth-Heinemann: Stoneham, MA, 1990.

11. (a) Rylander, P. N. *Catalytic Hydrogenation in Organic Syntheses*; Academic Press: New York, 1979. (b) Freifelder, M. *Catalytic Hydrogenation in Organic Synthesis. Procedures and Commentary*; John Wiley and Sons: New York, 1978.

12. For leading references, see: (a) Etter, M. C. *Acc. Chem. Res.* **1990**, *23*, 120–126. (b) Baker, E. N.; Hubbard, R. E. *Prog. Biophys. Molec. Biol.* **1984**, *44*, 97–179.

13. (a) Dado, G. P.; Desper, J. M.; Gellman, S. H.; *J. Am. Chem. Soc.* **1990**, *112*, 8630–8632. (b) see also: Gellman, S. H.; Dado, G. P.; Liang, G.-B.; Adams, B. R. *J. Am. Chem. Soc.* **1991**, *113*, 1164–1173 and references therein.

14. (a) Hackbart, W.; Hartmann, M. *J. Prakt. Chem.* **1961**, *September*, 1–3.

15. (a) Goldberg, I. *Chem. Ber.* **1907**, *40*, 4541. (b) Freeman, H. S.; Butler, J. R.; Freedman, L. D. *J. Org. Chem.* **1978**, *43*, 4975–4978. (c) Yamamoto,

T.; Kurata, Y. *Chem. Ind.* **1981**, 737–738. (d) Lindley, J. *Tetrahedron* **1984**, *40*, 1433–1456.

16. Bayley, H.; Standring, D. N.; Knowles, J. R. *Tetrahedron Lett.* **1978**, 3633–3634.

17. Buchler, J. W. In *The Porphyrins*; Dolphin, D., Ed.; Academic Press: New York, 1978; Chapter 10.

18. For a review of work performed with macrocyclic ligands containing one, two, or three amides see Kimura, E. *J. Coord. Chem.* **1986**, *15*, 1–28.

19. (a) Margerum, D. W.; Rybka, J. S. *Inorg. Chem.* **1980**, *19*, 2784–2790. (b) Rybka, J. S.; Margerum, D. W. *Inorg. Chem.* **1981**, *20*, 1453–1458.

20. This methodology is vaguely similar to that reported by Bartlett and Power in the synthesis of two-coordinate iron and cobalt complexes: Bartlett, R. A.; Power, P. P. *J. Am. Chem. Soc.* **1987**, *109*, 7563–7564.

21. Drake, N. L.; Anspon, H. D.; Draper, J. D.; Haywood, S. T.; Van Hook, J.; Melamed, S.; Peck, R. M.; Sterling, J.; Walton, E. W.; Whiton, A. *J. Am. Chem. Soc.* **1946**, *68*, 1536–1543.

22. (a) Collins, T. J.; Powell, R. D.; Slebodnick, C.; Uffelman, E. S. *J. Am. Chem. Soc.* in press. (b) Collins, T. J.; Kostka, K. L.; Uffelman, E. S. *Inorg. Chem.* in press.

23. Collins, T. J.; Nichols, T. R.; Uffelman, E. S. *J. Am. Chem. Soc.* **1991**, *113*, 4708–4709.

24. Collins, T. J.; Gordon-Wylie, S. W.; Paterno, S. to be published.

Chapter 3

Stable Chromium(V) Monooxo Complexes of Macrocyclic Tetraamido-*N* Ligands and a New ^{18}O-Labeling Reagent

Chromium(VI) oxo compounds are among the classic reagents available to perform oxidations of organic substrates in academic laboratories. The use of chromium(VI) synthetic reagents has been well reviewed,[1] as have been the structure, bonding, and reactivity of Cr(IV), Cr(V), and Cr(VI) oxo complexes.[2] Much early interest in Cr(V) arose as a result of its intermediacy in organic oxidations, and the coordination chemistry of Cr(V) has been recently reviewed.[3] Cr(V) monooxos have been demonstrated to be involved in catalytic oxidation of phosphines[4] and catalytic epoxidation of olefins.[5] Of the thirteen chromium oxo complexes crystallographically characterized to date, there have been five of Cr(VI),[6] six of Cr(V)[7], and two of Cr(IV).[8] Recently, Cr(V) has attracted attention because of postulates that Cr(V) intermediates are the real carcinogens in carcinogenic Cr(VI) species.[9] An objective of the Collins research program is to understand how the structural and electronic properties of specifically designed ancillary ligand complements affect the properties of new metal oxo species. It was found that the macrocyclic tetraamide ligands yielded indefinitely stable five-coordinate Cr(V) monooxos which are remarkable in being unreactive even with oxophilic reducing agents such as triphenylphosphine. These results confirm the high donor capacity of these macrocyclic ligands. In order to expand the number of ^{18}O-labeling reagents available for synthesizing terminal oxo ligands, a new ^{18}O-labeling reagent was developed. The crystal structures of the Cr(V) oxo complexes revealed nonplanar amides.

Background

The first stable Cr(V) monooxo was reported in 1978 (Figure 3.1) and

prepared by the reaction shown below.[7d]

$$2HCrO_4^- + 4C_2H_5(CH_3)C(OH)COOH + 4H^+ \longrightarrow$$

$$[(C_2H_5(CH_3)COCO_2)_2CrO]^- + Cr^{3+} + 2CH_3COC_2H_5 + 2CO_2 + 7H_2O$$

Clearly, starting with Cr(VI), 2-hydroxy-2-methylbutyric acid serves as both the reducing agent and the ligand in the reaction. The potassium salt of the complex was crystallographically characterized. The Cr–O bond distance of 1.554(14) is in between the current range of values found (1.519(12)[7e]–1.594(3)[7b]), as is the Cr–O stretching frequency of 994 cm^{-1} (910 cm^{-1}[7e]–1026 cm^{-1}[15a]). The EPR spectrum consisted of a sharp, single line at g=1.978 (I=0 for ^{52}Cr) and four hyperfine lines (9.55% ^{53}Cr, I=3/2, coupling constant not published).

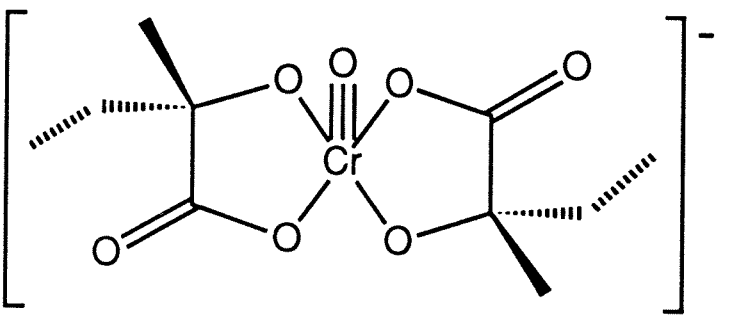

Figure 3.1. The first stable Cr(V) monooxo complex.

The first Cr(V) monooxo complex to be prepared by air oxidation was $[(Cp^*CrO)_2(\mu\text{-}O)_2]$, which contains a metal-metal single bond (Figure 3.2).[7e] It was prepared by stirring $[Cp^*Cr(CO)_2NO]$ for several hours in toluene saturated with O_2. The relatively long Cr–O bond of 1.594(3) Å and the relatively low energy Cr–O stretching frequency of 910 cm^{-1} can be ascribed to the *trans* bonding of the Cp* ring. Due to the metal-metal bond, the complex is diamagnetic.

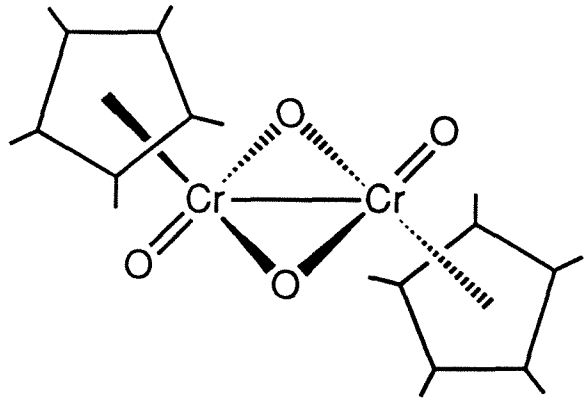

Figure 3.2. The first Cr(V) monooxo prepared from molecular oxygen.

In 1988, the Rauchfuss group demonstrated that Cr(V) may be used to perform catalytic oxygenations of substrates using molecular oxygen.[4] When dry O_2 is admitted to CH_2Cl_2 solutions of *trans*-[Cp*CrBr(μ-Br)]$_2$, Cp*CrOBr$_2$ forms in minutes (Figure 3.3).[4] Solutions 0.003 M in starting dimer and 0.25 M in PPh_3 exhibit an initial turnover number of 27 phosphines/20 min at 20 °C, yielding the phosphine oxides. Cp*CrOBr$_2$ does not oxygenate Et_2S, but CpCrOBr$_2$ does. Although the oxidation of phosphines is not a significant accomplishment, the repeated activation of molecular oxygen by a chromium organometallic complex is. The Cr–O bond distance of 1.58(2) Å and the Cr–O stretch of 934 cm^{-1} for Cp*CrOBr$_2$ is not surprising, given the similarities with [(Cp*CrO)$_2$(μ-O)$_2$].

In 1979, the Groves group studied the reactions of chlorotetraphenylporphinatochromium(III) (Cr^{III}TPPCl) with iodosylbenzene as a means of providing synthetic mimics of peroxidases and monooxygenases Figure 3.4.[5a] In the absence of substrate, the reaction generated [Cr^{V}(O)TPP]$^+$, which was stable in solution for several hours at room temperature. In the presence of olefin and iodosylbenzene, Cr^{III}TPPCl catalyzed epoxide formation. The Cr–

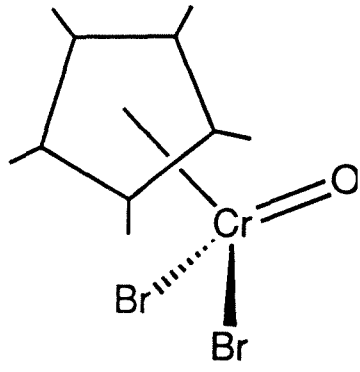

Figure 3.3. The first Cr(V) monooxo complex which could be employed in a catalytic cycle involving the activation of molecular oxygen.

O stretch was found to be 1026 cm^{-1}, higher than found in the organometallic complexes presumably because of the absence of a *trans* ligand. The EPR spectrum exhibited a nine line pattern at g=1.982 due to superhyperfine interactions with four spectroscopically equivalent nitrogens (a=2.85 gauss) and four nine line satelites due to hyperfine interactions (9.55% ^{53}Cr, I=3/2, a=23 gauss).[10] Detailed EPR studies have been performed on the analogous nitride complexes.[11] A crystal structure was subsequently performed on Cr^{IV}TPPO (Cr–O: 1.572(6) Å, Cr–N: 2.028(8), 2.031(7), 2.032(7), and 2.037(8) Å).[8a] The Cr atom sat 0.469 Å above the mean plane of the ligand donor atoms.

In 1985, the Kochi group published studies of the mechanism of chromium-catalysed epoxidations of olefins with iodosylbenzene using Salen ligands.[5b] Two crystal structures were performed. The structure of the five-coordinate cation (Figure 3.5) has a Cr–O bond distance of 1.545(2) Å and Cr–N bond distances of 1.969(2) and 1.991(2) Å.[7c] The Cr atom sits 0.533(1) Å above the mean plane of the Salen donors. The structure of the six-coordinate cation (Figure 3.6) has a Cr–O bond distance of 1.554(4) Å and Cr–N bond distances of 2.017(6) and 1.960(6) Å.[7c] The Cr atom sits 0.259(1) Å above the mean

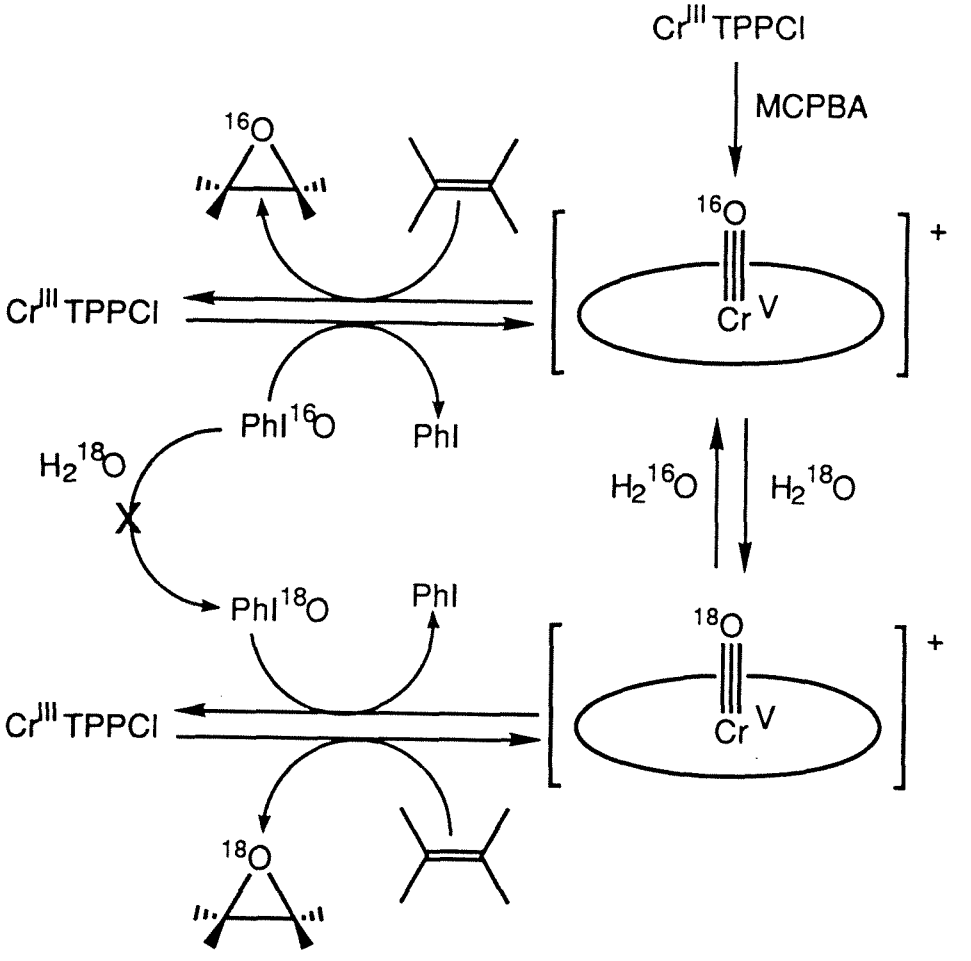

Figure 3.4. Groves mechanism for the CrTPPCl-catalyzed epoxidation of olefins with iodosylbenzene (TPP=tetraphenylporphyrin).

plane of the Salen donors. Depending on the Salen derivative used, the Cr–O stretch varied between 985–1007 cm^{-1}. The EPR exhibited a g value of 1.978, with a_N varying between 2.05–2.18 G, and a_{Cr} varying between 19.25–19.90 G, depending on the Salen derivative. In reactivity studies, it was found that the reactivity of the oxo complex with olefins was substantially increased in the presence of donor ligands.

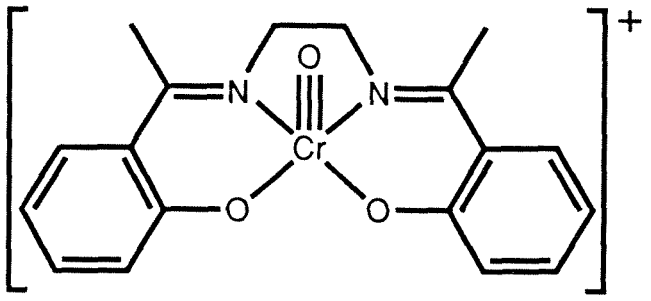

Figure 3.5. A five-coordinate cationic Cr(V) monooxo complex.

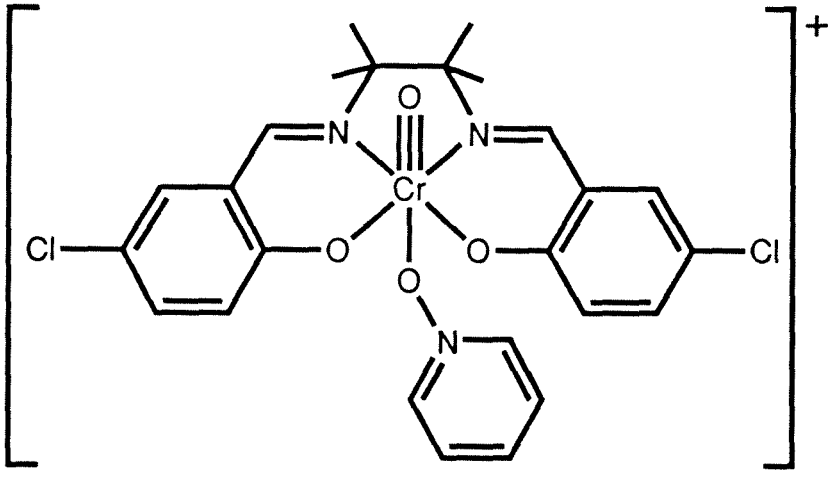

Figure 3.6. A six-coordinate cationic Cr(V) monooxo complex.

Results and Discussion

Because of the significance of chromium complexes to oxidation chemistry, the Collins group has had a long interest in further developing the high oxidation state chemistry of this element. Regrettably, as discussed in Chapter 1, some of the acyclic ligands which had been previously employed did not lead to the desired tetradentate mononuclear complexes, but led instead to dimeric compounds which featured both N- and O-bound amido donors. The macrocycles are constrained to be incapable of yielding dimeric complexes of this nature. Thus, employing the general synthetic method outlined in Chapter 2 generates intermediate Cr(II) complexes which are not isolated, but oxidized

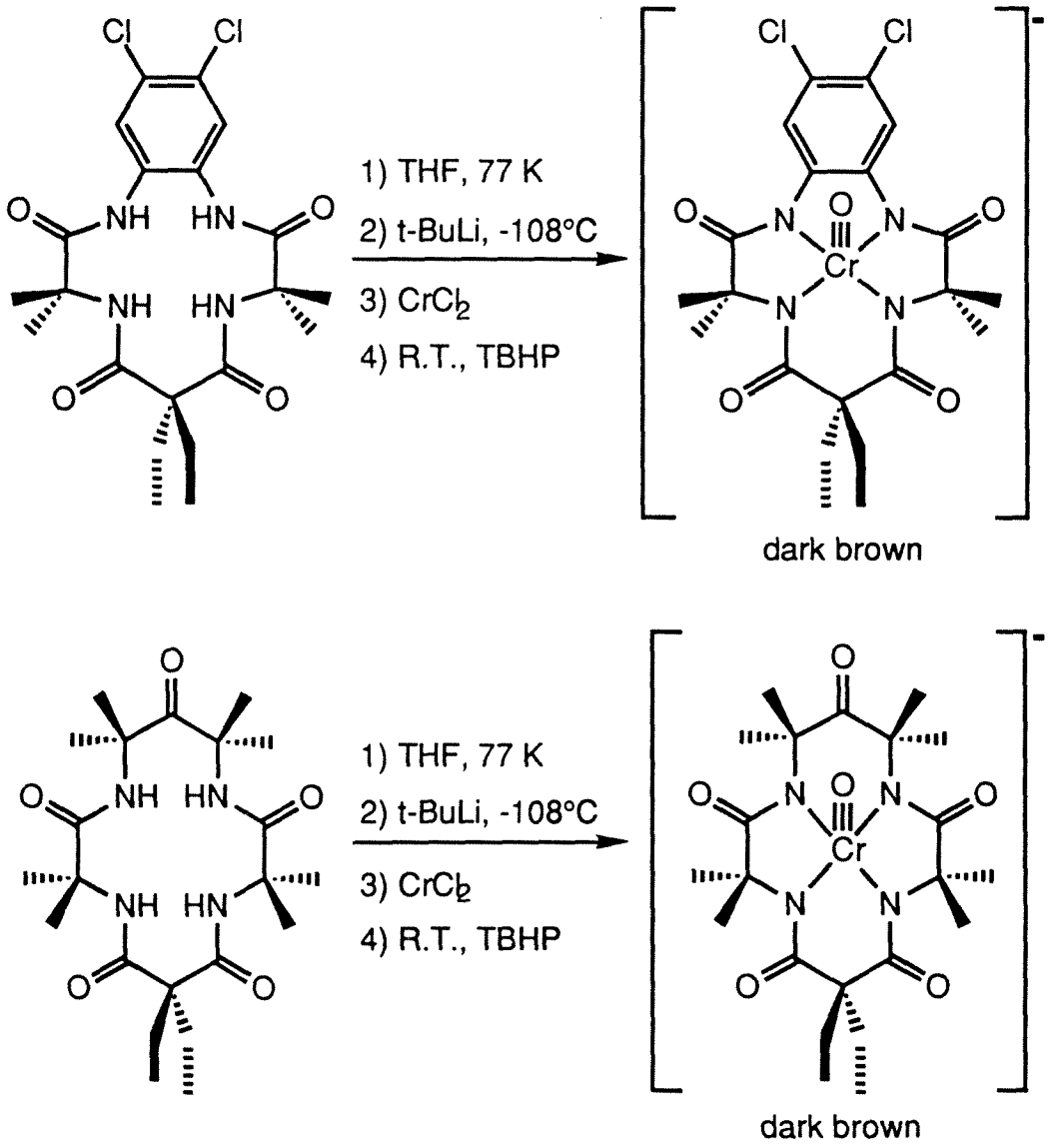

Figure 3.7. Syntheses of the five-coordinate Cr(V) monooxo complexes.

to the five-coordinate Cr(V) monooxos with TBHP (Figure 3.7).

The syntheses of the chromium(V) oxo complexes proceed in good yields. Obtaining the ^{18}O-labeled oxo complexes was an important goal. Both oxo complexes are stable in water, and the $[Me_4N]^+$ salts show no decomposition after standing as solutions in water for many weeks. Exchange of the ^{16}O-oxo

ligand with ^{18}O-labeled water is very slow under these conditions. Because of these factors, and because there is intrinsic value in developing new reagents for ^{18}O-labeling (many interesting oxo complexes are not water stable and are thus not amenable to oxo exchange), we decided to develop an ^{18}O-analogue of TBHP. The synthesis of TBHP involves conditions which are inappropriate and unavailable in most academic laboratories. Furthermore, TBHP is a liquid. This is a disadvantage because ^{18}O-reagents are expensive, and one would like to prepare analytically pure solids which can be crystallized and weighed accurately on milligram scales. However, 2,5-dihydroperoxy-2,5-dimethylhexane seemed like an excellent alternative. It possesses steric properties very similar to those of TBHP, the ^{16}O-version had been synthesized under relatively moderate conditions, and it is a solid at room temperature.[12] The much milder conditions which can be used to synthesize 2,5-dihydroperoxy-2,5-dimethylhexane compared to TBHP can be easily understood. First, 2,5-dimethylhexane has a much higher boiling point than methylpropane, thus, for any given temperature, 2,5-dimethylhexane will have a lower vapor pressure. Second, and most importantly, autoxidation of tertiary hydrocarbons proceeds by a radical chain mechanism which can be described by the following equations.*

$$In_2 \xrightarrow{R_i} 2In\cdot \qquad (1)$$

$$In\cdot + RH \longrightarrow InH + R\cdot \qquad (2)$$

$$R\cdot + O_2 \longrightarrow RO_2\cdot \qquad (3)$$

$$RO_2\cdot + RH \xrightarrow{k_p} RO_2H + R\cdot \qquad (4)$$

* This information is abstracted from the excellent discussion in reference 1(b).

$$R\cdot + RO_2\cdot \longrightarrow RO_2R \quad (5)$$

$$2RO_2\cdot \xrightarrow{2k_t} RO_4R \quad (6)$$

$$RO_4R \longrightarrow O_2 + \text{nonradical products} \quad (7)$$

The chain propagation step is usually critical. For 2,5-dimethylhexane the intermediate peroxy radical may smoothly abstract a hydrogen atom intramolecularly, because the reaction may be viewed as passing through a seven-membered ring transition state (Figure 3.8). This leads to highly efficient chain propagation. Under the conditions of this reaction, In_2 of equation 1 is adventitious peroxide in the starting hydrocarbon, at greater than 100 torr O_2 equation 3 is diffusion controlled, and the rate limiting step is hydrogen abstraction, equation 4. At greater than 100 torr O_2, equation 5 may be ignored. For tertiary hydrocarbons the nonradical products of equation 7 are dialkylperoxides. The alkylperoxy radical is relatively stable and is therefore selective (ROO–H bond strength = 90 kcal/mol). Because the bond strengths of the primary, secondary, and tertiary C–H bonds are 99, 94, and 90 kcal/mol, respectively, the autoxidations give high yields of alkylhydroperoxides at low hydrocarbon conversions. (The relative rates of attack at the primary, secondary, and tertiary C–H bonds of 2-methylpentane are 1:30:300 for alkylperoxy radicals.)

The synthetic procedure employed was a modification of the published procedure which involved the production of 400 g quantities of diperoxide. Aside from safety concerns, the amount of $^{18}O_2$ required would be prohibitively expensive. A simple procedure was found which conveniently yields the ^{18}O-labeled diperoxide in 300 mg analytically pure crystalline lots. The compound

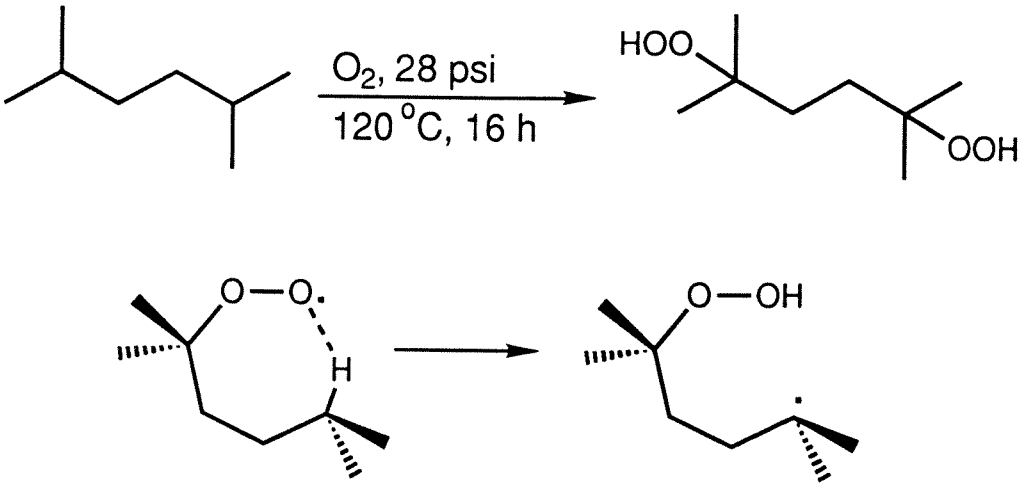

Figure 3.8. Synthetic conditions for producing 2,5-dihydroperoxy-2,5-dimethylhexane. The intramolecular hydrogen abstraction is also depicted.

seems to be very safe to work with and is stable for months at room temperature without observable decomposition.

As expected, 2,5-dihydroperoxy-2,5-dimethylhexane exhibits reactivity similar to TBHP and may be used to produce the ^{18}O-labeled oxos in high yield. The $\nu_{Cr\equiv{}^{16}O}$ band of $[(CH_3)_4N][Cr(O)(\eta^4\text{-DEMAMPA-DCB})]$ at 982 cm^{-1} is found at 944 cm^{-1} in the ^{18}O-labeled analogue. The $\nu_{Cr\equiv{}^{16}O}$ stretch of $[(CH_3)_4N][Cr(O)(\eta^4\text{-MAC*})]$ at 982 cm^{-1} is shifted by ^{18}O-labeling to 941 cm^{-1}. These results were confirmed by resonance Raman spectroscopy.[13]

Both complexes were crystallographically characterized (Figures 3.9 and 3.10). For $[(CH_3)_4N][Cr(O)(\eta^4\text{-DEMAMPA-DCB})]$ and $[(CH_3)_4N]$-$[Cr(O)(\eta^4\text{-MAC*})]$, the Cr≡O bond lengths are 1.569(2) Å and 1.580(6) Å, respectively, typical for the chromium(V) oxo triple bond. For $[(CH_3)_4N][Cr(O)(\eta^4\text{-DEMAMPA-DCB})]$, the four nitrogens lie in a plane (largest deviation 0.006 Å) with the chromium located 0.60 Å above the mean

plane, nearly equidistant from all four nitrogens. The entire chelate system remains virtually planar. For $[(CH_3)_4N][Cr(O)(\eta^4\text{-MAC*})]$, the four nitrogens alternate 0.12 Å above and below their mean plane, and the chromium sits 0.58 Å above the mean plane. All four amides in $[(CH_3)_4N][Cr(O)(\eta^4\text{-MAC*})]$ are nonplanar (see Chapter 9).

When a high oxidation state compound has been prepared, it is important to consider that ligand noninnocence, the ability of a ligand to become part or all of the redox active site of a complex, may be operative. The formal oxidation state of +V can be assigned to the chromium center in $[(CH_3)_4N][Cr(O)(\eta^4\text{-MAC*})]$ since $[\eta^4\text{-MAC*}]^{4-}$ is technically an innocent ligand. However, for $[(CH_3)_4N][Cr(O)(\eta^4\text{-DEMAMPA-DCB})]$, other resonance structures in which electrons are transferred from the ring to the metal with a reduction of the formal oxidation state at the metal center are possible contributors to an accurate resonance hybrid. The relevant structural, vibrational, and EPR properties of the compounds indicate that the assignment of the +V oxidation state to the chromium center is equally appropriate in both cases.

It is useful to compare the structural data for $[(CH_3)_4N][Cr(O)(\eta^4\text{-DEMAMPA-DCB})]$ with the structural data for two of the cobalt complexes (see Chapter 6). The cobalt chemistry of $(\eta^4\text{-DEMAMPA-DCB})^{4-}$ has allowed us to characterize complexes in which the ligand noninnocence plays a large factor in oxidations of the complexes (see Chapter 6). The structurally characterized square planar anion, $[Co(\eta^4\text{-DEMAMPA-DCB})]^-$, is clearly best described as Co(III), but the oxidation state of the structurally characterized square planar neutral molecule, $Co(\eta^4\text{-DEMAMPA-DCB})$, is ambiguous (see Chapter 6). In $[(CH_3)_4N][Cr(O)(\eta^4\text{-DEMAMPA-DCB})]$ and the Co anion,

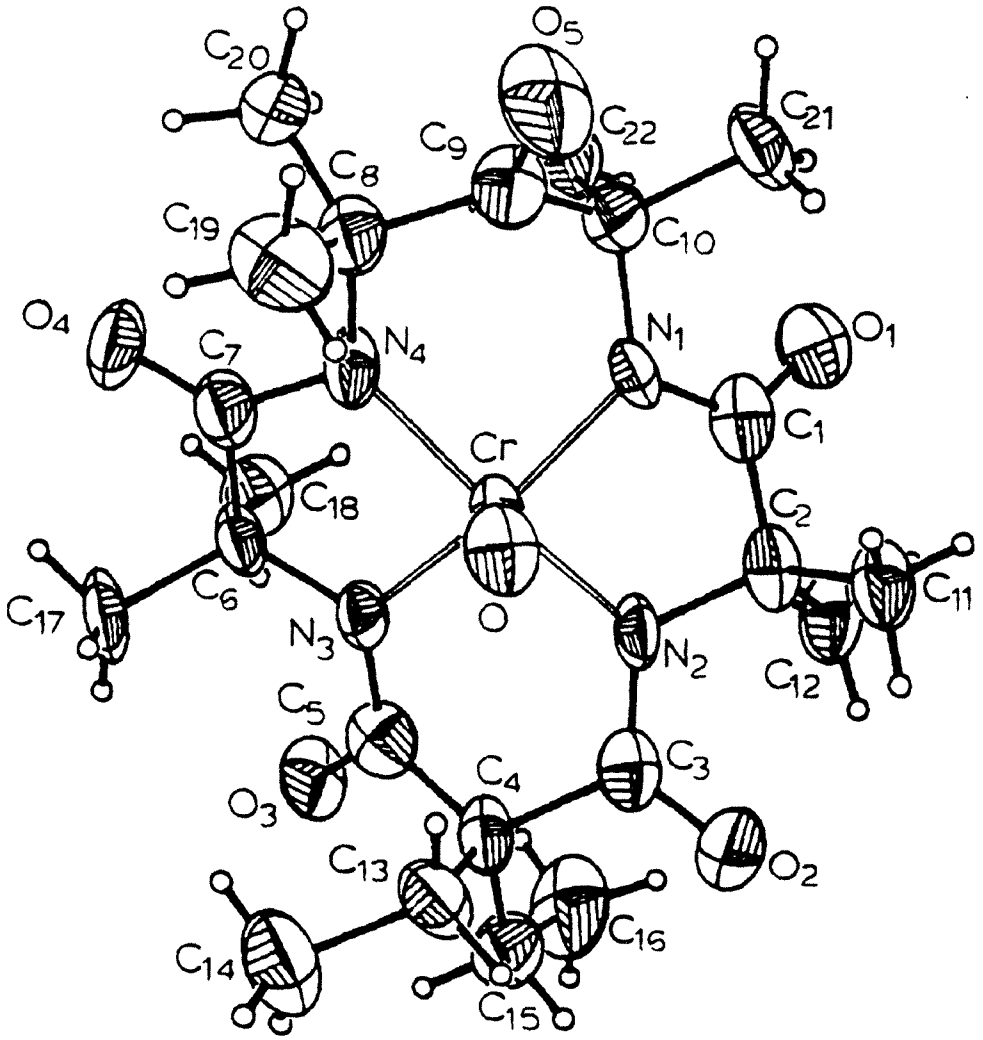

Figure 3.9. Molecular structure of $[Cr(O)(\eta^4\text{-MAC*})]^-$. ORTEP drawing with all nonhydrogen atoms drawn to encompass 50% of electron density.

Table 3.1. Bond Lengths in $[Cr(O)(\eta^4\text{-MAC*})]^-$			
Atoms	Length (Å)	Atoms	Length (Å)
CrO	1.580(6)	CrN1	1.917(6)
CrN2	1.948(7)	CrN3	1.941(5)
CrN4	1.957(7)	O1C1	1.24(1)
O2C3	1.25(1)	O3C5	1.23(1)

Table 3.1. Bond Lengths in $[Cr(O)(\eta^4\text{-MAC*})]^-$ (continued)			
Atoms	Length (Å)	Atoms	Length (Å)
O4C7	1.21(1)	O5C9	1.23(1)
N1C1	1.37(1)	N2C3	1.34(1)
N3C5	1.35(1)	N4C7	1.37(1)
N1C10	1.50(1)	N2C2	1.48(1)
N3C6	1.47(1)	N4C8	1.48(1)
C1C2	1.52(1)	C3C4	1.55(1)
C4C5	1.51(1)	C6C7	1.52(1)
C8C9	1.53(1)	C9C10	1.52(1)
C2C11	1.54(1)	C2C12	1.51(1)
C4C13	1.55(1)	C4C15	1.55(1)
C13C14	1.54(1)	C6C17	1.53(1)
C6C18	1.53(1)	C8C19	1.52(1)
C8C20	1.56(1)	C10C21	1.57(1)
C15C16	1.51(1)	C10C22	1.53(1)

Table 3.2. Bond Angles in $[Cr(O)(\eta^4\text{-MAC*})]^-$			
Atoms	Angle (°)	Atoms	Angle (°)
OCrN1	109.1(3)	OCrN2	103.6(3)
OCrN3	113.5(3)	OCrN4	103.0(3)
N1CrN2	82.0(3)	N1CrN3	137.4(3)
N1CrN4	89.3(3)	N2CrN3	87.5(3)
N2CrN4	153.3(3)	N3CrN4	81.9(3)
CrN1C1	116.2(5)	CrN1C10	124.9(5)

Table 3.2. Bond Angles in [Cr(O)(η^4-MAC*)]$^-$ (continued)			
Atoms	Angle (°)	Atoms	Angle (°)
CrN3C5	125.8(5)	CrN3C6	115.9(5)
CrN2C2	115.4(5)	CrN2C3	122.0(5)
CrN4C7	117.0(6)	CrN4C8	120.4(5)
C1N1C10	117.6(7)	C5N3C6	117.5(6)
C2N2C3	118.4(7)	C7N4C8	117.4(6)
O1C1N1	125.8(9)	O1C1C2	121.0(8)
N1C1C2	113.1(7)	O2C3N2	124.3(8)
O2C3C4	118.0(8)	N2C3C4	117.7(8)
O3C5N3	122.3(8)	O3C5C4	118.9(7)
N3C5C4	118.5(7)	N2C2C1	104.8(7)
N2C2C11	112.7(7)	N2C2C12	111.7(7)
C1C2C11	105.6(7)	C1C2C12	111.0(8)
C11C2C12	110.8(7)	C3C4C5	114.6(8)
C3C4C13	107.3(6)	C3C4C15	106.6(7)
O4C7N4	124.3(8)	O4C7C6	123.7(7)
N4C7C6	112.0(7)	O5C9C8	118.2(7)
O5C9C10	118.4(7)	C8C9C10	122.8(7)
N1C10C9	107.4(7)	N1C10C21	108.8(7)
N1C10C22	110.8(6)	C9C10C21	106.8(7)
C9C10C22	111.3(7)	C21C10C22	111.6(7)
C4C13C14	115.0(7)	C4C15C16	115.0(8)
C5C4C13	110.4(6)	C5C4C15	109.0(7)
C13C4C15	108.8(7)	N3C6C7	108.4(6)

Table 3.2. Bond Angles in [Cr(O)(η^4-MAC*)]$^-$ (continued)			
Atoms	Angle (°)	Atoms	Angle (°)
N3C6C17	113.0(7)	N3C6C18	113.1(6)
C7C6C17	104.6(6)	C7C6C18	106.2(7)
C17C6C18	110.9(6)	N4C8C9	107.8(6)
N4C8C19	110.7(7)	N4C8C20	114.6(7)
C9C8C19	109.9(7)	C9C8C20	104.3(7)
C19C8C20	109.3(7)		

the average distances for the N1–C9 and N4–C8 bonds are identical (1.41 Å) and are consistent with a C–N single bond. For the Co neutral, this bond distance is 1.353(6) Å, indicating the presence of some double bond character. For [$(CH_3)_4N$][Cr(O)(η^4-DEMAMPA-DCB)] and the Co anion, the aromatic C–C bonds alternate no more than 0.02 Å in distance, while for the Co neutral, these bond distances alternate as much as 0.07 Å. In the infrared, [$(CH_3)_4N$][Cr(O)(η^4-DEMAMPA-DCB)] and the Co anion are very similar in the region between 1550–1750 cm^{-1}. [$(CH_3)_4N$][Cr(O)(η^4-DEMAMPA-DCB)] has IR stretches at 1656, 1601, and 1575 cm^{-1} ([$(CH_3)_4N$][Cr(O)(η^4-MAC*)] has a ketone stretch at 1714 cm^{-1} and two very broad stretches at 1609 and 1585 cm^{-1}.). The anion, [Co(η^4-DEMAMPA-DCB)]$^-$, has IR stretches at 1648, 1593, 1571 cm^{-1}. In contrast, Co(η^4-DEMAMPA-DCB) has stretches at 1716, 1616, 1599 cm^{-1}. In general, complexes of (η^4-DEMAMPA-DCB)$^{4-}$ which have reduction couples at high potentials (greater than 1.0 V vs. NHE) have an amide IR band above 1700 cm^{-1}. Furthermore, the corresponding complexes of (η^4-MAC*)$^{4-}$ will not have this reduction wave. For in-

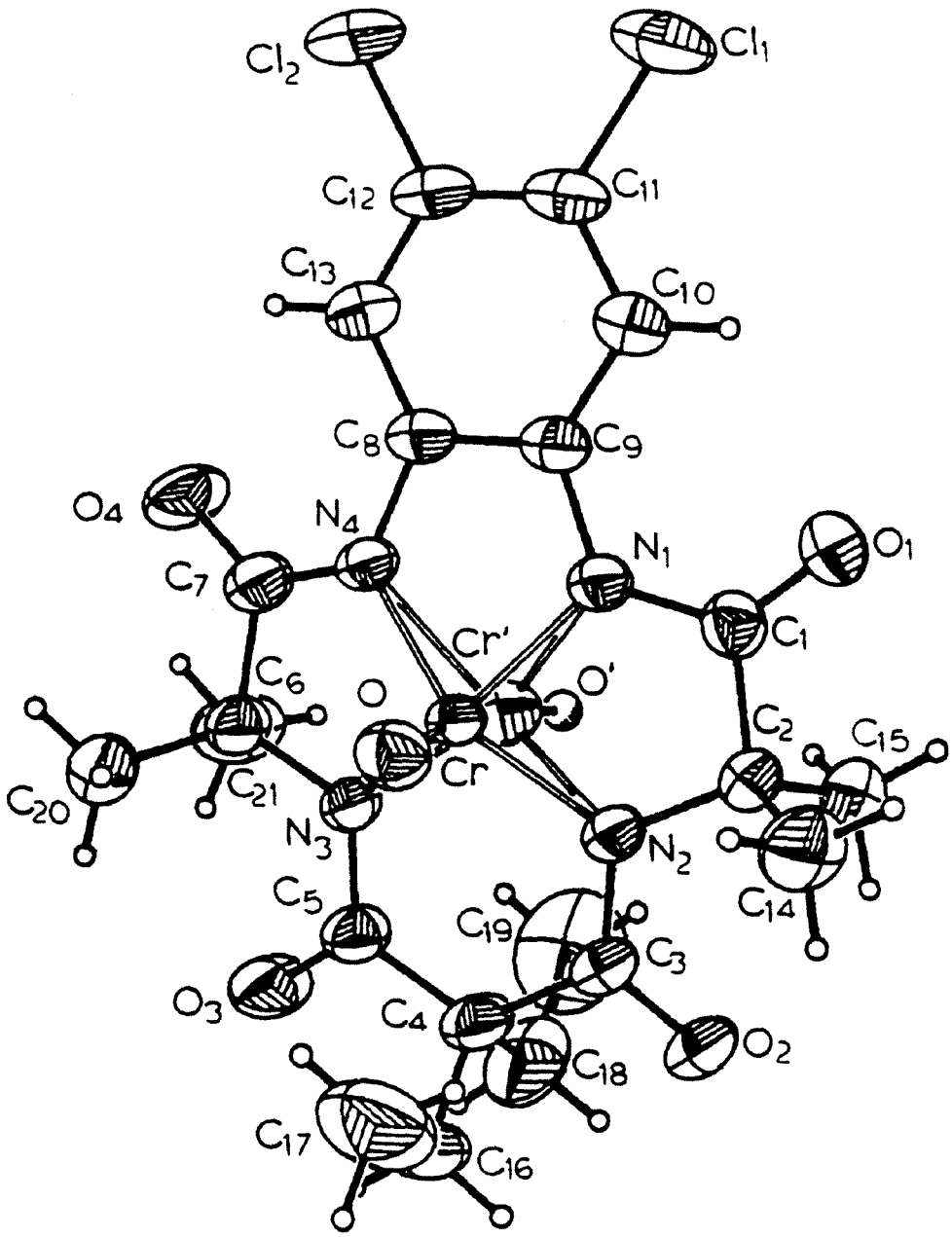

Figure 3.10. Molecular structure of $[Cr(O)(\eta^4\text{-DEMAMPA-DCB})]^-$. ORTEP drawing with all nonhydrogen atoms drawn to encompass 50% of electron density.

Table 3.3. Bond Lengths in [Cr(O)(η^4-DEMAMPA-DCB)]$^-$			
Atoms	Length (Å)	Atoms	Length (Å)
CrO	1.569(2)	Cr′O′	1.57(5)
CrN1	1.916(2)	Cr′N1	2.14(1)
CrN2	1.911(2)	Cr′N2	1.86(1)
CrN3	1.910(2)	Cr′N3	1.79(1)
CrN4	1.914(2)	Cr′N4	2.09(1)
N1C1	1.349(4)	N1C9	1.411(4)
N2C3	1.347(4)	N3C5	1.347(4)
N4C7	1.359(4)	N4C8	1.409(4)
N2C2	1.486(4)	N3C6	1.498(4)
Cl1C11	1.729(3)	ClC12	1.734(3)
C1C2	1.520(4)	C3C4	1.528(5)
C4C5	1.550(5)	C6C7	1.522(5)
C1O1	1.224(4)	C3O2	1.235(4)
C5O3	1.228(4)	C7O4	1.219(4)
C2C14	1.530(5)	C2C15	1.536(5)
C8C9	1.394(4)	C8C13	1.390(4)
C4C16	1.532(6)	C4C18	1.577(6)
C6C20	1.537(6)	C6C21	1.531(5)
C16C17	1.489(8)	C18C19	1.511(8)
C9C10	1.383(4)	C10C11	1.393(5)
C11C12	1.375(5)	C12C13	1.378(5)

Table 3.4. Bond Angles in [Cr(O)(η^4-DEMAMPA-DCB)]$^-$			
Atoms	Angle (°)	Atoms	Angle (°)
OCrN1	107.8(1)	O′Cr′N1	116(2)
OCrN2	108.4(1)	O′Cr′N2	105(2)
OCrN3	108.8(1)	O′Cr′N3	109(2)
OCrN4	108.2(1)	O′Cr′N4	120(2)
N1CrN2	81.5(1)	N1Cr′N2	76.7(4)
N1CrN3	142.4(1)	N1Cr′N3	133.8(7)
N1CrN4	79.6(1)	N1Cr′N4	70.8(4)
N2CrN3	94.7(1)	N2Cr′N3	100.6(6)
N2CrN4	142.5(1)	N2Cr′N4	132.7(7)
N3CrN4	81.4	N3Cr′N4	79.6(5)
CrN1C1	118.5(2)	Cr′N1C1	109.5(4)
CrN1C9	116.1(2)	Cr′N1C9	114.7(3)
CrN2C2	115.3(2)	Cr′N2C2	116.7(4)
CrN2C3	123.8(2)	Cr′N2C3	118.7(4)
CrN3C5	123.8(2)	Cr′N3C5	118.8(5)
CrN3C6	115.8(2)	Cr′N3C6	114.7(4)
CrN4C7	119.0(2)	Cr′N4C7	107.5(4)
CrN4C8	115.8(2)	Cr′N4C8	116.5(4)
C1N1C9	125.3(3)	C2N2C3	118.2(2)
C5N3C6	118.4(2)	C7N4C8	125.1(3)
N1C1O1	125.3(3)	C2C1O1	121.9(3)
N1C1C2	112.7(3)	N2C3O2	122.7(3)
C1C2N2	107.5(2)	C4C3O2	115.7(3)

Table 3.4. Bond Angles in [Cr(O)(η^4-DEMAMPA-DCB)]$^-$ (continued)

Atoms	Angle (°)	Atoms	Angle (°)
C1C2C14	106.7(3)	N2C3C4	121.4(3)
C1C2C15	106.8(3)	N3C5O3	122.5(3)
N2C2C14	112.2(3)	C4C5O3	115.7(3)
N2C2C15	111.1(3)	N3C5C4	121.7(3)
C14C2C15	112.2(3)	N4C7O4	125.4(3)
C3C4C5	121.9(3)	C6C7O4	122.1(3)
C3C4C16	108.0(3)	N4C7C6	112.5(3)
C3C4C18	104.8(3)	N4C8C9	112.3(3)
C5C4C16	106.9(3)	N4C8C13	127.6(3)
C5C4C18	105.0(3)	C9C8C13	120.1(3)
C16C4C18	109.7(3)	N1C9C8	111.7(3)
C7C6N3	107.2(2)	N1C9C10	127.9(3)
C7C6C20	107.2(3)	C8C9C10	120.4(3)
C7C6C21	106.6(3)	C9C10C11	118.8(3)
N3C6C20	111.5(3)	C10C11C12	120.7(3)
N3C6C21	111.3(3)	C10C11Cl1	117.9(2)
C20C6C21	112.7(3)	C12C11Cl1	121.4(3)
C4C16C17	114.0(4)	C11C12C13	120.7(3)
C4C18C19	113.7(4)	C11C12Cl2	121.3(3)
C13C12Cl2	118.0(2)	C12C13C8	119.3(3)

stance, cyclic voltammetry of [Cr(O)(η^4-DEMAMPA-DCB)]$^-$ shows a wave at 1.48 V (vs. NHE) corresponding to a Cr(O)(η^4-DEMAMPA-DCB)/[Cr(O)(η^4-DEMAMPA-DCB)]$^-$ couple. The [Cr(O)(η^4-MAC*)]$^-$ complex exhibits no electrochemical activity up to 2.2 V (vs. NHE). As will be seen in Chapter 6, [Co(η^4-MAC*)]$^-$ can not be oxidized to a neutral species corresponding to Co(η^4-DEMAMPA-DCB).

The EPR spectrum of [$(CH_3)_4N$][Cr(O)(η^4-MAC*)] (Figure 3.11), when compared with that for [$(CH_3)_4N$][Cr(O)(η^4-DEMAMPA-DCB)] (Figure 3.12), supports the contention that a formal oxidation state assignment of +V for the chromium center is equally appropriate for both complexes. The EPR spectrum for [$(CH_3)_4N$][Cr(O)(η^4-DEMAMPA-DCB)] can be interpreted as follows. The 90.45% of Cr nuclei having $I = 0$ gives rise to a strong nine-line first derivative signal at $g = 2.006$ through superhyperfine interactions with four spectroscopically equivalent nitrogen donors ($a_0 = 2.7$ G) ($2nI+1 = 2\cdot4\cdot1+1 = 9$, I = 1 for ^{14}N and $n = 4$). In addition, a hyperfine interaction with the ^{53}Cr ($I = 3/2$, 9.54%) of $A_0 = 17.9$ G gives rise to a weaker four-line feature, each component of which shows the nitrogen superhyperfine interactions. The EPR of [$(CH_3)_4N$][Cr(O)(η^4-MAC*)] is virtually identical. The hyperfine interaction with the ^{53}Cr is $A_0 = 17.8$ G ($g = 1.999$), and all four nitrogen donors are spectroscopically equivalent ($a_0 = 2.6$ G). These data are consistent with a chromium(V) centered radical for both complexes.

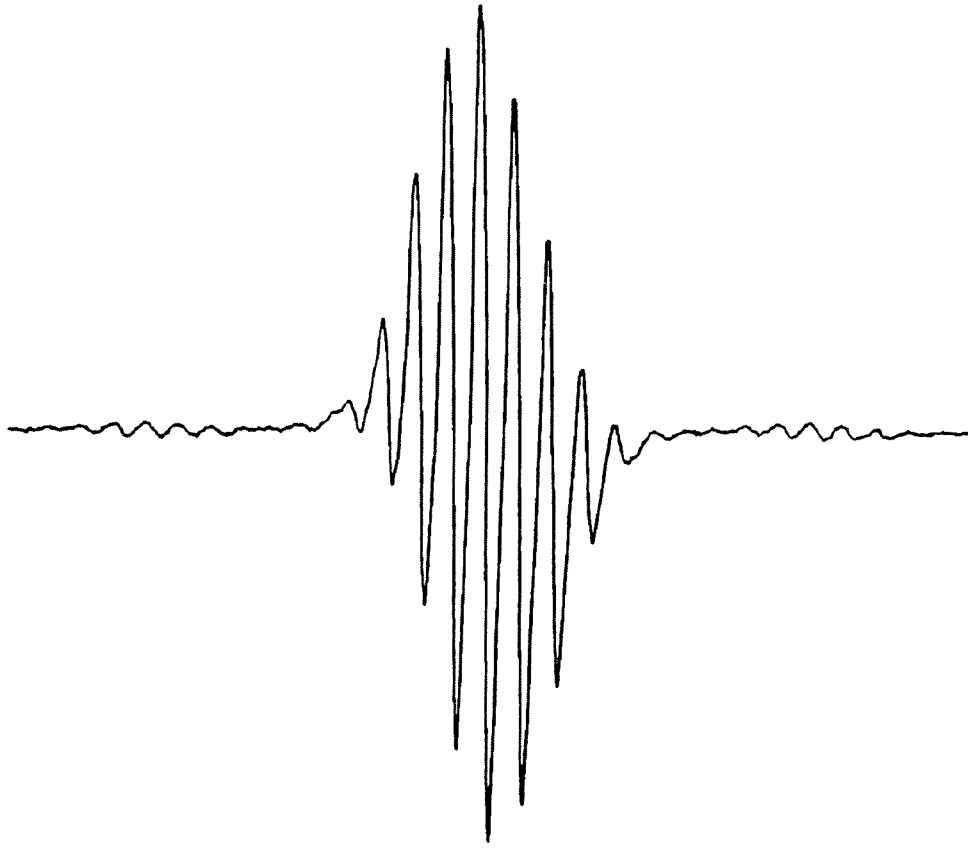

Figure 3.11. EPR spectrum of $[Cr(O)(\eta^4\text{-MAC*})]^-$ at 294 K, 9.34 GHz, in CH_3CN.

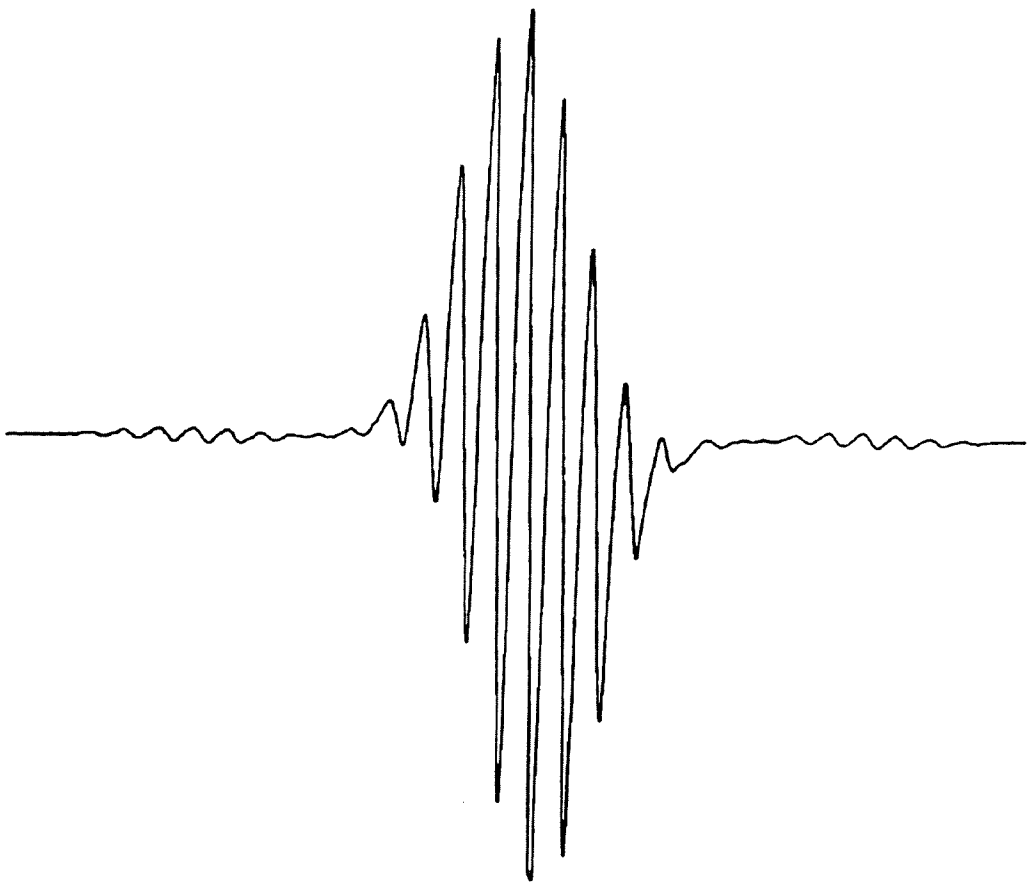

Figure 3.12. EPR spectrum of $[Cr(O)(\eta^4\text{-DEMAMPA-DCB})]^-$ at 292 K, 9.34 GHz, in CH_3CN.

Experimental

Materials. All solvents and reagents were reagent grade (Aldrich) except for THF (Aldrich, Sureseal), $CrCl_2$ (Alfa) and $^{18}O_2$ (EG & G Mound Applied Technologies) and were used as received.

Physical Measurements. ^1H and ^{13}C NMR were measured at 300 and 75.45 MHz, respectively, on an IBM NR/300 FT-NMR Spectrometer. ^1H and ^{13}C NMR data are reported in δ vs. $(CH_3)_4Si$ with the solvent ($CDCl_3$) as internal standard. EPR spectra were recorded on a Bruker ER300 Spectrometer. Infrared data were obtained on a Nicolet 5DXB FT-IR Spectrometer. Crystal structures were solved by Crystalytics Co. of Lincoln, Nebraska.

Electrochemistry. Sureseal anhydrous CH_2Cl_2 (Aldrich) was used as received. $[Bu_4N][ClO_4]$ (Fluka) was vacuum dried at 80 °C. In all cases, experiments were performed under N_2 with a supporting electrolyte concentration of 0.1 M. Cyclic voltammetry was performed in CH_2Cl_2 solutions of $[Bu_4N][ClO_4]$ at a 3 mm Pt disk working electrode with a silver wire quasi-reference electrode and a Pt foil counter electrode. At the conclusion of each experiment, ferrocene (Fc) was added as an internal potential standard. All formal potentials were taken as the average of anodic and cathodic peak potentials and are reported vs. the Fc^+/Fc couple. Plots of peak current vs. the square root of scan rate over the range 10–500 mV s^{-1} were made and found to be linear for couples that are stated to be reversible.

Synthetic Note. It should be noted that the experimental work reported here has been published in substantially similar form in *Inorg. Chem.*[14]

$[(CH_3)_4N][Cr(O)(\eta^4$-DEMAMPA-DCB)] and $[Ph_4P][Cr(O)(\eta^4$-DEMAMPA-DCB)]. H_4DEMAMPA-DCB (0.114 g) was dissolved in dry,

deoxygenated THF (18 mL), and *tert*-butyllithium in pentane (0.62 mL, 1.7 M solution) was added to the frozen solution under nitrogen. Anhydrous $CrCl_2$ (0.050 g) was added under nitrogen just before the THF finished thawing (−108 °C). As the suspension warmed to room temperature, a bright yellow precipitate (presumably a Cr(II) complex) collected on the flask walls. After stirring at room temperature (30 min), *tert*-butyl hydroperoxide (0.70 mL, 3.0 M in 2,2,4-trimethylpentane) was added. A dark brown solution developed rapidly with concomitant disappearance of the yellow precipitate. Li[Cr(O)(η^4-DEMAMPA-DCB)] was obtained in 75% isolated yield. Analytically pure [Ph_4P][Cr(O)(η^4-DEMAMPA-DCB)] was obtained (0.082 g, 38.8% yield from starting ligand) by dissolving the Li^+ salt in water, adding aqueous [Ph_4P]Cl, isolating the precipitate, and washing the precipitate with ether and pentane. (Anal. Calcd for [Ph_4P][Cr(O)(η^4-DEMAMPA-DCB)]: C, 61.78; H, 5.03; N, 6.41; P, 3.54. Found: C, 61.84; H, 5.09; N, 6.39; P, 3.47.) (Electronic spectrum of [Ph_4P][Cr(O)(η^4-DEMAMPA-DCB)] (CH_3CN—values in parentheses are molar absorptivities in $M^{-1}cm^{-1}$): 316 nm (9.9×10^3), 356 nm (5.6×10^3), ≈512 nm (shoulder) (≈8.6×10^2).) In a similar preparation, the $[(CH_3)_4N]^+$ salt was obtained by adding excess aqueous [$(CH_3)_4N$][Cl] to aqueous Li[Cr(O)(η^4-DEMAMPA-DCB)]. The water was removed in vacuo, and an CH_3CN/CH_2Cl_2 solution of the residue was treated with pentane to precipitate the LiCl and excess [$(CH_3)_4N$][Cl]. Large brown parallelepipeds, characterized by X-ray analysis, were obtained by evaporation from CH_3CN.

Synthesis of [$(CH_3)_4N$][Cr(O)(η^4-MAC*)] and [Et_4N][Cr(O)(η^4-MAC*)]. These analogues were prepared in a similar fashion by metathesizing aqueous Li[Cr(O)(η^4-MAC*)] with aqueous [$(CH_3)_4N$][Cl] and [Et_4N][F],

respectively, and X-ray quality crystals of $[(CH_3)_4N][Cr(O)(\eta^4\text{-MAC*})]$ were obtained by diffusion of pentane into an acetonitrile/dichloroethane solution. (Electronic spectrum of $[Et_4N][Cr(O)(\eta^4\text{-MAC*})]$ (CH_3CN—values in parentheses are molar absorptivities in $M^{-1}cm^{-1}$): 316 nm (8.8 x 10^3), 460 nm (3.2 x 10^3), ≈550 nm (shoulder) (≈1.9 x 10^3).)

$(CH_3)_2(H^{18}O^{18}O)CCH_2CH_2C(^{18}O^{18}OH)(CH_3)_2$. The synthesis of $(CH_3)_2(HOO)CCH_2CH_2C(OOH)(CH_3)_2$ was first reported in 1951.[12a] The title compound was produced using a method adapted from Rust's synthesis of the unlabeled material.[12b] 2,4-dimethylhexane (8.7 mL) was added to a glass bomb (123 mL) and the system was subjected to three freeze/pump/thaw/degas cycles. $^{18}O_2$ gas (96.9% ^{18}O, 0.5% ^{17}O, 2.6% ^{16}O) was added to the evacuated bomb to bring the total pressure to 27–29 psi (25 °C). The sealed bomb was placed in a silicone oil bath and heated (116–120 °C, 17 h). After the bomb had cooled to room temperature, air was admitted at ambient pressure (the pressure inside had dropped below room pressure). Upon standing, the reaction mixture separated into two phases—the lower phase being oily product, the upper phase being primarily unreacted hydrocarbon. (It is essential to run the reaction at low hydrocarbon conversion in order to obtain satisfactory yields of dihydroperoxide.) The contents of the bomb were washed into a flask with CH_2Cl_2 and CH_3CN and the solvents were removed under reduced pressure. The waxy solid residue was washed twice with a CH_2Cl_2 (5 mL) pentane (15 mL) mixture and then washed twice with pentane (10 mL). The resulting white powder was dried under reduced pressure, giving analytically pure material (0.309 g). This peroxide has shown no decomposition after months of storage at room temperature. Anal. Calcd for $C_8H_{18}{}^{96.9\%18,0.5\%17}O_4$: C,51.66;

H, 9.75. Found: 51.80; H, 9.64. ^{1}H NMR ($CDCl_3$): 8.09 (s, 2H, OOH), 1.65 (s, 4H, -CH_2-), 1.20 (s, 12H, -CH_3). ^{13}C NMR (broad-band decoupled, $CDCl_3$): 82.5 (COOH), 31.0 (-CH_2-), 24.2 (-CH_3).

X-ray Data Collection and Structure Refinement of [$(CH_3)_4$N][Cr(O)(η^4-MAC*)] and [$(CH_3)_4$N][Cr(O)(η^4-DEMAMPA-DCB)]. Crystal Data: Single crystals of [$(CH_3)_4$N][Cr(O)(η^4-MAC*)] at 20±1°C are orthorhombic, space group $P2_12_12_1$-D_2^4 (No. 19) with a = 9.210(3) Å, b = 16.352(4) Å, c = 19.957(5) Å, V = 3005(2) Å^3 and Z = 4 formula units (d_{calcd} = 1.240 g cm^{-3}; μ_a(CuK$\bar{\alpha}$) = 3.5 mm^{-1}). A total of 2557 independent absorption-corrected reflections having 2θ(CuK$\bar{\alpha}$) < 120.0° (the equivalent of 0.65 limiting CuK$\bar{\alpha}$ spheres) were collected on a computer-controlled Nicolet autodiffractometer using θ-2θ scans and Ni-filtered CuK$\bar{\alpha}$ radiation. Single crystals of [$(CH_3)_4$N][Cr(O)(η^4-DEMAMPA-DCB)] at 20±1°C are monoclinic, space group $P2_1/C$-C_{2h}^5 (No. 14), with a = 12.414(2) Å, b = 7.878(1) Å, c = 30.673(5) Å, β = 93.39(1)°, V = 2994.6(9) Å^3 and Z = 4 formula units (d_{calcd} = 1.352 g cm^{-3}; μ_a(MoK$\bar{\alpha}$) = 0.59 mm^{-1}). A total of 5488 independent reflections having 2θ(MoK$\bar{\alpha}$) < 50.7° (the equivalent of 0.80 limiting CuK$\bar{\alpha}$ spheres) were collected on a computer-controlled Nicolet autodiffractometer using full (0.9° wide) omega scans and graphite monochromated MoK$\bar{\alpha}$ radiation. The structures were solved using Direct Methods techniques with the Nicolet SHELXTL software package as modified at Crystalytics Company. The resulting structural parameters have been refined to convergence (R_1(unweighted, based on F) = 0.054 for 1634 independent reflections) for [$(CH_3)_4$N][Cr(O)(η^4-MAC*)] and (R_1(unweighted, based on F) = 0.040 for 3700 independent reflections) for [$(CH_3)_4$N][Cr(O)(η^4-DEMAMPA-DCB)] us-

ing counter-weighted cascade block-diagonal least-squares techniques and a structural model which incorporated anisotropic thermal parameters for non-hydrogen atoms and isotropic thermal parameters for all hydrogen atoms. The methyl groups were included in the refinement as idealized sp^3-rigid rotors. The remaining hydrogen atoms were fixed at idealized sp^2- or sp^3-hybridized positions with a C–H bond length of 0.96Å. The Cr≡O unit of $[(CH_3)_4N][Cr(O)(\eta^4$-DEMAMPA-DCB)] is disordered in the lattice, being 95% "above" the macrocycle (Cr and O) and 5% below it (Cr′ and O′). Oxygen atom O′ was refined isotropically.

References

1. (a) Cainelli, G.; Cardillo, G. *Chromium Oxidations in Organic Chemistry*; Springer-Verlag: New York, 1984. (b) Sheldon, R. A.; Kochi, J. K. *Metal Catalyzed Oxidations of Organic Compounds*; Academic Press: New York, 1981.

2. (a) Nugent, W. A.; Mayer, J. M. *Metal-Ligand Multiple Bonds*; Wiley-Interscience: New York, 1988. (b) Holm, R. H. *Chem. Rev.* **1987**, *87*, 1401–1449.

3. Mitewa, M.; Bontchev, P. R. *Coord. Chem. Rev.* **1985**, *61*, 241–272.

4. Morse, D. B.; Rauchfuss, T. B.; Wilson, S. R. *J. Am. Chem. Soc.* **1988**, *110*, 8234–8235.

5. (a) Groves, J. T.; Kruper, W. J., Jr. *J. Am. Chem. Soc.* **1979**, *101*, 7613–7615. (b) Samsel, E. G.; Srinivasan, K.; Kochi, J. K. *J. Am. Chem. Soc.* **1985**, *107*, 7606–7617.

6. (a) McGinnety, J. A. *Acta Crystallogr., Sect. B* **1972**, *B28*, 2845–2852. (b) Amirthalingam, V.; Grant, D. F.; Senol, A.; *Acta Crystallogr., Sect. B* **1972**, *B28*, 1340–1345. (c) Stensland, B.; Kierkegaard, P. *Acta Chem. Scand.* **1970**, *24*, 211-220. Stomberg, R. *Arkiv Kemi* **1963**, *22*, 29–47. (d) Stomberg, R.; Ainalem, I.-B. *Acta Chem. Scand.* **1968**, *22*, 1439–1451. (e) Stomberg, R. *Arkiv Kemi* **1965**, *24*, 111–131.

7. For structurally characterized Cr(V) oxos produced from molecular oxygen see references "a" and "b." For the other structurally characterized Cr(V) oxo complexes see "c"–"f": (a) Morse, D. B.; Rauchfuss, T. B.; Wilson, S. R. *J. Am. Chem. Soc.* **1988**, *110*, 8234–8235. (b) Herberhold, M.; Kremnitz, W.; Razavi, A.; Schöllhorn, H.; Thewalt, U. *Angew. Chem. Int. Ed. Engl.*

1985, *24*, 601–602. (c) Srinivasan, K.; Kochi, J. K. *Inorg. Chem.* **1985**, *24*, 4671–4679. (d) Krumpolc, M.; Deboer, B. G.; Roćek, J. *J. Am. Chem. Soc.* **1978**, *100*, 145–153. (e) Gahan, B.; Garner, D. C.; Hill, L. H.; Mabbs, F. E.; Hargrave, K. D.; McPhail, A. T. *J. Chem. Soc., Dalton Trans.* **1977**, 1726–1729. (f) Palmer, K. J.; *J. Am. Chem. Soc.* **1938**, *60*, 2360–2369. [an electron diffraction study]

8. (a) Groves, J. T.; Kruper, W. J. Jr.; Haushalter, R. C.; Butler, W. M. *Inorg. Chem.* **1982**, *21*, 1363–1368. (b) Budge, J. R.; Gatehouse, B. M. K.; Nesbit, M. C.; West, B. O. *J. Chem. Soc., Chem. Commun.* **1981**, 370–371.

9. Ms. Kimberly Kostka of the Collins group has provided samples of $[Cr(O)(\eta^4\text{-DEMAMPA-DCB})]^-$ to Peter Lay's group to screen the biological activity of these systems. For references in this area, see: (a) Bramley, R.; Farrell, R. P.; Ji, J.-Y.; Lay, P. A. *Aust. J. Chem.* **1990**, *43*, 263–279. (b) Farrell, R. P.; Judd, R. J.; Lay, P. A.; Bramley, R.; Ji, J.-Y. *Inorg. Chem.* **1989**, *28*, 3401–3403. (c) Farrell, R. P.; Judd, R. J.; Lay, P. A.; Dixon, N. E.; Baker, R. S. U.; Bonin, A. M. *Chem. Res. Toxicol.* **1989**, *2*, 227-229. (d) Bramley, R.; Ji, J.-Y.; Judd, R. J.; Lay, P. A. *Inorg. Chem.* **1990**, *29*, 3089–3094.

10. Groves, J. T.; Haushalter, R. C. *J. Chem. Soc., Chem. Commun.* **1981**, 1165–1166.

11. (a) Buchler, J. W.; Dreher, C.; Lay, K.-L.; Raap, A.; Gersonde, K. *Inorg. Chem.* **1983**, *22*, 879–884. (b) Groves, J. T.; Takahashi, T.; Butler, W. M. *Inorg. Chem.* **1983**, *22*, 884–887.

12. (a) Wibaut, J. P.; Strang, A. *Koninkl. Ned. Akad. Wetenschap. Proc. B* **1951**, *54*, 229–235. (b) Rust, F. F. *J. Am. Chem. Soc.* **1957**, *79*,

4000–4003.

13. Procyk, A.; Uffelman, E. S. unpublished results.

14. Collins, T. J.; Slebodnick, C.; Uffelman, E. S. *Inorg. Chem.* **1990**, *29*, 3432–3436.

Chapter 4

Water-Stable Manganese(V) Monooxo Complexes of Macrocyclic Tetraamido-*N* Ligands and the Definitive Assignment of a $\nu_{Mn^{V}\equiv O}$ Vibration

Although there are over 120,000 entries in the Chemical Abstracts Formula Index for manganese, fewer than ten unique fully characterized species of manganese(V), (VI), and (VII) are stable under normal conditions.[1,2] Manganese(V) oxo complexes are the subject of considerable current interest as reactive intermediates in oxidation reactions with porphyrin[3a-c] and salen[3d] systems, and manganese oxo complexes in lower oxidation states have a probable role in the oxygen evolving complex in photosynthesis.[4] Manganese is also present in the active sites of several enzymes that catalyze redox reactions of oxygen species—manganese superoxide dismutase[5] and azide insensitive catalase.[6] This chapter will briefly discuss the chemistry of Mn(VII) and Mn(VI), highlight a few investigations of Mn(V) and Mn(IV) oxos, and quickly summarize the crystal structure data of the Mn(V) nitrides. This will be followed by a discussion of the Collins group's preparation of the first Mn(V) oxo to be structurally charaterized. The rest of the chapter will present the chemistry of high valent manganese with the macrocycles of this thesis, which has yielded the first water-stable Mn(V) oxo, the first definitive assignment of a $\nu_{Mn^V\equiv O}$ vibration, and what appear to be stable neutral species from the one-electron oxidation of the Mn(V) oxo anions.

Background

The high valent chemistry of manganese has been reviewed.[7] The known complexes of Mn(VII), (VI), and (V), with the exception of the Mn(V) nitrido porphyrins and postulated Mn(V) oxo porphyrins (vide infra), have been succinctly summarized (Table 4.1).[7a] These are all oxo complexes, and except for the tetraoxomanganates, the compounds are unstable potent oxidants which are liable to detonation, particularly in the presence of a suitable fuel.

Table 4.1. Oxo Complexes of Mn(V), (VI), and (VII)	
Compound	Comments
MnO_4^{3-}	Blue anion—characterized in crystalline compounds, in concentrated alkalai solutions, and in melts.
MnO_4^{2-}	Green anion—stable in aqueous solutions with $[OH^-] > 1M$; crystalline salts.
MnO_4^-	Purple anion—reasonably robust in water and in crystalline salts.
Mn_2O_7	Very unstable red/green liquid. Susceptible to detonation, but IR and UV spectra recently obtained on matrix-isolated samples.[8a,e]
$HMnO_4$	Also as a dihydrate. Both crystalline,[8b] strong oxidizing agents, with parallels to $HClO_4$.
MnO_3F	Highly volatile.[7b] Microwave data give T_d with Mn–O = 1.586(5) and Mn–F = 1.724(5) Å. Dark green crystals at −78 °C. Very moisture sensitive and decomposes explosively.
$MnOCl_3$	Green liquid from $KMnO_4$ reduced in HSO_3Cl.[8c] Decomposes to $MnCl_3$ above 0 °C and to $[MnO_4]^{3-}$ in aqueous alkalai.
MnO_2Cl_2	Least stable of oxochlorides—decomposing at −30 °C. Brown solutions in CCl_4.[8c]

Table 4.1. Oxo Complexes of Mn(V), (VI), and (VII) (continued)	
Compound	Comments
MnO_3Cl	Green in CCl_4 solution. Detonates in air above 0 °C. Slowly hydrolysed to MnO_4^- and Cl^- in water.[8c]
$MnO_3 \cdot SO_3Cl$?	This species may exist in solution, but decomposes during isolation attempts to $MnO \cdot SO_3Cl$.[8d]

The relatively stable compound K_2MnO_4 is prepared by cautiously adding $KMnO_4$ to a hot aqueous solution of KOH. After about 15 minutes of refluxing, the dark purple color suddenly turns green. Adding hot aqueous KOH and rapidly cooling the solution precipitates K_2MnO_4 as a green solid.[9] The pure MnO_2 free compound has a room-temperature moment of 1.75 B. M. that is independent of field strength. The complex has been the subject of a single crystal EPR study,[10] and the significance of this study to this thesis work will be apparent (vide infra). In a single crystal study of 1% manganate doped into crystalline K_2CrO_4, the anisotropic g values were determined to be g_x=1.970, g_y=1.966, and g_z=1.938. A_x was found to be 2.5 × 10^{-3} cm^{-1}, while there were four solutions for A_z (±1.35 × 10^{-2} cm^{-1} or ±1.33 × 10^{-2} cm^{-1}), A_y (±3.3 × 10^{-3} cm^{-1} or ±2.2 × 10^{-3} cm^{-1}), and A_{yz} (±3.3 × 10^{-3} cm^{-1} or ±2.2 × 10^{-3} cm^{-1}).

Suslick's group has provided reasonable evidence that transient Mn(V) oxo porphyrin complexes can be used to hydroxylate alkanes. In what was an excellent demonstration of the control of selectivity by the steric

bulk of the ligand,[11] Mn(III) tetraphenylporphyrin (TPP), tetra(2′,4′,6′-trimethoxyphenyl)porphyrin (TTMPP), and tetra(2′,4′,6′-triphenylphenyl)porphyrin (TTPPP) acetates were used to mediate hydroxylation of 2,2-dimethylbutane by iodosylbenzene. The alkane, 2,2-dimethylbutane, has one secondary site and two different primary sites. With the TPP and TTMPP systems, 3,3-dimethylbutan-2-ol (the secondary hydroxylation product) was the predominant product ($\geq$90%). However, with TTPPP, the secondary alcohol is formed in only 25% yield, the yield of 2,2-dimethylbutanol (the statistically favored primary site) is 5%, and the yield of 3,3-dimethylbutan-1-ol (the least sterically hindered site of the alkane) is 70%.

Collman's group has very recently reinvestigated the mechanism of phase transfer catalytic olefin epoxidation with Mn(TMP)Cl (TMP = tetramesitylporphyrin) and hypochlorite anion.[12] This "Meunier system" has been the source of considerable study,[12] but such systems are still far from understood. Previous studies had indicated that this system exhibited saturation kinetics behavior with excess olefin. However, by studying these reactions with three different olefins (indene, styrene, and 1-methyl-cyclohexene) and three different axial ancillary ligands (4-(imidazol-1-yl)acetophenone, *tert*-butylpyridine, and N-phenylimidazole) at low hypochlorite to catalyst ratios (130:1), different conclusions were reached. In all of the reactions, leftover starting olefin, hypochlorite, and final epoxide were all quantified. With *tert*-BuPy as an ancillary ligand, no decomposition of the pyridine or hypochlorite was observed after over an hour and, if olefin was then added, normal catalysis was observed. If one of the more readily oxidized ancillary ligands was employed, both the ligand and hypochlorite concentrations diminished, with roughly six hypochlo-

rites being consumed per ligand, and if olefin was then added, catalysis still occurred because of the presence still of sufficient oxidant and axial ligand. In all cases, high olefin concentrations led to high efficiencies [(mol epoxide formed)/mol OCl^- added)] and low olefin concentrations led to low catalyst efficiencies. Collman proposed a mechanism which invoked several fates for the transient Mn(V) oxo (Figure 4.1). They estimated k_a to be $\approx 10k_b$.

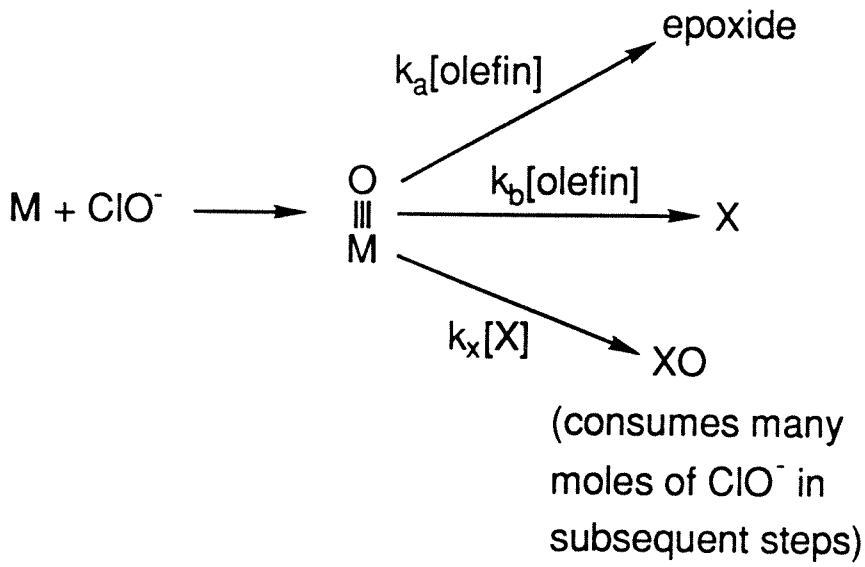

Figure 4.1. Collman's revised mechanistic ideas concerning the Mn(III)porphyrin mediated ClO^- epoxidation of olefins.

Bortolini and Meunier *claimed* to have isolated a Mn oxo porphyrin cation radical from the NaOCl oxidation of Mn(TPP)Cl.[13] Surprisingly, they proposed that the Mn=O stretch was at 950 cm^{-1} inspite of being unable to shift the band by exchange with ^{18}O-labeled water. Recent work by Groves et al. has provided strong evidence for the Mn=O stretch at ≈ 750 cm^{-1} for Mn(IV) porphyrins (vide infra).[14] The diamagnetic Mn(V)≡O system of this thesis, $[Mn(O)(\eta^4\text{-DEMAMPA-DCB})]^-$, is slow to exchange the oxo ligand with wa-

ter and exhibits a Mn(V)≡O stretch at 979 cm^{-1} (vide infra).[15] However, Mn(V) would be completely incompatible for Meunier's system because of the other spectroscopic data he presented. Meunier's assignment of the Mn=O band should be regarded with skepticism.

Kochi's group studied the Mn(III)Salen mediated epoxidation of olefins by iodosylbenzene.[3d] They found that when a clear brown solution of Mn(III)Salen in MeCN was treated with iodosylbenzene, it immediately turned brown. This brown compound was unstable and decomposed in solution after 2–3 hours. Although addition of olefin to this intermediate discharged the color, the rate difference only was significant in the first 10% of the reaction, compared to the disappearance of color without olefin. This led the authors to speculate that this intermediate was really a Mn(IV) μ-oxodimer. By using 75% ^{18}O-labeled iodosylbenzene, they obtained 75% ^{18}O-labeled epoxide. By using ^{18}O-labeled water and ^{16}O-iodosylbenzene, they obtained some ^{18}O-labeled epoxide. Conversely, by using ^{16}O-water and ^{18}O-labeled iodosylbenzene, they obtained some ^{16}O-epoxide. They were able to demonstrate that the iodosylbenzene and water did not undergo O-atom exchange. They therefore proposed the mechanism illustrated (Figure 4.2), with the Mn(V) oxo being the species which undergoes O-atom exchange with water. It should be noted that they presented no clear evidence for the intermediate.

Groves and Stern[3a] have performed thorough studies on the synthesis, characterization and reactivity of oxomanganese(IV) porphyrin complexes. The methods of preparation are summarized in Figure 4.3. The EPR of these species all gave strong broad resonances at $g \approx 4$ and weak unresolved signals at $g \approx 2$, consistent with a high spin S=3/2 formulation. The Mn=O stretch

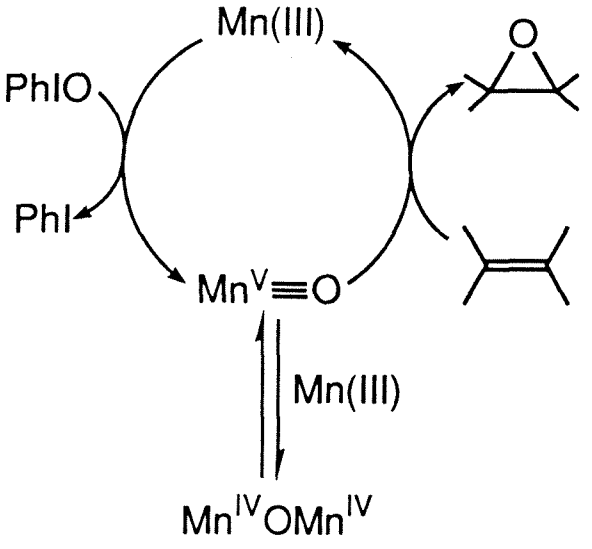

Figure 4.2. Kochi's mechanism concerning the Mn(III)Salen mediated iodosylbenzene epoxidation of olefins.

for the five coordinate species was found at 754 cm^{-1}, and the stretch for the six coordinate complex (with hydroxide *trans* to the oxo) was 712 cm^{-1}. These data are all consistent with a Mn–O double bond (Figure 4.4). It was found that the Mn(IV) oxo was a competent olefin epoxidation catalyst.

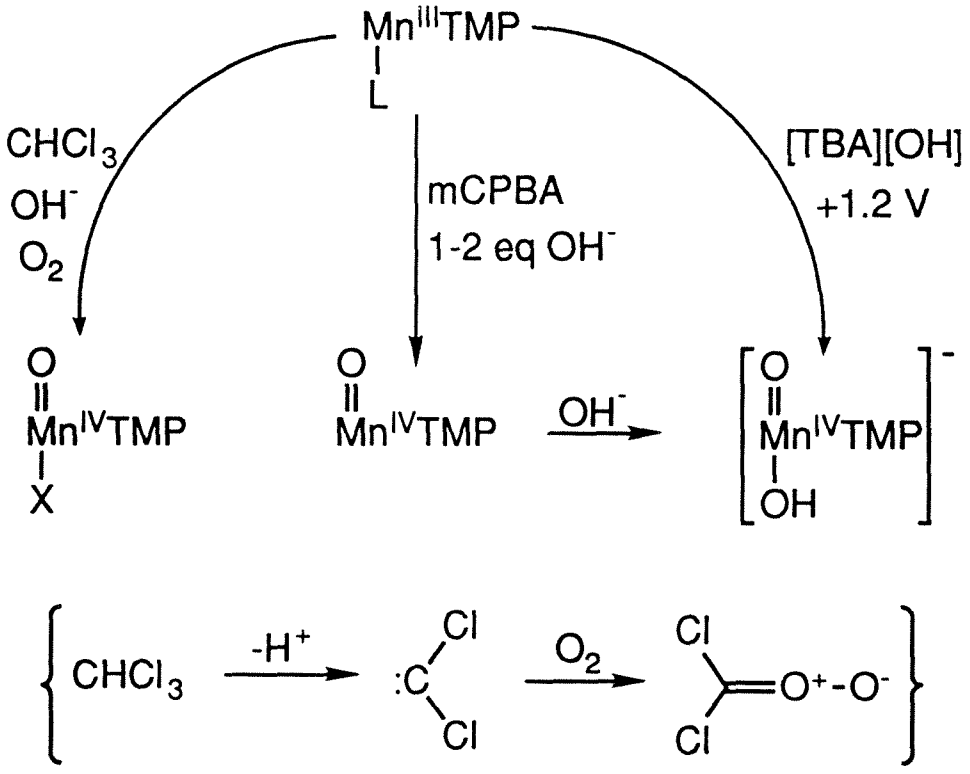

Figure 4.3. Groves' methods of synthesizing various Mn^{IV} oxo porphyrin species, including the postulate for the active oxidizing species in the O_2 method.

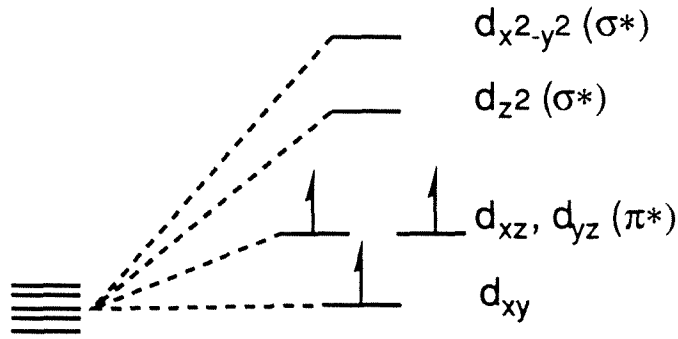

Figure 4.4. Groves' scheme showing the three unpaired electrons in the t_{2g} orbital set for Mn^{IV} oxo porphyrin species. The non-bonding orbital is brought closer to the π^* orbitals than in Cr or Fe analogues by exchange terms.

Manganese nitrido porphyrins[16] were prepared by the oxidation of Mn(III) porphyrin halide complexes with hypochlorite or iodosylbenzene in the presence of excess ammonia. These dark red neutral compounds are highly stable diamagnetic complexes which give excellent NMR and mass spectra. The $\nu_{Mn\equiv N}$ band occurs at 1036–1049 cm^{-1} for different porphyrin derivatives. X-ray crystal structures reveal square pyramidal geometries, with Mn 0.39–0.43 Å above the porphyrin nitrogen atom plane, average Mn–N (porphyrin) bond distances of 2.02 Å, and a short axial Mn–N bond distance of 1.51–1.52 Å. Interestingly, one of the structures[16b] exhibited disorder in the Mn≡N group, with the group being above or below the plane of the porphyrin 50% each. The IR and UV-vis spectra show no evidence of π-cation radical character in the porphyrin rings. Unlike the Mn(V) oxos postulated as intermediates in olefin epoxidation and alkane hydroxylation, the Mn(V) nitrides are very stable unreactive complexes.

Prior to the efforts of the Collins group, there was little concrete data on Mn(V) and (VI) complexes. Then, in 1989, Collins and Gordon-Wylie pub-

lished the first structure of a Mn(V) monooxo complex, Na[Mn(O)(η^4-HMPA-B)].[2] This achievement with the acyclic ligands was realized by oxidizing the Mn(III) anion with 90% TBHP in the absence of solvent, quickly precipitating the complex and recrystallizing in a glove box. In the structure, the Mn atom sits 0.62 Å above the plane of the donor atoms, the Mn–O_{oxo} bond distance is 1.548(4) Å, the Mn–N distances are 1.870(5) and 1.874(5) Å, and the Mn–O distances are 1.831(4) and 1.825(4) Å. The complex decomposes in wet solvents, but it is stable in solution for several hours in anhydrous media. The complex is stable for several days in the solid state. This stability is literally orders of magnitude greater than what had been previously achieved for such species, but the aqueous incompatibility imposes limitations, particularly for oxo-exchange with isotopically labeled water.

Results and Discussion

Oxo complexes of the macrocycles are readily prepared by the method illustrated in Figure 4.5. Unlike the acyclic system, the oxos are best prepared by oxidation of the Mn(II) intermediate, without the isolation of any intermediate oxidation state compounds. Once formed, the Mn(V) oxos of the macrocycles are indefinitely stable either in solution or the solid state. The results of the structural study for [Et_4N][Mn(O)(η^4-DEMAMPA-DCB)] are shown in Figure 4.6. The Mn≡O distance of 1.555(4) Å is similar to that found in the acyclic complex. The four nitrogens lie nearly in a plane (largest deviation 0.026 Å) and the manganese atom sits 0.60 Å above the mean plane, virtually equidistant from all four nitrogens (1.878(5) Å from both aromatic amide nitrogens and 1.904(4) and 1.895(4) Å from the aliphatic amide nitrogens). The bond distances in the benzene ring are consistent with an aromatic

unit and the bond distances from the ring to the amide nitrogen atoms are consistent with a single bond between the two sp^2 atoms. Noninnocence in the aromatic ligand is not expected because the relevant d_π orbitals are strongly interacting with the oxo ligand. The amide nonplanarity found in this structure will be discussed in Chapter 9. It is interesting to note that the structure with the acyclic ligand exhibits no amide nonplanarity. It is also interesting to note that, like one of the structures of the Mn porphyrin nitrides which has a planar macrocycle and exhibits disorder in the Mn–O unit, the structure of $[Et_4N][Mn(O)(\eta^4\text{-DEMAMPA-DCB})]$, which also has a planar macrocycle, also exhibits Mn–O disorder.

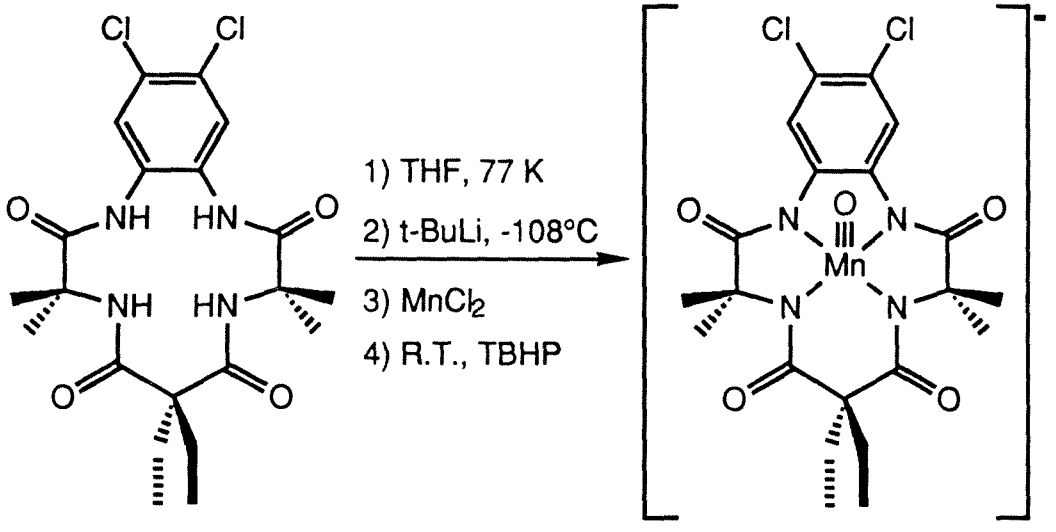

Figure 4.5. Synthesis of a water stable, structurally characterized Mn(V) monooxo.

Unlike, the acyclic system, which decomposes rapidly in water, the macrocyclic system is indefinitely stable in water, and this provided the opportunity to easily label the Mn oxo using ^{18}O-labeled water. The stability was critical, since even after 48 hours in neat ^{18}O-labeled water, exchange had only

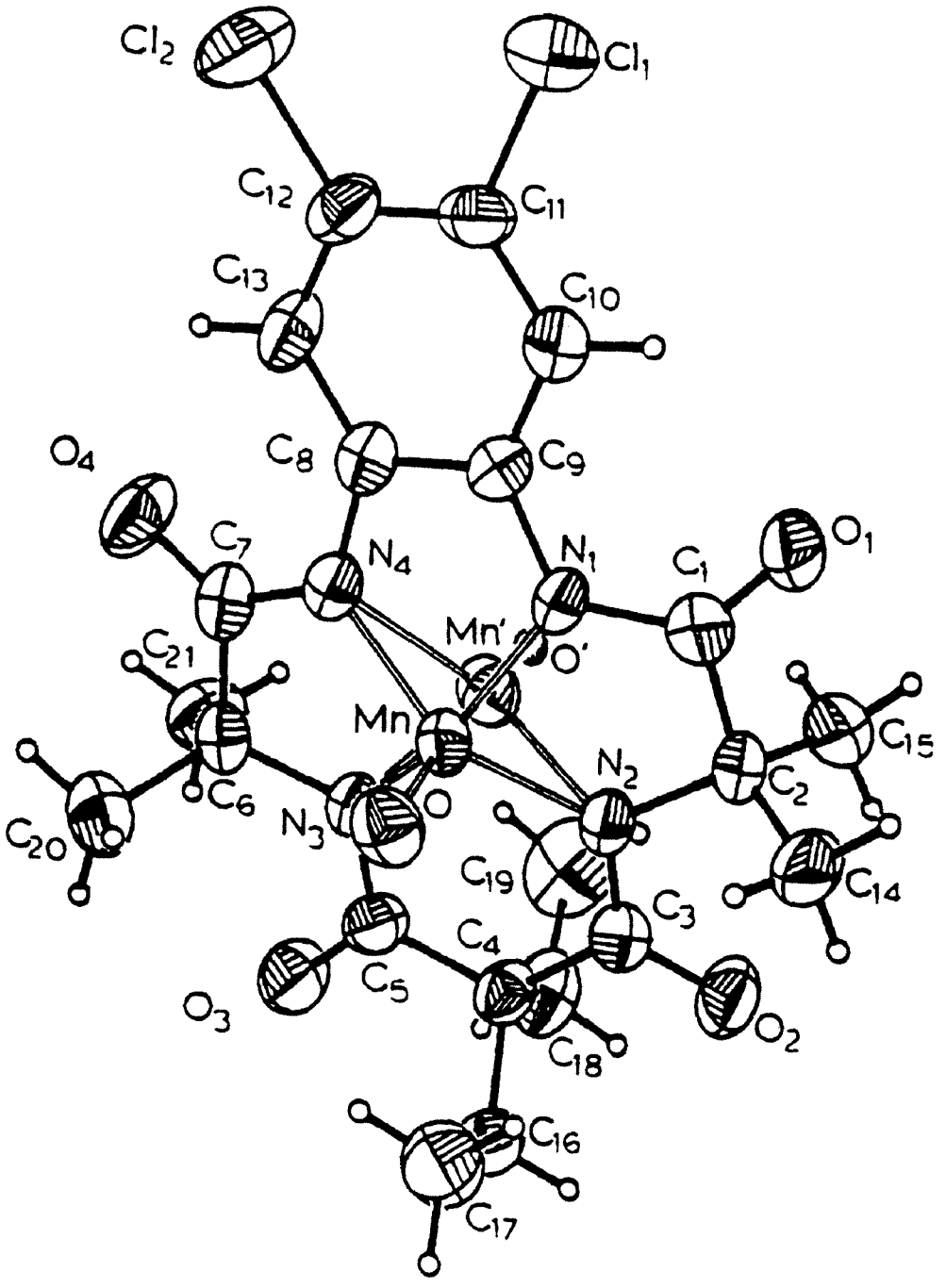

Figure 4.6. Molecular structure of $[Mn(O)(\eta^4\text{-DEMAMPA-DCB})]^-$. ORTEP drawing with all nonhydrogen atoms drawn to encompass 50% of electron density. There is disorder in the Mn–O unit (92% "above" the plane and 8% "below" the plane).

Table 4.2. Bond Lengths in [Mn(O)(η^4-DEMAMPA-DCB)]$^-$			
Atoms	Length (Å)	Atoms	Length (Å)
MnO	1.555(4)	Mn′O′	1.55(5)
MnN1	1.878(5)	Mn′N1	2.19(1)
MnN2	1.904(4)	Mn′N2	1.88(1)
MnN3	1.895(4)	Mn′N3	1.82(1)
MnN4	1.878(4)	Mn′N4	2.09(1)
N1C1	1.344(7)	N1C9	1.392(7)
N2C3	1.355(7)	N3C5	1.366(7)
N4C7	1.352(7)	N4C8	1.400(7)
N2C2	1.497(7)	N3C6	1.489(7)
Cl1C11	1.739(6)	ClC12	1.720(6)
C1C2	1.514(8)	C3C4	1.530(8)
C4C5	1.521(8)	C6C7	1.516(8)
C1O1	1.228(8)	C3O2	1.224(7)
C5O3	1.223(7)	C7O4	1.227(7)
C2C14	1.515(8)	C2C15	1.548(8)
C8C9	1.411(8)	C8C13	1.388(8)
C4C16	1.554(8)	C4C18	1.558(8)
C6C20	1.549(8)	C6C21	1.529(8)
C16C17	1.515(8)	C18C19	1.486(10)
C9C10	1.403(9)	C10C11	1.364(9)
C11C12	1.389(9)	C12C13	1.382(9)

Table 4.3. Bond Angles in [Mn(O)(η^4-DEMAMPA-DCB)]$^-$			
Atoms	Angle (°)	Atoms	Angle (°)
OMnN1	107.8(2)	O′Mn′N1	124(2)
OMnN2	109.6(2)	O′Mn′N2	111(2)
OMnN3	107.6(2)	O′Mn′N3	108(2)
OMnN4	109.0(2)	O′Mn′N4	120(2)
N1MnN2	81.8(2)	N1Mn′N2	74.5(4)
N1MnN3	143.9(2)	N1Mn′N3	126.8(6)
N1MnN4	80.2(2)	N1Mn′N4	68.9(4)
N2MnN3	92.9(2)	N2Mn′N3	96.1(6)
N2MnN4	140.8(2)	N2Mn′N4	127.8(6)
N3MnN4	81.9(2)	N3Mn′N4	78.3(5)
MnN1C1	118.9(4)	Mn′N1C1	108.1(5)
MnN1C9	116.4(4)	Mn′N1C9	113.5(5)
MnN2C2	115.5(3)	Mn′N2C2	116.3(5)
MnN2C3	126.4(4)	Mn′N2C3	117.4(5)
MnN3C5	124.5(4)	Mn′N3C5	120.5(5)
MnN3C6	114.5(3)	Mn′N3C6	114.9(5)
MnN4C7	118.5(4)	Mn′N4C7	106.1(5)
MnN4C8	117.0(3)	Mn′N4C8	116.0(5)
C1N1C9	124.7(5)	C2N2C3	116.2(4)
C5N3C6	117.2(4)	C7N4C8	124.4(5)
N1C1O1	124.9(5)	C2C1O1	121.5(5)
N1C1C2	113.6(5)	N2C3O2	122.5(5)
C1C2N2	106.1(4)	C4C3O2	116.8(5)

Table 4.3. Bond Angles in [Mn(O)(η^4-DEMAMPA-DCB)]$^-$ (continued)

Atoms	Angle (°)	Atoms	Angle (°)
C1C2C14	107.6(5)	N2C3C4	120.7(5)
C1C2C15	106.3(5)	N3C5O3	122.3(5)
N2C2C14	112.9(5)	C4C5O3	116.9(5)
N2C2C15	110.2(5)	N3C5C4	120.8(5)
C14C2C15	113.3(5)	N4C7O4	125.0(5)
C3C4C5	121.9(5)	C6C7O4	122.2(5)
C3C4C16	107.2(4)	N4C7C6	112.7(5)
C3C4C18	106.7(5)	N4C8C9	110.7(5)
C5C4C16	108.3(5)	N4C8C13	129.3(5)
C5C4C18	105.1(4)	C9C8C13	120.1(5)
C16C4C18	106.7(5)	N1C9C8	111.6(5)
C7C6N3	106.3(4)	N1C9C10	128.6(5)
C7C6C20	105.8(5)	C8C9C10	119.7(5)
C7C6C21	107.9(5)	C9C10C11	118.8(5)
N3C6C20	112.4(4)	C10C11C12	121.9(6)
N3C6C21	112.2(4)	C10C11Cl1	118.0(5)
C20C6C21	111.7(5)	C12C11Cl1	120.0(5)
C4C16C17	112.1(5)	C11C12C13	120.0(5)
C4C18C19	114.3(6)	C11C12Cl2	121.1(5)
C13C12Cl2	118.9(5)	C12C13C8	119.5(5)

proceeded about 70% to completion. Comparison of the IR spectra of the ^{18}O and ^{16}O complexes to those of the chromyls (see Chapter 3) indicated that the oxo stretches were in virtually the same place: 982 cm^{-1} for the ^{16}O-derivative and 942 cm^{-1} for the ^{18}O-derivative. [The 1500–1700 cm^{-1} regions are also similar. $[Mn(O)(\eta^4\text{-DEMAMPA-DCB})]^-$ has stretches at 1650, 1605, and 1582 cm^{-1}, while $[Cr(O)(\eta^4\text{-DEMAMPA-DCB})]^-$ has stretches at 1656, 1601, and 1575 cm^{-1}.] However, unlike the chromyls, which gave only modest resonance enhancement of the Cr–O stretch in the Raman spectra, the manganyls gave remarkable resonance enhancement. Figure 4.7 shows the off-resonance Raman spectrum of the compound in a Na_2SO_4 pellet, while Figure 4.8 shows the on-resonance spectrum of the compound in a Na_2SO_4 pellet. Figure 4.9 shows the on-resonance spectrum of the complex in a KBr pellet, while Figure 4.10 unambiguously shows the shift of the Mn–O stretch after partial ^{18}O-labeling. The $\nu_{Mn\equiv O}$ bands are: ^{16}O-labeled 979 cm^{-1}, ^{18}O-labeled 942 cm^{-1}. These data can be contrasted to the vibrational properties of high spin d^3 Mn^{IV}=O units in porphyrin complexes; for the five-coordinate species in that study, $\nu_{Mn=O}$ occurs at 754 cm^{-1} (vide supra). Clearly, the low spin d^2 Mn(V) oxo complex has a formal triple bond between the Mn and oxygen atoms, while the high spin d^3 Mn(IV) oxo has a formal double bond between the Mn and oxygen atoms. The resonance Raman spectra of the Cr and Mn porphyrin nitrides have been studied and similarly exhibit modest enhancement for Cr and strong enhancement for Mn.[17] This difference was rationalized based on the planarity of the porphyrin ring in the Mn nitride vs. the buckled nature of the porphyrin ring in the Cr nitride. Since the structures of the chromyl and manganyl of $(\eta^4\text{-DEMAMPA-DCB})^{4-}$ are virtually

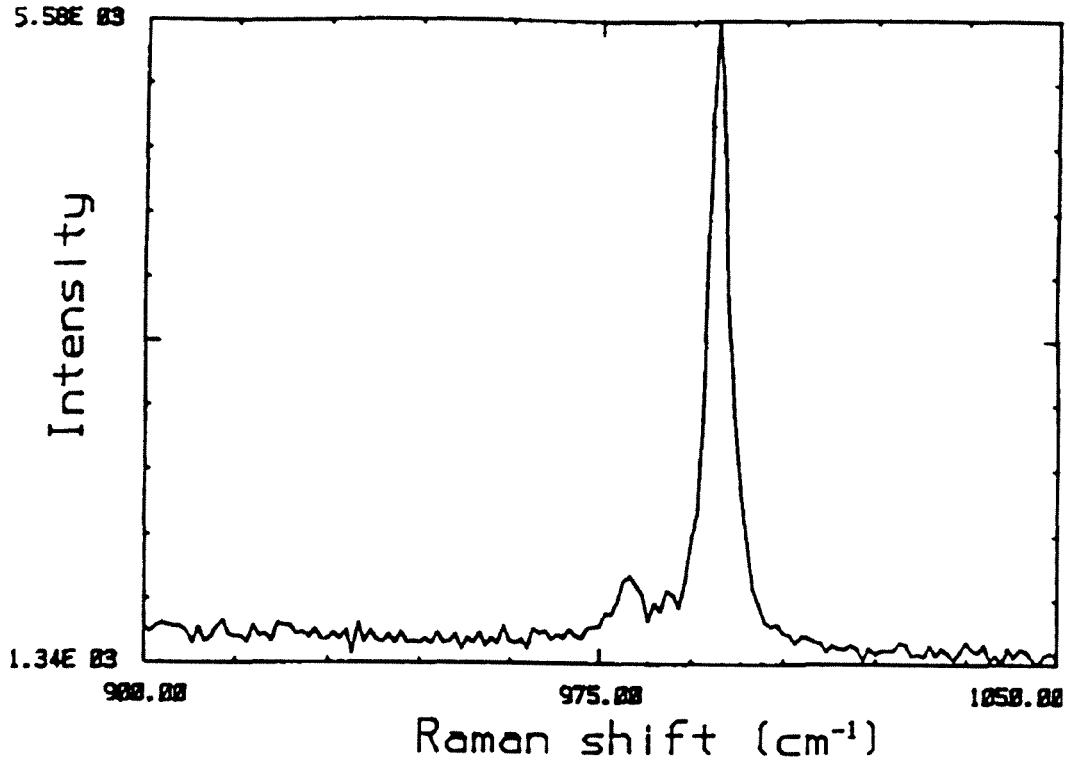

Figure 4.7. Resonance Raman spectrum of $[Et_4N][Mn(O)(\eta^4\text{-DEMAMPA-DCB})]$ in a Na_2SO_4 pellet. Excitation is off resonance (λ_{ex}=647.0 nm). The peak at 994 cm^{-1} is due to SO_4^{2-}, while the weak band at 980 cm^{-1} is due to the complex.

superimposable, this explanation probably needs to be re-evaluated.

Like the low spin diamagnetic complex of the acyclic ligand, the complex of the macrocyclic ligand also shows the expected diamagnetic ^1H NMR spectrum of a low spin d^2 square pyramidal complex complex with C_s symmetry (Figure 4.11). The chemical shifts and coupling constants observed are consistent with those found in other diamagnetic complexes of these ligands.

The macrocyclic complexes are quite distinct from the acyclic complexes in exhibiting reversible oxidations at high potentials. The cyclic voltammogram of $[Mn(O)(\eta^4\text{-DEMAMPA-DCB})]^-$ is shown (Figure 4.12) and so is that

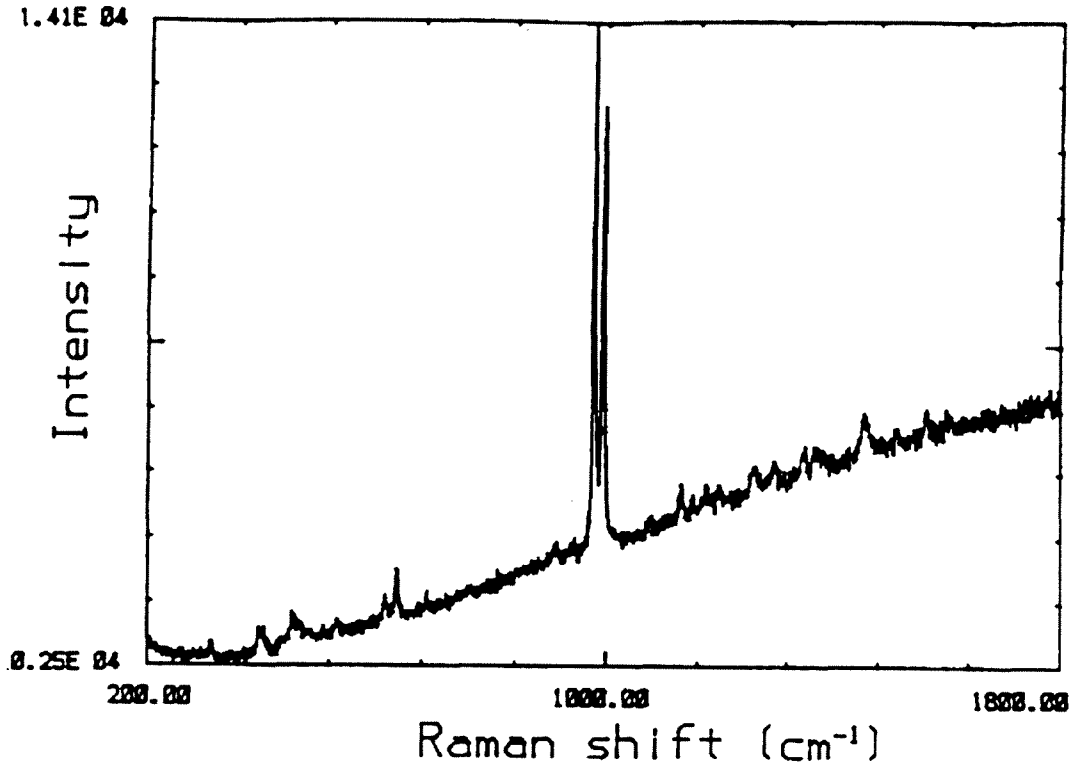

Figure 4.8. Resonance Raman spectrum of $[Et_4N][Mn(O)(\eta^4\text{-DEMAMPA-DCB})]$ in a Na_2SO_4 pellet. Excitation is on resonance (λ_{ex}=488.0 nm). The peak at 996 cm^{-1} is due to SO_4^{2-}, while the strong band at 979 cm^{-1} is due to the complex.

for $[Mn(O)(\eta^4\text{-DEMAMPA-DMOB})]^-$ (Figure 4.13). These reversible couples are remarkable in that the oxidized species would be formally Mn(VI) monooxos, but it is likely that ligand noninnocence plays a big role in these oxidations. EPR spectra taken after bulk electrolysis are interesting (Figures 4.14 and 4.15). Both spectra show the six line pattern expected for hyperfine interactions with ^{55}Mn (I=5/2, 100% abundance). The data obtained for MnO_4^{2-} (vide supra) have similar g values (1.97 for the manganate, 2.038 for the macrocyclic complex), and similar ^{55}Mn hyperfine interactions ($\approx$30 G to $\approx$140 G for the different A tensors of the manganate). It remains to be clearly

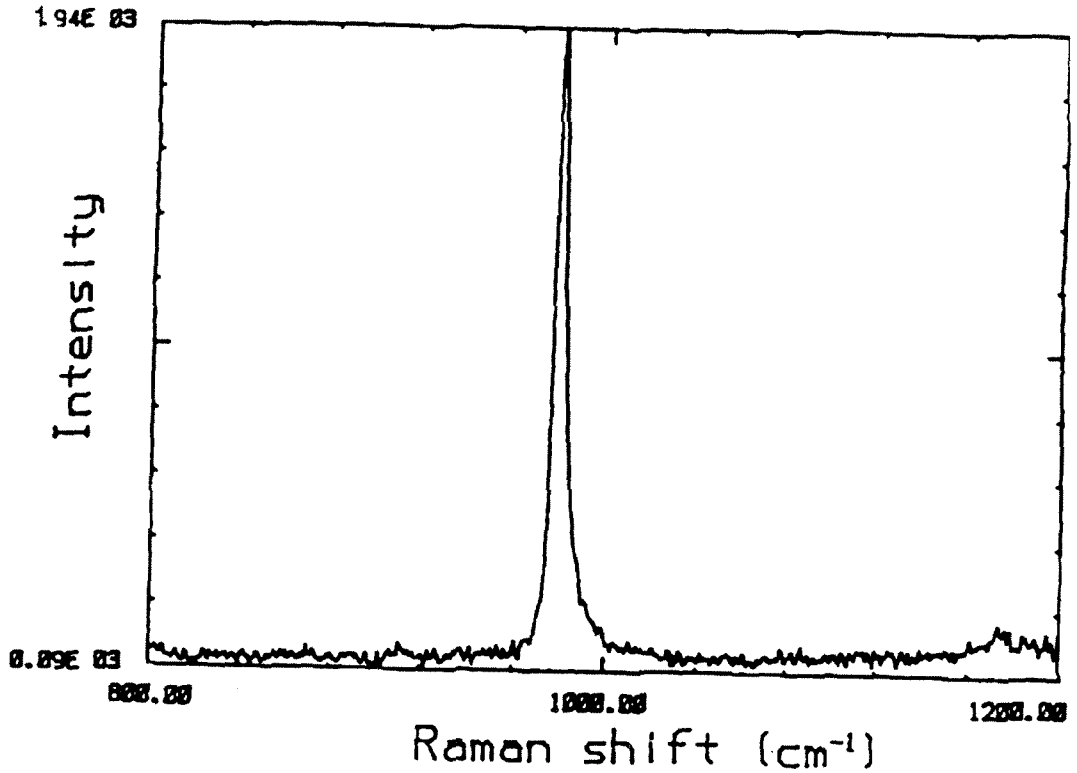

Figure 4.9. Resonance Raman spectrum of $[Et_4N][Mn(O)(\eta^4\text{-DEMAMPA-DCB})]$ in a KBr pellet. Excitation is on resonance (λ_{ex}=406.7 nm). The strong band at 979 cm^{-1} is due to the complex.

demonstrated that these EPR spectra correspond to $Mn(O)(\eta^4$-DEMAMPA-DCB) or $Mn(O)(\eta^4$-DEMAMPA-DMOB). José Workman in the Collins group is studying the electrochemical characterization of these complexes and other derivatives, and has collaborated with Alexander Procyk of the Bocian group to extend the resonance Raman characterization.[18]

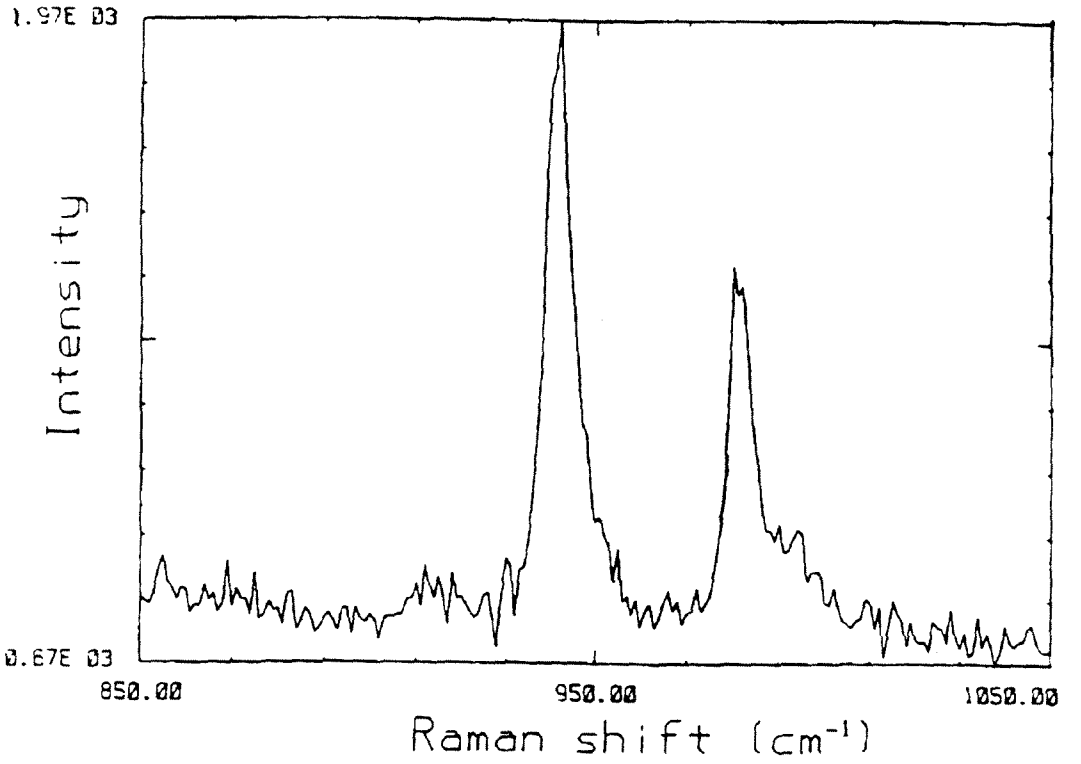

Figure 4.10. Resonance Raman spectrum of $[Et_4N][Mn(O)(\eta^4\text{-DEMAMPA-DCB})]$, which was prepared after stirring the Li salt in $H_2{}^{18}O$ for 48 h under N_2, in a KBr pellet. Excitation is on resonance (λ_{ex}=406.7 nm). The strong bands at 942 and 981 cm^{-1} are due to the ^{18}O-labeled and ^{16}O-labeled complexes respectively.

NEXT PAGE: Figure 4.11. ^1H NMR (300 MHz, CD_2Cl_2) of $[Et_4N][Mn(O)(\eta^4\text{-DEMAMPA-DCB})]$ (δppm: 8.59, s, 2H(aromatic); 3.23, br, 8H($[(CH_3\underline{CH_2})_4N]^+$); 2.02, q, 2H($CH_3\underline{CH_2}$-); 1.94, q, 2H($CH_3\underline{CH_2}$-); 1.86, s, 6H($C(\underline{CH_3})CH_3$); 1.80, s, 6H($C(CH_3)(\underline{CH_3})$); 1.35, br, 12H($[(\underline{CH_3}CH_2)_4N]^+$); 0.86, t, 3H($\underline{CH_3}CH_2$-); 0.56, t, 3H($\underline{CH_3}CH_2$-) [x = $CHDCl_2$ signals—used as reference, o = H_2O).

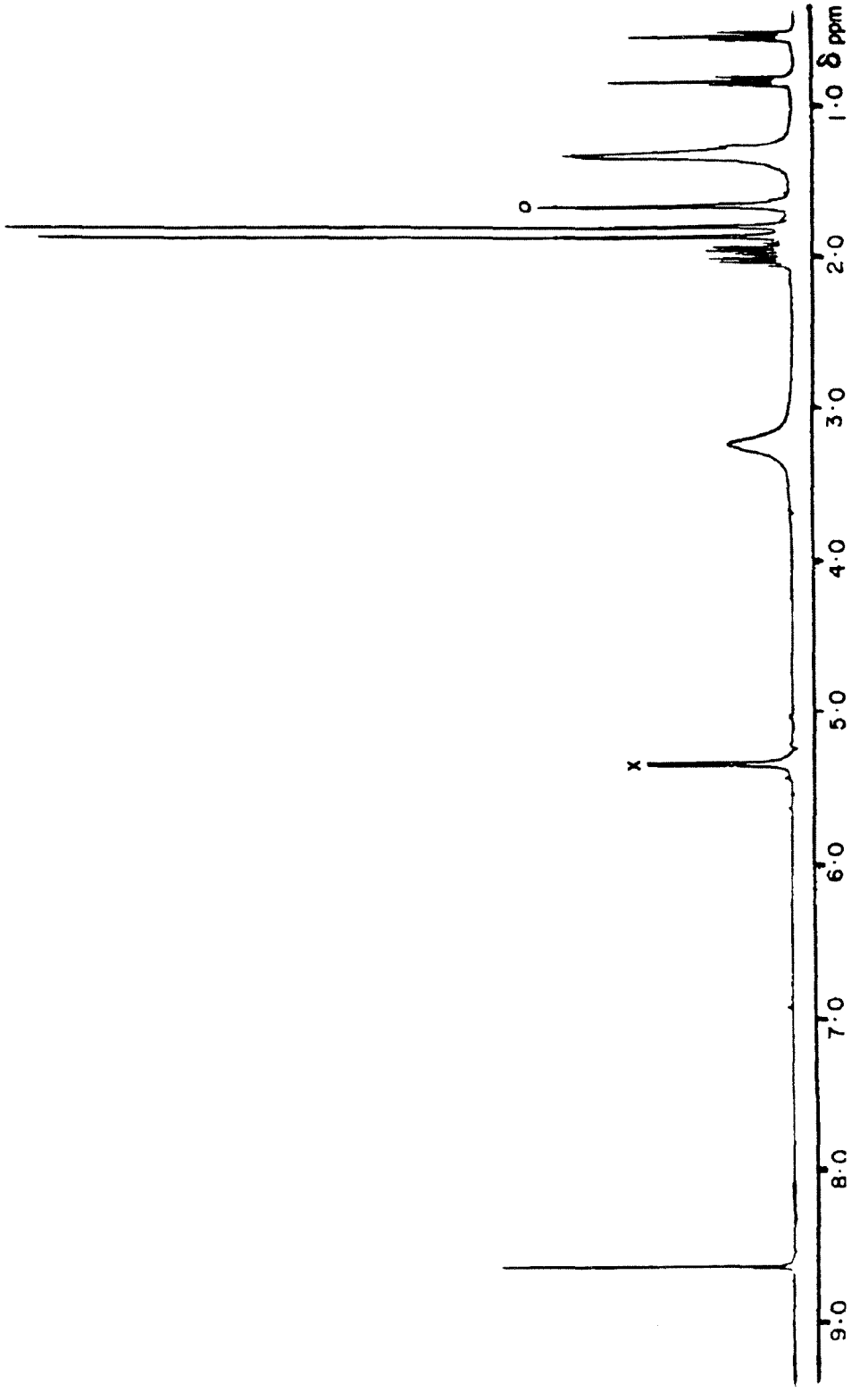
o
x
1·0 δ ppm
2·0
3·0
4·0
5·0
6·0
7·0
8·0
9·0

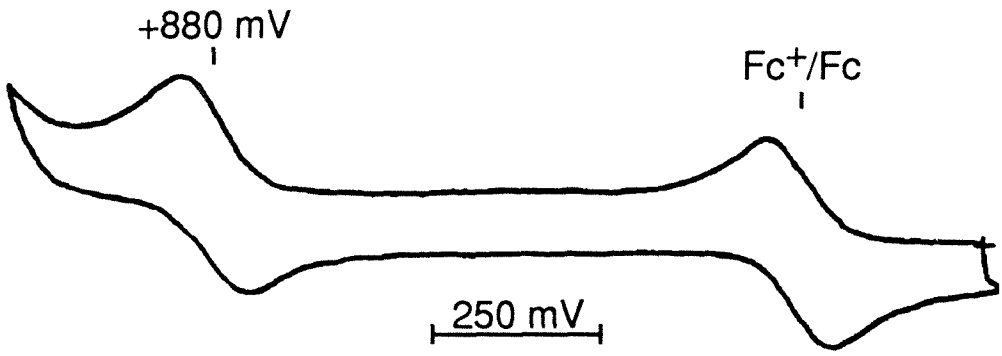

Figure 4.12. Cyclic voltammogram of $[Mn(O)(\eta^4\text{-DEMAMPA-DCB})]^-$ and ferrocene at 200 mV/s in a 0.1 M solution of $[Bu_4N][ClO_4]$ in CH_2Cl_2. The Mn couple is +880 mV vs. Fc^+/Fc.

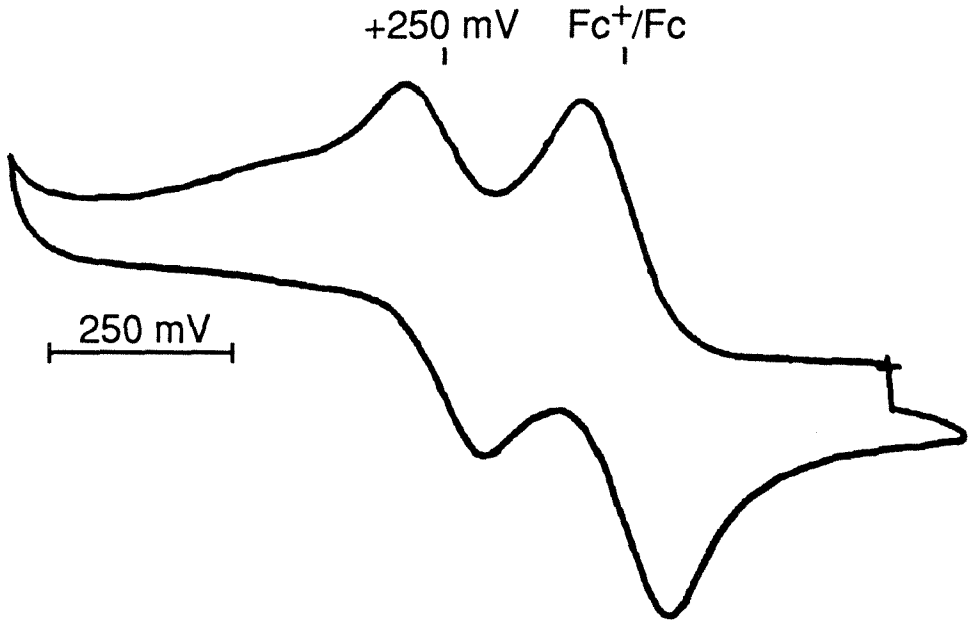

Figure 4.13. Cyclic voltammogram of $[Mn(O)(\eta^4\text{-DEMAMPA-DMOB})]^-$ and ferrocene at 200 mV/s in a 0.1 M solution of $[Bu_4N][ClO_4]$ in CH_2Cl_2. The Mn couple is +250 mV vs. Fc^+/Fc.

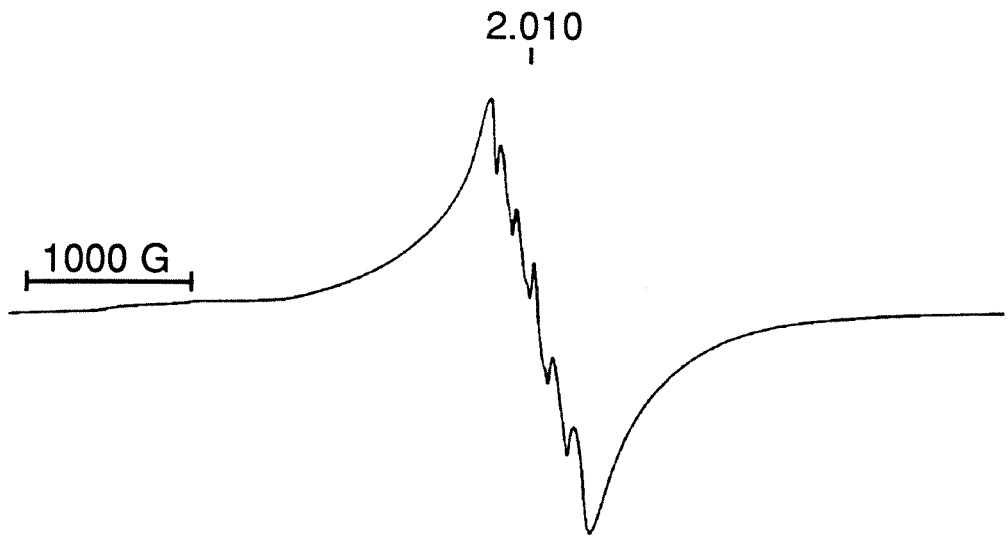

Figure 4.14. EPR spectrum of Mn(O)(η^4-DEMAMPA-DCB) at 154 K, 9.34 GHz, in a 0.1 M solution of $[Bu_4N][ClO_4]$ in CH_2Cl_2 (three scan average, 6000 G scan range, 3050 G mid-range), A_{Mn}=50 G (low field)–120 G (high field).

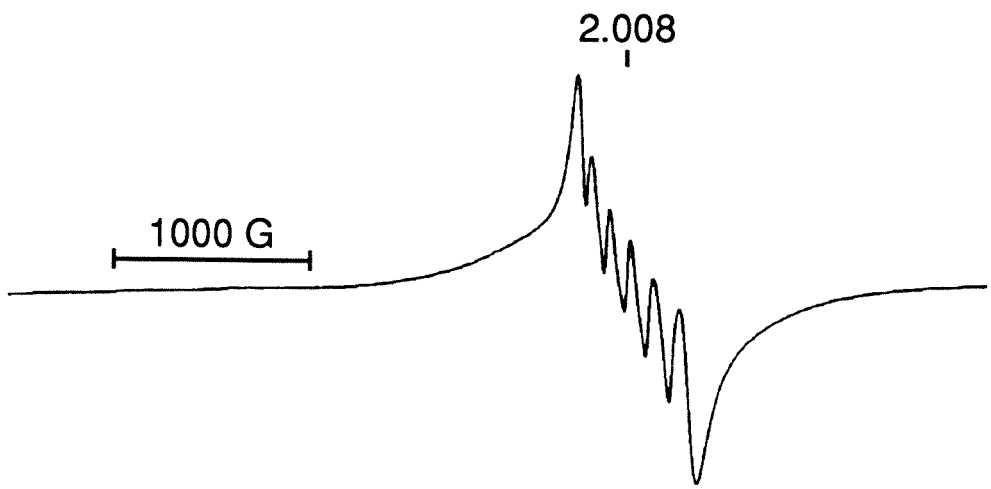

Figure 4.15. EPR spectrum of Mn(O)(η^4-DEMAMPA-DMOB) at 150 K, 9.33 GHz, in MeCN (three scan average, 5000 G scan range, 2550 G mid-range), A_{Mn}=70 G (low field)–125 G (high field).

Experimental

Materials. All solvents and reagents were reagent grade (Aldrich) except for THF and benzene (Aldrich, Sureseal) and were used as received except as described for electrochemical measurements.

Physical Measurements. ^{1}H NMR were measured at 300 MHz on an IBM NR/300 FT-NMR Spectrometer. ^{1}H NMR data are reported in δ vs. $(CH_3)_4Si$ with the solvent as internal standard. EPR spectra were recorded on a Bruker ER300 Spectrometer. Infrared data were obtained on a Nicolet 5DXB FT-IR Spectrometer. UV-vis data were obtained on a Perkin-Elmer Lambda Array 3840 Spectrophotometer. Crystal structures were solved by Crystalytics Co. of Lincoln, Nebraska.

Electrochemical Data. Cyclic voltammetry was performed on a Princeton Applied Research Model 173/179 potentiostat/digital coulometer equipped with positive feedback IR compensation and a Model 175 universal programmer. Current voltage curves were recorded on a Houston Instruments Model 2000 X-Y recorder.

Sureseal anhydrous CH_2Cl_2 (Aldrich) was used as received. $[Bu_4N][ClO_4]$ (Fluka) was vacuum dried at 80 °C. In all cases experiments were performed under N_2 with a supporting electrolyte concentration of 0.1 M. Cyclic voltammetry was performed in CH_2Cl_2 solutions of $[Bu_4N][ClO_4]$ at a 3 mm Pt disk working electrode with a silver wire quasi-reference electrode and a Pt foil counter electrode. At the conclusion of each experiment, ferrocene (Fc) was added as an internal potential standard. All formal potentials were taken as the average of anodic and cathodic peak potentials and are reported vs. the Fc^+/Fc couple. Peak-to-peak separation of the Fc^+/Fc couple was similar to

that of the Mn couples in all cases. Plots of peak current vs. the square root of scan rate over the range 10–500 mV s^{-1} were made and found to be linear for couples that are stated to be reversible. Bulk electrolysis was performed in CH_2Cl_2 solutions of $[Bu_4N][ClO_4]$ in a standard three-compartment cell at Pt gauze working and counter electrodes with a silver wire quasi-reference electrode.

Synthetic Note. The experimental work reported here has been published in substantially similar form in *J. Am. Chem. Soc.*[15]

$[Et_4N][Mn(O)(\eta^4$-DEMAMPA-DCB)]. H_4DEMAMPA-DCB (58 mg, 0.12 mmol) was dissolved in dry, deoxygenated THF, and a stoichiometric amount of lithium bis(trimethylsilyl)amide (1.0 M solution in THF) was added at 20 °C under N_2 and stirred (5 min). A 25% excess of anhydrous $MnCl_2$ was added and the mixture was stirred (2 h) to yield a yellowish-white suspension, presumably a manganese(II) complex. A fivefold excess of *tert*-butyl hydroperoxide (3.0 M solution in 2,2,4-trimethylpentane) was added, and the mixture was stirred overnight to yield a dark greenish-brown solution. The solvents were removed under vacuum, and the solid residue was washed with CH_2Cl_2, extracted with CH_3CN and passed through a diatomaceous earth pad to give $Li[Mn(O)(\eta^4$-DEMAMPA-DCB)] (yield approximately 75%). A stoichiometric amount of $[Et_4N]Cl$ was added to an CH_3CN solution of the complex, and the CH_3CN was then removed in vacuo. The residue was extracted with CH_2Cl_2 to yield a solution of $[Et_4N][Mn(O)(\eta^4$-DEMAMPA-DCB)], which gave green X-ray quality crystals from CH_2Cl_2/C_6H_6. An oxygen-(18) substituted species was produced by dissolving $Li[Mn(O)(\eta^4$-DEMAMPA-DCB)] (10 mg) in $H_2{}^{18}O$ (1 ml), stirring for 48 h under N_2, removing the excess water in vacuo,

then crystallizing as the $[Et_4N]^+$ salt as described above. This complex can also be synthesized using the *tert*-butyllithium/−108 °C method of preparing Li[Cr(O)(η^4-DEMAMPA-DCB)] (see Chapter 3).

X-ray Data Collection and Structure Refinement of [Et_4N][Mn-(O)(η^4-DEMAMPA-DCB)]. Single crystals of $[(C_2H_5)_4N]$[Mn(O)(η^4-DEMAMPA-DCB)] at 20± 1 °C are monoclinic, space group $P2_1/c\text{-}C_{2h}^5$ (No. 14) with a = 9.853(2) Å, b = 14.890(3) Å, c = 22.432(5) Å, β = 95.43(1)°, V = 3276(1) Å^3 and Z = 4 (d_{calcd} = 1.356 g cm^{-3}; μ_a(CuK$\bar{\alpha}$) = 5.2 mm^{-1}). A total of 4505 independent absorption-corrected reflections having 2θ(CuK$\bar{\alpha}$) < 115.0° were collected using θ-2θ scans and Ni-filtered CuK$\bar{\alpha}$ radiation. The structural parameters have been refined to a convergence of R_1(unweighted, based on F) = 0.046 for 2447 independent reflections having $2\theta_{CuK\bar{\alpha}}$ < 115.0° and I > 3σ(I). There was disorder in the Mn–O unit (92% "above" the plane and 8% "below" the plane).

References

1. (a) Nugent, W. A.; Mayer, J. M. *Metal-Ligand Multiple Bonds*; Wiley-Interscience: New York, 1988. (b) Cotton, F. A., Wilkinson, G. *Advanced Inorganic Chemistry, 5th Edn.*; Wiley: New York, 1988.

2. Collins, T. J.; Gordon-Wylie, S. W. *J. Am. Chem. Soc.* **1989**, *111*, 4511–4513.

3. For a set of references on this rapidly developing area, see: (a) Groves, J. T.; Stern, M. K. *J. Am. Chem. Soc.*, **1988**, *110*, 8628–8638. Also see: (b) Anelli, P. L.; Banfi, S.; Montanari, F.; Quici, S. *J. Chem. Soc., Chem. Commun.* **1989**, 779-780. (c) Holm, R. H. *Chem. Rev.* **1987**, *87*, 1401–1449. (d) Srinivasan, K.; Michaud, P.; Kochi, J. K. *J. Am. Chem. Soc.* **1986**, *108*, 2309–2320.

4. (a) Amesz, J.; *Biochim. Biophys. Acta* **1983**, *726*, 1–12. (b) Babcock, G. T. in *New Comprehensive Biochemistry - Photosynthesis*, Amesz, J., ed.; Elsevier: Amsterdam, 1988. (c) Pecoraro, V. L. *Photochem. Photobiol.* **1988**, *48*, 249–264.

5. Ludwig, M.; Pattridge, K. A.; Stallings, W. C. *Manganese in Metabolism and Enzyme Function*; Academic press: New York, 1986; Chapter 21, p 405.

6. Beyer, W., Jr.; Frodovich, I. *Manganese in Metabolism and Enzyme Function*; Academic press: New York, 1986; Chapter 12, p 193.

7. (a) Chiswell, B.; McKenzie, E. D.; Lindoy, L. F. In *Comprehensive Coordination Chemistry* Wilkinson, G., Ed. in chief, Gillard, R. D.; McCleverty, J. A., Eds.; Pergamon: New York, 1987; Vol. 4, Chapter 41. (b) Levason, W.; McAuliffe, C. A. *Coord. Chem. Rev.* **1972**, *7*, 353–384.

8. (a) Levason, W.; Ogden, J. S.; Turff, J. W. *J. Chem. Soc., Dalton Trans.* **1983**, 2699–2702. (b) Frigerio, N. A. *J. Am. Chem. Soc.* **1969**, *91*, 6200–6201. (c) Briggs, T. S. *J. Inorg. Nucl. Chem.* **1968**, *30*, 2866–2869. (d) Siddiqi, Z. A.; Lutfullah, S. A.; Zaidi, A.; Siddiqi, K. S. *Bull. Soc. Chim. Fr., Part I* **1980**, 228–230. (e) The crystal structure of this compound has been obtained by immediately cooling an X-ray capillary after filling it with liquid Mn_2O_7. Simon, A.; Dronskowski, R.; Krebs, B.; Hettich, B. *Angew. Chem. Int. Ed. Engl.* **1987**, *26*, 139–140.

9. Nyholm, R. S.; Woolliams, P. R. *Inorg. Synth.* **1968**, *11*, 56–61.

10. Carrington, A.; Ingram, D. J. E.; Lott, K. A. K.; Schonland, D. S.; Symons, M. C. R. *Proc. R. Soc.* **1960**, *A254*, 101–110.

11. Cook, B. R.; Reinert, T. J.; Suslick, K. S. *J. Am. Chem. Soc.* **1986**, *108*, 7281.

12. Collman, J. P.; Brauman, J. I.; Hampton, P. D.; Tanaka, H.; Bohle, D. S.; Hembre, R. T. *J. Am. Chem. Soc.* **1990**, *112*, 7980–7984.

13. Bortolini, O.; Meunier, B.; *J. Chem. Soc., Chem. Commun.* **1983**, 1364–1366.

14. Czernuszewicz, R. S.; Su, Y. O.; Stern, M. K.; Macor, K. A.; Kim, D.; Groves, J. T.; Spiro, T. G. *J. Am. Chem. Soc.* **1988**, *110*, 4158–4165.

15. Collins, T. J.; Powell, R. D.; Slebodnick, C.; Uffelman, E. S. *J. Am. Chem. Soc.* **1990**, *112*, 899–901.

16. (a) Buchler, J. W.; Dreher, C.; Lay, K. L. *Z. Naturforsch., Teil B.* **1982**, *37*, 1155. (b) Hill, C. L.; Hollander, F. J. *J. Am. Chem. Soc.* **1982**, *104*, 7318. (c) Buchler, J. W.; Dreher, C.; Lay, K. L.; Lee, Y. J. A.; Scheidt, W. R. *Inorg. Chem.* **1983**, *22*, 888.

17. Campochiaro, C.; Hofmann, J. A. Jr.; Bocian, D. F. *Inorg. Chem.* **1985**, *24*, 449–450.

18. Workman, J. W.; Powell, R. D.; Procyk, A.; Collins, T. J.; Bocian, D. F. submitted for publication.

Chapter 5

Stable Mononuclear Five-Coordinate Fe(IV) Complexes of Macrocyclic Tetraamido-*N* Ligands

Highly oxidized iron complexes are significant as reactive intermediates in many biological and biomimetic redox processes.[1] Despite this significance, high valent iron coordination chemistry is limited. Few stable, well-defined compounds of iron(IV) exist,[2] and the V and VI oxidation states are established only for the tetraoxo polyanions.[2] This chapter will briefly discuss the chemistry of Fe(IV), Fe(V), and Fe(VI), and will summarize some of the salient features of high valent iron in biological systems. The rest of the chapter will present the chemistry of high valent iron with the macrocycles of this thesis. The compound, $[Et_4N][FeCl(\eta^4\text{-MAC*})]$, is of particular importance, being the first mononuclear five-coordinate iron(IV) complex to be characterized by X-ray crystallography.

Background

Non-biological high valent iron chemistry

The chemistry of high valent iron has been reviewed.[2,3] The only Fe(VI) compound known is the ferrate ion, FeO_4^{2-}. There are a number of ways of preparing FeO_4^{2-} salts,[4] but the method which seems to give the purest samples of potassium, rubidium, cesium, and barium salts was developed by Audette and Quail.[4] The method is lengthy, but consists essentially of chilling very basic, very concentrated aqueous solutions of MOCl with powdered ferric nitrate nonahydrate, adding more base, and then rapidly filtering the purple precipitate. This precipitate is dried with benzene washes, and then washed twenty times in a centrifuge with portions of absolute methanol. Considerable further washing yielded salts of 99.8% purity in overall yields of 50–60%. The dianion is reasonably stable in the solid state, and has magnetic moments between 2.67–2.92 B. M. for the different salts, which all obey the Curie-Weiss law

between 85–303 K. The vibrational spectra of these species have been studied by IR and Raman spectroscopies, which show absorbances at 832, 790, 340, and 322 cm^{-1}.[4,5] The electronic structure and molecular orbital description of FeO_4^{2-} has been based on the scheme of Viste and Gray developed for permanganate ion.[6]

Most of the Fe(IV) chemistry prior to this thesis had been done with non-innocent ligands such as dithiocarbamates, *o*-phenylenediarsines, and dithiolene/dithiolates. This work will be quickly summarized.

The first well characterized complex which was claimed to contain Fe(IV) was $[Fe(diars)_2X_2]^{2+}$ (X = Cl, Br; diars = *o*-phenylenebisdimethylarsine).[7] These dark black compounds are best prepared by oxidizing the monocations with 15 N nitric acid, adding 42% HBF_4, and collecting the dark black precipitate (the perchlorate salt is highly explosive). The complexes are hygroscopic (with decomposition), but may be stored briefly under vacuum in the absence of light. Most solvents which dissolve the complexes cause rapid decomposition, but the complexes are sparingly soluble in nitromethane, with a half-life of fifteen minutes. At room temperature the magnetic susceptibility of the chloro complex was 2.76 B. M. and that for the bromo complex was 3.17 B. M. The Mössbauer spectra of these compounds were collected on samples containing 90% ^{57}Fe.[8] For the dichloro complex, the center shift was 0.12 mm s^{-1} (298 K, with respect to metallic iron) and the quadrupole splitting was 3.22 mm s^{-1}. The sign of the electric field gradient was determined to be positive in an external field of 50 kG. Assuming D_{4h} symmetry, it was claimed that this positive q value indicated that the ground state was $^3A_{2g}$. For the dibromo complex at 298 K, the center shift was 0.17 mm s^{-1} and the quadrupole splitting was

3.16 mm s^{-1}.

Iron(IV) has been claimed in the tris-*N,N*-disubstituted dithiocarbamate cations, which can be prepared by oxidation of the corresponding Fe(III) complexes with BF_3/air[9a] or with I_2.[9b] These black complexes undergo slow decomposition at room temperature. The C–N bands increase 30–40 cm^{-1} upon oxidation. The room temperature magnetic moments of the complexes varied from 3.15–3.37 B. M. The Mössbauer spectra show isomer shifts of 0.10–0.13 mm s^{-1} at 300 K, with quadrupole splittings of 2.00–2.54 mm s^{-1}. For Fe(III) tris-dithiocarbamates, isomer shifts of 0.29 mm s^{-1} are observed. The nature of the BF_3/air oxidation was not elucidated. Electrochemical measurements of complexes of this type give an Fe(IV)/Fe(III) couple varying between 0.41–0.61 V in acetone vs. Ag/AgCl (approximately 0.60–0.80 V vs. NHE).[10] The crystal structure of the pyrrolidyl derivative ($(CH_2)_4NCS_2^-$) was performed.[11] No structural anomalies were observed in the ligand framework, and the average Fe-S distance contracted 0.11 Å from the corresponding Fe-S average distance in the Fe(III) complex. All of the Mössbauer,[12] structural, and electrochemical data were consistent with the formal Fe(IV) oxidation state assignment. Similarly, $[Fe^{IV}(DED)_3]^{2-}$ (DED = 1,1-dicarboethoxy-2,2-ethylenedithiolate, Figure 5.1) has been prepared by the reaction of K_2DED with $Fe(ClO_4)_3 \cdot H_2O$ in water in the presence of air.[13] Dark black crystals of the benzyltriphenylphosphonium salt were structurally characterized and revealed the ligand to be insignificantly different compared to the ligand in $[Ni^{II}(DED)_2]^{2-}$. The Fe(IV)/Fe(III) couple occurred at the notably low potential of −1.20 V (vs. Ag/AgI, in CH_2Cl_2).

There are two crystal structures of five-coordinate iron where a formal ox-

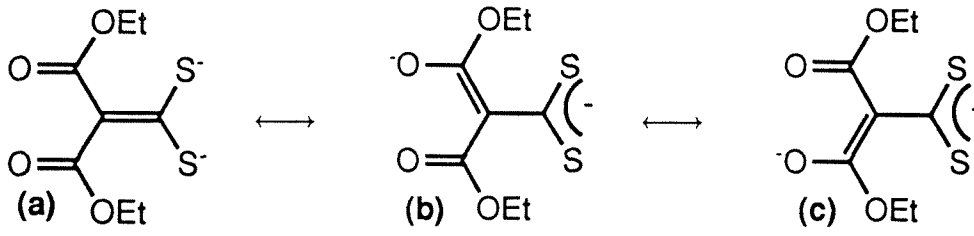

Figure 5.1. Resonance structures of the DED (1,1-dicarboethoxy-2,2-ethylenedithiolate) ligand.

idation state assignment is inappropriate due to the use of noninnocent dithiolate ligands. The triphenylarsine complex of bis(1,2-bis(trifluoromethyl)-1,2-ethylenedithiolato)iron could be considered a five-coordinate Fe(IV) complex. However, the C-S bond lengths of 1.702 Å are considerably shorter than those found in low oxidation state maleonitriledithiolate complexes (1.71–1.75 Å). This led the investigators to consider the complex a dithiolene compound.[14a] The crystal structure of bis(1,2-diphenyl-1,2-ethylenedithiolato)trimethoxyphosphineiron has C–S bond lengths of 1.717 Å.[14b] Although the authors assigned a formal oxidation state of iron(IV), the noninnocence of the ligand makes this uncertain. There does not appear to be any Mössbauer data on these two compounds.

The best characterised complex of five-coordinate iron(IV) is the dimer, μ-carbido-bis(5,10,15,20-tetraphenylporphinatoiron).[15] The diamagnetic complex was prepared by the reaction of Fe(TPP) with CI_4. The Fe–C distance is 1.675 Å, the Fe-out-of-plane distance is 0.26 Å, the Fe-C-Fe angle is 180°, and the average Fe–$N_{porphyrin}$ bond length is 1.980 Å. The Mössbauer spectrum has an isomer shift of 0.10 mm s^{-1} and quadrupole splitting of 1.88 mm s^{-1}.[16] The complex is similar to the bridging nitrido complex (TPP)Fe-N-Fe(TPP),[17]

which has an Fe–$N_{nitride}$ bond length of 1.660 Å, an Fe-out-of-plane distance of 0.32 Å, an Fe-N-Fe angle of 180°, and an average Fe–$N_{porphyrin}$ bond length of 1.991 Å. The compound, (TPP)Fe-N-Fe(TPP), has a temperature independent magnetic moment of 2.04 B. M., and the Mössbauer spectrum has an isomer shift of 0.18 mm s^{-1} and quadrupole splitting of 1.08 mm s^{-1}.[16] The diamagnetic [(TPP)Fe-N-Fe(TPP)]$^+$ complex seems to be Fe(IV) by Mössbauer, with an isomer shift of 0.03 mm s^{-1} and quadrupole splitting of 2.00 mm s^{-1}.[16] The low spin electronic structure of these complexes has been explained by Tatsumi and Hoffman.[18]

Six-coordinate iron(IV) has been prepared from a six-coordinate iron(III) porphyrin cation radical complex by Groves and coworkers.[19] Treatment of Fe(TMP)(ClO_4) with solid Fe(ClO_4)$_3$ in CH_2Cl_2 for several hours yielded the bright green porphyrin cation radical complex Fe(TMP)(ClO_4)$_2$ (The assignment of oxidation to the porphyrin ring was supported by the long wavelength absorbance band near 800 nm and an intense IR band at 1270 cm^{-1}; both of these features are diagnostic of porphyrin cation radicals.). This compound was then treated with two equivalents of NaOMe in MeOH at −78 °C, generating deep red solutions of Fe^{IV}(TMP)(OMe)$_2$. The oxidation state assignment of this compound was supported by Mössbauer spectroscopy, which had an isomer shift of −0.025 mm s^{-1} and quadrupole splitting of 2.10 mm s^{-1}. The Mössbauer data were consistent with an $S = 1$ ground state, which was supported by the solution magnetic moment of 2.9 ± 0.2 B. M. from 193–229 K.

Goff's group reported that Fe(TPP)F in CH_2Cl_2 has a binding constant for a second fluoride ion of 4×10^3 M^{-1} at 25 °C.[20] This compound underwent a reversible oxidation at fast scan speeds at 0.16 V vs. Fc^+/Fc in CH_2Cl_2. The

compound was unstable and was postulated to disproportionate to Fe(TPP)F and the prophyrin cation radical, Fe(O)(TPP)F, in the presence of trace water. Due to its instability, the $Fe^{IV}(TPP)F_2$ species was poorly characterized, although the authors noted that production of the porphyrin cation radical, $Fe(TPP)F^+$, occurs at a potential that is 0.41 V higher, supporting the iron(IV) formulation for the oxidized difluoro species.

Biological high valent iron chemistry

The cytochromes P-450[1a,21] are monooxygenase enzymes of critical importance to a number of living organisms. They are responsible for many steps in the synthesis of steroids, fatty acids, and prostaglandins and are also involved in the oxidative metabolism of drugs and other foreign substances. The role of cytochromes P-450 in sterol synthesis and metabolism has been reviewed.[22] The enzymes all are b-type cytochromes which contain iron-protoporphyrin IX at the active site. What distinguishes the P-450 enzymes from the iron-porphyrin oxygen transport proteins is the unusual coordination of thiolate in one of the axial positions. There is speculation that this strong donor group is critical to the O-O scission that must occur to yield the catalytically reactive species.[23] The P-450 enzymes catalyse six categories of oxidative reactions[24]: (1) carbon hydroxylation—the formation of an alcohol at a methyl, methylene, or methine position (2) heteroatom release—the oxidative cleavage of the heteroatomic portion of a molecule, resulting from hydroxylation adjacent to the heteroatom and subsequent release of the heteroatom to form a carbonyl compound (3) heteroatom oxygenation—the conversion of a heteroatom substrate to its corresponding heteroatom oxide (4) epoxidation—the formation of oxirane derivatives from olefins and aromatic compounds (5) oxidative

group transfer—a 1,2 carbon shift of a group with concomitant incorporation of oxygen as a carbonyl at the C-1 position (6) olefinic suicide destruction—the inactivation of the enzyme by itself. The mechanism for carbon hydroxylation has been termed the oxygen rebound mechanism. There are several noteworthy aspects of this mechanism (Figure 1.16). First, the resting state of the enzyme is in equilibrium between a five-coordinate form and a six-coordinate form and binding of substrate shifts the equilibrium towards the five-coordinate form. Thus, as the sequence proceeds, the substrate is already close to what will become the reactive center, and this must contribute substantially to the lifetime of the enzyme, which does not have ligands which are particularly resistant to oxidative degradation. The structures of both of these two ferric forms have been crystallographically determined.[25] Second, the five-coordinate form obtains an electron from NADH or NADPH via an electron-transfer chain. This compound binds dioxygen to form a low-spin six-coordinate ferrous complex (There are many model systems for such a complex.[26]). This species then obtains an electron and two protons to form the reactive species, which is believed to be an iron(IV) oxo porphyrin cation radical. This species hydroxylates the substrate to an alcohol and regenerates the ferric complex.

There is considerable evidence in support of the iron(IV) oxo porphyrin cation radical species postulated as the active complex in the P-450 enzymes, only some salient aspects will be presented here. Groves and coworkers[27] have oxidized chloro-5,10,15,20-tetramesitylporphinatoiron(III) with 1.5 equivalents of *m*-chloroperoxybenzoic acid in CH_2Cl_2/MeOH at -78 °C to produce a green intermediate which has a magnetic susceptibility of 4.2 B. M. (Evans method), and a quadrupole doublet centered at 0.05 mm s^{-1} (quadrupole splitting of

1.49 mm s^{-1}) in the Mössbauer. Extensive Mössbauer studies at different temperatures and different fields were consistent with an Fe(IV) S=1 system tightly coupled with an S=1/2 porphyrin cation radical system. The NMR and visible spectra of this species also supported this formulation. Also consistent with this formulation was the rapid epoxidation of olefins by the intermediate at temperatures of −40 °C. Nakamoto's group[28] obtained resonance Raman spectra of oxoiron(IV) porphyrins by photolyzing iron(II) dioxygen complexes in dioxygen matrices at 15 K. They obtained an Fe–O band at 852 cm^{-1} which shifted to 818 cm^{-1} with $^{18}O_2$ and shifted to 856 cm^{-1} with ^{54}Fe. These data were consistent with a five-coordinate Fe^{IV}=O species. The authors noted that the lower Fe^{IV}=O band in HRP-II (787 cm^{-1}[29a]) and ferrylmyoglobin (797 cm^{-1}[29b]) is due to the coordination of the proximal imidazole in the sixth coordination site. In a similar study, Nakamoto's group laser photolyzed films of N_3Fe(TPP) at 30 K, obtaining N≡Fe^{V}(TPP).[30] The N≡Fe vibration at 876 cm^{-1} shifted to 854 cm^{-1} with ^{15}N and to 879 cm^{-1} with ^{54}Fe.

The peroxidases and the catalases are found in almost every aerobic organism and are related by their functions and active sites.[1i,31] Catalase converts hydrogen peroxide to water and oxygen; peroxidase uses hydrogen peroxide to perform substrate oxidations. A number of crystal structures exist of both enzyme types in their resting forms. These enzymes all have Fe(III) porphyrins at their active sites, with an axially bound imidazole. The presence or absence of a sixth ligand (e. g., water) is not clear. Oxidation of the ferric porphyrin with hydrogen peroxide or other O-atom transfer oxidants (e. g., alkylhydroperoxides, peracids) all yield the same intermediate, called Compound I. Magnetic susceptibility measurements and Mössbauer spectroscopy have revealed that

Compound I contains an S=1, Fe(IV) center, with the additional oxidizing equivalent stored in the ligands. The Compound I from Cytochrome c peroxidase has a Soret band similar to that observed for the Compound II (vide infra) of other peroxidase and catalase systems and, unlike the Compound I's of other enzymes, has a narrow line free-radical-like EPR observable at 77 K. This has been attributed to either a tryptophanyl radical, or a thioether cation radical. The Compound I of the other peroxidases is now generally believed to be an iron(IV) porphyrin cation radical. Compound II of these enzymes can be formed either by reduction of Compound I by one electron, or by reacting hydrogen peroxide with a reduced (Fe^{II}) form of the native enzyme. This compound also has an S=1, Fe(IV) center, but is not a porphyrin cation radical. These systems are all believed to contain an Fe^{IV}=O bond, and as was stated above, there is resonance Raman evidence for such a species in HRP-II.

The methane monooxygenase (MMO) enzymes have recently been reviewed by Fox and Lipscomb.[32] MMO catalyses the following reaction in methanotrophic bacteria:

$$NADH + H^+ + CH_4 + O_2 \rightarrow CH_3OH + NAD^+ + H_2O$$

It will also react with a number of other substrates, taking alkanes to alcohols, alkenes to epoxides, aromatics to phenols, pyridine to pyridine N-oxide, and dimethyl ether to methanol and formaldehyde. It is a three-component enzyme consisting of a hydroxylase, which contains two μ-hydroxo iron dimers responsible for the hydrocarbon oxidations, a reductase responsible for providing reducing equivalents that generate the diferrous state of the hydroxylase (which is the O_2 reactive form), and a less well-characterized protein called "compo-

nent B." The hydroxylase is a competent catalyst by itself in the presence of chemical reducing agents and molecular oxygen. No other known oxygenase contains a μ-hydroxo or μ-oxo iron dimer. The existence and nature of this dimer has been primarily explored by Mössbauer, EPR, and UV-vis spectroscopies. The resting state of the hydroxylase contains the dimer in its diferric form. The Mössbauer spectrum exhibits a quadrupole doublet with an isomer shift of 0.5 mm s^{-1} and ΔE_Q of 1.07 mm s^{-1}. The Mössbauer spectrum at 4.2 K in 6 Tesla applied field provided strong evidence that this compound is diamagnetic, with antiferromagnetic coupling between the iron centers yielding an S = 0 system. Upon complete reduction of the hydroxylase to the diferrous state, an integer spin EPR spectrum is observed at $g = 16$. Comparison of the EPR data to similar data for model complexes and the azide complex of deoxyhemerythrin demonstrated that this form of the hydroxylase contains ferromagnetically coupled high spin iron(II). Extensive single turnover reactivity studies of the reduced hydroxylase with oxygen and substrate allowed Fox and Lipscomb to postulate the catalytic cycle shown in Figure 5.2 for the hydroxylase of MMO. Certain aspects of the reactivity of MMO have been mimicked in model studies.[33]

Interesting biological systems which employ ferrous or ferric oxo-bridged dimers are hemerythrin (the nonheme oxygen transport protein of some lower organisms),[34] ribonucleotide reductase,[35] rubrerythrin,[36] and purple acid phosphatase.[37] The biology and chemistry of oxo-bridged polyiron centers has recently been reviewed by Lippard.[38]

Results and Discussion

Insertion of iron into the macrocycles of this thesis can be accomplished as

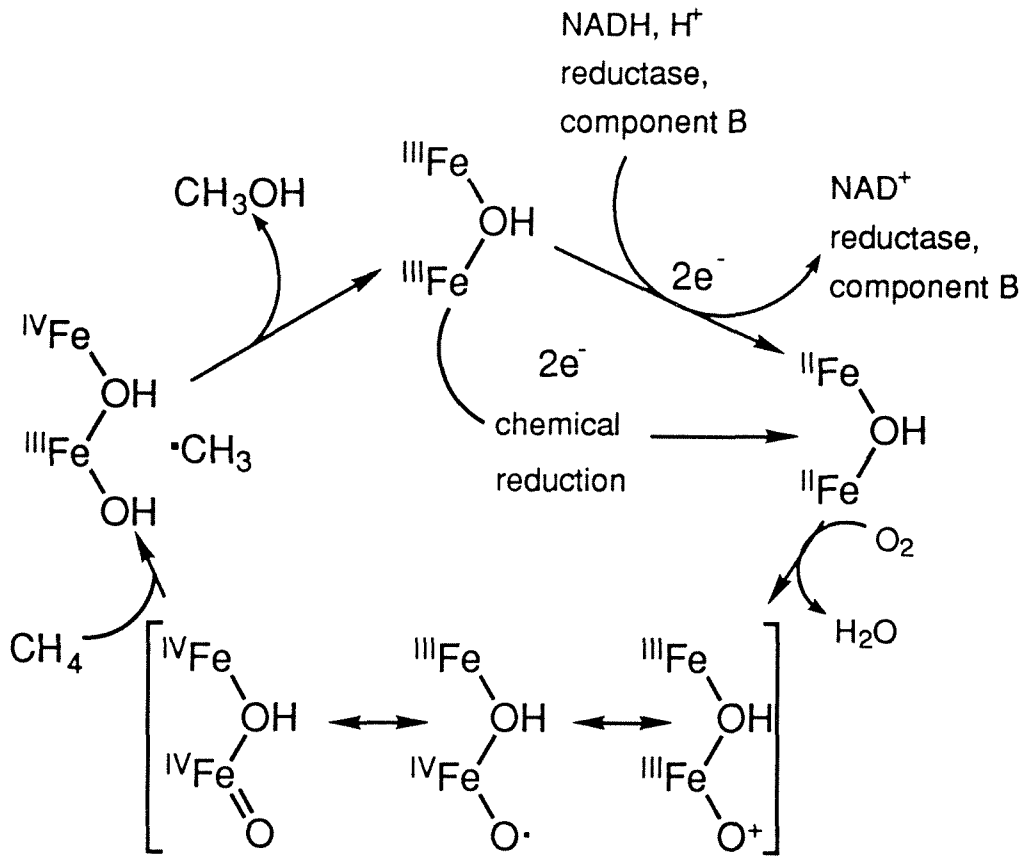

Figure 5.2. The catalytic cycle for methane monooxygenase proposed by Fox and Lipscomb.

shown in Scheme 5.1. $FeBr_2$ or FeI_2 may also be used, but a lower isolated yield results. The iron(II) intermediate is pale green and is probably square planar, since it is isoelectronic with the crystallographically characterised Co(III) complexes (see Chapter 6). One would expect d^6 iron(II) to have even less afinity for axial ligands than d^6 Co(III). The iron(II) complexes are all very air sensitive and are oxidized by dry air to the five-coordinate Fe(III) complexes. These iron(III) complexes are generally hygroscopic, but are remarkably resistant to hydrolysis. The cations of $[Fe^{III}Cl(\eta^4\text{-DEMAMPA-DCB})]^{2-}$ may be exchanged by passing methanolic solutions of the lithium salt down ion-exchange columns.

Scheme 5.1. Preparation of the Fe(III) five-coordinate axial chloride complexes.

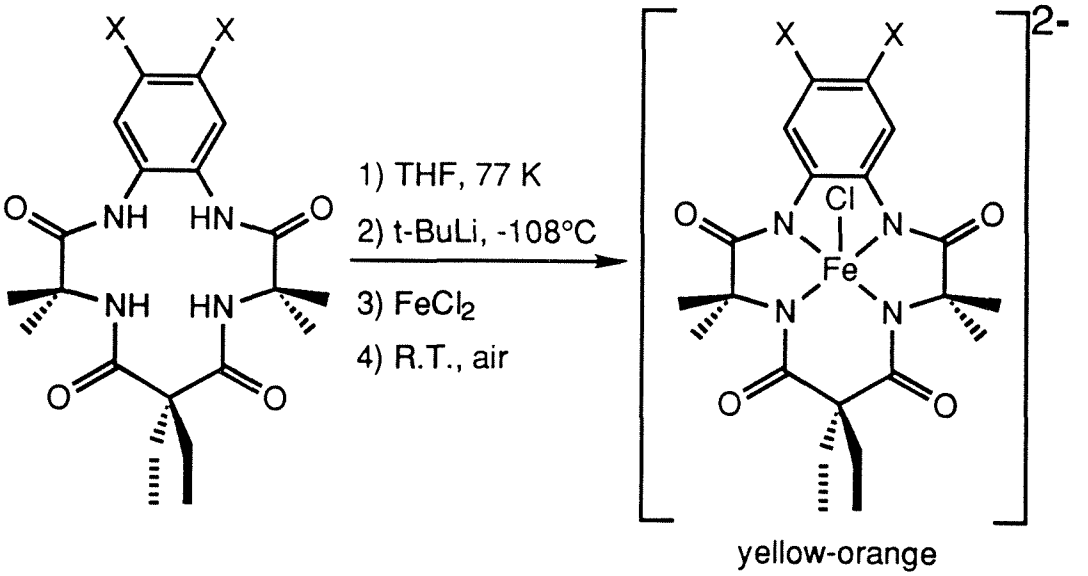

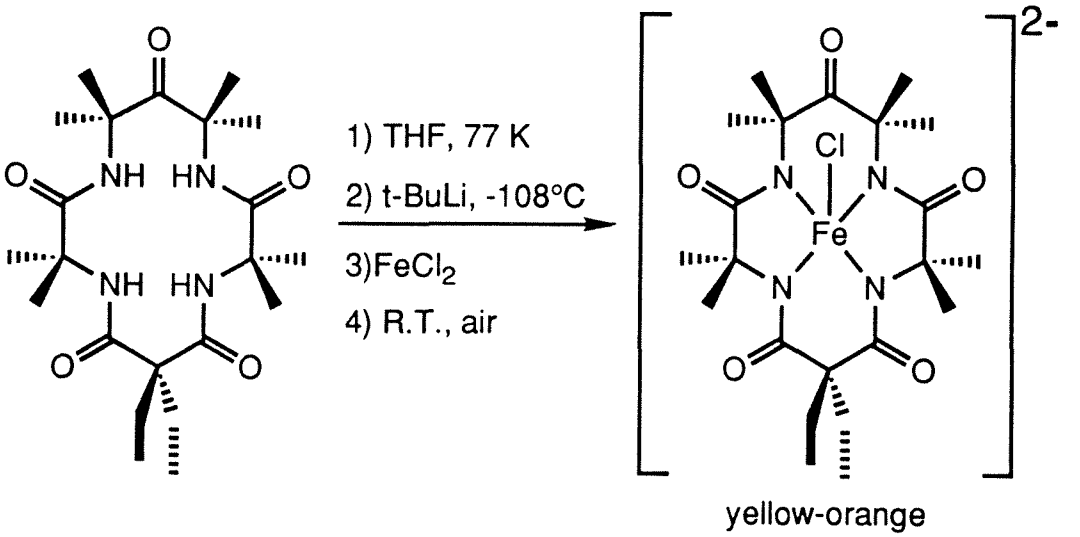

The Fe(III) compounds may be oxidized by a number of means to give a number of different products, depending on the oxidant used and the reaction conditions. Two types of reaction will be discussed here, the reaction of these compounds with electron transfer oxidants (and their electrochemical behavior) and the reaction of $[Fe^{III}Cl(\eta^4\text{-DEMAMPA-DCB})]^{2-}$ with TBHP under basic

conditions.

Both macrocyclic systems exhibit reversible $Fe^{IV/III}$ couples. Cyclic voltammetry of $[Et_4N]_2[Fe^{III}Cl(\eta^4\text{-MAC*})]$ shows a reversible $Fe^{IV/III}$ couple at $E_f = -65$ mV vs. Fc^+/Fc in CH_2Cl_2 (ca. 645 mV vs. NHE) with $[Bu_4N][ClO_4]$ (0.1 M) as supporting electrolyte (Figure 5.3). Cyclic voltammetry of $[Et_4N]_2[Fe^{III}Cl(\eta^4\text{-DEMAMPA-DCB})]$ shows a reversible $Fe^{IV/III}$ couple at $E_f = +60$ mV vs. Fc^+/Fc in CH_2Cl_2 (ca. 770 mV vs. NHE) and another reversible couple at +690 mV vs. Fc^+/Fc in CH_2Cl_2 (ca. 1400 mV vs. NHE) with $[Bu_4N][ClO_4]$ (0.1 M) as supporting electrolyte (Figure 5.4). These formal potentials can be compared with the $Fe^{IV/III}$ couple for the six-coordinate difluoro(tetraphenylporphyrinato)iron system which occurs at +160 mV vs. Fc^+/Fc in acetonitrile.[20] The considerable stabilization of the iron(IV) oxidation state in $[Et_4N][FeCl(\eta^4\text{-MAC*})]$ can be attributed to the strong donor capacity of $(\eta^4\text{-MAC*})^{4-}$. The oxidation state assignment for $[Et_4N][FeCl(\eta^4\text{-DEMAMPA-DCB})]$ could be considered as +IV, even though the crystal structure exhibits some of the bond changes associated with ligand noninnocence (see Chapter 6). The difference between the $Fe^{IV/III}$ potentials for $[Fe^{III}Cl(\eta^4\text{-MAC*})]^-$ and $[Fe^{III}Cl(\eta^4\text{-DEMAMPA-DCB})]^-$ is very similar to the difference between the $Ni^{III/II}$ potentials for $[Ni^{III}(\eta^4\text{-MAC*})]^-$ and $[Ni^{III}(\eta^4\text{-DEMAMPA-DCB})]^-$, which occur at lower formal potentials by almost 500 mV. It is also important to note that $[Co^{III}(\eta^4\text{-MAC*})]^-$ exhibits no redox chemistry within 1.0 V of the $[Co(\eta^4\text{-DEMAMPA-DCB})]/[Co^{III}(\eta^4\text{-DEMAMPA-DCB})]^-$ couple. It appears that formal oxidation state assignments to complexes of $(\eta^4\text{-DEMAMPA-DCB})^{4-}$ have some relevance when the electrochemistry of the species in question parallels the electrochemistry of the

complexes of $(\eta^4\text{-MAC*})^{4-}$. The high wave at 1.40 V for $[Et_4N]_2[Fe^{III}Cl(\eta^4\text{-DEMAMPA-DCB})]$ probably has a significant amount of ligand character.

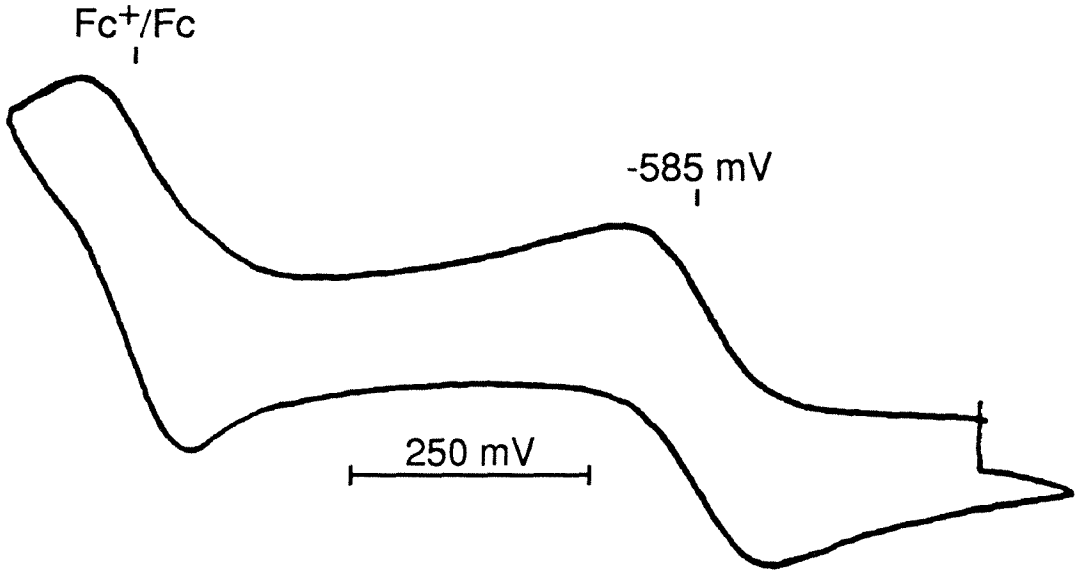

Figure 5.3. Cyclic voltammetry of $[Et_4N]_2[FeCl(\eta^4\text{-MAC*})]$ (0.1 M $[Bu_4N][ClO_4]$, CH_2Cl_2, 1.05 V sweep width, 200 mV/s). Top voltammogram is with added ferrocene; bottom voltammogram is without added ferrocene.

Although the Cambridge Crystallographic Database lists over 500 structures for five-coordinate iron, five-coordinate iron(IV) had been established in the solid state only for the dinuclear μ-carbido complex $[(TPP)Fe]_2C$ (vide supra).[15] The five-coordinate Fe(IV) species of both macrocyclic ligands may be produced by oxidizing the Fe(III) complexes with $(NH_4)_2Ce(NO_3)_6$ in

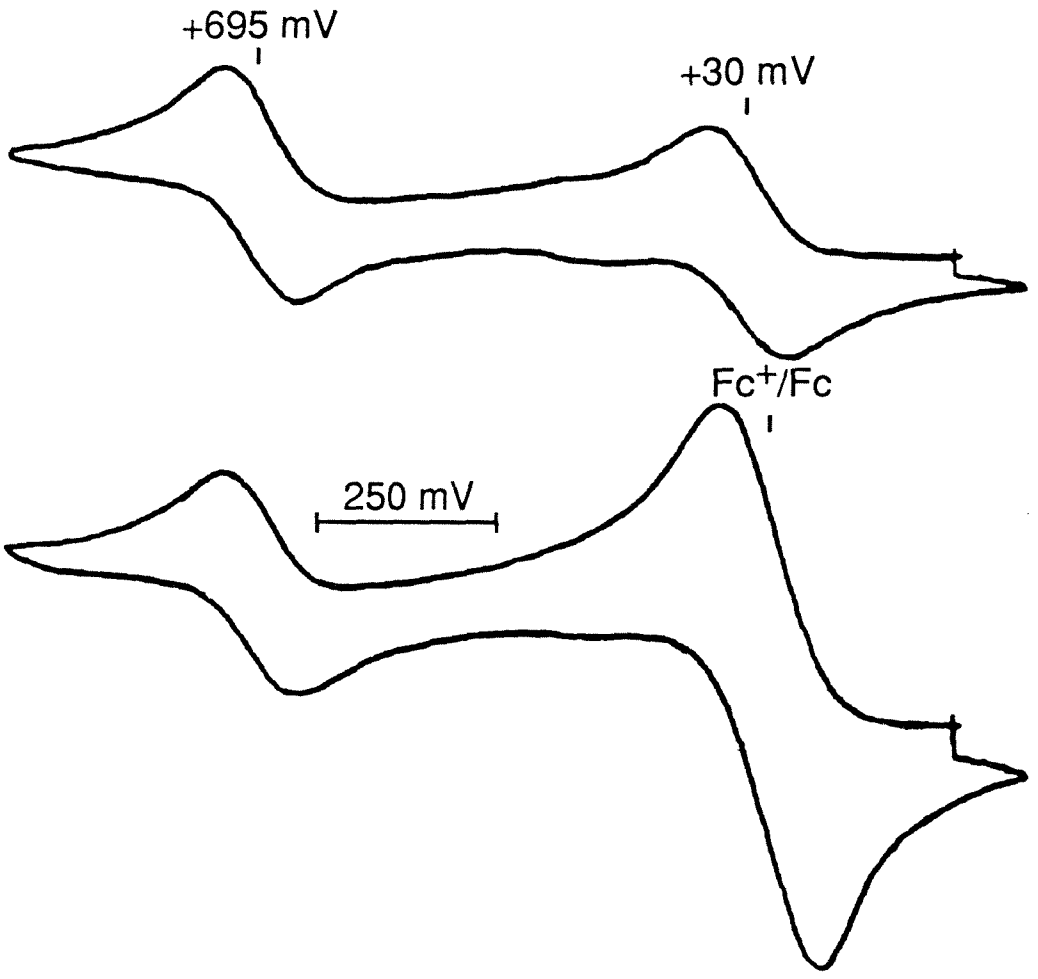

Figure 5.4. Cyclic voltammetry of $[Et_4N]_2[FeCl(\eta^4\text{-DEMAMPA-DCB})]$ (0.1 M $[Bu_4N][ClO_4]$, CH_2Cl_2, 1.400 V sweep width, 200 mV/s). Top voltammogram is without added ferrocene; bottom voltammogram is with added ferrocene.

CH_2Cl_2. The dark brown compound, $[Et_4N][FeCl(\eta^4\text{-MAC*})]$, has the crystal structure shown in Figure 5.5. The structure is best described as a distorted square pyramid: the four amide nitrogens lie in a plane ($\pm$ 0.01 Å), with the Fe atom sitting 0.42 Å above the plane. The Fe–Cl distance is 2.309(3) Å, and the average Fe–N distance is 1.902 Å (about 0.08 Å shorter than for the porphyrin μ-carbido and μ-nitrido complexes discussed above[15,17]). As will be discussed

in Chapter 9, the complex exhibits some amide nonplanarity. For dark purple [Et_4N][FeCl(η^4-DEMAMPA-DCB)] (Figure 5.6), the average Fe–N distance is 0.03 Å shorter than for [Et_4N][FeCl(η^4-MAC*)], and the Fe–Cl distance is 0.103 Å shorter. The aromatic ring carbon to amide nitrogen bonds average 1.374 Å, in between the average distance for [Co(η^4-DEMAMPA-DCB)]$^-$ (1.410 Å) and the average distance for Co(η^4-DEMAMPA-DCB) (1.353 Å).

Zero-field Mössbauer spectra of [Et_4N][FeCl(η^4-MAC*)] in acetonitrile consist of a single doublet. The quadrupole splitting, ΔE_Q, is nearly independent of temperature. The spectrum obtained at 150 K (Figure 5.7) has $\Delta E_Q = 0.87$ mm s^{-1} and the isomer shift is $\delta_{Fe} = -0.03$ mm s^{-1}.[39] Spectra measured at 4.2 K in fields greater than 0.5 T show well-resolved magnetic hyperfine interactions (internal field, −20.5 T), proving that the ground state has electronic spin S > 0 (Figures 5.8 and 5.9).[40] The isomer shift is an excellent indicator of the oxidation state. The value obtained here, $\delta_{Fe} = +0.01$ mm s^{-1} at 4.2 K, compares very well with those of ferryl S = 1 hemes ($\delta_{Fe} = 0.03$–0.11 mm s^{-1} at 4.2 K), lending firm support for an iron(IV) oxidation state.[41] EPR and Mössbauer studies of these systems and derivatives are currently under vigorous investigation by the Collins and Münck groups.[42]

The compound, [Et_4N]$_2$[Fe^{III}Cl(η^4-DEMAMPA-DCB)], undergoes a number of oxidation reactions; its reaction with *tert*-butyl hydroperoxide in basic acetonitrile will be discussed here. The reaction of [Et_4N]$_2$[Fe^{III}Cl(η^4-DEMAMPA-DCB)] with *tert*-butylamine and TBHP in acetonitrile proceeds to produce an inky blue color from the starting pale yellow solution. This dark blue color persists at room temperature for approximately five minutes. Dr. L. James Wright[43] pursued this chemistry and rapidly determined that

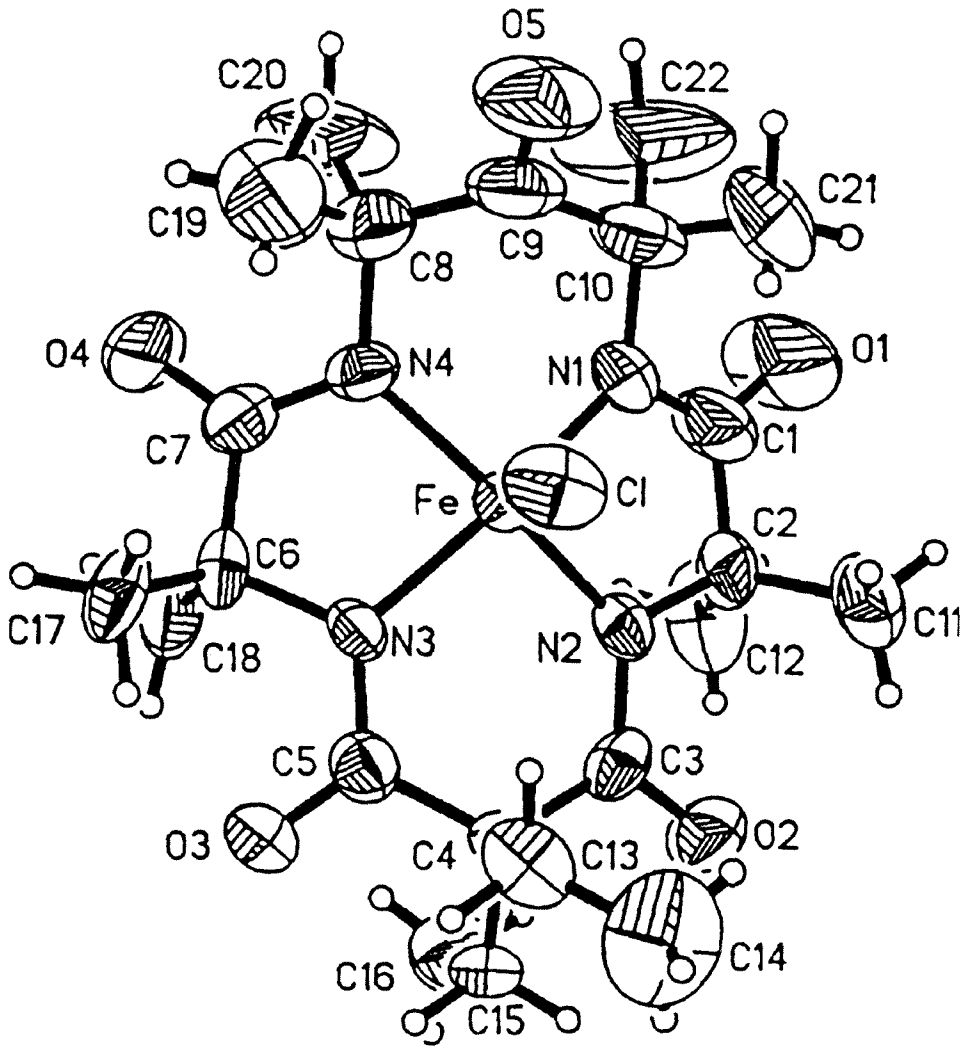

Figure 5.5. Molecular structure of $[FeCl(\eta^4\text{-MAC*})]^-$. ORTEP drawing with all nonhydrogen atoms drawn to encompass 50% of electron density.

Table 5.1. Bond Lengths in $[FeCl(\eta^4\text{-MAC*})]^-$			
Atoms	Length (Å)	Atoms	Length (Å)
FeCl	2.309(3)	FeN1	1.879(7)
FeN2	1.892(7)	FeN3	1.926(6)
FeN4	1.909(6)	O1C1	1.211(15)
O2C3	1.239(11)	O3C5	1.227(11)

Table 5.1. Bond Lengths in [FeCl(η^4-MAC*)]$^-$ (continued)			
Atoms	Length (Å)	Atoms	Length (Å)
O4C7	1.228(11)	O5C9	1.221(14)
N1C1	1.375(14)	N2C3	1.369(11)
N3C5	1.342(11)	N4C7	1.365(12)
N1C10	1.485(14)	N2C2	1.479(11)
N3C6	1.475(10)	N4C8	1.487(12)
C1C2	1.502(15)	C3C4	1.520(12)
C4C5	1.533(12)	C6C7	1.509(13)
C8C9	1.490(15)	C9C10	1.540(17)
C2C11	1.534(14)	C2C12	1.540(15)
C4C13	1.560(13)	C4C15	1.534(12)
C13C14	1.471(19)	C6C17	1.497(13)
C6C18	1.525(14)	C8C19	1.499(22)
C8C20	1.498(23)	C10C21	1.548(20)
C15C16	1.510(14)	C10C22	1.524(21)

Table 5.2. Bond Angles in [FeCl(η^4-MAC*)]$^-$			
Atoms	Angle (°)	Atoms	Angle (°)
ClFeN1	99.0(2)	ClFeN2	106.7(2)
ClFeN3	106.3(2)	ClFeN4	98.5(2)
N1FeN2	84.0(3)	N1FeN3	154.6(3)
N1FeN4	89.9(4)	N2FeN3	90.7(3)
N2FeN4	154.6(3)	N3FeN4	84.4(3)
FeN1C1	115.8(7)	FeN1C10	125.6(7)

Table 5.2. Bond Angles in [FeCl(η^4-MAC*)]$^-$ (continued)			
Atoms	Angle (°)	Atoms	Angle (°)
FeN3C5	126.7(6)	FeN3C6	115.0(5)
FeN2C2	116.4(5)	FeN2C3	126.2(6)
FeN4C7	115.2(6)	FeN4C8	126.2(6)
C1N1C10	118.1(8)	C5N3C6	118.1(7)
C2N2C3	117.4(7)	C7N4C8	118.3(7)
O1C1N1	125.4(11)	O1C1C2	119.5(11)
N1C1C2	115.0(9)	O2C3N2	121.9(8)
O2C3C4	116.0(8)	N2C3C4	122.1(7)
O3C5N3	121.6(8)	O3C5C4	117.1(8)
N3C5C4	121.4(7)	N2C2C1	106.9(7)
N2C2C11	112.7(7)	N2C2C12	109.1(8)
C1C2C11	105.1(8)	C1C2C12	110.6(8)
C11C2C12	112.2(8)	C3C4C5	115.5(7)
C3C4C13	110.4(7)	C3C4C15	108.3(7)
O4C7N4	124.9(9)	O4C7C6	119.4(9)
N4C7C6	115.4(8)	O5C9C8	118.2(11)
O5C9C10	117.1(10)	C8C9C10	124.2(10)
N1C10C9	110.8(9)	N1C10C21	108.6(10)
N1C10C22	113.6(12)	C9C10C21	106.7(12)
C9C10C22	106.1(12)	C21C10C22	110.8(14)
C4C13C14	116.6(9)	C4C15C16	115.0(8)
C5C4C13	104.4(7)	C5C4C15	107.1(7)
C13C4C15	111.2(7)	N3C6C7	108.2(7)

Table 5.2. Bond Angles in [FeCl(η^4-MAC*)]$^-$ (continued)			
Atoms	Angle (°)	Atoms	Angle (°)
N3C6C17	114.1(7)	N3C6C18	110.2(7)
C7C6C17	104.6(6)	C7C6C18	106.2(7)
C17C6C18	108.1(7)	N4C8C9	110.6(8)
N4C8C19	107.8(10)	N4C8C20	112.9(10)
C9C8C19	110.3(10)	C9C8C20	109.1(11)
C19C8C20	106.0(12)		

the same blue species could be produced using $[Et_4N]OH$ in place of *tert*-butylamine. He was able to produce pure $[Ph_4P]^+$ salts of the blue species which have lifetimes of many days in solution at room temperature and indefinite lifetimes in the solid state in the absence of light. The IR spectrum indicates that the ligand has not suffered decomposition and reveals bands in the amide region at 1723, 1623, and 1564 cm^{-1}, consistent with the amide bands of Co(η^4-DEMAMPA-DCB) (see Chapter 6). The compound absorbs in the visible region at 607 nm (ϵ=9.39×10^9). The compound was subjected to FAB MS with the instrumentation set to detect anions. Although the complex appeared to react with the sulfolane matrix before the MS was performed, the MS still revealed Fe-bound ligand species. The electrochemistry of the compound is shown in Figure 5.10, and indicates that the blue compound is only a *very weak* electron transfer oxidant. The species has a paramagnetic NMR, and no detectable EPR, suggesting that it is a paramagnetic even spin system. The Mössbauer spectrum of the species is shown in Figure 5.11 and a Mössbauer spectrum of a monoprotonated species is shown in Figure 5.12.

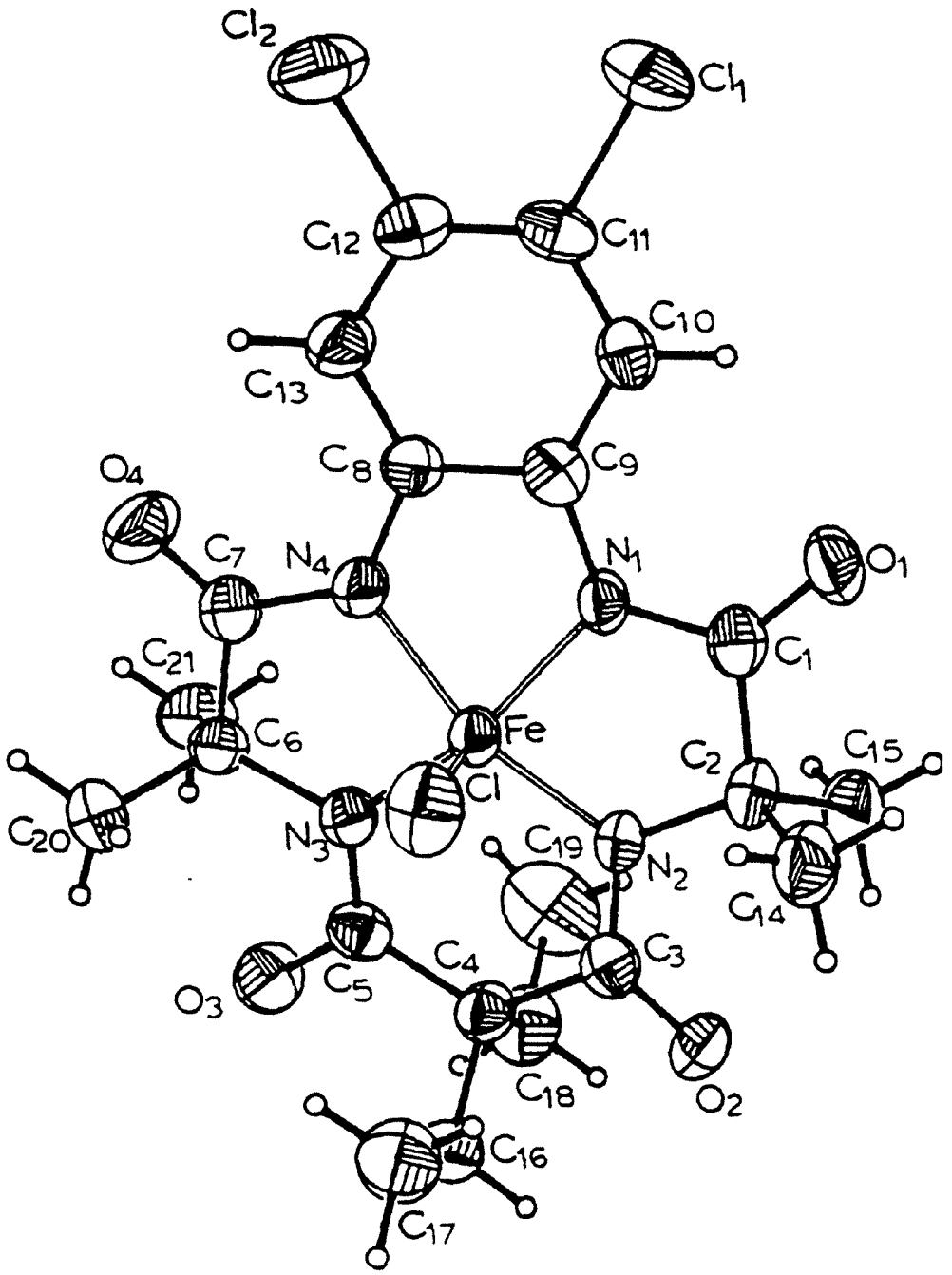

Figure 5.6. Molecular structure of [FeCl(η^4-DEMAMPA-DCB)]$^-$. ORTEP drawing with all nonhydrogen atoms drawn to encompass 50% of electron density.

Table 5.3. Bond Lengths in [FeCl(η^4-DEMAMPA-DCB)]$^-$			
Atoms	Length (Å)	Atoms	Length (Å)
FeCl	2.203(1)	FeN1	1.865(3)
FeN2	1.869(3)	FeN3	1.876(3)
FeN4	1.864(3)	Cl1C11	1.730(5)
Cl2C12	1.728(5)	C1O1	1.214(5)
C3O2	1.232(6)	C5O3	1.250(5)
C7O4	1.214(6)	N1C1	1.391(5)
N1C9	1.376(6)	N2C2	1.489(5)
N2C3	1.353(6)	N3C5	1.337(6)
N3C6	1.488(6)	N4C7	1.378(6)
N4C8	1.372(5)	C1C2	1.531(6)
C3C4	1.551(6)	C4C5	1.540(6)
C6C7	1.532(6)	C8C9	1.425(6)
C9C10	1.396(6)	C10C11	1.373(6)
C8C13	1.396(6)	C2C14	1.538(7)
C2C15	1.539(6)	C4C16	1.538(7)
C4C18	1.555(6)	C6C20	1.526(7)
C6C21	1.532(7)	C16C17	1.513(7)
C18C19	1.497(8)	C11C12	1.393(7)
C12C13	1.375(7)		

Table 5.4. Bond Angles in [FeCl(η^4-DEMAMPA-DCB)]$^-$			
Atoms	Angle (°)	Atoms	Angle (°)
ClFeN1	101.9(1)	ClFeN2	102.9(1)

Table 5.4. Bond Angles in [FeCl(η^4-DEMAMPA-DCB)]$^-$ (continued)			
Atoms	Angle (°)	Atoms	Angle (°)
ClFeN3	105.0(1)	ClFeN4	99.1(1)
ClFeN1	101.9(1)	ClFeN2	102.9(1)
ClFeN3	105.0(1)	ClFeN4	99.1(1)
N1FeN2	84.8(1)	N1FeN3	151.5(2)
N1FeN4	81.9(1)	N2FeN3	98.0(1)
N2FeN4	156.2(1)	N3FeN4	84.9(1)
FeN1C1	117.2(3)	FeN1C9	116.2(3)
FeN2C2	114.4(2)	FeN2C3	124.6(3)
FeN3C5	126.6(3)	FeN3C6	115.0(3)
FeN4C7	117.4(3)	FeN4C8	115.8(3)
C1N1C9	126.5(3)	C2N2C3	118.2(3)
C5N3C6	118.0(3)	C7N4C8	126.7(4)
N1C1O1	124.4(4)	N1C1C2	112.1(3)
O1C1C2	123.5(4)	N2C3O2	123.5(4)
N2C3C4	120.4(4)	C4C3O2	116.0(4)
N3C5O3	123.0(4)	N3C5C4	121.8(4)
C4C5O3	123.0(4)	N4C7O4	124.4(4)
N4C7C6	112.3(4)	C6C7O4	123.3(4)
N4C8C9	112.1(4)	N4C8C13	128.0(4)
C9C8C13	119.9(4)	N1C9C8	111.5(4)
N1C9C10	128.8(4)	C8C9C10	119.7(4)
C9C10C11	118.8(4)	C10C11Cl1	118.5(3)
C12C11Cl1	119.9(4)	C10C11C12	121.6(4)

Table 5.4. Bond Angles in [FeCl(η^4-DEMAMPA-DCB)]$^-$ (continued)			
Atoms	Angle (°)	Atoms	Angle (°)
C11C12Cl2	121.0(4)	C13C12Cl2	118.4(4)
C11C12C13	120.6(4)	C12C13C8	119.2(4)
C1C2N2	107.1(3)	C1C2C14	106.8(4)
C1C2C15	107.0(4)	N2C2C14	112.6(4)
N2C2C15	111.8(4)	C14C2C15	111.2(4)
C3C4C5	122.2(4)	C3C4C16	108.2(4)
C3C4C18	105.1(3)	C5C4C16	107.0(4)
C5C4C18	106.3(4)	C16C4C18	107.2(4)
N3C6C7	108.2(3)	N3C6C20	112.8(4)
N3C6C21	111.5(4)	C7C6C20	107.4(4)
C7C6C21	104.8(4)	C20C6C21	111.7(4)
C4C16C17	114.1(4)	C4C18C19	114.6(5)

(The monoprotonated species may be reversed to the unprotonated species with pyridine.) The blue species was sent for combustion analysis. The numbers found were: C, 61.77; H, 5.09; N, 6.50; P, 3.31. The theoretical numbers for $[Ph_4P]_2[O(Fe(\eta^4\text{-DEMAMPA-DCB}))_2]$ (an iron(IV) μ-oxo species) are: C, 62.08; H, 5.09; N, 6.44; P, 3.56. The theoretical numbers for $[Ph_4P]_2[O_2(Fe(\eta^4\text{-DEMAMPA-DCB}))_2]$ (an iron(IV) μ-peroxo species) are: C, 61.52; H, 5.05; N, 6.38; P, 3.53. A μ-oxo species of this type would be significant to scientists studying MMO, while a μ-peroxo species of this type would be significant to studies of photosynthesis. The instability of the complex at such a low potential would argue against the μ-oxo system, since these ligands are so resistant

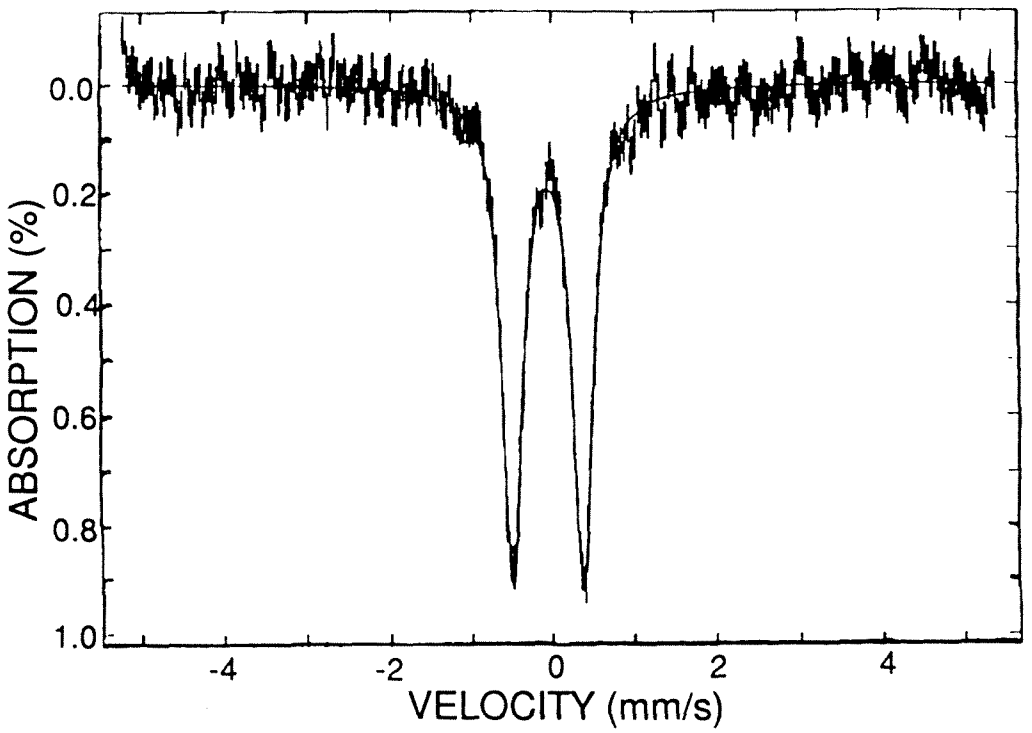

Figure 5.7. Mössbauer spectrum of $[Et_4N][FeCl(\eta^4\text{-MAC*})]$ in acetonitrile recorded at 150 K in zero-field. $\delta_{Fe} = -0.03$ mm s^{-1}, $\Delta E_Q = 0.87$ mm s^{-1}. The solid line results from fitting two Lorentzians (full width 0.30 mm s^{-1}) to the data.

to oxidative and hydrolytic decomposition. A system with an O–O bond could explain the instability. Clearly, this blue compound, even if it is neither of the species postulated here, is a very interesting molecule. Mr. Michael Bartos of the Collins group is actively pursuing the chemistry and spectroscopy of this species and its derivatives.

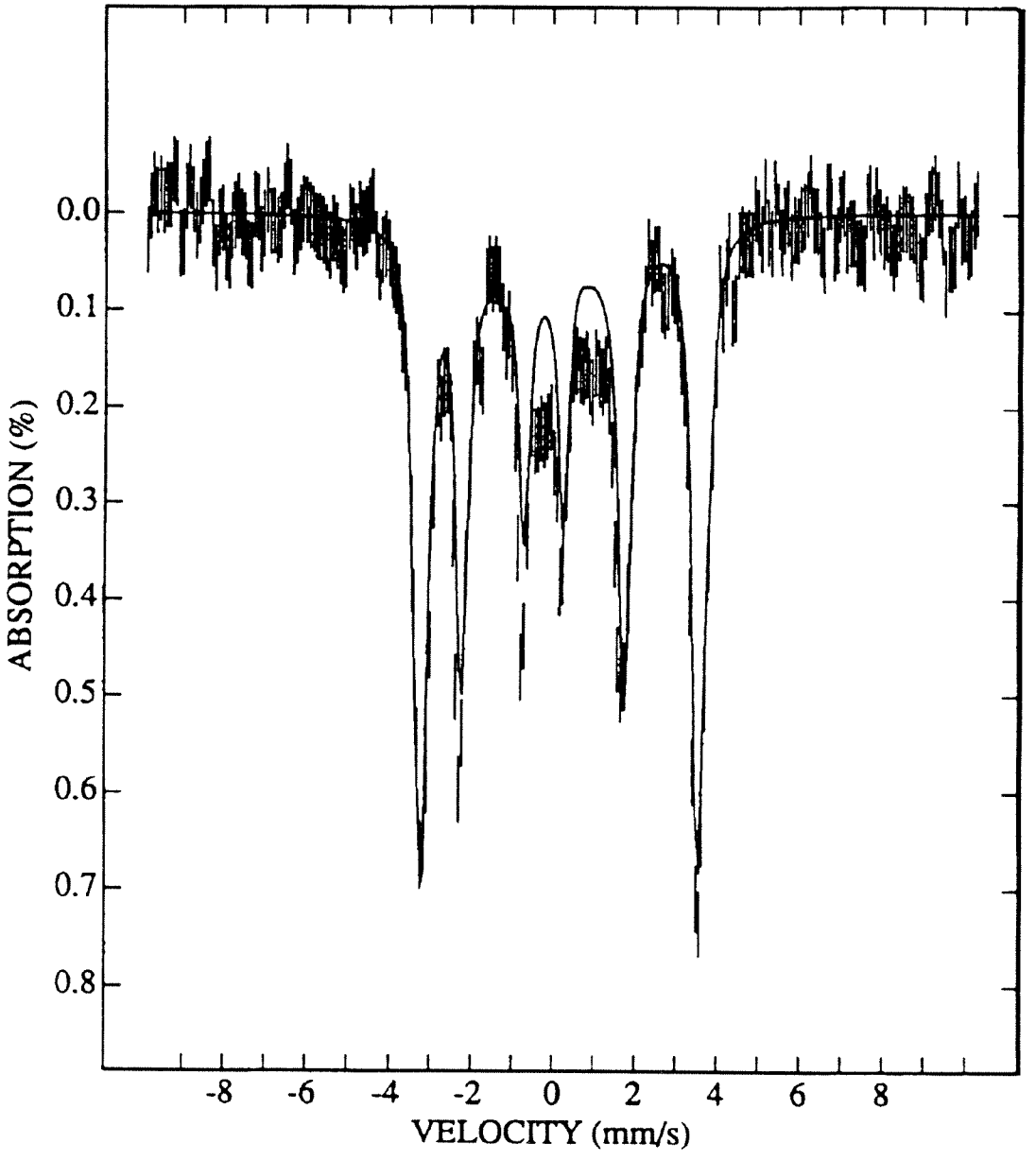

Figure 5.8. Mössbauer spectrum of $[Et_4N][FeCl(\eta^4\text{-MAC*})]$ in acetonitrile recorded at 4.2 K in 10 kG field.

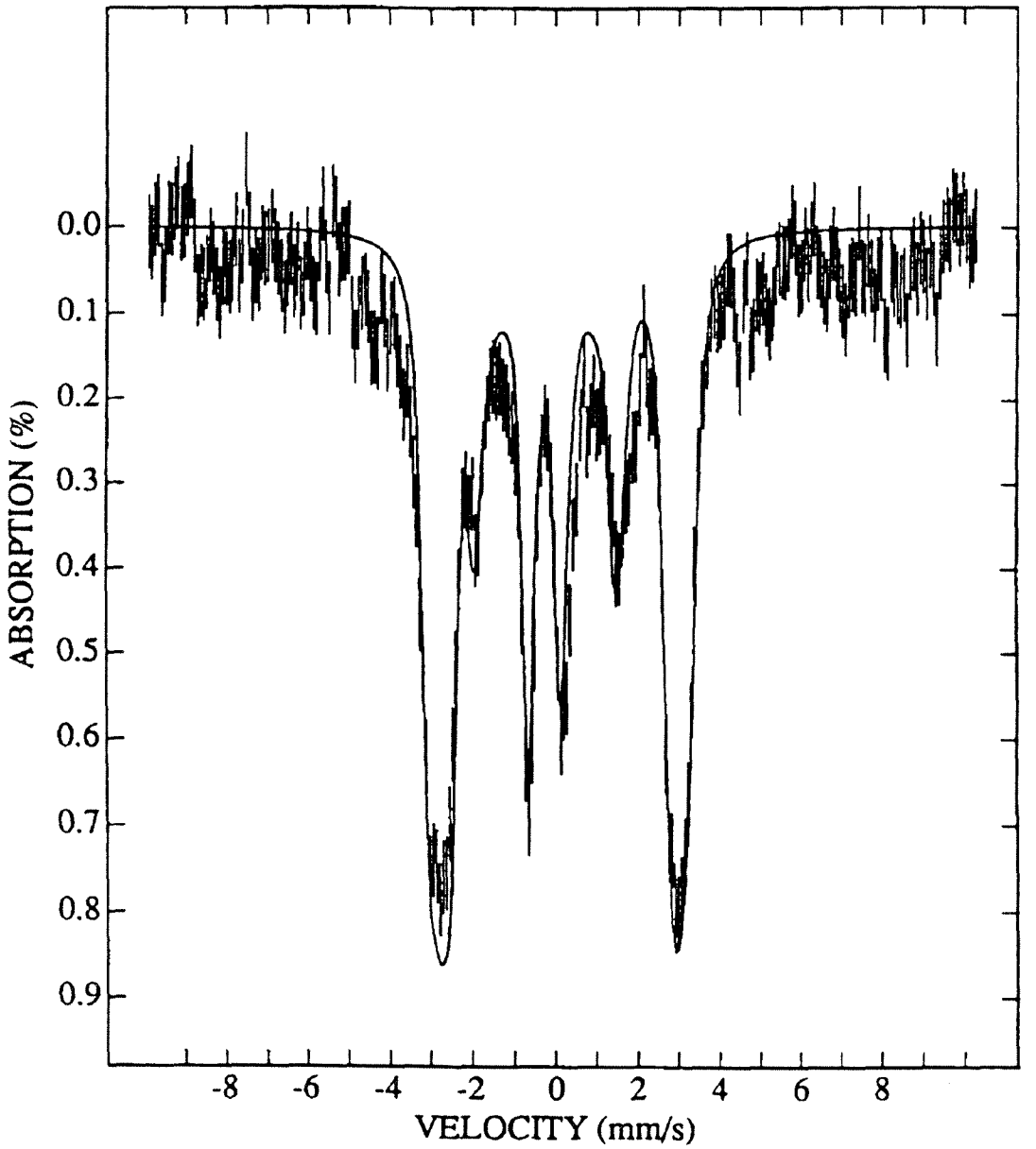

Figure 5.9. Mössbauer spectrum of $[Et_4N][FeCl(\eta^4\text{-MAC}^*)]$ in acetonitrile recorded at 4.2 K in 60 kG field.

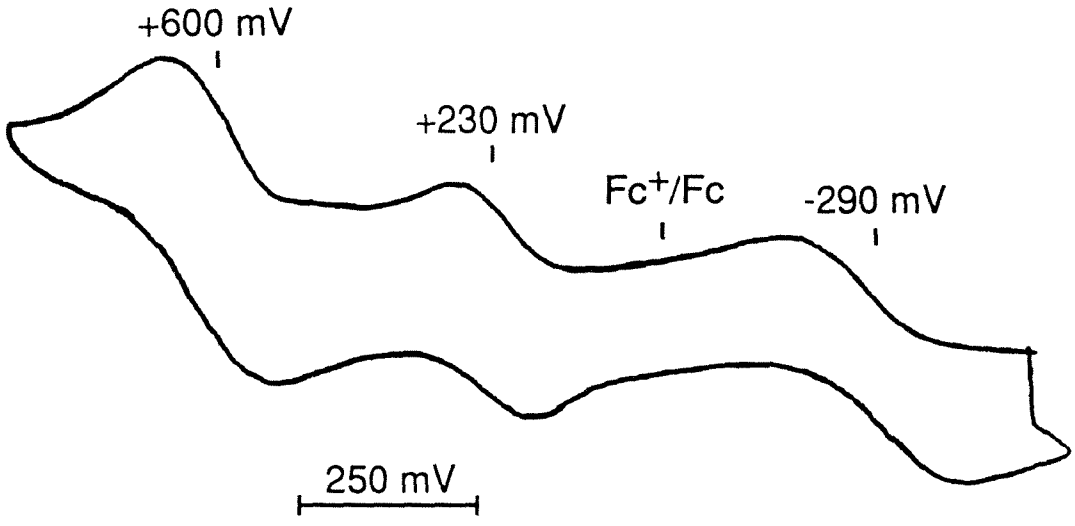

Figure 5.10. Cyclic voltammetry of the blue iron compound (0.1 M $[Bu_4N][ClO_4]$, CH_2Cl_2, 1.450 V sweep width, 200 mV/s). To avoid clutter, a voltammogram without added ferrocene is shown, and the midpoint of the Fc^+/Fc wave from a voltammogran with added ferrocene is indicated.

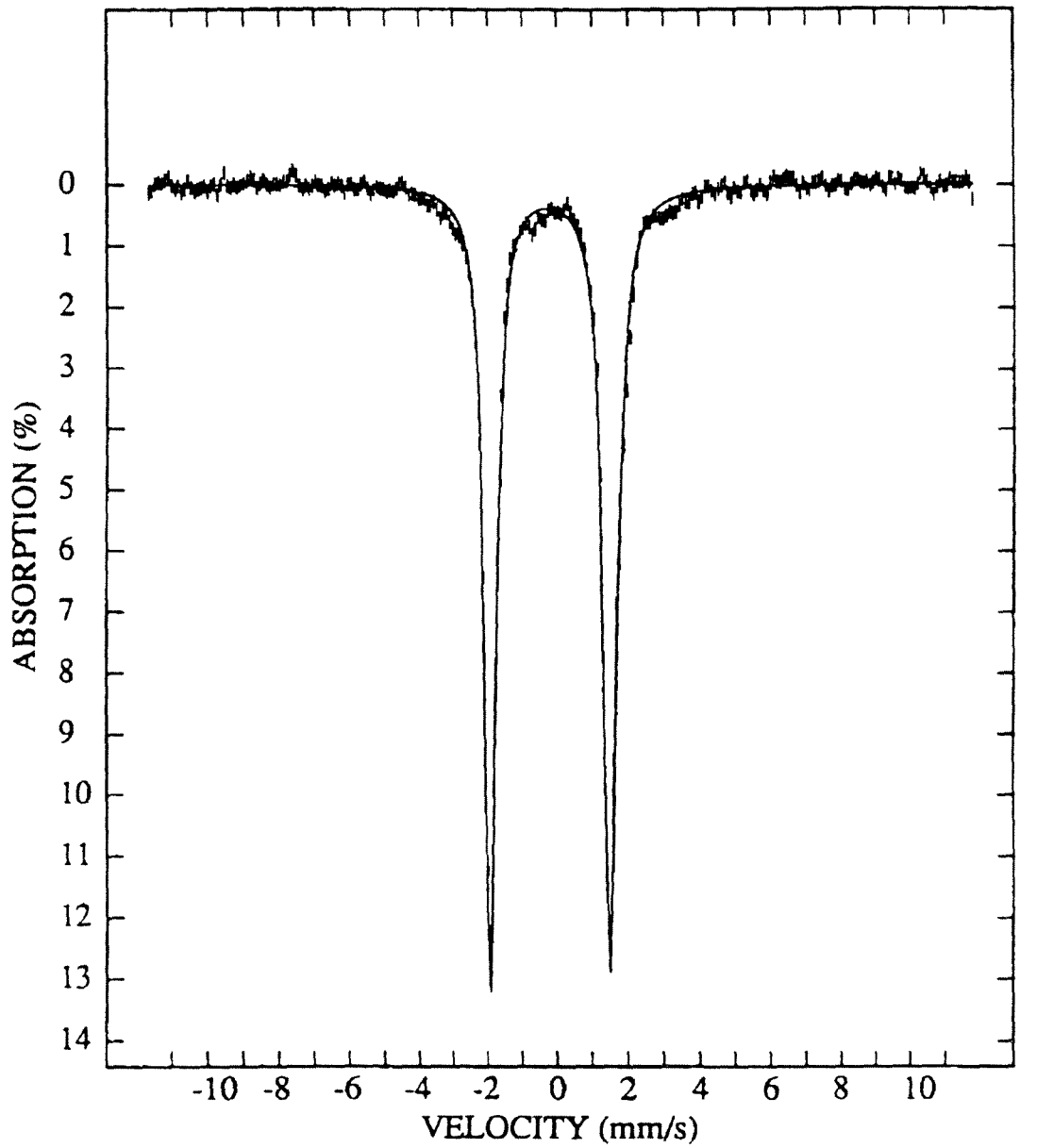

Figure 5.11. Mössbauer spectrum of the blue iron compound in acetonitrile recorded at 4.2 K in 600 G field. $\delta_{Fe} = -0.18$ mm s^{-1}, $\Delta E_Q = 3.42$ mm s^{-1}.

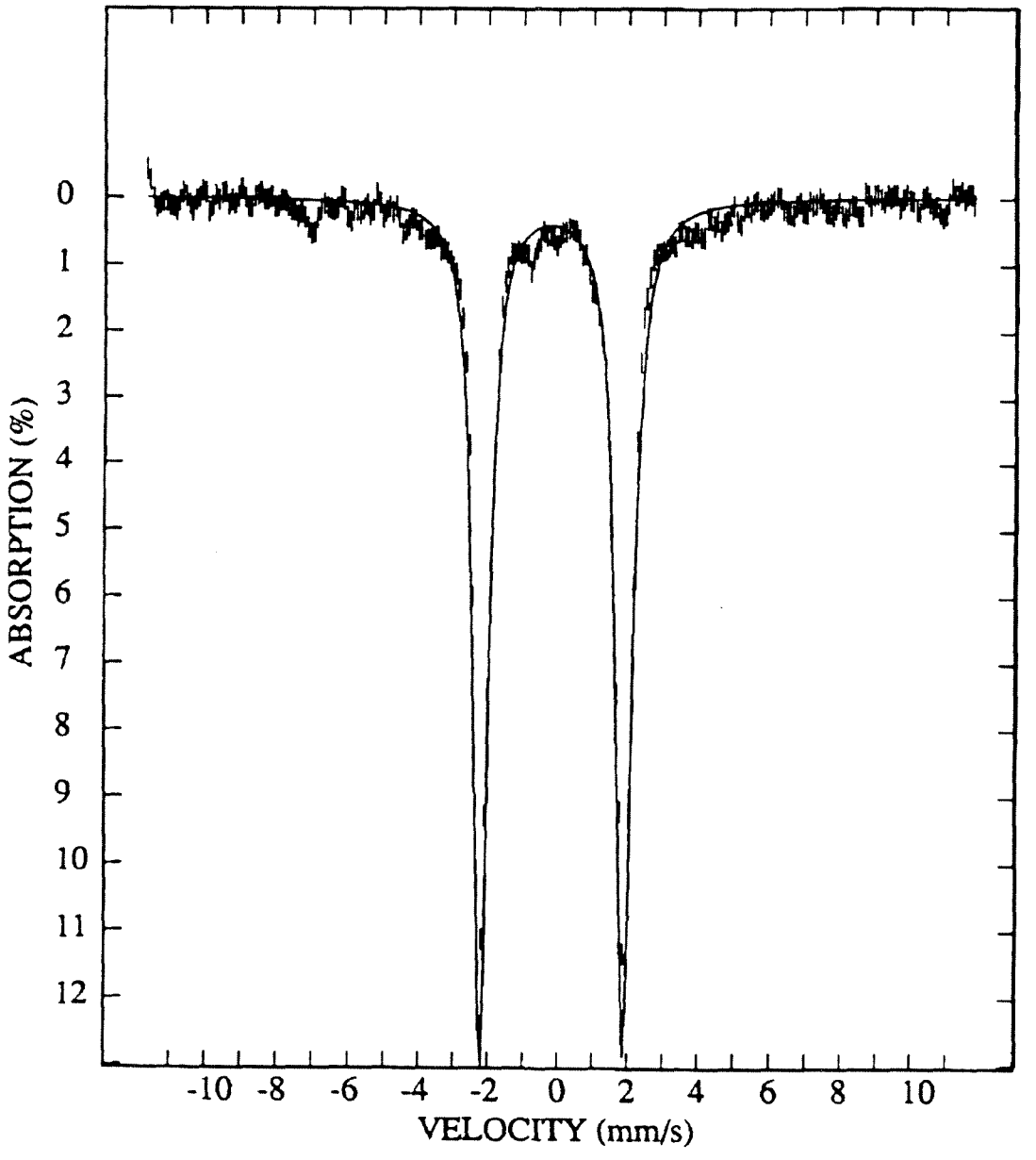

Figure 5.12. Mössbauer spectrum of the protonated blue iron compound in acetonitrile recorded at 4.2 K in 600 G field. $\delta_{Fe} = -0.18$ mm s^{-1}, $\Delta E_Q = 4.13$.

Experimental

Materials. All solvents and reagents were reagent grade (Aldrich) except for THF and benzene (Aldrich, Sureseal) and were used as received except as described for electrochemical measurements.

Physical Measurements. ^{1}H NMR were measured at 300 MHz on an IBM NR/300 FT-NMR Spectrometer. ^{1}H NMR data are reported in δ vs. $(CH_3)_4Si$ with the solvent as internal standard. EPR spectra were recorded on a Bruker ER300 Spectrometer. Infrared data were obtained on a Nicolet 5DXB FT-IR Spectrometer. Crystal structures were solved by Crystalytics Co. of Lincoln, Nebraska.

Electrochemical Data. Cyclic voltammetry was performed on a Princeton Applied Research Model 173/179 potentiostat/digital coulometer equipped with positive feedback IR compensation and a Model 175 universal programmer. Current voltage curves were recorded on a Houston Instruments Model 2000 X-Y recorder.

Sureseal anhydrous CH_2Cl_2 (Aldrich) and $[Et_4N][PF_6]$ (Fluka) were used as received. $[Bu_4N][ClO_4]$ (Fluka) was vacuum dried at 80 °C. In all cases experiments were performed under N_2 with a supporting electrolyte concentration of 0.1 M. Cyclic voltammetry was performed in CH_2Cl_2 solutions of $[Bu_4N][ClO_4]$ at a 3 mm Pt disk working electrode with a silver wire quasi-reference electrode and a Pt foil counter electrode. At the conclusion of each experiment ferrocene (Fc) was added as an internal potential standard. All formal potentials were taken as the average of anodic and cathodic peak potentials and are reported vs. the Fc^+/Fc couple. Peak-to-peak separation of the Fc^+/Fc couple was similar to that of the iron couples in all cases. Plots of

peak current vs. the square root of scan rate over the range 10–500 mV s^{-1} were made and found to be linear for couples that are stated to be reversible.

Synthetic Note. It should be noted that some of the experimental work reported here has been published in substantially similar form in *J. Am. Chem. Soc.*[44]

[Et_4N][FeCl(η^4-MAC*)]. H_4MAC* (70 mg) was dissolved in dry, deoxygenated THF (24 mL), and a stoichiometric amount of *tert*-butyllithium (0.41 mL, 1.7 M in pentane, 4 equiv, Aldrich) was added to the frozen solution under nitrogen. $FeCl_2$ (anydrous, 29 mg, 1.2 equiv, Alfa) was added under nitrogen when the THF solution thawed (−108 °C). As the stirred suspension warmed to 20 °C, a dark green precipitate (presumably an Fe(II) complex) collected on the flask walls. After stirring at 20 °C (30 min), air was admitted through a calcium chloride drying tube and an orange precipitate rapidly developed as the green precipitate disappeared. This precipitate was stirred (30 min), then the THF was removed under reduced pressure to yield an orange solid. The solid was washed with CH_2Cl_2, dissolved in MeOH, and filtered through celite. [Et_4N]F·xH_2O (116 mg, Aldrich) was added and the MeOH removed under reduced pressure. The resulting orange-brown residue was dissolved in CH_2Cl_2 (20 mL) and filtered through a celite pad. $(NH_4)_2Ce(NO_3)_6$ (0.1 g, Aldrich) was added to the orange CH_2Cl_2 solution, immediately producing a dark brown solution. After stirring (15 min), Na_2SO_4 (0.2 g) was added, the reaction mixture was passed through a celite pad, the mother liquor was collected, and the volume was reduced to 3 mL. Et_2O was layered on the CH_2Cl_2 solution and dark brown X-ray quality crystals of [Et_4N][FeCl(η^4-MAC*)] formed upon diffusion of the two solvents at 4 °C (21.5 mg, 18.8%

yield).

[Et_4N][FeCl(η^4-DEMAMPA-DCB)]. H_4DEMAMPA-DCB (458 mg) was dissolved in dry, deoxygenated THF (65 mL), and a stoichiometric amount of *tert*-butyllithium (2.29 mL, 1.7 M in pentane, 4 equiv, Aldrich) was added to the frozen solution under nitrogen. $FeCl_2$ (anydrous, 131 mg, Alfa) was added under nitrogen when the THF solution thawed (−108 °C). As the stirred suspension warmed to 20 °C, a dark green precipitate (presumably an Fe(II) complex) collected on the flask walls. After stirring at 20 °C (30 min), air was admitted through a calcium chloride drying tube and an orange precipitate rapidly developed as the green precipitate disappeared. This precipitate was stirred (30 min), then the THF was removed under reduced pressure to yield an orange solid. The solid was washed with CH_2Cl_2, dissolved in MeOH, and filtered through celite. Removing the MeOH under reduced pressure resulted in a nearly quantitative yield of crude Li_2[FeCl(η^4-DEMAMPA-DCB)]. Some of this material was dissolved in MeOH, excess [Et_4N]F·$x H_2O$ was added and the MeOH removed under reduced pressure. The resulting orange-brown residue was dissolved in CH_2Cl_2 and filtered through a celite pad. $(NH_4)_2Ce(NO_3)_6$ (Aldrich) was added to the orange CH_2Cl_2 solution, immediately producing a dark purple solution. After stirring (15 min), Na_2SO_4 was added, the reaction mixture was passed through a celite pad, the mother liquor was collected, and the volume was reduced to a few mL. Et_2O was layered on the CH_2Cl_2 solution and dark purple X-ray quality crystals of [Et_4N][FeCl(η^4-DEMAMPA-DCB)] formed upon diffusion of the two solvents at 4 °C. These crystals were manually separated form colorless crystals of [Et_4N]F·$x H_2O$.

Crystal Data. Single crystals of [Et_4N][FeCl(η^4-MAC*)] at 20 ± 1 °C

are orthorhombic, space group $Pna2_1$-C_{2v}^9 (No. 33) with a = 15.341(3) Å, b = 15.261(3) Å, c = 14.920(4) Å, α = 90.00°, β = 90.00°, γ = 90.00°, V = 3493(2) Å^3, and Z = 4 (d_{calcd} = 1.248 g cm^{-3}; μ_a(MoK$\bar{\alpha}$) = 0.55 mm^{-1}). A total of 2920 independent reflections having 2θ(MoK$\bar{\alpha}$) < 48.3° (the equivalent of 0.7 limiting CuK$\bar{\alpha}$ spheres) were collected on a computer-controlled Nicolet autodiffractometer using full (0.90°-wide) ω scans and graphite-monochromated MoK$\bar{\alpha}$ radiation. The structure was solved using "Direct Methods" techniques with the Nicolet SHELXTL software package as modified at Crystalytics Company. The resulting structural parameters have been refined to a convergence of R_1(unweighted, based on F) = 0.051 for 1796 independent reflections having $2\theta_{MoK\bar{\alpha}}$ < 48.3° and I > 3σ(I) using counter-weighted full-matrix least-squares techniques and a structural model which incorporated anisotropic thermal parameters for all nonhydrogen atoms except cation carbon atoms $C_{1a'}$, $C_{2a'}$, $C_{3a'}$, and $C_{4a'}$ (which were isotropically refined) and isotropic thermal parameters for all anion hydrogen atoms. Hydrogen atoms for the cation were not included in the structural model. The methyl groups of the anion were included in the refinement as idealized sp^3-hybridized rigid rotors and gave final values for the C-C-H angles which ranged from 97°–123°. The remaining hydrogen atoms were fixed at idealized sp^3-hybridized positions with a C-H bond length of 0.96 Å. The four ethyl groups of the cation appear to be disordered in the lattice with two alternate (74% and 26% occupancy) resolvable orientations. Methylene carbon atoms C_{1a}, C_{2a}, C_{3a}, and C_{4a} with N and the methyl carbon atoms represent the major (74%) orientation for the cation while $C_{1a'}$, $C_{2a'}$, $C_{3a'}$, and $C_{4a'}$ with N and the methyl carbon atoms represent the minor (26%) orientation.

Crystal Data. Single crystals of $[Et_4N][FeCl(\eta^4\text{-DEMAMPA-DCB})]$ at 20± 1 °C are monclinic, space group $P2_1/c\text{-}C_{2h}^5$ (No. 14) with a = 9.958(2) Å, b = 14.956(3) Å, c = 22.688(5) Å, β = 93.83(2)°, V = 3372(1) Å^3 and Z = 4 (d_{calcd} = 1.357 g cm^{-3}; $\mu_a(CuK\bar{\alpha})$ = 6.17 mm^{-1}). A total of 4626 independent absorption-corrected reflections having $2\theta(CuK\bar{\alpha}) < 115.0°$ were collected using θ-2θ scans and Ni-filtered CuK$\bar{\alpha}$ radiation. The structure was solved using "Direct Methods" techniques with the Nicolet SHELXTL software package as modified at Crystalytics Company. The resulting structural parameters have been refined to a convergence of R_1(unweighted, based on F) = 0.037 for 2680 independent reflections having $2\theta_{CuK\bar{\alpha}} < 115.0°$ and $I > 3\sigma(I)$. The 10 methyl groups were refined as rigid rotors with sp^3-hybridized geometry and a C-H bond length of 0.96 Å. The initial orientation of each methyl group was determined from difference Fourier positions for the hydrogen atoms. The final orietation of each methyl group was determined by three rotational parameters. The refined positions for the rigid rotor methyl groups gave C-C-H angles which ranged from 103°–118°. The remaining hydrogen atoms were included in the structure factor calculations as idealized atoms (assuming sp^2- or sp^3-hybridization of the carbon atoms and a C-H bond length of 0.96 Å) "riding" on their respective carbon atoms. The isotropic thermal paprameter of each hydrogen atom was fixed at 1.2 times the equivalent isotropic thermal parameter of the carbon to which it is covalently bonded.

References

1. See for example, (a) *Cytochrome P-450; Structure, Mechanism, and Biochemistry*; Ortiz de Montellano, P. R., Ed.; Plenum: New York, 1986. (b) Holm R. H. *Chem. Rev.* **1987**, *87*, 1404–1449. (c) *Metal Ion Activation of Dioxygen*; Spiro, T. G., Ed.; Wiley: New York, 1980. (d) *Oxygenases*; Hayashi, O., Ed.; Academic Press: New York-London, 1976. (e) *Activation and Functionalization of Alkanes*; Hill, C. L., Ed.; John Wiley & Sons: New York, 1989. (f) Sheldon, R. A.; Kochi, J. K. *Metal Catalyzed Oxidations of Organic Compounds*; Academic Press: New York, 1981. (g) Baldwin, J. E.; Abraham, E. *Natural Products Reports* **1988**, 129–145. (i) Dunford, *Peroxidases*, in *Adv. Inorg. Biochem.* Vol. 4, Eichorn, G. L.; Marzilli, L. G. Ed's; Elsevier Biomedical: New York, 1982, 41–68.

2. Nelson, F. M. *Iron(III) and Higher Oxidation States* in *Comprehensive Coordination Chemistry* Vol. 4, Wilkinson, G.; Guillard, R. G.; McCleverty, J. A., Eds.; Pergamon: Oxford, 1987, pp. 217–276.

3. Levason, W.; McAuliffe, C. A. *Coord. Chem. Rev.* **1974**, *12*, 151-184.

4. Audette, R. J.; Quail, J. W. *Inorg. Chem.* **1972**, *11*, 1904–1908.

5. (a) Gonzalez-Vilchez, F.; Griffith, W. P. *J. Chem. Soc., Dalton Trans.* **1972**, 1416–1421. (b) Griffith, W. P. *J. Chem. Soc., A* **1966**, 1467–1468.

6. Viste, A.; Gray, H. B. *Inorg. Chem.* **1964**, *8*, 1113–1123.

7. Hazeldean, G. S. F.; Nyholm, R. S.; Parish, R. V. *J. Chem. Soc., A* **1966**, 162–165.

8. Páez, E. A.; Oosterhuis, W. T.; Weaver, D. L. *J. Chem. Soc., Chem. Commun.* **1970**, 506–507.

9. (a) Pasek, E. A.; Straub, D. K. *Inorg. Chem.* **1972**, *11*, 259–263. (b)

Pasek, E. A.; Straub, D. K. *Inorg. Chim. Acta* **1977**, *21*, 23–27.

10. Chant, R.; Hendrickson, A. R.; Martin, R. L.; Rohde, N. M. *Aust. J. Chem.* **1973**, *26*, 2533–2536.

11. Martin, R. L.; Rohde, N. M.; Robertson, G. B.; Taylor, D. *J. Am. Chem. Soc.* **1974**, *96*, 3647–3649.

12. Petrouleas, V.; Petridis, D. *Inorg. Chem.* **1977**, *16*, 1306–1309.

13. (a) Hollander, F. J.; Pedelty, R.; Coucouvanis, D. *J. Am. Chem. Soc.* **1974**, *96*, 4032–4034. (b) Coucouvanis, D.; Hollander, F. J.; Pedelty, R. *Inorg. Chem.* **1977**, *16*, 2691–2696.

14. (a) Epstein, E. F.; Bernal, I. *Inorg. Chim. Acta* **1977**, *25*, 145–155. (b) Miyamae, H.; Sato, S.; Saito, Y.; Sakai, K.; Fukuyama, M. *Acta Cryst.* **1977**, *B33*, 3942–3944.

15. Goedken, V. L.; Deakin, M. R.; Bottomley, L. A. *J. Chem. Soc., Chem. Commun.* **1982**, 607–608.

16. English, D. R.; Hendrickson, D. N.; Suslick, K. S. *Inorg. Chem.* **1983**, *22*, 367–368.

17. Scheidt, W. R.; Summerville, D. A.; Cohen, I. A. *J. Am. Chem. Soc.* **1976**, *98*, 6623–6628.

18. (a) Tatsumi, K.; Hoffman R.; Whangbo, M.-H. *J. Chem. Soc., Chem. Commun.* **1980**, 509–511. (b) Tatsumi, K.; Hoffman R. *J. Am. Chem. Soc.* **1981**, *103*, 3328–3341.

19. (a) Groves, J. T.; Quinn, R.; McMurry, T. J.; Lang, G.; Boso, B. *J. Chem. Soc., Chem. Commun.* **1984**, 1455–1456. (b) Groves, J. T.; Quinn, R.; McMurry, T. J.; Nakamura, M.; Lang, G.; Boso, B. *J. Am. Chem. Soc.* **1985**, *107*, 354–360.

20. Hickman, D. L.; Nanthakumar, A.; Goff, H. M. *J. Am. Chem. Soc.* **1988**, *110*, 6384–6390.

21. Mansuy, D.; Battioni, P. In *Activation and Functionalization of Alkanes*; Hill, C. L., Ed.; John Wiley & Sons: New York, 1989; pp 195–218.

22. Jefcoate, C. B. In *Cytochrome P-450; Structure, Mechanism, and Biochemistry*; Ortiz de Montellano, P. R., Ed.; Plenum: New York, 1986; pp 387–428.

23. (a) Ortiz de Montellano, P. R. In *Cytochrome P-450; Structure, Mechanism, and Biochemistry*; Ortiz de Montellano, P. R., Ed.; Plenum: New York, 1986; pp 226 and 256. (b) Dawson, J. H.; Sono, M. *Chem. Rev.* **1987**, *87*, 1255–1276.

24. Guengerich, F. P.; Macdonald, T. L. *Acc. Chem. Res.* **1984**, *17*, 9–16.

25. (a) Poulos, T. L.; Finzel, B. C.; Gunzulas, I. C.; Wagner, G. C.; Kraut, J. *J. Biol. Chem.* **1985**, *260*, 16122. (b) Poulos, T. L.; Finzel, B. C.; Howard, A. J. *Biochemistry* **1986**, *25*, 5314.

26. For references, see: Collman, J. P. *Acc. Chem. Res.* **1977**, *10*, 265–272.

27. (a) Groves, J. T.; Haushalter, R. C.; Nakamura, M.; Nemo, T. E.; Evans, B. J. *J. Am. Chem. Soc.* **1981**, *103*, 2884–2886. (b) Boso, B.; Lang, G.; McMurry, T. J.; Groves, J. T. *J. Chem. Phys.* **1983**, *79*, 1122–1126. (c) Groves, J. T. *J. Chem. Ed.* **1985**, *62*, 928–931.

28. (a) Bajdor, K.; Nakamoto, K. *J. Am. Chem. Soc.* **1984**, *106*, 3045–3046. (b) Proniewicz, L. M.; Bajdor, K.; Nakamoto, K. *J. Phys. Chem.* **1986**, *90*, 1760–1766.

29. (a) Hashimoto, S.; Tatsuno, Y.; Kitagawa, T. *Proc. Jpn. Acad., Ser. B*

1984, *60*, 345. (b) Sitter, A. J.; Reczek, C. M.; Terner, J. *Biochim. Biophys. Acta* **1985**, *828*, 229.

30. Wagner, W.-D.; Nakamoto, K. *J. Am. Chem. Soc.* **1988**, *110*, 4044–4045.

31. For a review see: Frew, J. E.; Jones, P. In *Advances in Inorganic and Bioinorganic Mechanisms*; Academic Press: New York, 1984; Vol. 3, pp 175–212.

32. Fox, B. G.; Lipscomb, J. D. In *Biological Oxidation Systems*; Reddy, C. C.; Hamilton, G. A.; Madyastha, K. M., Eds.; Academic Press: New York, 1990; Vol. 1, pp 367–388.

33. (a) Murch, B. P.; Bradley, F. C.; Que, L. Jr. *J. Am. Chem. Soc.* **1986**, *108*, 5027–5028. (b) Kitajima, N.; Fukui, H.; Moro-oka, Y. *J. Chem. Soc., Chem. Commun.* **1988**, 485–486. (c) Vincent, J. B.; Huffman, J. C.; Christou, G.; Li, Q.; Nanny, M. A.; Hendrickson, D. N.; Fong, R. H.; Fish, R. H. *J. Am. Chem. Soc.* **1988**, *110*, 6898–6900.

34. (a) Wilkins, P. C.; Wilkins, R. G. *Chem. Rev.* **1987**, *79*, 195–214. (b) Klotz, I. M.; Kurtz, D. M. *Acc. Chem. Res.* **1984**, *17*, 17–22.

35. Sahlin, M.; Gräslund, A.; Petersson, L.; Ehrenberg, A.; Sjöberg, B.-M. *Biochemistry* **1989**, *28*, 2618–2625.

36. LeGall, J.; Prickril, B. C.; Moura, I.; Xavier, A. V.; Moura, J. J. G.; Huynh, B.-H. *Biochemistry* **1988**, *27*, 1636–1642.

37. Averill, B. A.; Davis, J. C.; Burman, S.; Zirino, T.; Sanders-Loehr, J.; Loehr, T. M.; Sage, J. T.; Debrunner, P. G. *J. Am. Chem. Soc.* **1987**, *109*, 3760–3767.

38. Lippard, S. J. *Angew. Chem. Int. Ed. Engl.* **1988**, *27*, 344–361.

39. δ_{Fe} values for Fe(III) complexes range from 0.2 mm s^{-1} to 0.6 mm s^{-1}. In a preliminary study of $[Et_4N]_2[Fe^{III}Cl(\eta^4\text{-MAC*})]$, a $\delta_{Fe} \approx 0.25$ mm s^{-1} at 4.2 K was observed.

40. The 300 MHz ^1H NMR spectrum of $[Et_4N][FeCl(\eta^4\text{-MAC*})]$ in $CDCl_3$ at 20 °C exhibits broad paramagnetically shifted features spread over a range of 50 ppm.

41. See Table 1 in Schulz, C. E.; Rutter, R.; Sage, J. T.; Debrunner, P. G.; Hager, L. P. *Biochem* **1984**, *23*, 4743–4754.

42. Ms. Kimberly Kostka of the Collins group and Dr. Brian Fox of the Münck group have pursued a detailed investigation of the EPR and Mössbauer properties of the Fe(III) and Fe(IV) systems of $(\eta^4\text{-MAC*})^{4-}$. Dr. Michael Hendrich has collaborated with Ms. Kostka to obtain the first integer spin EPR of an Fe(IV) species with this system. Mr. Michael Bartos of the Collins group and Dr. Fox are conducting intensive studies of the EPR and Mössbauer properties of the Fe(III) and Fe(IV) systems of $(\eta^4\text{-DEMAMPA-DCB*})^{4-}$ and its derivatives.

43. Dr. L. James Wright, visiting professor to CMU from the University of Auckland, New Zealand, 1989–1990.

44. Collins, T. J.; Kostka, K. L.; Münck, E.; Uffelman, E. S. *J. Am. Chem. Soc.* **1990**, *112*, 5637–5639.

Chapter 6

Stable Highly Oxidizing Square Planar Cobalt Complexes of Macrocyclic Tetraamido-*N* Ligands

Inorganic chemists have historically been interested in cobalt chemistry for several reasons. One reason is that some cobalt complexes are known to be reversible dioxygen carriers, and this topic has been reviewed.[1] Another reason is that vitamin B12, which has a cobalt-carbon bond, is the only biologically occurring organometallic complex.[2] This interest in vitamin B12 has led to some of the few examples of Co(IV) chemistry. This chapter will briefly introduce the literature of Co(IV) and square planar Co(III) complexes, and will then discuss the cobalt chemistry of the macrocycles. The isolation and characterization of an unprecedented class of square planar cobalt compounds with high positive formal reduction potentials indicates that the macrocycles possess the rare property of being compatible with strongly oxidizing coordination environments. It is also shown that an unusual and potentially useful combination of properties characterize the new class of cobalt compounds presented in this thesis: high positive formal potential, coordinative unsaturation of the oxidized species, intense coloration of the oxidized species with a clearly visible color change upon reduction, and high solubility of the oxidized form in nonpolar solvents with low solubility of the reduced form.

Background

For years, the only well-characterized complexes of Co(IV) were the inorganic salts Ba_2CoO_4[3a] and Cs_2CoF_6.[3b] More recently, Co(IV) monoalkyls have been studied in solution as part of the exploration of vitamin B12 reactivity.[4] Halpern's group studied a series of different six-coordinate organobis(dioximato)cobalt(IV) complexes (Figure 6.1).[5] These compounds were amenable to EPR spectroscopy. The small superhyperfine coupling constants observed in these species for both axial ($A_C \approx 1$ G for ^{13}C CH_3) and

equatorial (A_N = 2.3 G) ligands was explained by postulating that the odd electron resides in the dπ orbital in the plane of the dioxime ligand. Although the dioxime ligands are noninnocent, the relatively small Co hyperfine coupling constant (A_{Co} = 24.5–34.8 G for several complexes) was explained by low symmetry mixing of a 4p orbital with the 3d orbital and having the hyperfine interactions be of opposite sign and, thus, partially cancelling. Based on the model, an orbital which was 70% 3d and 30% 4p was invoked. The compounds had $Co^{IV/III}$ couples ranging from 0.849–0.902 V vs. SCE. At temperatures above the solvent freezing point, the compounds exhibited isotropic g values between 2.012 and 2.033, and isotropic A_{Co} values between 24.5–34.8 G. For the anisotropic spectra, $g_{\|}$ and $g_{\perp}$ differed from each other by 0.006 or less for the range of complexes, while $A_{\|}$ was typically six times larger than $A_{\perp}$. None of the compounds was characterized in the solid state, since they decomposed after several hours at −20 °C.

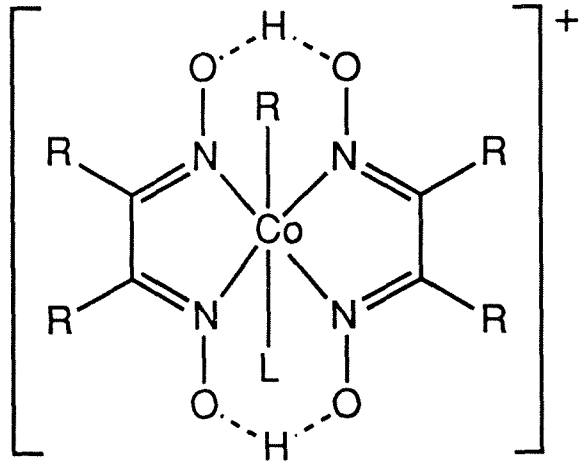

Figure 6.1. Six-coordinate organobis(dioximato)cobalt(IV) compounds studied by EPR by Halpern's group. These compounds decomposed after several hours at −20 °C.

Russian workers studied a series of different six-coordinate alkyl-

Salencobalt(IV) complexes (Figure 6.2).[6] These unstable compounds had rhombic EPR spectra. For the butyl complex, g_1=2.213, A_1=72 G, g_2 was calculated to be 2.090, A_2 was calculated to be 40 G, and g_3=1.993, and A_3=27 G. There was no resolvable superhyperfine coupling. These authors also explained their results in terms of mixing a 4p orbital with the 3d orbital on the metal, estimating that the unpaired electron resides in an orbital which is 90% 3d and 10% 4p.

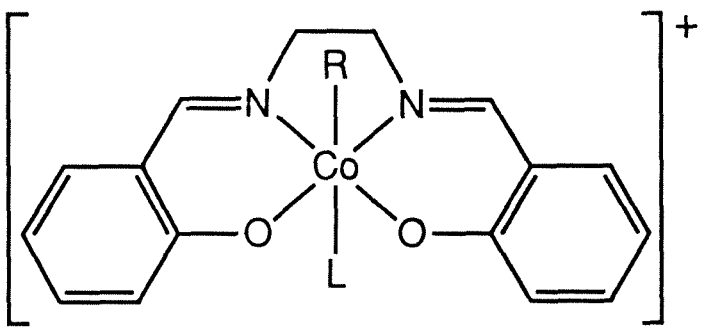

Figure 6.2. Unstable six-coordinate alkyl-Salencobalt(IV) complexes studied by Vol'pin's group.

Bower and Tennant prepared the compound which is the least ambiguous organometallic example of Co(IV), tetrakis(1-norbornyl)cobalt(IV).[7a] Theopold's group was successful in structurally characterizing the molecule, confirming that it was indeed tetrahedral, with Co–C bond distances of 1.92 Å.[7c] The group demonstrated that the compound was reduced by one electron at −2.02 V (vs. Fc^+/Fc in THF). More significantly, Theopold's group demonstrated that the compound was oxidized by one electron at −0.65 V (vs. Fc^+/Fc in THF) and was thus able to prepare the first well-characterized Co(V) complex.[7d] The anionic Co(III) and the neutral Co(IV) compounds both gave the expected paramagnetic NMR, while the cationic Co(V) gave the

diamagnetic NMR anticipated for a low-spin d^4 tetrahedral species.

The Collins group prepared an octahedral cobalt complex of CHBA-DCB, *trans*-Co(η^4CHBA-DCB)(*tert*-butylpyridine)$_2$, which has become accepted as an example of octahedral cobalt(IV),[8a] inspite of ambiguities associated with ligand noninnocence (Figure 1.17).[8b] The low temperature EPR parameters were consistent with those from previously accepted cobalt(IV) complexes (g=2.011, A_{Co}=16 G). The complex had a reversible $Co^{IV/III}$ couple of 0.39 V (vs. Fc^+/Fc in MeCN) and another reversible couple at 0.84 V (vs. Fc^+/Fc in MeCN).

The chemistry of cobalt(III) is voluminous for five- and six-coordinate species, but is limited for the square planar geometry.[9] Prior to the Collins group's research, the dozen known structures of square planar Co(III) were all of anions.[9] However, methylating the square planar Co(III) anions of the HMPA-B[10a] or HMPA-DMP[10b] ligands generated stable solutions of the first neutral square planar Co(III) complexes (Figure 6.3).[10b] The square planar anionic cobalt(III) complexes[10c] and chiral analogues[10d] were also found to act as catalytic oxidants of styrene to styrene oxide using iodosyl benzene as the stoichiometric oxidant. In a typical experiment, 24 turnovers were obtained in 24 hours with 69% catalyst recovered. The epoxidation reaction was tentatively proposed to involve a Co(V) oxo (isoelectronic with Fe(IV) oxo), although Valentine's results with Al^{III}TPP- and Zn^{II}TPP-mediated iodosylbenzene epoxidation of olefins[11] should cause this speculation to be cautiously regarded. As mentioned in Chapter 1 (Figure 1.12), Kochi's group also studied similar epoxidation reactions.[12a] However, it is almost certain that the mechanisms they ascribed to their oxidations are meaningless for several reasons.

First, the structure of their proposed catalyst is certainly incorrect, based on consideration of the literature precedent of Co(III) with strongly donating ligand complements,[9] and because a structure they characterized as a derivative was completely different from that of their earlier proposed catalyst (Figure 1.12).[12b] Second, Kochi's proposal of a Co–O double bond for a Co(IV) oxo ignores the fact that Co(IV) is d^5, making the bond order 1.5 for a system approximated by C_{4v} symmetry. Kochi's comparison of such a species with Fe(IV) (d^4) species is without merit.

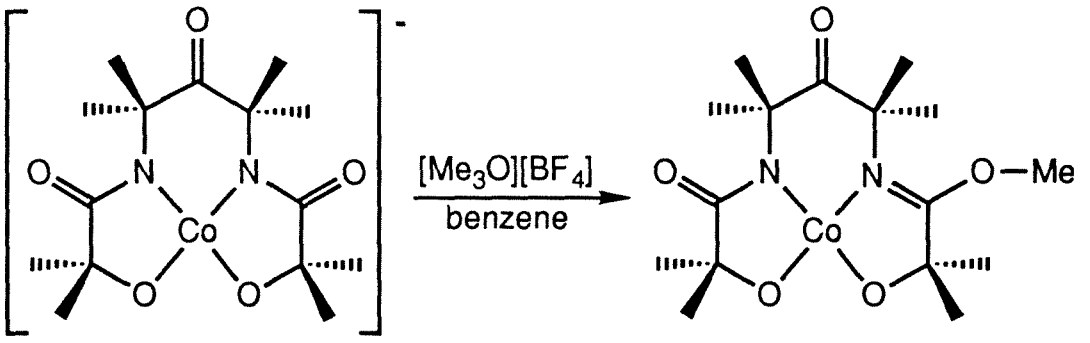

Figure 6.3. The preparation of the first neutral square planar Co(III) complex.

Treatment of paramagnetic $[Co(\eta^4\text{-HMPA-DMP})]^-$ with excess cyanide generated a diamagnetic *cis*-β complex which contained nonplanar amides (Figure 6.4).[13] This result extended the class of amides nonplanar due to electronic effects to an aliphatic ligand for the first time and extended this class to a metal other than osmium for the first time.

Results and Discussion

Cobalt has been inserted into each of the macrocycles, in high yields, to give the first macrocyclic square planar cobalt(III) complexes (Figure 6.5). The

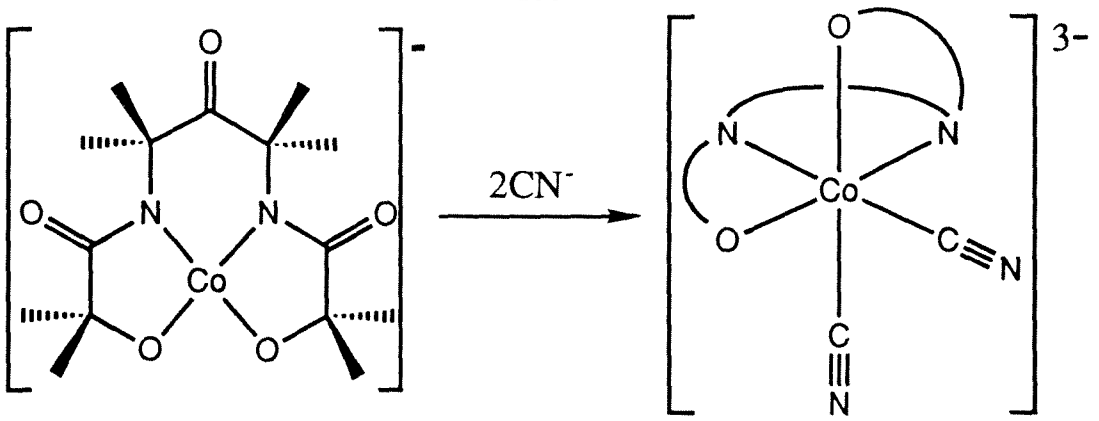

Figure 6.4. The preparation of *cis*-β-[Co(CN)$_2$(η^4-HMPA-DMP)]$^{3-}$.

cobalt anions have been isolated as their Li^+, $[Me_4N]^+$, $[Et_4N]^+$, $[Ph_4P]^+$, and $[Bu_4N]^+$ salts. The cobalt(III) complexes of (η^4-DEMAMPA-DCB)$^{4-}$, (η^4-DEMAMPA-B)$^{4-}$, and (η^4-DEMAMPA-DMOB)$^{4-}$ are all dark purple in the solid state and in solution, the cobalt(III) complex of (η^4-MAC*)$^{4-}$ is red, and the UV-vis spectra remain effectively constant in aprotic coordinating and non-coordinating solvents for all of the complexes.

The cobalt(III) complexes exhibit well-resolved, paramagnetically-shifted ^{1}H NMR spectra typical of square planar cobalt(III) (S = 1) systems.[9f,j,k] The NMR spectra characteristic of the complexes are shown in Figures 6.6 and 6.7. The dependence of the proton chemical shifts on the solvent donor properties is small, further indicating that the four-coordinate planar structures established in the solid state (see below) are also the most likely structures in aprotic solutions. In water, in which only the Li^+ salts have appreciable solubility, the behavior is more complex (Figure 6.8). The complexes will not bind classic σ-donors such as halide anions, water, nitrogen bases, phosphines, etc. at room temperature. However, they will bind π-acids such as cyanide or *tert*-butyl isocyanide to give diamagnetic complexes. The monocyanide complexes are

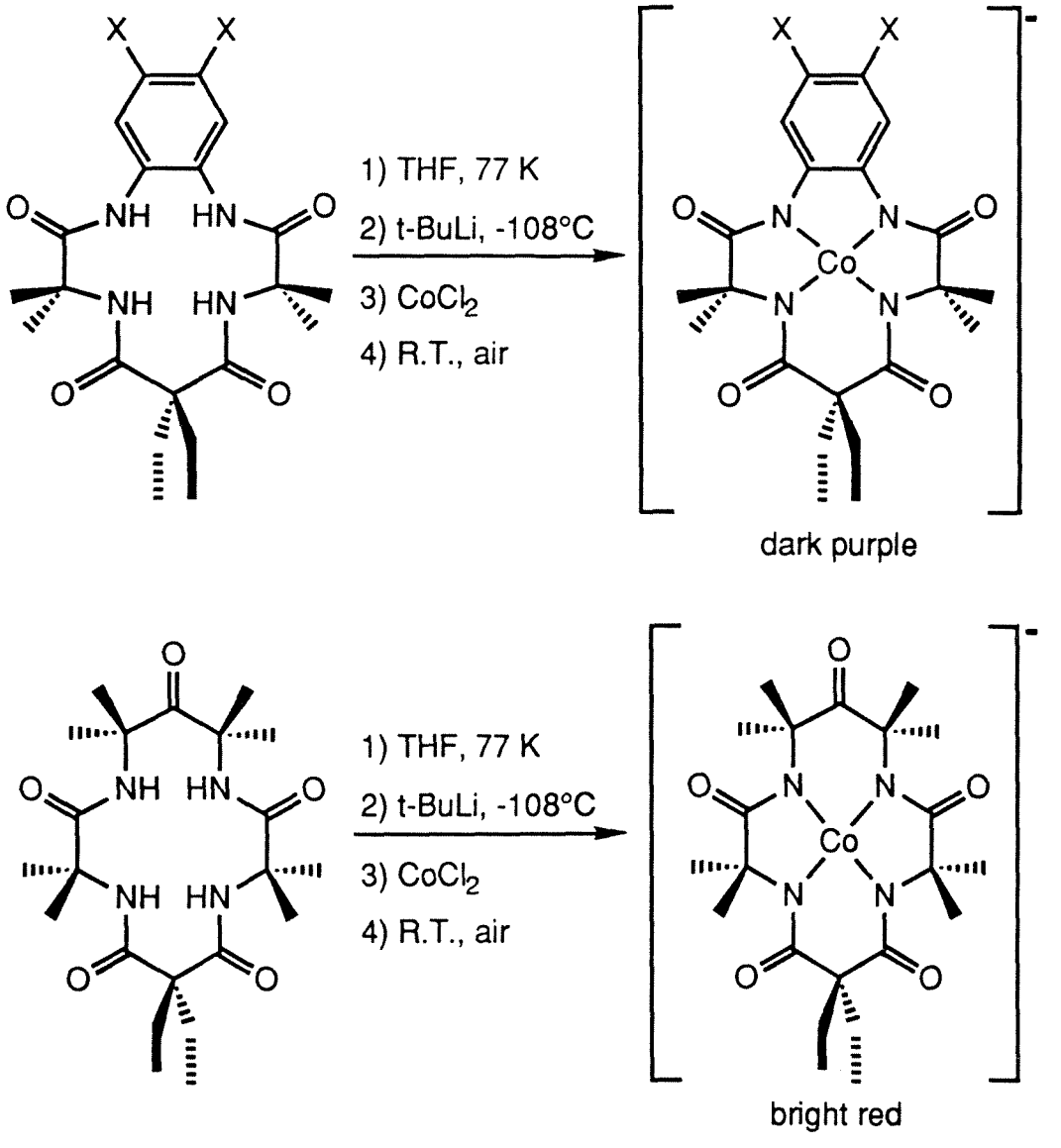

Figure 6.5. Reaction conditions for inserting cobalt into the macrocycles.

green, and the *trans* bis cyanide complexes are yellow.[14] Various Grignards and aryl and alkyllithiums generate insoluble green complexes which slowly revert to starting material on exposure to air or water.

The Co(III) complexes are even more remarkably acid stable than the Cr, Mn, and Fe complexes. Strong acids, such as *p*-toluenesulfonic acid, gener-

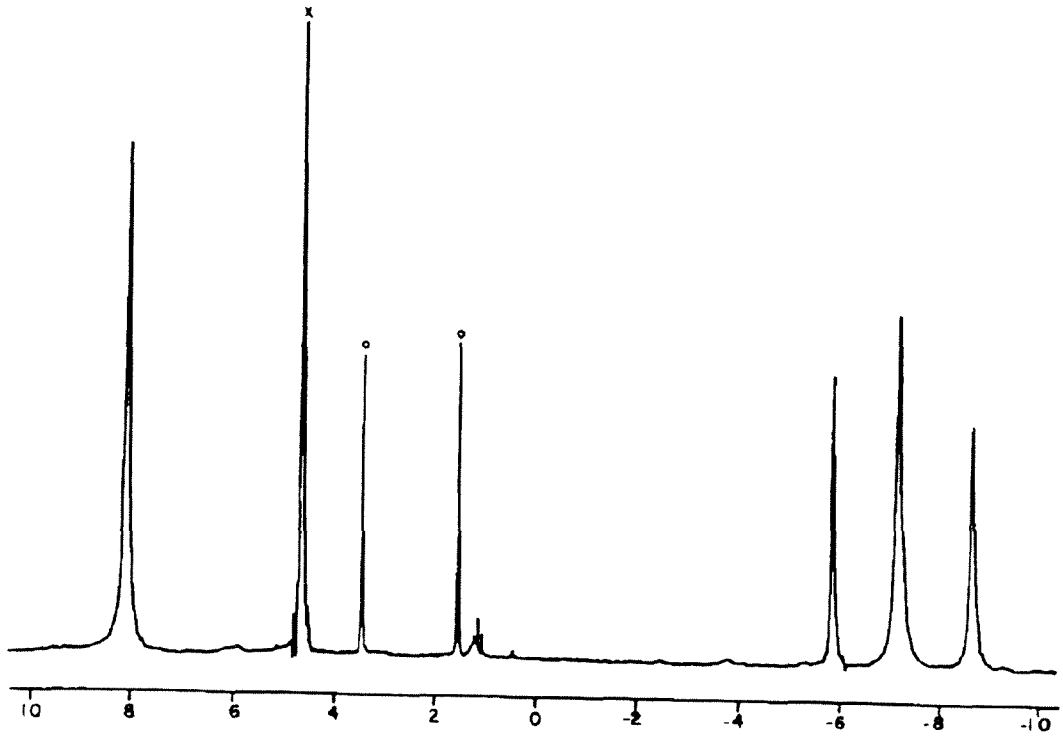

Figure 6.6. ^{1}H NMR spectrum (300 MHz, D_2O) of Li[Co(η^4-MAC*)] (δppm: 8.10, br, 12H; -5.85, br, 4H; -7.19, br, 12H; -8.66, br, 6H [x = HOD—used as reference, o = THF signals]).

ate diamagnetic, axially symmetric pale yellow complexes in EtOH.[15] Heating these acidic ethanolic solutions regenerates the dark red or purple colors and cooling causes the yellow color to reappear. Addition of base regenerates the red or purple anions. Protonation of the anions probably occurs at the amide oxygens, generating hydroxyimine donors. These weaker donors enable Co(III) to add the axial ligands which causes spin-pairing of intermediate-spin d^6 to give low-spin d^6. Neutral paramagnetic monoprotonated species may be precipitated from water using HBF_4 (vide infra). Considering the extremely basic conditions needed to insert metals into the macrocycles, this tremendous acid stability is remarkable. The complexes are also very robust to base hydrolysis,

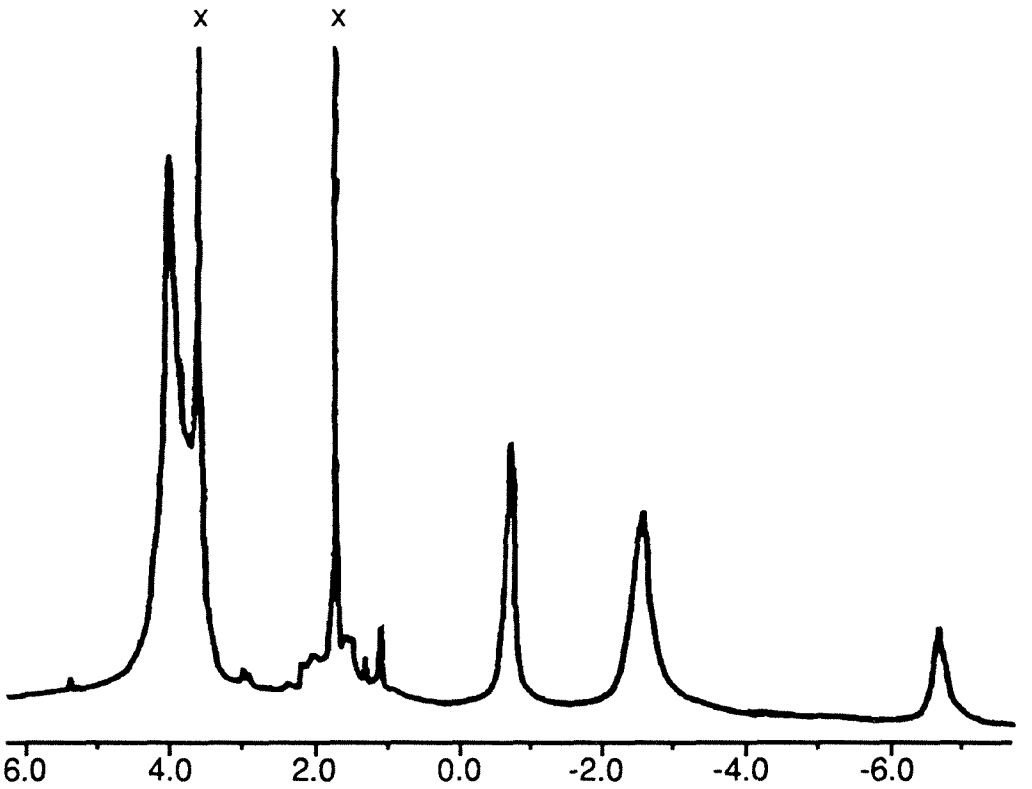

Figure 6.7. ^{1}H NMR spectrum (300 MHz, THF) of Li[Co(η^4-DEMAMPA-DCB)] (δppm: 3.96, br, 12H; -0.69, br, 4H; -2.64, br, 6H; -6.80, br, 2H [x = THF signals—used as reference]). The ^{1}H NMR spectrum (300 MHz) in CD_3CN of Li[Co(η^4-DEMAMPA-DCB)] is very similar (δppm: 3.92, br, 12H; -0.80, br, 4H; -2.82, br, 6H; -6.58, br, 2H). Note that sharp diamagnetic spikes which had no integratable intensity have been omitted from this figure.

since the $[Bu_4N]^+$ salts may be prepared by precipitations from solutions of the Li^+ salts with $[Bu_4N][OH]$.

The anion, $[Co(\eta^4\text{-MAC*})]^-$, was the first structurally characterized macrocyclic square planar Co(III) complex (Figure 6.9). The average Co–N bond distance of 1.85 Å is not unusual for square planar Co(III) (average Co–N bond distances: 1.818 Å,[10a] 1.82 Å,[10d], cf 1.892 Å for *trans*-Co(η^4CHBA-DCB)(*tert*-butylpyridine)$_2$[8b]). Although the complex is best described as

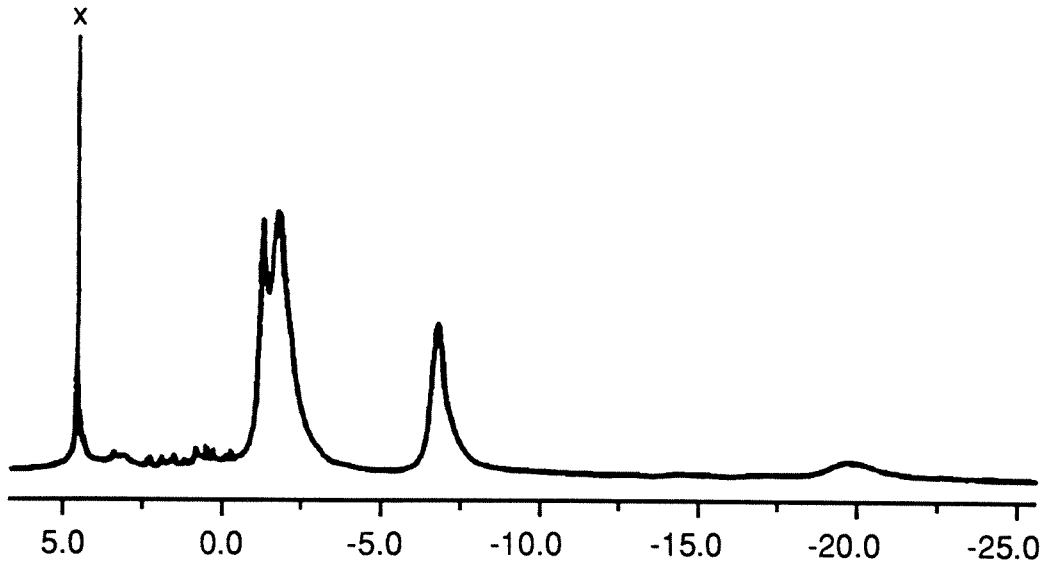

Figure 6.8. ^{1}H NMR spectrum (300 MHz, D_2O) of Li[Co(η^4-DEMAMPA-DCB)] (δppm: -1.18, br, 4H; -1.70, br, 12H; -6.66, br, 6H; -19.70, br, 2H [x = HOD signal—used as reference]). Note that sharp diamagnetic spikes which had no integratable intensity have been omitted from this figure.

square planar, the ligand is ruffled, and the nitrogens alternate 0.23 Å above and below their mean plane, with Co 0.03 Å above this plane. The complex crystallizes to give two independent anions. In both, there is one significantly nonplanar amide, and as will be discussed in Chapter 9, this was the first inorganic example of amide nonplanarity due solely to ring strain in the absence of ancillary ligands. The complex does not exhibit any electrochemical activity up to 2.0 V vs. NHE.

By contrast, each of the square planar cobalt(III) anions of the benzene-bridged macrocycles can be oxidized by one electron in CH_2Cl_2 to give stable square planar neutral molecules which can be produced by bulk electrolysis or chemical oxidation: E_f(Co(η^4-DEMAMPA-DCB)/[Co^{III}(η^4-

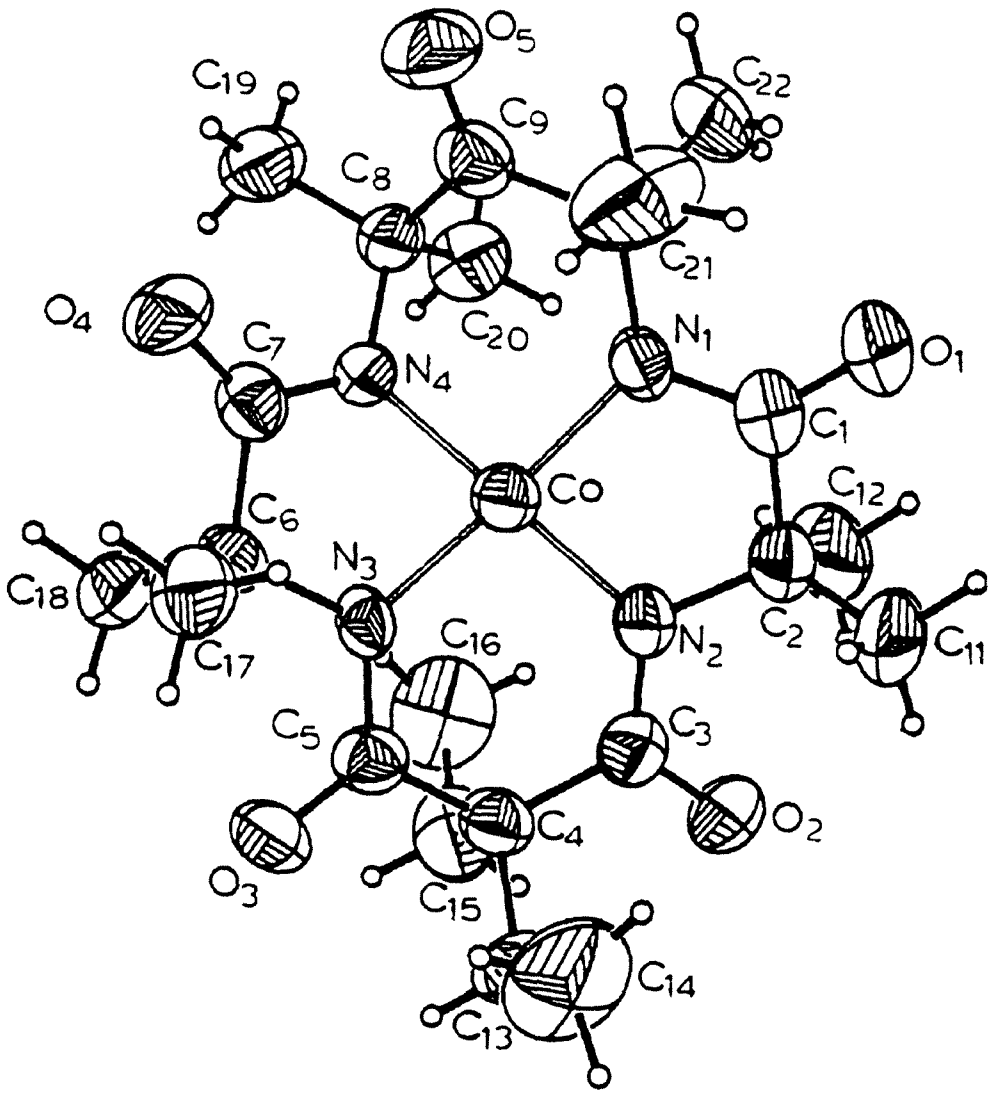

Figure 6.9. Molecular structure of anion 1 of $[Me_4N][Co(\eta^4\text{-MAC*})]$. ORTEP drawing with all nonhydrogen atoms drawn to encompass 50% of electron density.

Table 6.1. Bond Lengths in $[Co(MAC*)]^-$ anion 1			
Atoms	Length (Å)	Atoms	Length (Å)
CoN1	1.865(5)	CoN2	1.837(5)
CoN3	1.845(5)	CoN4	1.844(5)
O1C1	1.230(9)	O2C3	1.235(9)

Table 6.1. Bond Lengths in $[Co(MAC^*)]^-$ anion 1 (continued)			
Atoms	Length (Å)	Atoms	Length (Å)
O3C5	1.233(8)	O4C7	1.225(9)
O5C9	1.209(9)	N1C1	1.342(9)
N2C3	1.348(8)	N3C5	1.354(8)
N4C7	1.361(9)	N1C10	1.494(8)
N2C2	1.486(9)	N3C6	1.471(9)
N4C8	1.498(7)	C1C2	1.53(1)
C3C4	1.53(1)	C4C5	1.53(1)
C6C7	1.52(1)	C8C9	1.52(1)
C9C10	1.54(1)	C2C11	1.53(1)
C2C12	1.55(1)	C4C13	1.54(1)
C4C15	1.57(1)	C13C14	1.52(2)
C15C16	1.49(1)	C6C17	1.52(1)
C6C18	1.53(1)	C8C19	1.54(1)
C8C20	1.53(1)	C10C21	1.51(1)
C10C22	1.58(1)		

Table 6.2. Bond Lengths in $[Co(MAC^*)]^-$ anion 2			
Atoms	Length (Å)	Atoms	Length (Å)
CoN1	1.846(5)	CoN2	1.841(6)
CoN3	1.838(5)	CoN4	1.863(5)
O1C1	1.215(9)	O2C3	1.233(10)
O3C5	1.228(9)	O4C7	1.238(8)

Table 6.2. Bond Lengths in [Co(MAC*)]$^-$ anion 2 (continued)			
Atoms	Length (Å)	Atoms	Length (Å)
O5C9	1.206(9)	N1C1	1.350(10)
N2C3	1.364(9)	N3C5	1.367(8)
N4C7	1.348(9)	N1C10	1.483(9)
N2C2	1.485(9)	N3C6	1.499(9)
N4C8	1.493(9)	C1C2	1.54(1)
C3C4	1.51(1)	C4C5	1.53(1)
C6C7	1.53(1)	C8C9	1.54(1)
C9C10	1.49(1)	C2C11	1.51(1)
C2C12	1.54(1)	C4C13	1.54(1)
C4C15	1.54(1)	C13C14	1.51(1)
C15C16	1.51(1)	C6C17	1.54(1)
C6C18	1.54(1)	C8C19	1.53(1)
C8C20	1.56(1)	C10C21	1.53(1)
C10C22	1.53(1)		

Table 6.3. Bond Angles in [Co(MAC*)]$^-$ anion 1			
Atoms	Angle (°)	Atoms	Angle (°)
N1CoN2	87.6(2)	N1CoN3	163.5(3)
N1CoN4	94.6(2)	N2CoN3	96.8(2)
N2CoN4	167.4(3)	N3CoN4	84.6(2)
CoN1C1	114.1(4)	CoN1C10	125.3(4)

Table 6.3. Bond Angles in $[Co(MAC^*)]^-$ anion 1 (continued)			
Atoms	Angle (°)	Atoms	Angle (°)
CoN2C2	114.3(4)	CoN2C3	117.3(6)
CoN3C5	128.6(5)	CoN3C6	112.9(3)
CoN4C7	110.6(4)	CoN4C8	122.0(4)
C1N1C10	118.3(6)	C2N2C3	117.3(6)
C5N3C6	118.3(5)	C7N4C8	122.7(5)
N1C1O1	126.3(7)	N1C1C2	115.2(6)
O1C1C2	118.5(6)	N2C3O2	123.1(6)
N2C3C4	120.7(6)	O2C3C4	116.3(6)
N3C5O3	122.6(7)	N3C5C4	119.4(5)
O3C5C4	117.7(6)	N4C7O4	125.5(5)
N4C7C6	112.5(6)	O4C7C6	122.0(6)
C8C9C10	120.0(6)	C8C9O5	121.6(6)
C10C9O5	118.3(7)	C1C2C11	107.7(7)
C1C2C12	106.4(6)	N2C2C1	106.5(6)
N2C2C12	111.2(7)	C11C2C12	106.4(6)
C3C4C5	120.7(6)	C3C4C13	108.2(6)
C3C4C15	106.8(6)	C5C4C13	107.4(6)
C5C4C15	105.3(6)	C13C4C15	107.8(6)
C7C6C17	108.4(6)	C7C6C18	103.9(5)
N3C6C7	106.2(5)	N3C6C17	112.3(6)
N3C6C18	113.3(6)	C17C6C18	112.1(6)
N4C8C9	105.4(5)	N4C8C19	112.9(5)
N4C8C20	107.4(5)	C9C8C19	111.4(6)

Table 6.3. Bond Angles in $[Co(MAC^*)]^-$ anion 1 (continued)			
Atoms	Angle (°)	Atoms	Angle (°)
C9C8C20	111.3(6)	C19C8C20	108.4(6)
N1C10C9	114.4(6)	N1C10C21	109.8(6)
N1C10C22	110.6(7)	C9C10C21	109.3(7)
C9C10C22	99.3(5)	C21C10C22	113.2(7)
C4C13C14	114.1(7)	C4C15C16	116.5(7)
N2C2C11	113.2(6)		

Table 6.4. Bond Angles in $[Co(MAC^*)]^-$ anion 2			
Atoms	Angle (°)	Atoms	Angle (°)
N1CoN2	85.1(2)	N1CoN3	168.7(2)
N1CoN4	94.1(2)	N2CoN3	96.2(2)
N2CoN4	166.1(2)	N3CoN4	87.4(2)
CoN1C1	112.8(4)	CoN1C10	121.9(5)
CoN2C2	113.4(4)	CoN2C3	117.6(6)
CoN3C5	128.5(5)	CoN3C6	114.4(4)
CoN4C7	114.9(4)	CoN4C8	127.3(4)
C1N1C10	122.9(6)	C2N2C3	117.6(6)
C5N3C6	116.2(6)	C7N4C8	116.1(5)
N1C1O1	128.2(7)	N1C1C2	112.5(6)
O1C1C2	119.1(7)	N2C3O2	122.0(7)
N2C3C4	120.4(7)	O2C3C4	117.4(6)
N3C5O3	123.5(7)	N3C5C4	119.8(6)
O3C5C4	116.6(6)	N4C7O4	127.6(6)

Table 6.4. Bond Angles in $[Co(MAC^*)]^-$ anion 2 (continued)			
Atoms	Angle (°)	Atoms	Angle (°)
N4C7C6	114.8(6)	O4C7C6	117.7(6)
C8C9C10	121.5(6)	C8C9O5	116.8(6)
C10C9O5	121.8(6)	C1C2C11	109.3(6)
C1C2C12	104.8(5)	N2C2C1	106.2(6)
N2C2C12	112.6(6)	C11C2C12	111.6(7)
C3C4C5	121.3(6)	C3C4C13	107.4(7)
C3C4C15	107.6(6)	C5C4C13	106.6(6)
C5C4C15	106.2(7)	C13C4C15	107.0(6)
C7C6C17	108.8(5)	C7C6C18	105.1(6)
N3C6C7	106.6(5)	N3C6C17	112.3(6)
N3C6C18	111.2(5)	C17C6C18	112.3(6)
N4C8C9	112.3(5)	N4C8C19	108.4(6)
N4C8C20	112.4(7)	C9C8C19	109.1(7)
C9C8C20	103.2(6)	C19C8C20	111.3(6)
N1C10C9	104.6(5)	N1C10C21	114.4(7)
N1C10C22	107.1(6)	C9C10C21	111.4(6)
C9C10C22	112.6(7)	C21C10C22	106.8(6)
C4C13C14	113.4(7)	C4C15C16	114.9(7)
N2C2C11	111.9(5)		

DEMAMPA-DCB)]$^-$) = 0.550 V (Figure 6.10) (vs. Fc^+/Fc, ca. 1.26 V vs. NHE), E_f(Co(η^4-DEMAMPA-B)/[Co^{III}(η^4-DEMAMPA-B)]$^-$) = 0.385 V (vs. Fc^+/Fc, ca. 1.09 V vs. NHE), E_f(Co(η^4-DEMAMPA-DMOB)/[Co^{III}(η^4-DEMAMPA-DMOB)]$^-$) = −0.010 V (vs. Fc^+/Fc, ca. 0.70 V vs. NHE). As

has been discussed in Chapters 3–5, this family of ligands is capable of supporting crystalline highly oxidized species such as mononuclear five-coordinate iron(IV) chloro and manganese(V) oxo and chromium(V) oxo. As a result of the negative charge and strong donor capacity of the macrocyclic tetraamido-*N* ligands, these tetraamido-*N* complexes are not strongly oxidizing and, in fact, are remarkably inert. Co(η^4-DEMAMPA-DCB), Co(η^4-DEMAMPA-B), and CoDEMAMPA-DMOB) can all be isolated as crystalline compounds, and the existence of the stable neutral species shows that the dichloro- and diproteo-substituted ligands are indeed stable in strongly oxidizing complexes. The methoxy groups lower the formal potential of Co(η^4-DEMAMPA-DMOB) such that the complex is only mildly oxidizing. The long-term stability of the strong electron transfer oxidants, Co(η^4-DEMAMPA-DCB) and Co(η^4-DEMAMPA-B), demonstrates the resistance of the macrocyclic tetraamido-*N* ligands to oxidative degradation. This is an important finding, since it shows that these macrocyclic ligands, known to be excellent for stabilizing high valent metal centers, are also compatible with strongly oxidizing systems and establishes that complexes with *cis*-amido-*N* donors can be resistant to reductive degradation processes, such as N-N bond formation or homolytic M-N bond cleavage.

As expected, the oxidation results in a pronounced increase in the C–O IR stretching frequencies ([Bu_4N][Co^{III}(η^4-DEMAMPA-DCB)]: IR (Nujol): $\bar{\nu}$[cm^{-1}] = 1648, 1593, 1571; Co(η^4-DEMAMPA-DCB): IR (Nujol): $\bar{\nu}$[cm^{-1}] = 1716, 1616, 1599.). Remarkably, the band at 1716 cm^{-1} is higher than any of the amide bands in the free ligand (see experimental, Chapter 2). The complex was also examined by FAB mass spec. Because the complex is highly oxidizing, it was anticipated that the cation spectrum would show considerable

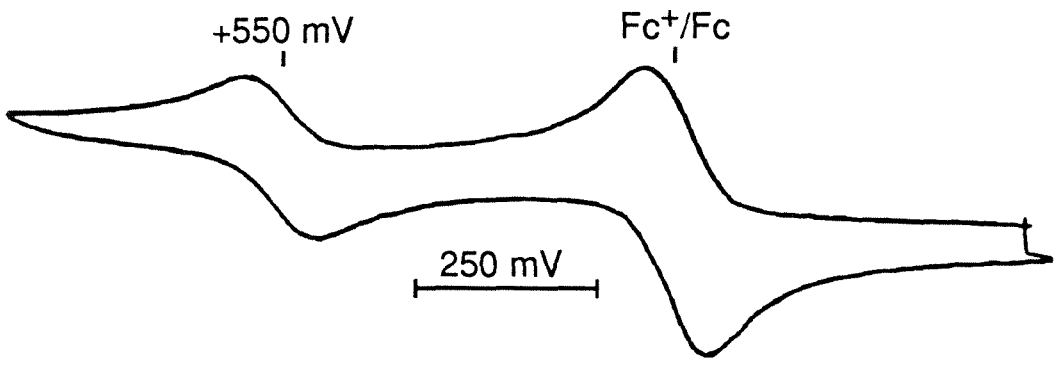

Figure 6.10. Cyclic voltammetry of $[Co^{III}(\eta^4\text{-DEMAMPA-DCB})]^-$ and ferrocene in CH_2Cl_2 (0.1 M $[Bu_4N][ClO_4]$ supporting electrolyte, 1.450 V sweep-width).

fragmentation, with very little of the molecular ion apparent. Conversely, since the anion was obviously very stable, it was anticipated that the anion spectrum would exhibit very little fragmentation. This was found to be the case, since the base peak in the anion spectrogram (525) was the molecular ion. It is anticipated that negative anion FABS will be an important tool in characterizing highly oxidizing neutral complexes.

The solubility of Co(η^4-DEMAMPA-DCB) in benzene is 60 mM; it dissolves in nujol, silicone grease, and is even somewhat pentane soluble. Thus, Co(η^4-DEMAMPA-DCB) is a noteworthy complex, a potent electron transfer oxidant soluble in hydrocarbons. Although these neutrals are very stable, demonstrating the resistance to oxidative degradation of this ligand system, they are reactive in the presence of oxidizable substrates. The Co(η^4-DEMAMPA-DCB) complex reacts instantaneously with alcohols, and very slowly with water, to give H[Co(η^4-DEMAMPA-DCB)]. This was verified by synthesizing the compound by dissolving Li[Co(η^4-DEMAMPA-DCB)] in wa-

ter and precipitating a neutral complex by adding HBF_4. The spectral and physical properties of the material produced by acidification and the material produced by reduction are identical. The monoprotonated complex gives a very much broadened paramagnetic NMR in acetone.

Co(η^4-DEMAMPA-DCB) is the first crystallographically characterized neutral square planar cobalt complex in an oxidation state higher than +II. The molecular structures of $[Co^{III}(\eta^4$-DEMAMPA-DCB$)]^-$ and Co(η^4-DEMAMPA-DCB) are shown in Figures 6.11 and 6.12, respectively. The coordination environments around each cobalt center are best described as square planar. For the $[Co^{III}(\eta^4$-DEMAMPA-DCB$)]^-$ anion, the four nitrogen atoms each deviate from their mean plane by no more than 0.02 Å, with the Co atom sitting in this mean plane. For Co(η^4-DEMAMPA-DCB), the four nitrogen atoms each deviate from their mean plane by no more than 0.05 Å, and the Co atom sits in this mean plane. At the 3σ confidence level, the average Co–N bond distances, 1.814(4) Å for Co(η^4-DEMAMPA-DCB) and 1.825(2) Å for $[Co^{III}(\eta^4$-DEMAMPA-DCB$)]^-$, are indistinguishable. The most significant structural difference is found in the shortening of the two aromatic C to N bond distances and the distortions that occur in the aromatic ring upon oxidation. For Co(η^4-DEMAMPA-DCB), a twofold crystallographic rotation axis passes through Co and C4. The N1-C5/N1′-C5′ (1.353(6) Å) and C6-C7/C6′-C7′ (1.350(8) Å) distances of this neutral molecule show evidence of significantly higher bond orders than the comparable bonds of the anion: Bond Distances [Å]: N1-C9, 1.406(3); N4-C8, 1.415(3); C10-C11, 1.386(4); C12-C13, 1.387(4). Although the differences are less pronounced, a trend to lower bond orders is suggested in the distances for the C5-C5′ (1.432(9)), C5-C6/C5′-C6′

(1.398(7) Å), and C7-C7′ (1.428(10) Å) bonds of the neutral species when compared with the comparable bonds of the anion: Bond distances [Å]: C8-C9, 1.411(4); C8-C13, 1.376(4); C9-C10, 1.387(4); C11-C12, 1.380(4). These changes suggest that ligand-centered oxidation is important in the neutral species since the trends in the data can be rationalized by invoking structures similar to those indicated in Figure 6.13.[16] Significantly, the ligand character of the oxidation is also supported by the absence of electrochemical activity for $[Co^{III}(\eta^4\text{-MAC*})]^-$. While the X-ray data for $[Co^{III}(\eta^4\text{-DEMAMPA-DCB})]^-$ and $Co(\eta^4\text{-DEMAMPA-DCB})$ suggest the involvement of the ligand extended π system in the site of oxidation, EPR evidence clearly shows that the metal is the primary location of the unpaired electron in the highly oxidizing S=1/2 molecules.

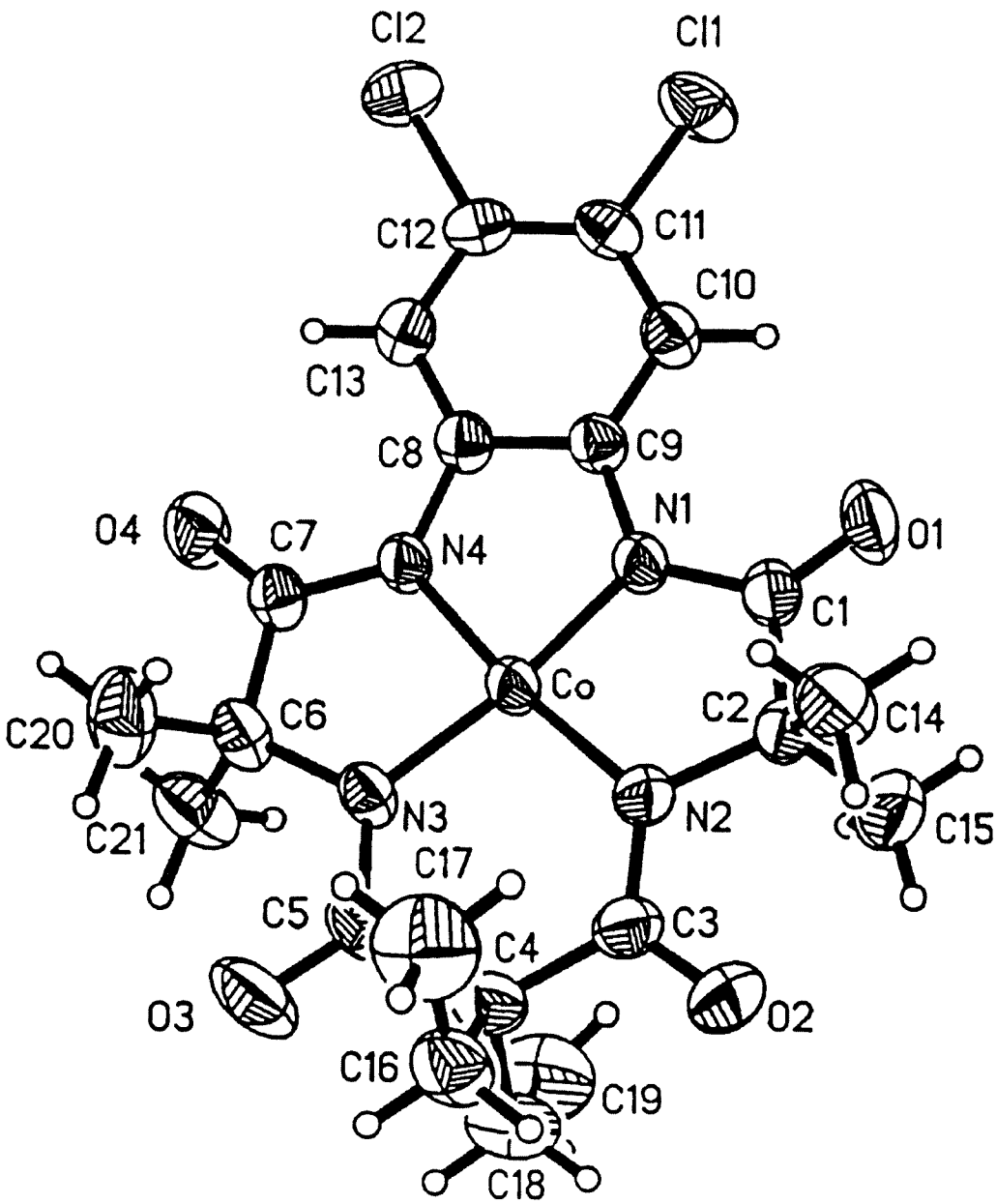

Figure 6.11. Molecular structure of anion of $[Ph_4P][Co^{III}(\eta^4\text{-DEMAMPA-DCB})]$. ORTEP drawing with all nonhydrogen atoms drawn to encompass 50% of electron density.

Table 6.5. Bond Lengths in $[Co^{III}(\eta^4$-DEMAMPA-DCB)]$^-$			
Atoms	Length (Å)	Atoms	Length (Å)
CoN1	1.827(2)	CoN2	1.823(2)
CoN3	1.829(2)	CoN4	1.819(2)
Cl1C11	1.740(3)	Cl2C12	1.738(3)
O1C1	1.219(4)	O2C3	1.232(4)
O3C5	1.231(4)	O4C7	1.218(3)
N1C1	1.365(4)	N1C9	1.406(3)
N2C3	1.358(4)	N3C5	1.358(3)
N4C7	1.359(4)	N4C8	1.415(3)
N2C2	1.493(4)	N3C6	1.490(4)
C1C2	1.534(4)	C3C4	1.542(4)
C4C5	1.539(5)	C6C7	1.533(4)
C8C9	1.411(4)	C8C13	1.376(4)
C9C10	1.387(4)	C10C11	1.386(4)
C11C12	1.380(4)	C12C13	1.387(4)
C2C14	1.526(5)	C2C15	1.520(5)
C4C16	1.548(5)	C4C18	1.550(5)
C6C20	1.529(5)	C6C21	1.527(5)
C16C17	1.519(5)	C18C19	1.516(6)

Table 6.6. Bond Angles in $[Co^{III}(\eta^4$-DEMAMPA-DCB)]$^-$			
Atoms	Angle (°)	Atoms	Angle (°)
N1CoN2	87.1(1)	N2CoN3	101.3(1)
N2CoN4	171.7(1)	N1CoN3	171.5(1)

Table 6.6. Bond Angles in $[Co^{III}(\eta^4$-DEMAMPA-DCB)]$^-$ (continued)

Atoms	Angle (°)	Atoms	Angle (°)
N1CoN4	84.7(1)	N3CoN4	86.9(1)
CoN1C1	117.7(2)	CoN1C9	115.9(2)
CoN2C2	126.5(2)	CoN3C5	126.8(2)
CoN3C6	114.8(2)	CoN4C7	118.0(2)
CoN4C8	115.9(2)	CoN2C3	126.5(2)
C1N1C9	126.4(2)	C2N2C3	118.3(2)
C5N3C6	118.4(2)	C7N4C8	126.0(2)
O1C1N1	124.9(3)	O1C1C2	123.0(3)
N1C1C2	112.1(2)	O2C3N2	122.9(3)
O2C3C4	115.7(3)	N2C3C4	121.4(3)
O3C5N3	122.8(3)	O3C5C4	115.9(3)
N3C5C4	121.3(3)	O4C7N4	125.5(3)
O4C7C6	122.3(3)	N4C7C6	112.2(2)
N2C2C1	108.0(2)	N2C2C14	111.0(3)
C1C2C14	106.3(3)	N2C2C15	112.6(3)
C1C2C15	107.5(3)	C14C2C15	111.2(3)
C3C4C5	122.3(2)	C3C4C16	106.8(3)
C5C4C16	106.5(3)	C3C4C18	106.2(3)
C5C4C18	106.5(3)	C16C4C18	107.8(2)
N4C8C9	111.6(2)	N4C8C13	127.8(3)
C9C8C13	120.5(2)	N1C9C8	111.8(2)
N1C9C10	128.9(3)	C8C9C10	119.3(2)
C9C10C11	119.7(3)	Cl1C11C10	119.5(2)

Table 6.6. Bond Angles in $[Co^{III}(\eta^4\text{-DEMAMPA-DCB})]^-$ (continued)

Atoms	Angle (°)	Atoms	Angle (°)
Cl1C11C12	120.3(2)	C10C11C12	120.2(3)
Cl2C12C11	120.8(2)	Cl2C12C13	118.3(2)
C11C12C13	120.9(3)	C8C13C12	119.1(3)
C4C16C17	112.7(3)	C4C18C19	113.8(3)
N3C6C7	107.8(2)	N3C6C20	112.0(3)
C7C6C20	105.1(2)	N3C6C21	112.0(2)
C7C6C21	107.7(3)	C20C6C21	111.8(3)

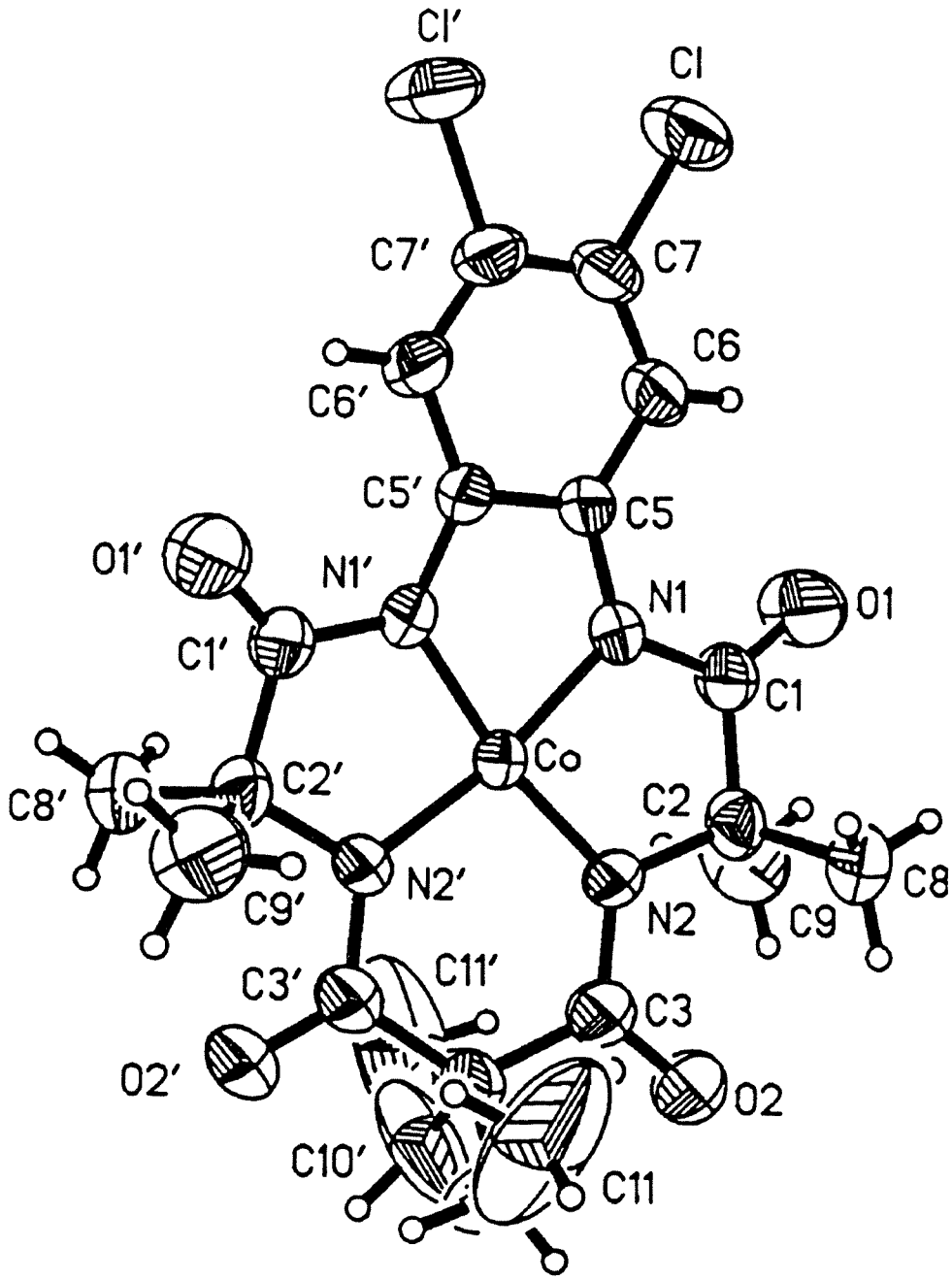

Figure 6.12. Molecular structure of Co(η^4-DEMAMPA-DCB). ORTEP drawing with all nonhydrogen atoms drawn to encompass 50% of electron density. A twofold crystallographic rotation axis passes through Co and C4.

Table 6.7. Bond Lengths in Co(η^4-DEMAMPA-DCB)			
Atoms	Length (Å)	Atoms	Length (Å)
CoN1	1.823(4)	CoN2	1.805(4)
O1C1	1.201(7)	O2C3	1.227(7)
N1C1	1.386(6)	N1C5	1.353(6)
N2C3	1.367(7)	N2C2	1.503(7)
C1C2	1.522(8)	C3C4	1.539(7)
C5C6	1.398(7)	C6C7	1.350(8)
C5C5′	1.432(9)	C7C7′	1.428(10)
C2C8	1.531(8)	C2C9	1.520(9)
C4C10	1.539(11)	C4C11	1.496(19)
ClC7	1.724(6)		

Table 6.8. Bond Angles in Co(η^4-DEMAMPA-DCB)			
Atoms	Angle (°)	Atoms	Angle (°)
N1CoN2	87.5(2)	N2CoN1′	170.3(2)
N1CoN1′	83.4(2)	N2CoN2′	101.9(3)
CoN1C1	116.8(3)	CoN1C5	116.8(3)
CoN2C2	115.7(3)	CoN2C3	126.2(3)
C1N1C5	126.5(4)	C2N2C3	117.8(4)
O1C1N1	124.2(5)	N1C1C2	112.7(4)
O1C1C2	123.2(5)	O2C3N2	122.3(5)
O2C3C4	117.1(5)	N2C3C4	120.5(5)
N1C5C6	128.3(4)	N1C5C5′	111.5(2)
C6C5C5′	120.2(3)	C5C6C7	118.3(5)

Table 6.8. Bond Angles in Co(η^4-DEMAMPA-DCB) (continued)			
Atoms	Angle (°)	Atoms	Angle (°)
ClC7C6	119.0(4)	ClC7C7′	119.5(2)
C6C7C7′	121.5(3)	N2C2C8	111.3(4)
N2C2C1	107.1(4)	C1C2C8	105.6(4)
N2C2C9	111.0(5)	C1C2C9	108.8(5)
C8C2C9	112.6(5)	C3C4C10	106.0(5)
C3C4C3′	122.4(7)	C3C4C10′	106.2(5)
C10C4C10′	109.9(10)	C4C10C11	113.3(9)

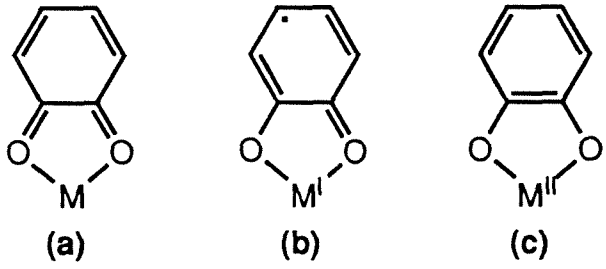

Figure 6.13. Transition metal complexes of (a) *o*-benzoquinone, (b) *o*-semiquinone, and (c) catecholate ligands. "The electronic structure of the metal-quinone chelate ring can be viewed in terms of three isoelectronic forms related by the distribution of formal charge over ligand and metal."[16]

The EPR data for the oxidized square planar cobalt complexes in glasses of anhydrous toluene at 4–7 K are presented in Figures 6.14–6.16. The spectra for the three different complexes are rhombic and clearly show that the unpaired electron is strongly interacting with the metal center in each case. At this point, we are avoiding calling the compounds Co(IV) species, since there are mechanisms for the noninnocent ligand to share its delocalized *paired* π-electrons with the metal or for a ligand radical to couple with S=1 Co(III). The struc-

tural changes observed are strong evidence for structures of the type shown in Figure 6.13 which lower the formal oxidation state at cobalt. Spin quantitation against aqueous $Cu(ClO_4)_2$ for Co(η^4-DEMAMPA-DCB) shows that there is 1 ± 0.1 unpaired electron per cobalt center. All three complexes exhibit g_1 at 2.558–2.571, g_2 at 2.168–2.187 (A_2: 15–19 G), and g_3 at 2.017–2.024. There is no change in the deep blue color of toluene glasses of Co(η^4-DEMAMPA-DCB), Co(η^4-DEMAMPA-B) or Co(η^4-DEMAMPA-DMOB) saturated with water. The EPR spectrum of a toluene glass containing Co(η^4-DEMAMPA-DMOB) and saturated with $H_2{}^{17}O$ (45% ^{17}O) is indistinguishable from that of a dry glass. These data indicate that trace water in the toluene does not coordinate to the vacant axial sites of the neutral species.

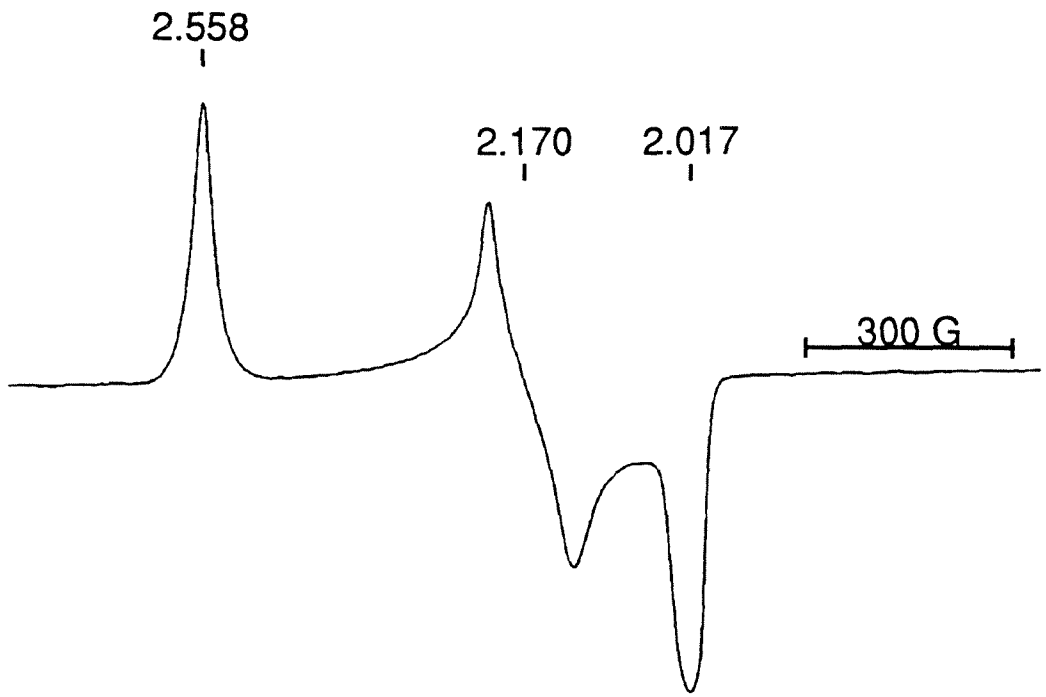

Figure 6.14. EPR spectrum of Co(η^4-DEMAMPA-DCB), at 5.9 K, 9.46 GHz, in toluene (six scan average, 1500 G scan range, 3100 G mid-range), hyperfine coupling to Co (A_2) $\approx$15 G.

When apical ligands are coordinated to these complexes, the EPR spectra obtained have nearly isotropic g values. When pyridine (Figures 6.17–6.19) or acetonitrile (Figures 6.20–6.22) is added to toluene solutions of the neutral species at room temperature, no color change from dark blue occurs. However, upon cooling, the color changes to dark purple, and upon warming back to room temperature, the dark blue color returns. EPR examination of these purple complexes at low temperature reveals spectra with collapsed anisotropy. These spectra are similar to the spectra previously obtained by the Halpern and Collins groups for six-coordinate Co(IV).[5,8b] However, the hyperfine coupling to Co for the pyridine adducts of Co(η^4-DEMAMPA-DCB) and

Figure 6.15. EPR spectrum of Co(η^4-DEMAMPA-B) at 6.3 K, 9.46 GHz, in toluene (1500 G scan range, 3100 G mid-range), hyperfine coupling to Co (A_2) $\approx$19 G.

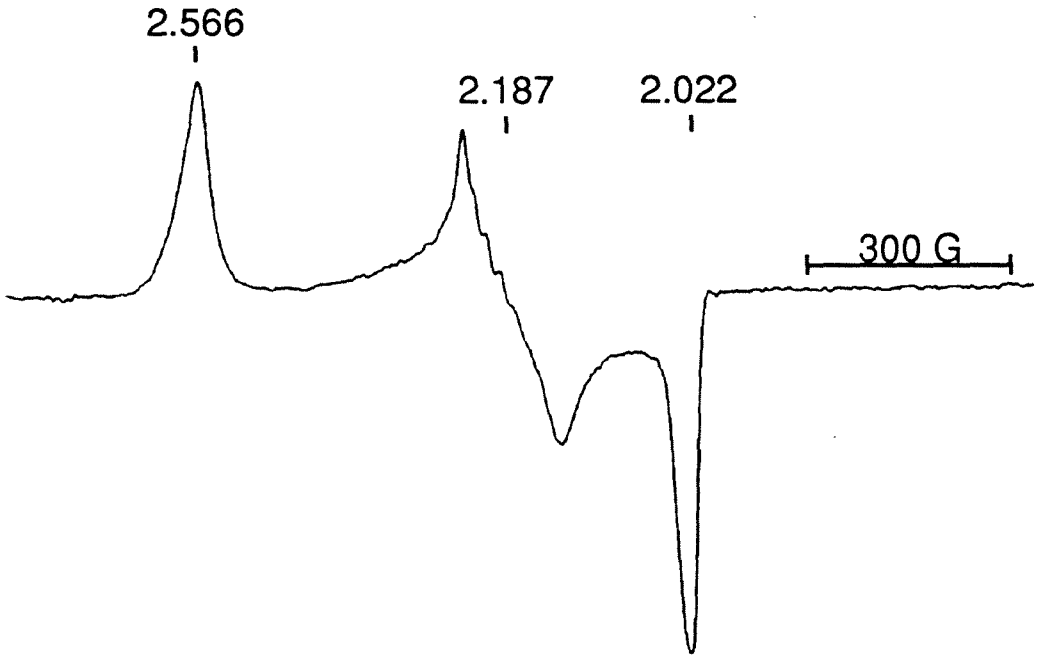

Figure 6.16. EPR spectrum of Co(η^4-DEMAMPA-DMOB) at 4.6 K, 9.46 GHz, in toluene (four scan average, 1500 G scan range, 3100 G mid-range), hyperfine coupling to Co (A_2) $\approx$19 G.

Co(η^4-DEMAMPA-B) (about 39 G for both) is substantially larger (16–35 G) than that found in the previous Halpern or Collins systems. The hyperfine coupling to cobalt for the pyridine adduct of Co(η^4-DEMAMPA-DMOB) is much smaller (about 18 G). Interestingly, the general appearance of the EPR spectra of the acetonitrile adducts is similar, but the hyperfine coupling to Co is smaller, especially for Co(η^4-DEMAMPA-DMOB). It is currently unkown if these pyridine and acetonitrile EPR spectra are of five- or six-coordinate species or a mixture of both. The Co(η^4-DEMAMPA-DCB) complex forms an adduct with [Ph_4P][Cl] at room temperature. Future investigations should be aimed at crystallizing this species and obtaining its EPR. One would predict that the structure of such an adduct will have bond distances in the ligand which will have shifted back towards the Co(III) values, since less electron donation will be required of the macrocycle. Given the EPR results from the literature and the EPR results presented here, the tetrakis(1-norbornyl)cobalt(IV) complex is probably the only uncontroversial Co(IV) complex besides the simple Ba_2CoO_4 and Cs_2CoF_6 salts. Obtaining EPR spectra of the tetrakis(1-norbornyl)cobalt(IV) complex is a worthy objective.

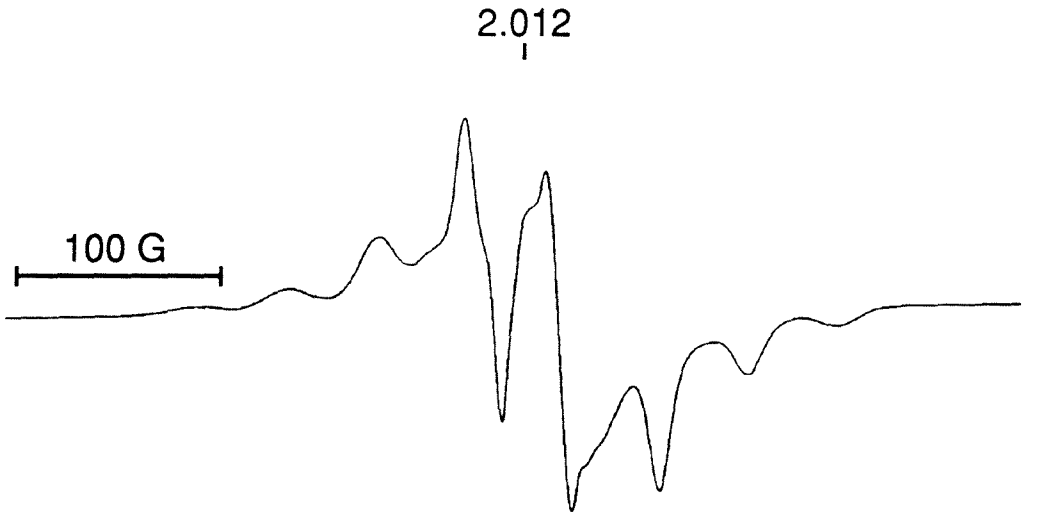

Figure 6.17. EPR spectrum of Co(η^4-DEMAMPA-DCB), at 7.4 K, 9.46 GHz, in toluene/pyridine (500 G scan range, 3350 G mid-range), hyperfine coupling to Co ≈39 G.

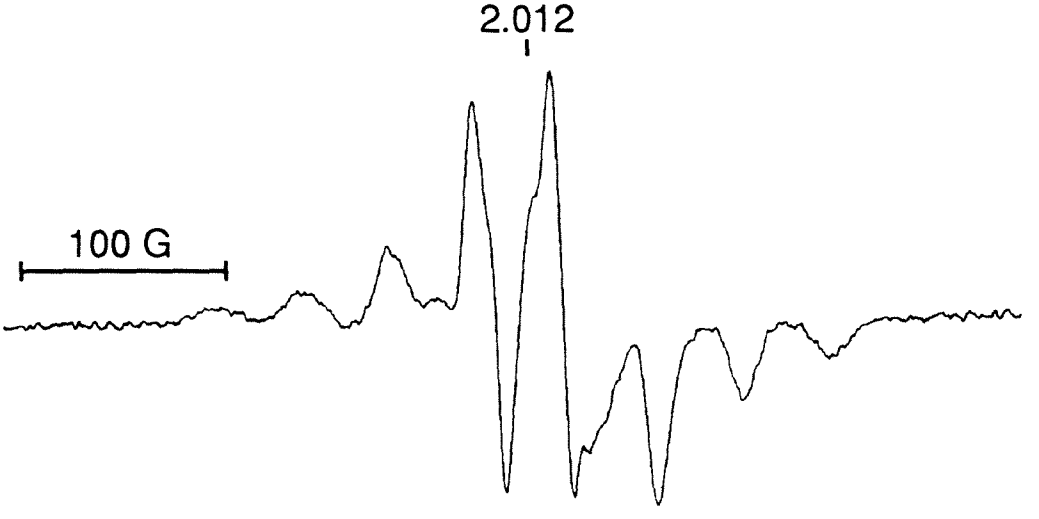

Figure 6.18. EPR spectrum of Co(η^4-DEMAMPA-B), at 6.3 K, 9.46 GHz, in toluene/pyridine (500 G scan range, 3350 G mid-range), hyperfine coupling to Co ≈38 G.

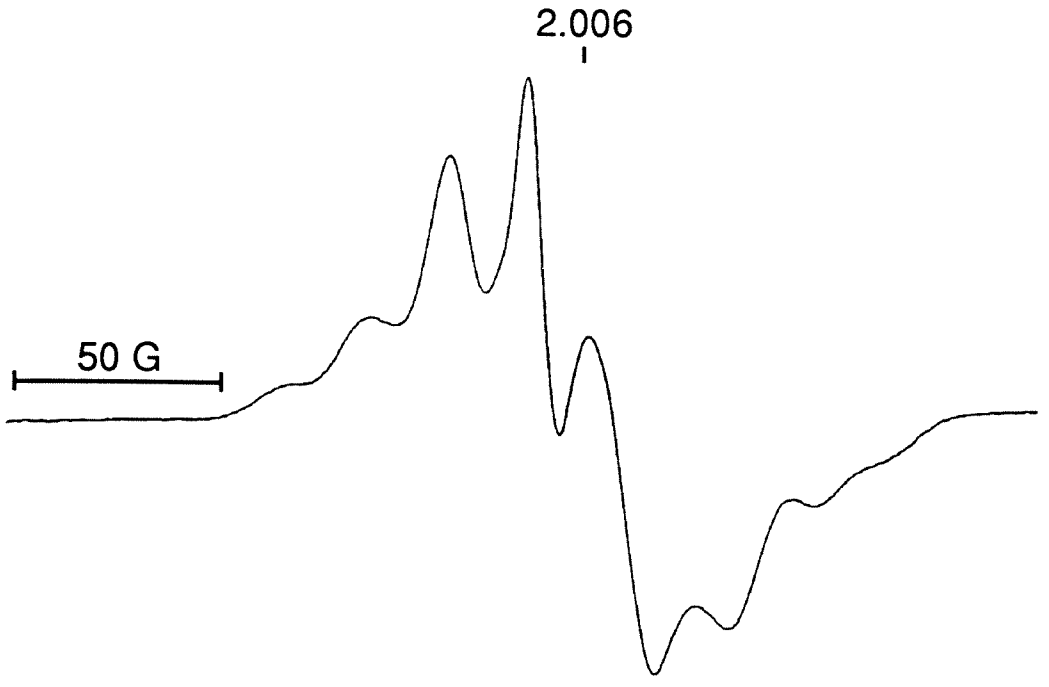

Figure 6.19. EPR spectrum of Co(η^4-DEMAMPA-DMOB), at 4.6 K, 9.46 GHz, in toluene/pyridine (250 G scan range, 3350 G mid-range), hyperfine coupling to Co (A_2) $\approx$18 G.

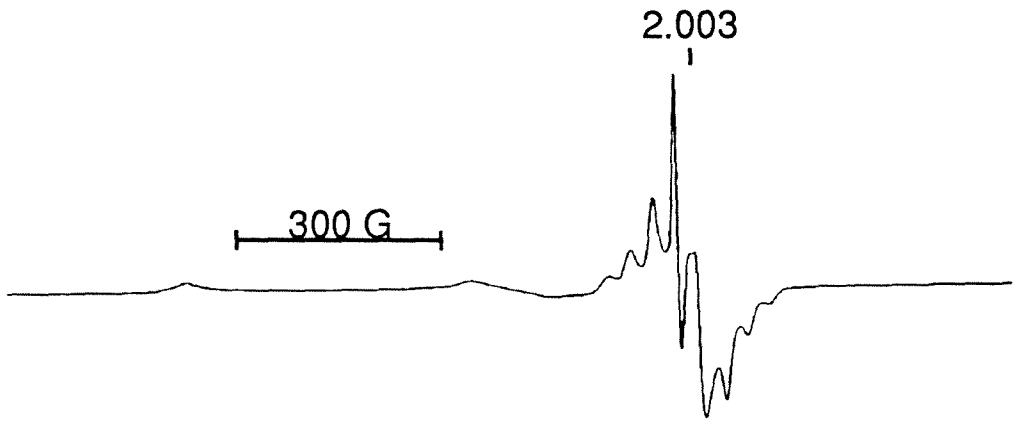

Figure 6.20. EPR spectrum of Co(η^4-DEMAMPA-DCB), at 6.8 K, 9.46 GHz, in toluene/MeCN (1500 G scan range, 3100 G mid-range), hyperfine coupling to Co ≈29 G. Residual axially unligated Co(η^4-DEMAMPA-DCB) is clearly present.

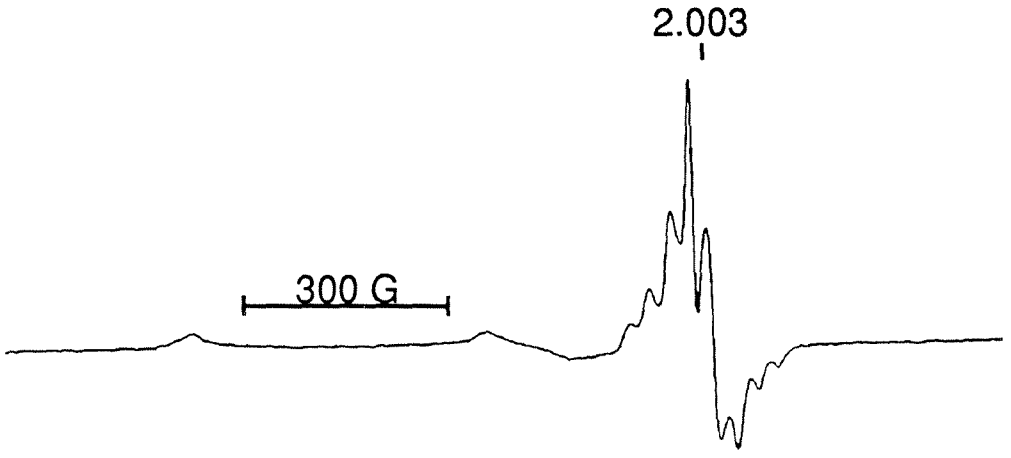

Figure 6.21. EPR spectrum of Co(η^4-DEMAMPA-B), at 6.3 K, 9.46 GHz, in toluene/MeCN (1500 G scan range, 3100 G mid-range), hyperfine coupling to Co ≈29 G. Residual axially unligated Co(η^4-DEMAMPA-B) is clearly present.

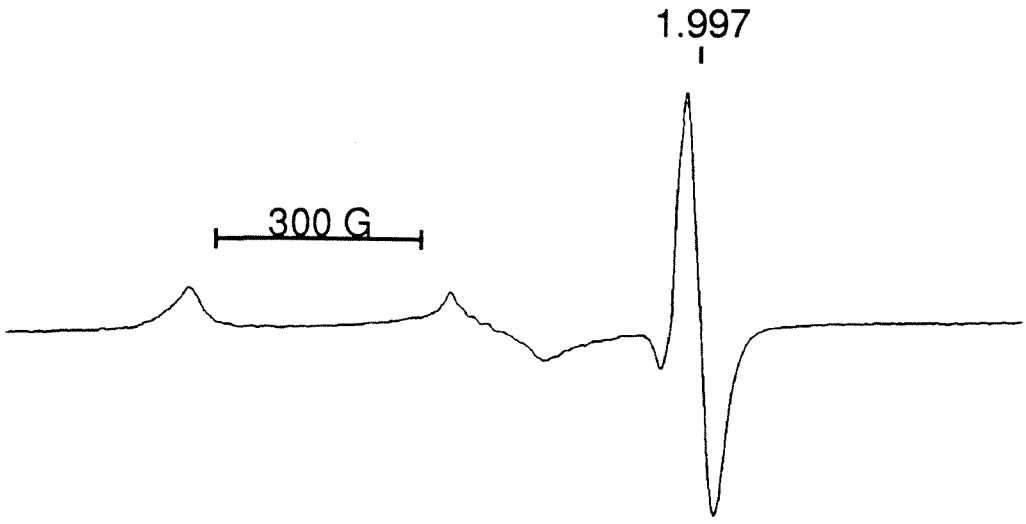

Figure 6.22. EPR spectrum of Co(η^4-DEMAMPA-DMOB), at 4.6 K, 9.46 GHz, in toluene/MeCN (1500 G scan range, 3100 G mid-range). Residual axially unligated Co(η^4-DEMAMPA-DMOB) is clearly present.

Experimental

Materials. All solvents and reagents were reagent grade (Aldrich) except for THF and benzene (Aldrich, Sureseal) and were used as received except as described for electrochemical measurements.

Physical Measurements. ^{1}H NMR were measured at 300 MHz on an IBM NR/300 FT-NMR Spectrometer. ^{1}H NMR data are reported in δ vs. $(CH_3)_4Si$ with the solvent as internal standard. EPR spectra were recorded on a Bruker ER300 Spectrometer. Infrared data were obtained on a Nicolet 5DXB FT-IR Spectrometer. UV-vis data were obtained on a Perkin-Elmer Lambda Array 3840 Spectrophotometer. Crystal structures were solved by Crystalytics Co. of Lincoln, Nebraska.

Electrochemical Data. Cyclic voltammetry was performed on a Princeton Applied Research Model 173/179 potentiostat/digital coulometer equipped with positive feedback IR compensation and a Model 175 universal programmer. Current voltage curves were recorded on a Houston Instruments Model 2000 X-Y recorder.

Sureseal anhydrous CH_2Cl_2 (Aldrich) and $[Et_4N][PF_6]$ (Fluka) were used as received. $[Bu_4N][ClO_4]$ (Fluka) was vacuum dried at 80 °C. In all cases experiments were performed under N_2 with a supporting electrolyte concentration of 0.1 M. Cyclic voltammetry was performed in CH_2Cl_2 solutions of $[Bu_4N][ClO_4]$ at a 3 mm Pt disk working electrode with a silver wire quasi-reference electrode and a Pt foil counter electrode. At the conclusion of each experiment, ferrocene (Fc) was added as an internal potential standard. All formal potentials were taken as the average of anodic and cathodic peak potentials and are reported vs. the Fc^+/Fc couple. Peak-to-peak separation of

the Fc^+/Fc couple was similar to that of the cobalt couples in all cases. Plots of peak current vs. the square root of scan rate over the range 10–500 mV s^{-1} were made and found to be linear for couples that are stated to be reversible. Bulk electrolysis was performed in CH_2Cl_2 solutions of $[Et_4N][PF_6]$ in a standard three-compartment cell at Pt gauze working and counter electrodes with a silver wire quasi-reference electrode.

Synthetic Note. The experimental work reported here has been published in substantially similar form in *Angew. Chem. Int. Ed. Engl.* and *J. Am. Chem. Soc.*[17]

$[Me_4N][Co(\eta^4$-MAC*)]. H_4MAC* was dissolved in dry, deoxygenated THF, and a stoichiometric amount of *tert*-butyllithium was added to the frozen solution under nitrogen. $CoCl_2$ was added under nitrogen as soon as the THF finished thawing (−108 °C). As the suspension warmed to room temperature, a yellow-green precipitate (presumably a Co(II) complex) collected on the flask walls. After 30 minutes at room temperature, air was admitted and a bright red solution rapidly developed with concomitant disappearance of the yellow-green precipitate. Crude $Li[Co(\eta^4$-MAC*)] was obtained in 95% yield. The $[Me_4N]^+$ salt was obtained by adding excess $[Me_4N][Cl]$ in water to an aqueous solution of the complex. The water was removed in vacuo, and an CH_3CN/CH_2Cl_2 solution of the residue was treated with pentane to precipitate the LiCl and excess $[Me_4N][Cl]$. Bright red rectangular parallelepipeds, characterized by X-ray analysis, were obtained by diffusion of pentane into a dichloromethane/chloroform solution of $[Me_4N][Co(\eta^4$-MAC*)].

$Li[Co^{III}(\eta^4$-DEMAMPA-DCB)]. A dry, deoxygenated THF (60 mL) solution of H_4DEMAMPA-DCB (0.504 g) was frozen with liquid N_2, and *tert*-

butyllithium (2.52 mL, 1.7 M in pentane) was added under N_2. After warming, anhydrous $CoCl_2$ (0.175 g, 1.3 equiv) was added just before the THF finished thawing (−108 °C). Upon further warming, a green precipitate (presumably a Co(II) complex) gradually developed. After stirring (20 °C, 30 min), air was admitted, rapidly converting the green-yellow suspension to a dark purple solution. The mixture was filtered through silica gel, and the purple compound was eluted with acetone. The solution was evaporated to dryness under reduced pressure, and the resultant solid was washed copiously with CH_2Cl_2 yielding the product as a purple powder (0.536 g, 93.5%). ^{1}H NMR (CD_3CN): 3.88 (br, 12H), -0.85 (br, 4H), -2.81 (br, 6H), -6.55 (br, 2H). ^{1}H NMR (THF-d_8): 3.98 (br, 12H), -0.70 (br, 4H), -2.65 (br, 6H), -6.82 (br, 2H). ^{1}H NMR (D_2O): -1.60 (br, 4H), -2.50 (br, 12H), -7.37 (br, 6H), -21.12 (br, 2H).

[Ph_4P][Co^{III}(η^4-DEMAMPA-DCB)] and [Bu_4N][Co^{III}(η^4-DEMAMPA-DCB)]. Aqueous [Ph_4P]Cl (excess) was added to aqueous Li[Co^{III}-(η^4-DEMAMPA-DCB)], and the precipitate was collected. X-ray quality crystals were grown by vapor diffusion of pentane into a 1,2-dichloroethane solution. Anal. Calcd for [Ph_4P][Co^{III}(η^4-DEMAMPA-DCB)]: C, 62.44; H, 5.12; N, 6.47. Found: C, 62.38; H, 4.99; N, 6.40. UV-vis (CH_2Cl_2): λ_{max} [nm] (ϵ) = 430 (3350), 516 (9150), 612 (2970). ^{1}H NMR of [Ph_4P][Co^{III}(η^4-DEMAMPA-DCB)] ($CDCl_3$): 7.32 (br, 8H, $[Ph_4P]^+$), 6.95 (br, 8H, $[Ph_4P]^+$), 6.76 (br, 4H, $[Ph_4P]^+$), 4.15 (br, 12H), -0.95 (br, 4H), -2.90 (br, 6H), -5.72 (br, 2H). Crystalline [Bu_4N][Co^{III}(η^4-DEMAMPA-DCB)] was prepared analogously using [Bu_4N]Cl. IR [Bu_4N][Co^{III}(η^4-DEMAMPA-DCB)] (Nujol): $\bar{\nu}$[cm^{-1}] = 1648, 1593, 1571.

H[Co^{III}(η^4-DEMAMPA-DCB)]. Aqueous HBF_4 was added to aqueous

$Li[Co^{III}(\eta^4\text{-DEMAMPA-DCB})]$ (0.075 g), and the precipitate (0.049 g) was collected and crystallized by vapor diffusion of pentane into an acetone solution. IR (Nujol): $\bar{\nu}[cm^{-1}] = 1671, 1618, 1611$. UV-vis (acetone): λ_{max} [nm](ϵ) = 342 (3400), 430 (3500), 516 (8400). MS (70 eV): m/z 526 (M^+, 8%). Melting point = 312 °C. ^{1}H NMR (acetone-d_6): only one broad peak located (-9.5 ppm). The complex is also produced by reduction of $Co(\eta^4$-DEMAMPA-DCB) with H_2O.

$Co(\eta^4$-DEMAMPA-DCB). In an inert atmosphere chamber, $Li[Co^{III}(\eta^4$-DEMAMPA-DCB)] (0.137 g) and excess $(NH_4)_2Ce(NO_3)_6$ were ground together on a sintered glass crucible in dry benzene. The benzene developed an intense blue color as $Co(\eta^4$-DEMAMPA-DCB) formed. The blue solution was filtered away from the solids, fresh benzene was added to the crucible, and grinding was repeated. This grinding and collection procedure was repeated until the blue color in the benzene extracts had diminished significantly. Removal of the benzene under reduced pressure yielded the metallic red-purple powdery product (0.069 g, 51%). X-ray quality crystals were grown by vapor diffusion of pentane into a benzene solution. UV-vis (benzene): λ_{max} [nm] (ϵ) = 344 (4900), 386 (4500), 524 (7400), 626 (26000), 670 (shoulder 9800). IR (Nujol): $\bar{\nu}[cm^{-1}] = 1716, 1616, 1599$. FAB MS of $Co(\eta^4$-DEMAMPA-DCB) (sulpholane matrix, *anions* detected): m/z 525 (M^-, 100%).

$Li[Co^{III}(\eta^4$-DEMAMPA-B)]. A dry, deoxygenated THF (38 mL) solution of H_4DEMAMPA-B (0.210 g) was frozen with liquid N_2, and *tert*-butyllithium (1.1 mL, 1.7 M in pentane) was added under N_2. After warming, anhydrous $CoCl_2$ (0.085 g) was added just before the THF finished thawing (−108 °C). Upon further warming, a green precipitate (presumably a Co(II)

complex) gradually developed. After stirring (20 °C, 30 min), air was admitted, rapidly converting the green-yellow suspension to a dark purple solution. The mixture was filtered through silica gel, and the purple compound was eluted with acetone. The solution was evaporated to dryness under reduced pressure, and the resultant solid was washed copiously with CH_2Cl_2 yielding the product as a purple powder (0.206 g, 85.0%).

[Bu$_4$N][Co^{III}(η^4-DEMAMPA-B)]. Excess aqueous [Bu$_4$N]Cl was added to aqueous Li[Co^{III}(η^4-DEMAMPA-B)] (0.114 g), the precipitate was collected and dissolved in 50:50 EtOH/H_2O, and crystals of [Bu$_4$N][Co^{III}(η^4-DEMAMPA-B)] (0.115 g) grew upon evaporation of the EtOH. Anal. Calcd for [Bu$_4$N][Co^{III}(η^4-DEMAMPA-B)]: C, 63.50; H, 8.93; N, 10.01. Found: C, 63.39; H, 8.72; N, 9.97. UV-vis (CH_2Cl_2): λ_{max} [nm] (ϵ) = 426 (2700), 516 (9000), 630 (2400). ^{1}H NMR ($CDCl_3$): 3.69 (br, [Bu$_4$N]$^+$, 8H), 2.69 (br, [Bu$_4$N]$^+$, 8H), 1.68 (br, [Bu$_4$N]$^+$, 8H), 0.77 (br, [Bu$_4$N]$^+$, 12H), -0.69 (br 12H), -0.94 (br, 6H), -2.72 (br, 4H), -4.35 (br, 2H), -21.64 (br, 2H). IR (Nujol): $\bar{\nu}$[cm^{-1}] = 1648, 1635, 1590, 1572.

Co(η^4-DEMAMPA-B). Li[Co^{III}(η^4-DEMAMPA-B)] (33 mg) and excess $(NH_4)_2Ce(NO_3)_6$ (300 mg) were suspended in dry CH_2Cl_2 (5 mL) and stirred (1 h). The resulting dark blue solution was filtered from the suspension and the CH_2Cl_2 was removed under vacuum. The solids were re-suspended in CH_2Cl_2 (5 mL) and stirred again (1 h). The resulting dark blue solution was filtered from the suspension and combined with the previously obtained product. The CH_2Cl_2 was again removed under vacuum, benzene was added, and the benzene was removed under vacuum to give a metallic purple solid (16 mg, 49%). UV-vis (benzene): λ_{max} [nm] (ϵ) = 525 (6000), 614 (15000),

630 (3000). Anal. Calcd for $Co^{III}(\eta^4$-DEMAMPA-B)·C_6H_6·$3H_2O$: C, 55.01; H, 6.50; N, 9.50. Found: C, 55.30; H, 6.64; N, 9.26. IR (CH_2Cl_2): $\bar{\nu}[cm^{-1}]$ = 1720, 1640, 1593.

Li[$Co^{III}(\eta^4$-DEMAMPA-DMOB)]. To a frozen solution of H_4DEMAMPA-DMOB (0.108 g) in dry, deoxygenated THF (25 mL) under N_2 was added *tert*-butyllithium (0.58 mL, 1.7 M in pentane) followed immediately upon thawing by anhydrous $CoCl_2$ (0.047 g, 1.3 equiv). The mixture was allowed to warm to room temperature and was stirred (1 h) under N_2 to give a green suspension (presumably a Co(II) complex). Air was admitted, and a dark red-purple solution developed rapidly. The solution was filtered, evaporated to dryness, washed twice with CH_2Cl_2, then extracted with MeOH and filtered through a pad of diatomaceous earth. Evaporation yielded the product as a dark purple-red solid. (0.061 g). ^{1}H NMR (CD_3OD): 12.85 (s, 6H), 2.48 (br, 12H), 1.32 (br, 2H), 0.05 (br, 4H), -2.11 (br, 6H).

[Et_4N][$Co^{III}(\eta^4$-DEMAMPA-DMOB)]. To a solution of Li[$Co^{III}(\eta^4$-DEMAMPA-DMOB)] (0.040 g) in MeOH was added [Et_4N]F·H_2O (0.020 g), and the mixture was stirred (10 min). The solvent was removed under reduced pressure, and the resulting solid was extracted with CH_2Cl_2 and filtered through a diatomaceous earth pad. Diffusion of Et_2O into a CH_2Cl_2 solution yielded the pure compound as dark red-purple crystals (0.042 g, 85%). Anal. Calcd for [Et_4N][$Co^{III}(\eta^4$-DEMAMPA-DMOB)]·$0.5H_2O$: C, 56.70; H, 7.83; N, 10.66. Found: C, 56.95; H, 7.79; N, 10.65. ^{1}H NMR (CD_3OD): 12.80 (br, 6H); 3.12 (q, 8H, CH_2 of $[Et_4N]^+$), 2.41 (br, 12H), 1.33 (br, 2H), 1.05 (t, 12 H, Me of $[Et_4N]^+$), -0.02 (br, 4H), -2.16 (br, 6H). IR (Nujol): $\bar{\nu}[cm^{-1}]$ = 1648, 1621, 1588, 1570.

Co(η^4-DEMAMPA-DMOB). Li[Co^{III}(η^4-DEMAMPA-DMOB)] (0.058 g) was stirred with excess $(NH_4)_2Ce(NO_3)_6$ suspended in dry CH_2Cl_2. A deep blue color developed in the mixture containing the purple suspended Li[Co^{III}(η^4-DEMAMPA-DMOB)]. Stirring was continued until all the purple solid had reacted (2.5 h). The intense blue solution was filtered and evaporated to dryness. The residue was extracted with benzene and filtered. Large metallic purple-red single crystals of the product were obtained from benzene/pentane solution (0.048 g, 84%). Anal. Calcd for Co(η^4-DEMAMPA-DMOB)·$0.5C_6H_6$: C, 56.12; H, 5.89; N, 10.07. Found: C, 56.10; H, 5.96; N, 10.09. IR (Nujol): $\bar{\nu}[cm^{-1}]$ = 1701, 1690, 1627, 1616, 1593. UV-vis (benzene): λ_{max} [nm](ϵ) = 654 (40,000). The concentration of a saturated solution in benzene was 24 mM.

X-ray Data Collection and Structure Refinement of [$(CH_3)_4N$]-[Co(η^4-MAC*)]·H_2O. Crystal Data: Single crystals of [$(CH_3)_4N$][Co(η^4-**MAC***)]·H_2O at 20± 1 °C are monclinic, space group $P2_1/C$-C_{2h}^5 (No. 14) with a = 17.221(3) Å, b = 19.075(6) Å, c = 21.797(6) Å, β = 109.74(2)°, V = 6739(3) $Å^3$ and Z = 8 formula units (d_{calcd} = 1.137 g cm^{-3}; μ_a(CuK$\bar{\alpha}$) = 5.2 mm^{-1}). A total of 9248 independent absorption-corrected reflections having 2θ(CuK$\bar{\alpha}$) < 115.0° (the equivalent of 0.6 limiting CuK$\bar{\alpha}$ spheres) were collected on a computer-controlled Nicolet autodiffractometer using θ-2θ scans and Ni-filtered CuK$\bar{\alpha}$ radiation. The structure was solved using Direct Methods techniques with the Nicolet SHELXTL software package as modified at Crystalytics Company. The resulting structural parameters have been refined to convergence (R_1(unweighted, based on F) = 0.054 for 4033 independent reflections having $2\theta_{CuK\bar{\alpha}}$ < 115.0° and I > 3σ(I)) using counter-weighted cascade block-diagonal least-squares techniques and a structural model which

incorporated anisotropic thermal parameters for 88 nonhydrogen atoms and isotropic thermal parameters for all hydrogen atoms. The 28 methyl groups were included in the refinement as idealized sp^3-rigid rotors. The remaining hydrogen atoms were fixed at idealized sp^3-hybridized positions with a C–H bond length of 0.96Å. The value listed for calculated density is exclusive of disordered halocarbon solvent in the lattice. Complete details deposited with the Cambridge Crystallographic Data Centre.

X-ray Data Collection and Structure Refinement of [Ph_4P]-[Co^{III}(η^4-DEMAMPA-DCB)] and Co(η^4-DEMAMPA-DCB). Crystal Data: Single crystals of [Ph_4P][Co^{III}(η^4-DEMAMPA-DCB)] are triclinic (space group $P\bar{1}$-C_i^1 (No. 2) at 20± 1 °C), with a = 11.429(3) Å, b = 13.245(3) Å, c = 14.227(3) Å, α = 97.11(2)°, β = 92.74(2)°, γ = 96.21(2)°, V = 2120.5(9) Å^3, and Z = 2. A total of 7757 independent reflections having $2\theta(MoK\bar{\alpha}) <$ 50.7° (the equivalent of 0.80 limiting CuK$\bar{\alpha}$ spheres) were collected on a computer-controlled Nicolet autodiffractometer using full (0.90°-wide) ω scans and graphite-monochromated MoK$\bar{\alpha}$ radiation. Single crystals of Co(η^4-DEMAMPA-DCB) are tetragonal (space group $P4_12_12$-D_4^4 (No. 92) at 20±1 °C), with a = 10.515(2) Å, c = 21.681(3) Å, V = 2397.3(9) Å^3, and Z = 4. A total of 1665 independent reflections having $2\theta(MoK\bar{\alpha}) <$ 55° (the equivalent of 1.0 limiting CuK$\bar{\alpha}$ spheres) were collected on a computer-controlled Nicolet autodiffractometer using full (1.5°-wide) ω scans and graphite-monochromated MoK$\bar{\alpha}$ radiation. The structures were solved using Direct Methods techniques with the Nicolet SHELXTL software package as modified at Crystalytics Company. The resulting structural parameters have been refined to convergence R_1(unweighted, based on F) = 0.037 for 5243 independent re-

flections having $2\theta_{MoK\bar{\alpha}} < 50.7°$ and $I > 3\sigma(I)$ for $[Ph_4P][Co^{III}(\eta^4\text{-DEMAMPA-DCB})]$ and R_1(unweighted, based on F) = 0.041 for 1163 independent reflections having $2\theta_{MoK\bar{\alpha}} < 55.0°$ and $I > 3\sigma(I)$ for $Co(\eta^4\text{-DEMAMPA-DCB})$ using counter-weighted cascade block-diagonal least-squares techniques and a structural model which incorporated anisotropic thermal parameters for non-hydrogen atoms and isotropic thermal parameters for all hydrogen atoms. The methyl groups were included in the refinement as idealized sp^3-rigid rotors and gave final values for the C-C-H angles which ranged from 105° to 112° for $[Ph_4P][Co^{III}(\eta^4\text{-DEMAMPA-DCB})]$ and from 102° to 120° for $Co(\eta^4\text{-DEMAMPA-DCB})$. The remaining hydrogen atoms were fixed at idealized sp^2- or sp^3-hybridized positions with a C–H bond length of 0.96 Å. The oxygen atom of a partial water molecule of crystallization was refined to an occupancy factor of 0.30(1) for $[Ph_4P][Co^{III}(\eta^4\text{-DEMAMPA-DCB})]$. For $Co(\eta^4\text{-DEMAMPA-DCB})$, the correctness of the enantiomeric description was verified by a series of refinement cycles in which the multiplier of $\Delta f''$ was varied; this multiplier refined to a value of 1.0(1).

References

1. Boca, R. *Coord. Chem. Rev.* **1983**, *50*, 1. Valentine, J. S. *Chem. Rev.* **1973**, *73*, 235. Chen, D.; Martell, A. E. *Inorg. Chem.* **1987**, *26*, 1026.

2. Collman, J. P.; Hegedus, L. S.; Norton, J. R.; Finke, R. G. *Principles and Applications of Organotransition Metal Chemistry*, 2nd ed.; University Science Books: Mill Valley, CA, 1987.

3. (a) Scholder, R. V.; *Bull. Soc. Chim. Fr.* **1965**, 1112–1114. (b) Hoppe, R.; *Rec. Trav. Chim. Pays-Bas.* **1956**, *75*, 569–575.

4. For a review, see: Vol'pin, M. E.; Levitin, I. Ya.; Sigan, A. L.; Nikitaev, A. T. *J. Organomet. Chem.* **1985**, *279*, 263–280.

5. (a) Halpern, J.; Chan, M. S.; Hanson, J.; Roche, J. S.; Topich, J. A. *J. Am. Chem. Soc.* **1975**, *97*, 1606–1608. (b) Tobich, J.; Halpern, J. *Inorg. Chem.* **1979**, *18*, 1339–1343.

6. Nikitaeva, G. A.; Nikitaev, A. T.; Zamaraev, K. I.; Sigan, A. L.; Levitin, I. Ya.; Vol'pin, M. E. *Zh. Strukt. Khim.* **1978**, *19*, 282–287.

7. (a) Bower, B. K.; Tennent, H. G. *J. Am. Chem. Soc.* **1972**, *94*, 2512. (b) Byrne, E. K.; Richeson, D. S.; Theopold, K. H. *J. Chem. Soc., Chem. Commun.* **1986**, 182. (c) Byrne, E. K.; Richeson, D. S.; Theopold, K. H. *J. Chem. Soc., Chem. Commun.* **1986**, 1491–1492. (d) Byrne, E. K.; Theopold, K. H. *J. Am. Chem. Soc.* **1987**, *109*, 1282–1283.

8. (a) Cotton, F. A.; Wilkinson, G. *Advanced Inorganic Chemistry*, 5th ed.; Wiley-Interscience: New York, 1988. (b) Anson, F. C.; Collins, T. J.; Coots, R. J.; Gipson, S. L.; Richmond, T. G. *J. Am. Chem. Soc.* **1984**, *106*, 5037.

9. For other examples of the rare Co(III) square planar geometry see: (a)

Eisenberg, R.; Dori, Z.; Gray, H. B.; Ibers, J. A. *Inorg. Chem.* **1968**, *7*, 741. (b) Baker-Hawkes, M. J.; Billig, E.; Gray, H. B. *J. Am. Chem. Soc.* **1966**, *88*, 4870. (c) Dorfman, J. R.; Rao, Ch. P.; Holm, R. H. *Inorg. Chem.* **1985**, *24*, 453. (d) Fikar, R.; Koch, S. A.; Millar, M. M. *Inorg. Chem.* **1985**, *24*, 3311. (e) Rao, Ch. P.; Dorfman, J. R.; Holm, R. H. *Inorg. Chem.* **1986**, *25*, 428. (f) van der Put, P. J.; Schilperoord, A. A. *Inorg. Chem.* **1974**, *13*, 2476. (g) Bour, J. J.; Beurskins, P. T.; Steggerda, J. J. *J. Chem. Soc., Chem. Commun.* **1972**, 221. (h) Birker, P. J. M. W. L.; Bour, J. J.; Steggerda *Inorg. Chem.* **1973**, *12*, 1254. (i) Birker, P. J. M. W. L.; Beurskins, P. T. *J. R. Neth. Chem. Soc.* **1974**, *93* 218. (j) Brewer, J. C.; Collins, T. J.; Smith, M. R.; Santarsiero, B. D. *J. Am. Chem. Soc.* **1988**, *110*, 423–428. (k) Collins, T. J.; Richmond, T. G.; Santarsiero, B. D.; Treco, B. G. R. T. *J. Am. Chem. Soc.* **1986**, *108*, 2088–2090. References a–f concern aliphatic and aromatic thiolate ligands. References g–i concern innocent biuret ligands.

10. (a) Collins, T. J.; Richmond, T. G.; Santarsiero, B. D.; Treco, B. G. R. T. *J. Am. Chem. Soc.* **1986**, *108*, 2088–2090. (b) Brewer, J. C.; Collins, T. J.; Smith, M. R.; Santarsiero, B. D. *J. Am. Chem. Soc.* **1988**, *110*, 423–428. (c) Collins, T. J.; Ozaki, S.; Richmond, T. G. *J. Chem. Soc., Chem. Commun.* **1987**, 803–804. (d) Ozaki, S.; Mimura, H.; Yasuhara, N.; Masui, M.; Yamagata, Y.; Tomita, K.; Collins, T. J. *J. Chem. Soc., Perkin Trans. 2* **1990**, 353–360.

11. Nam, W.; Valentine, J. S. *J. Am. Chem. Soc.* **1990**, *112*, 4977-4979.

12. (a) Koola, J. D.; Kochi, J. K. *J. Org. Chem.* **1987**, *52*, 4545–4553. (b) Koola, J. D.; Kochi, J. K. *Inorg. Chim. Acta* **1987**, *133*, 119–127.

13. Collins, T. J.; Workman, J. M. *Angew. Chem. Int. Ed. Engl.* **1989**,

28, 912–914.

14. ^{1}H NMR (CD_3OH) of a mixture of $[Co^{III}(CN)(\eta^4$-DEMAMPA-DCB)$]^{2-}$ and $[Co^{III}(CN)_2(\eta^4$-DEMAMPA-DCB$)]^{3-}$: 8.73 (s, mono-CN^-), 8.49 (s, bis-CN^-), 2.00 (q, 7.2 Hz), 1.90 (2×q-overlapping), 1.82 and 1.81 (overlapping singlets), 1.20 (t, 7.2 Hz, bis-CN^-), 0.93 (t, 7.2 Hz, mono-CN^-), 0.62 (t, 7.2 Hz, mono-CN^-).

15. ^{1}H NMR (CD_3CN) of $[Co(\eta^4$-MAC*$)]^-$ and *p*-toluenesulfonic acid (only $[Co(\eta^4$-MAC*$)]^-$ resonances listed): 2.14 (q, 4H, 8.2 Hz), 1.76 (s, 12H), 1.68 (s, 12H), 0.54 (t, 6H, 8.2 Hz).

16. Pierpont, C. G.; Buchanan, R. M. *Coord. Chem. Rev.* **1981**, *38*, 45–87.

17. (a) Collins, T. J.; Uffelman, E. S. *Angew. Chem. Int. Ed. Engl.* **1989**, *28*, 1509–1511. (b) Collins, T. J.; Powell, R. D.; Slebodnick, C.; Uffelman, E. S. *J. Am. Chem. Soc.* in press.

Chapter 7

A Square Planar Nickel(III) Complex of an Innocent Macrocyclic Tetraamido-*N* Ligand

High valent nickel chemistry[1] has attracted increasing attention due to the possible biological significance of the +III oxidation state in hydrogenase enzymes.[2] High valent nickel species may also be intermediates in newly discovered catalytic oxidations.[3] High valent nickel intermediates have also been implicated in the sequence-specific oxidative cleavage of DNA by a designed metalloprotein.[4] Five- and six-coordinate nickel species in which the +III formal oxidation state is unambiguous have been structurally characterized.[5] This chapter discusses the synthesis, first structural characterization, and spectroscopic properties of a four-coordinate nickel(III) complex of the innocent ligand system, $[Et_4N][Ni(\eta^4\text{-MAC*})]$. Low potential Ni(III) is found in nickel hydrogenases,[6] and it is interesting to note that the innocent abiological ligand, $(\eta^4\text{-MAC*})^{4-}$, can also produce highly stabilized nickel(III); the Ni(III)/Ni(II) couple of $[Ni(\eta^4\text{-MAC*})]^-$ occurs at -0.58 V vs. Fc^+/Fc (CH_2Cl_2, 0.1 M $[Bu_4N][ClO_4]$ supporting electrolyte, 0.13 V vs. NHE).[6c] EPR spectroscopy has been of special significance to the study of enzymatic systems containing nickel(III),[2] and this chapter will present a number of EPR results with $[Ni(\eta^4\text{-MAC*})]^-$. Structural and spectroscopic comparisons will be made between $[Ni(\eta^4\text{-MAC*})]^-$ and $[Ni(\eta^4\text{-DEMAMPA-DCB})]^-$.

Background

The important Ni(III) peptide studies of Margerum's group have been recently reviewed[2c] and will be discussed more explicitly in the "Results and Discussion" section.

The study of Ni(III) chemistry originated with Jensen's report of $(Et_3P)_2NiBr_3$ in 1936.[7] It was not until 1969, however, that a structure of such a complex was obtained. The Meek and Ibers groups characterized the trigonal

bipyramidal complex $(PhMe_2P)_2NiBr_3$, which was prepared by bromine oxidation of $(PhMe_2P)_2NiBr_2$.[8] The average axial Ni–P distance was 2.268(2) Å and the average Ni–Br distance was 2.353(2) Å. The complex did not give an observable EPR spectrum even at 77 K in toluene, but the magnetic moment of the complex was determined to be 2.09 B. M.

Burrows' group has published a series of studies of the use of nickel complexes to catalyze the oxygen atom transfer reaction of OCl^- with olefins under phase transfer conditions.[3] The studies have focussed primarily on systems such as Ni^{II}(salen) and Ni^{II}(dibenzyldioxocyclam). In recently, published results, Ni^{II}(salen) buffered at pH=9.3 with slow addition of OCl^- to solutions of *trans*-β-methylstyrene gave 3840 turnovers in six minutes. Loss of *E,Z*-stereochemistry, chlorination of alkene, and alkene bond cleavage products were features of this reaction. Although the Burrows group reactivity results are spectacular, the mechanistic information is sparse—Ni^{III} apical chloride, hypochlorite, and oxo-radical species have all been postulated without supporting evidence. Their studies are ongoing, but have already established that very high turnover rates can be achieved for alkene epoxidation with inexpensive oxidants and catalysts. In a similar study, Kochi studied the epoxidation of olefins with nickel cyclams and proposed the intermediacy of Ni(IV) oxos with Ni–O double bonds.[9] However, such a proposal completely ignores the fact that Ni(IV) would be d^6 and be completely incapable of forming multiple bonds with oxygen in approximate C_{4v} symmetry.

Dervan's group has synthesized the DNA-binding domain of Hin recombinase (residues 139–190) and attached the tripeptide copper binding domain of serum albumin (GGH) to the N-terminus. The resultant 55 residue protein

was metallated at the copper binding site with $Ni(OAc)_2$. The resultant metalloprotein was capable of binding DNA at four 13-base pair sites and, with the addition of one equivalent of monoperoxyphthalic acid, cleaved the DNA at the four positions with a pattern characteristic of a non-diffusable oxidant. The rapidity of the reaction, coupled with its precision and the known terminal DNA products, were cited in support of a high valent nickel species as the active reagent.[4]

De Castro's group has recently studied the adduct formation of noninnocent Ni^{III}(3,5-dichlorosalen) complexes with pyridines.[10] In the absence of pyridine, the Ni(III/II) couple occurs at 0.435 V vs. Fc^+/Fc, and the authors surmised that one or two solvent molecules occupied the axial coordination sites. At room temperature the EPR exhibited an isotropic g of 2.175 (in frozen glasses the EPR spectra were highly anisotropic with $g_x = 2.238$, $g_y = 2.204$, and $g_z = 2.023$). The complexes decay to EPR silent species at room temperature in 10 minutes in DMF. When pyridine was added, the g values moved ($g_x = 2.180$, $g_y = 2.160$, and $g_z = 2.025$ and $a_x = 16.2$ G, $a_y = 17.8$ G, and $a_z = 22.5$ G), supporting a six coordinate tetragonally distorted complex with the lone electron in the d_{z^2} orbital. The authors discussed their EPR simulation model in some detail.

The insoluble blue-black bis(biuretato)nickel(III) anion can be prepared as the potassium salt by oxidizing $K_2Ni(biuret)_2$ with $K_2S_2O_8$ in 5 N KOH solutions at room temperature.[11] Studies of the potassium salt of this Ni(III) complex were hampered by its total insolubility, but the Ni(III/II) couple was measured in aqueous base using the Ni(II) salt and determined to be 0.50 V vs. SCE. It was found that $K[Ni(biuret)_2]$ had a magnetic moment of 2.5 B. M,

and it was speculated that the complex was square planar. Attempts to increase the solubility with alkyl-substituted biurets failed in the synthesis.

Because many "nickel(III)" complexes of noninnocent ligands have interesting solid state electronic and magnetic properties, a large structural literature exists.[12] These compounds originated with the Ni dithiolene/dithiolate studies of Holm's group in the early 1960s, and quickly became the subject of vigorous debate.[13] Both the formal oxidation state assignment (Ni^{III} vs. Ni^{II} ligand radical cation) and the ground state electronic structure ($^2B_{3g}$ [...$b_{3g}{}^1$ $a_g{}^0$] vs. ^2A_g[...$a_g{}^1$ $b_{1g}{}^0$]) of these complexes were disputed. McCleverty published a thorough presentation of both sides of these chemical arguments in a comprehensive review of metal 1,2-dithiolene and related complexes.[13a] Briefly stated, the low value of hyperfine interaction with ^{61}Ni enriched complexes (as low, in some examples, as 4 G) argued against the Ni(III) formalism, while the threefold anisotropy of the g tensor in these systems argued against the ^2A_g groundstate. The later papers pertaining to this work indicated that the molecular orbital in which the odd electron was located had at least 50% ligand character.[13g,h] McCleverty's assessment of these systems is still pertinent: "The use of formal oxidation states in such systems must be misleading."

Drago's group published a paper on octahedral nickel(III) complexes of pyridine oxime ligands (Figure 7.1).[14] Although the black compounds were unstable in solution, they were stable as solids. The paper also summarized data that indicated that the "nickel(III)" complexes of dithiolates, diarsines, and triarsines are really nickel(II) ligand cation radical complexes. Drago's octahedral nickel(III) complexes gave rhombic EPR spectra at 77 K (g_1 = 2.08, g_2 = 2.10, and g_3 = 2.14).

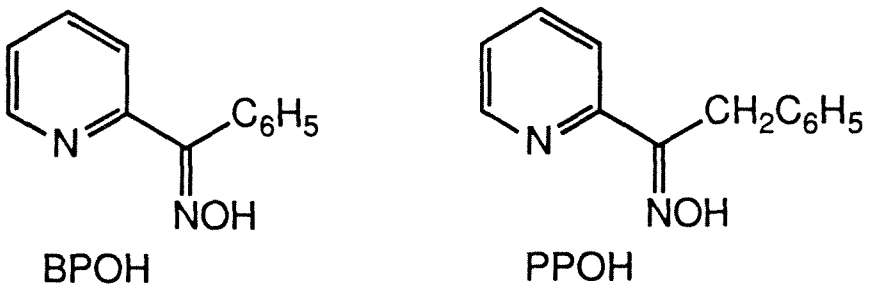

Figure 7.1. Drago's pyridine oxime ligands.

The Murmann group published a paper with a square planar crystallographically characterized species which the authors viewed as a nickel(II) complex of a radical type ligand stabilized through metal-ligand π-bonding (Figure 7.2).[15] It was noted that if the diamagnetic complex (which slowly decomposed in solution) was not viewed in this manner, it would be a four-coordinate low spin Ni(IV) complex (which can be considered unlikely). Beyond the question of oxidation state assignment, the complex contains a very short Ni–N bond distance (1.804(2) Å), although the authors were incorrect in thinking it the shortest Ni–N bond reported until then. Shorter Ni–N bond distances were found in an octaaza macrocyclic complex of Ni(II) (1.786(4) and 1.795(3) Å) prepared by Goedken's group.[16]

Considerable work has been done with partially oxidized nickel bisglyoximates.[17] A definitive paper on these complexes featuring the diphenylglyoximate ligand conclusively demonstrated that the oxidation of Ni^{II}(bisdiphenylglyoximate) with iodine produces crystals consisting of stacked nickel complexes and stacked iodine atoms with both being in fractional oxidation states[17c]. The authors studied the system with low temperature X-ray crystallography, Raman spectroscopy, X-ray photoelectron spectroscopy, solid

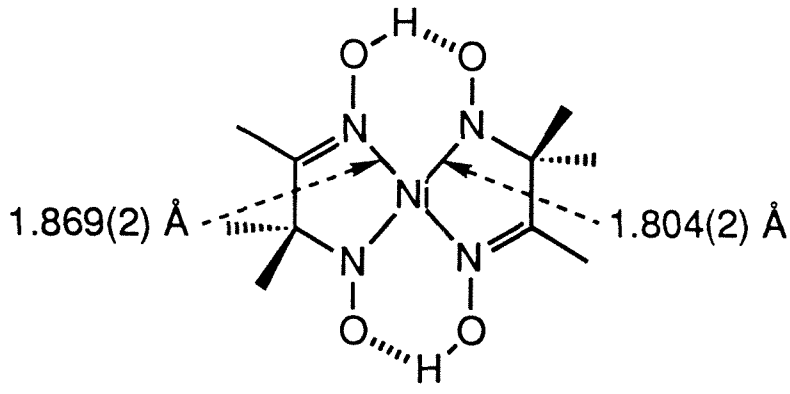

Figure 7.2. Murmann's neutral nickel complex of a formally tetraanionic ligand.

state conductivity, and ^{129}I Mössbauer spectroscopy. They conclusively demonstrated that these square planar nickel complexes are best viewed not as Ni(III) species with I^- counterions, but as Ni(2.2) species with I_5^- counterions. The Ni–Ni separation in this mixed valence system was 3.223(2) Å.

Wolberg and Manassen studied the electrochemical oxidation of Ni^{II}TPP in benzonitrile solutions.[18] The complex oxidized at approximately 0.95 V vs. SCE and at low temperature gave an EPR consistent with a Ni(III) species with $g_\perp$ (2.295) > $g_\parallel$ (2.116) (77 K). After standing, the Ni(III) species disappeared and a new species ascribed to the Ni(II) porphyrin cation radical appeared (g_{av} = 2.026). It must be emphasized that the line widths and noise of the spectra precluded being able to tell if benzonitrile was coordinated axially to either species, since superhyperfine coupling to ^{14}N of benzonitrile would not be distinguishable with the spectral quality obtained.

Busch's group was the first to synthesize an extended series of Ni(III) complexes and study them by EPR.[19a,c] The $[Ni(TAAB)]^{2+}$ complex (Figure 7.3) gives a representative example of some of the phenomena encountered. $[Ni(TAAB)]^{2+}$ exhibits a "quasi-Nernstian" oxidation wave at 1.24 V vs. SCE

in MeCN. This species gives an EPR spectrum with $g_\perp$ (2.198) > $g_\parallel$ (2.031), and superhyperfine coupling to two MeCN ^{14}N's with $a_\perp$ (17 G) < $a_\parallel$ (21.6 G). This is the expected spectrum for tetragonally distorted octahedral Ni(III) with the odd electron in a d_{z^2} orbital. In addition, $[Ni(TAAB)]^{2+}$ exhibits a Nernstian reduction wave at −0.64 V vs. SCE. Although this could be considered a formal Ni(I) product, Busch and coworkers argued that, because the TAAB ligand can become aromatic when it is a dianionic ligand, the complex is better viewed as a Ni(III) complex of $(TAAB)^{2-}$. The complex gave an EPR spectrum with $g_\parallel$ (2.160) > $g_\perp$ (2.023), which the authors attributed to a square planar complex with the lone electron in the d_{xy} orbital. However, this spectrum might also be consistent with a Ni(I) d^9 formulation in which the odd electron is in a $d_{x^2-y^2}$ orbital.

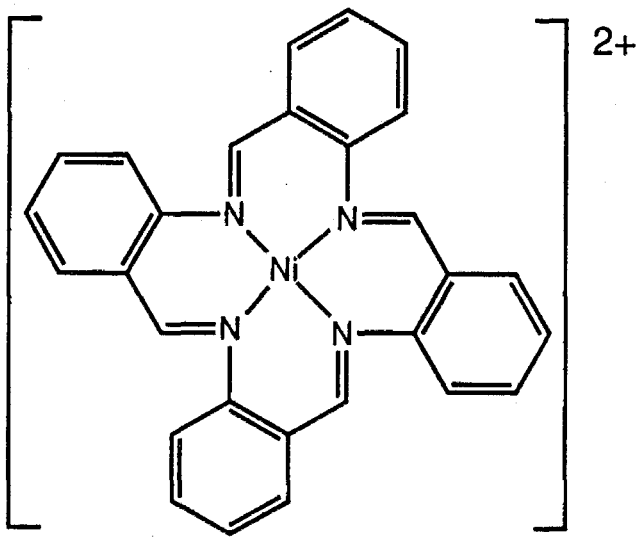

Figure 7.3. Busch's $NiTAAB^{2+}$ system.

Four recent papers of model compounds have appeared with significance to understanding the nickel hydrogenases. Millar's group has overcome the propensity of nickel thiolates to oligomerize by prepar-

ing the nickel(II) complex of bicyclo[2.2.1]heptane-*exo-cis*-2,3-dithiolate (S_2-norbornane).[19b] $[Et_4N]_2[Ni^{II}(S_2\text{-norbornane})]$ was crystallographically characterised, and it has a reversible nickel(III/II) couple at −0.76 V vs. SCE in DMF and −0.46 V vs. SCE in MeOH. The significance of this result is that the nickel(III/II) couple for hydrogenases can be from −0.390 to −0.640 V vs. SCE. When exposed to air, $[Et_4N]_2[Ni(S_2\text{-norbornane})]$ is oxidized to the nickel(III) complex, which exhibits an EPR spectrum with $g_{\|}$ (2.14) > $g_{\perp}$ (2.05), which the authors attributed to a square planar complex with the lone electron in the d_{xy} orbital. The complex is apparently stable in solution for 24 hours in DMF. Holm's group has recently structurally characterized $[Ph_3PCH_2Ph][Ni(pdtc)_2]$ [pdtc = pyridine-2,6-bis(monothiocarboxylate)$^{2-}$].[6b] The tetragonally distorted octahedral compound exhibits a Ni(III/II) couple of -0.085 V vs. SCE in DMF. Its EPR spectrum has $g_{\perp}$ (2.137) > $g_{\|}$ (2.038), which caused the authors to assign the odd electron to the d_{z^2} orbital. Superhyperfine coupling was observed to nitrogen, with an $a_{\perp}$ of 16.2 G and an $a_{\|}$ of 21.1 G. In another recent paper, Holm's group has published the EPR and redox couples of several tetradentate amido-*N*/thiolate systems. In most instances, the Ni(III/II) couples, although low, were still 200 mV positive of the hydrogenases when solvent effects were taken into account.[6c] So far, Millar's compound appears to be the only model system with a Ni(III/II) couple that approximates that of the enzymes. Finally, it must be stated that Zimmer and Crabtree have developed the first nickel-containing hydrogenase model which is functional for H_2/D exchange.[20] They used the system shown in Figure 7.4. Zimmer and Crabtree found that the Ni^{I} form of the molecule (produced at −1.05 V vs. SCE, no Ni(III/II) couple was found) was the active species and

performed 7.5 turnovers of H/D exchange between EtOH and D_2 in five minutes at 25 °C and 1 atm of D_2. More work with Ni(I) and Ni(III) species is clearly needed.

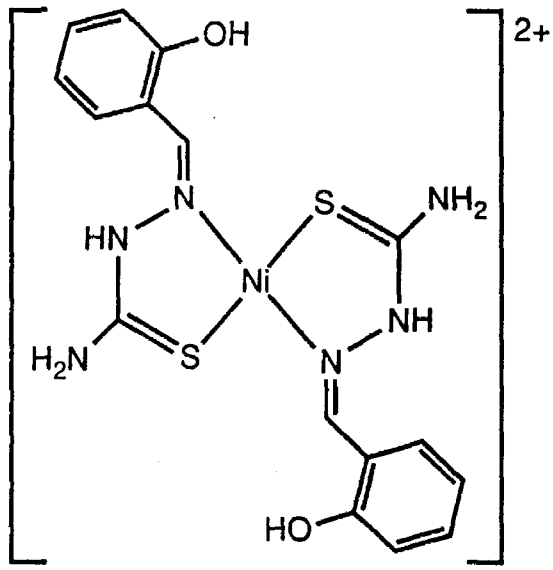

Figure 7.4. The postulated solution state structure of a nickel-containing functional hydrogenase prior to reduction.

Results and Discussion

Attempts to insert Ni into the macrocycles using simple anhydrous nickel halides (e.g., $NiBr_2$) and the strong base/anhydrous THF method developed for Cr, Mn, Fe, and Co were unsuccessful, probably because these starting nickel compounds are totally insoluble in THF and appear to be kinetically unreactive under these conditions. Tetrahedral and square planar diphosphine nickel dihalides are well known,[21] and considerations of solubility and kinetic reactivity led to the use of commercially available $(Ph_3P)_2NiBr_2$, a paramagnetic, tetrahedral, crystallographically characterized[21a] compound. It was assumed that the organic Ph_3P groups would lead to reasonable solubility. It is well known that tetrahedral complexes of the first row transition metals are

generally substitutionally labile, and use of this material made the Ni insertions facile (Figure 7.5).

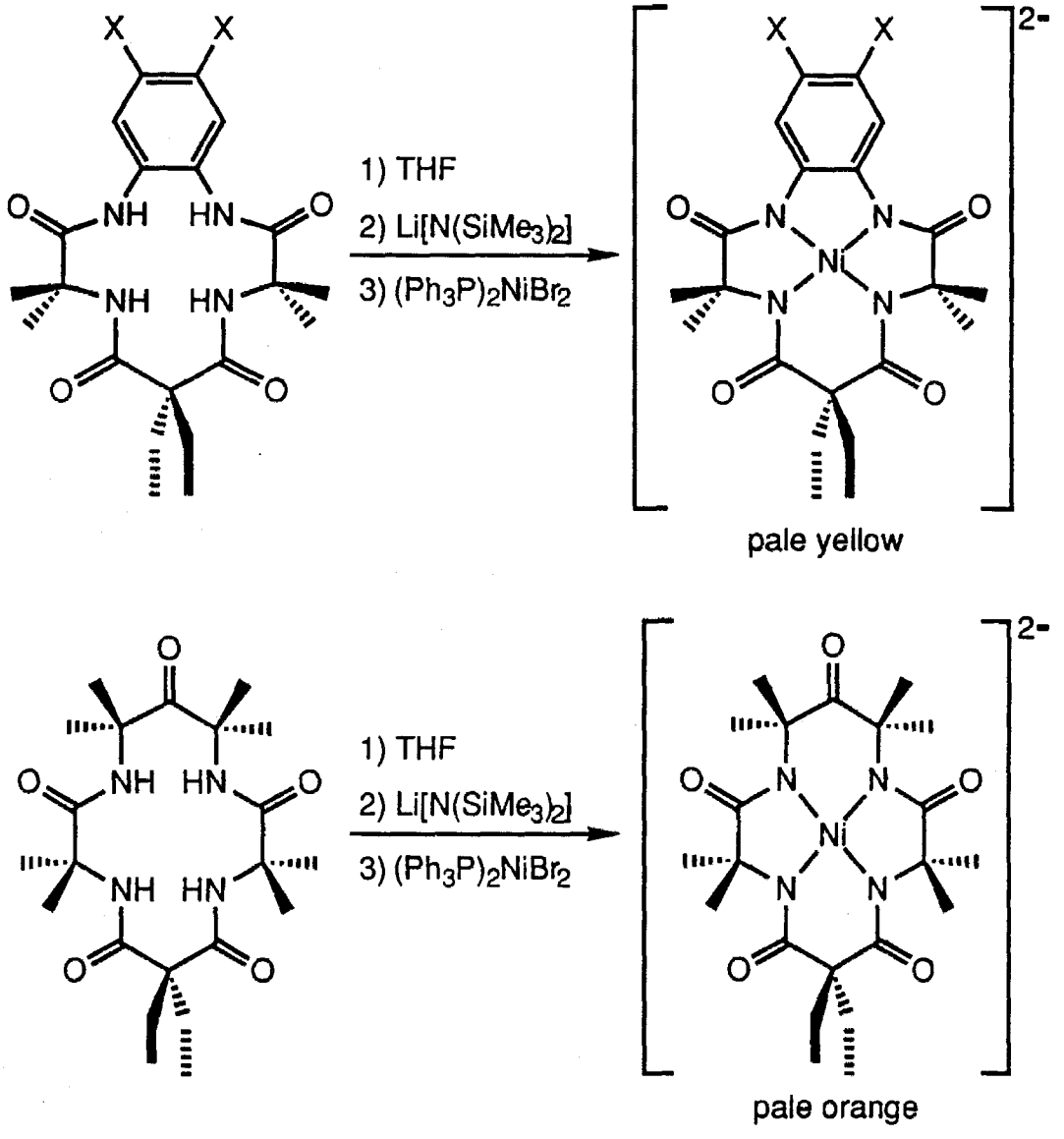

Figure 7.5. Synthesis of the macrocyclic Ni(II) complexes.

The Ni(II) compounds are stable in mild aqueous acid and base and are stable for more than a year in aqueous solution at neutral pH. They do not bind classic σ-donors or π-acids at room temperature. The Ni(II) salts give very

low amide C–O stretches in the IR,[22] consistent with the low valent dianionic character of the central metal ion. The complexes also exhibit absorptions in the visible region whose low molar absorptivities are consistent with d-d transitions.[23]

The complexes exhibit sharp ^{1}H NMR spectra that are consistent with square planar Ni(II) complexes of C_{2v} symmetry (Figures 7.6 and 7.7). However, at lower temperatures (in CD_2Cl_2), the signals of the complexes broaden. This is not due to the slowing of exchange processes, because the signals for the counter cations also broaden. In fact, at 230 K, the lock signal for the NMR solvent is completely broadened into the baseline—the complexes clearly go paramagnetic at low temperatures. This process can be visually observed by taking a 2,5-dimethyltetrahydrofuran/CH_2Cl_2 solution of one of the Ni(II) compounds and cooling it in liquid nitrogen. As the solution cools the pale yellow or pale orange color fades, and the solvent glass becomes colorless. When the glass is permitted to thaw and warm to room temperature, the starting color reappears. At least three processes might be considered to cause this paramagnetic transition at low temperature. First, it is possible that the affinity of the complexes for axial ligands increases to the point that one or two axial ligands bind at low temperature, lifting one of the d orbitals close to the highest unoccuppied d orbital so that the gap between them becomes less than the spin-pairing energy. Considering the nature of metal complexes with these macrocyclic ligands, it is unlikely that CH_2Cl_2 or trace water would bind to Ni(II) axially, even at low temperatures. Second, it is possible that dioxygen forms adducts with the complexes at low temperatures. Kimura has observed such species with pentadentate dioxacyclam Ni complexes.[24] Such an adduct

would almost necessarily be paramagnetic. However, the Ni(II) compounds continue to change color at low temperature even after several freeze-pump-thaw cycles under nitrogen. Third, it is possible that a conformational change in the complex occurs at low temperature to reduce the d orbital splittings. The fit of Ni(III) to (η^4-DEMAMPA-DCB)$^{4-}$ is excellent (vide infra). It is possible that Ni(II) is too large to comfortably fit in the ligand. It is possible that at room temperature the ligand can accomodate a strain which generates a geometry approximating square planar. However, at low temperature, the surrounding medium might have insufficient energy to maintain the ligand strain, and the complex could relax to some domed or ruffled configuration which lowers the d orbital splitting. Clearly, the cause of this low temperature Ni(II) paramagnetism merits further investigation.

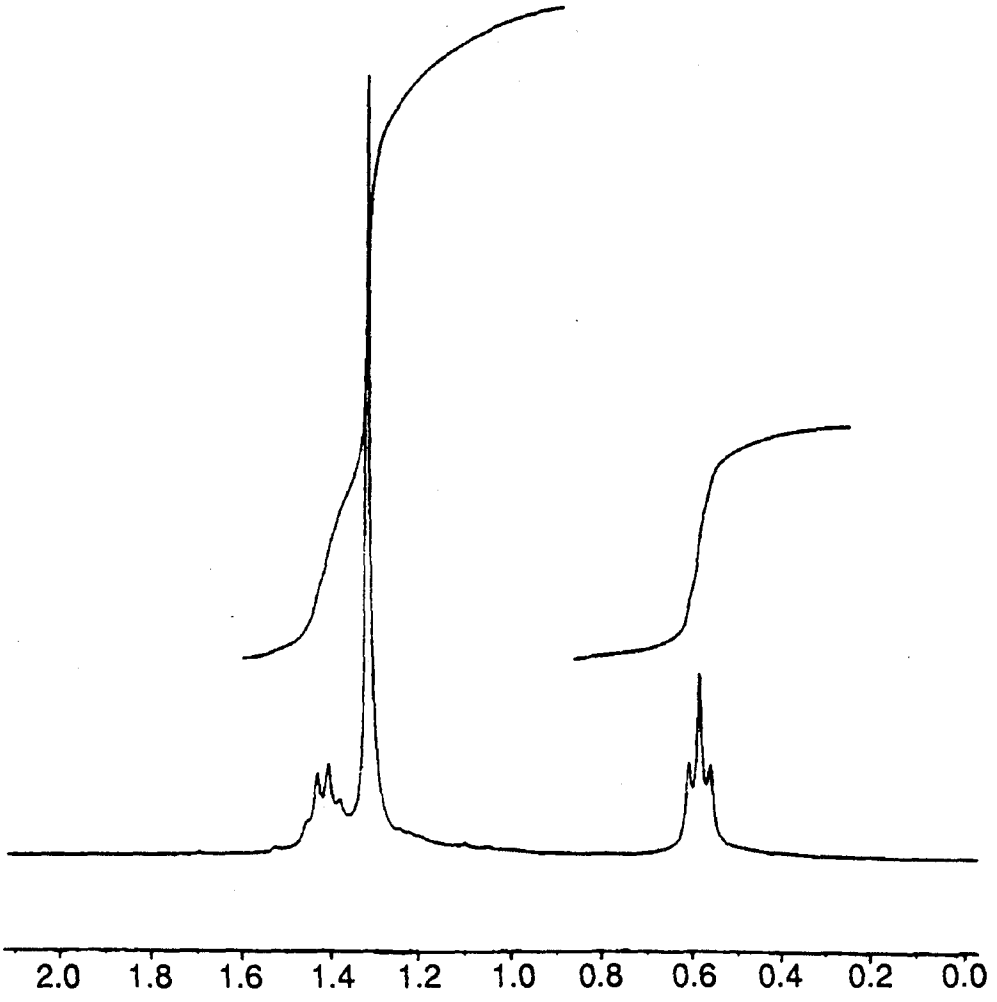

Figure 7.6. ^{1}H NMR spectrum (300 MHz, D_2O, 293 K) of Li_2[Ni(η^4-DEMAMPA-DCB)] (δppm: 8.02, s, 2H, off scale of figure; 1.43, q, 4H, J=6.9 Hz; 1.32, s, 12H; 0.58, t, 6H, J=6.9 Hz [HOD—4.65—used as reference, off scale of figure]).

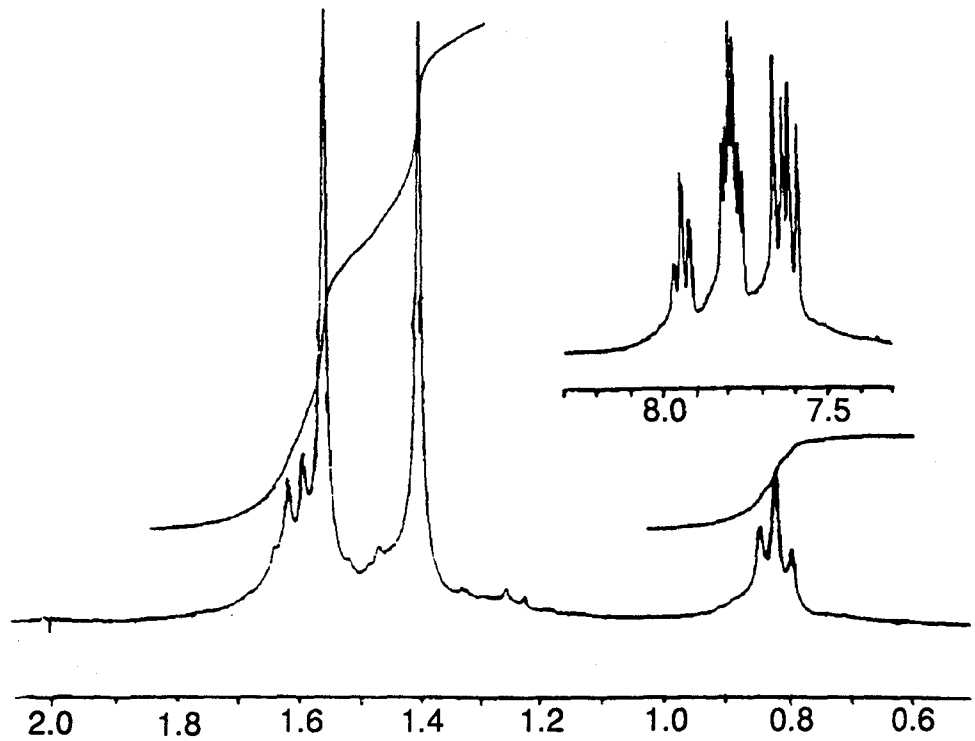

Figure 7.7. ^{1}H NMR spectrum (300 MHz, CD_2Cl_2, 293 K) of $[PPh_4]_2[Ni(\eta^4$-MAC*)] (δppm: 1.60, q, 4H, J=7.4 Hz; 1.56, s, 12H; 1.40, s, 12H; 0.83, t, 6H, J=7.4 Hz; 7.3–8.3, $[PPh_4]^+$ resonances [$CHDCl_2$—5.32—used as reference, off scale of figure]).

Orange [Ni(η^4-MAC*)]$^{2-}$ and yellow [Ni(η^4-DEMAMPA-DCB)]$^{2-}$ can both be oxidized to the purple nickel(III) complexes (Figure 7.8) using a wide variety of oxidizing agents, including bromine, chlorine, benzoyl peroxide, silver nitrate, *tert*-butyl hypochlorite, the magnesium salt of monoperoxyphthalic acid, or ceric ammonium nitrate. Bromine and chlorine tend to oxidize the complexes beyond purple to a green or dark yellow color. Benzoyl peroxide yields the purple complexes even after stirring with the nickel(II) for several hours and is the preferred oxidant for the preparation of the square planar Ni(III) species.

Cyclic voltammetry reveals the potential of the Ni(III/II) couples (Figure 7.9 and Figure 7.10). Note that the formal potential of the Ni(III)/Ni(II) couple of [Ni(η^4-MAC*)]$^-$ occurs at the low value of +0.130 V vs. NHE. In fact, if the correction factor of ca. 600 mV vs. NHE is made for the Ag/$AgNO_3$ electrode in acetonitrile (see reference 20 in Chapter 5), the Ni(III)/Ni(II) couple of [Ni(η^4-MAC*)]$^-$ is lower than any of those observed for the macrocyclic complexes shown in Figure 1.3. In the absence of contrary evidence a coordination environment consisting of four deprotonated amido-*N* ligands is unrealistic in a biological medium. However, low potential Ni(III) is found in nickel hydrogenases (vide supra) and it is interesting to note that an innocent abiological ligand complement can also produce highly stabilized nickel(III). The Ni(III/II) couple for [Ni(η^4-DEMAMPA-DCB)]$^-$ occurs 190 mV higher at 0.320 V vs. NHE. The complex has another reversible couple at 1.210 V vs. NHE. This couple is analogous to the couple found at 1.250 V vs. NHE for Co(η^4-DEMAMPA-DCB) (see Chapter 6). As expected, the amide stretches in the IR increase with oxidation.[25]

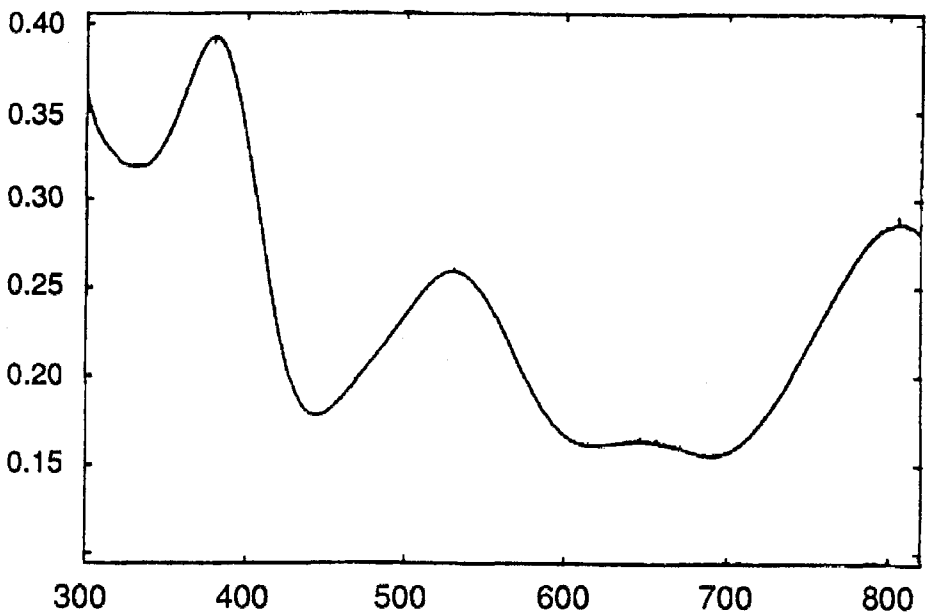

Figure 7.8. UV-vis spectrum of [Bu_4][Ni(η^4-MAC*)] in CH_2Cl_2. 380 nm (5.48×10^3 M^{-1} cm^{-1}), 532 nm (3.62×10^3 M^{-1} cm^{-1}), 650 nm (2.33×10^3 M^{-1} cm^{-1}), 808 nm (4.18×10^3 M^{-1} cm^{-1}).

Table 7.1. UV-vis Data for [Ni(η^4-MAC*)]$^-$

Solvent	$\lambda_1(\epsilon)$	$\lambda_1(\epsilon)$	$\lambda_1(\epsilon)$	$\lambda_1(\epsilon)$
CH_2Cl_2	380(5480)	532(3620)	650(2330)	808(4180)
MeCN	380(5450)	530(3590)	650(2260)	806(3980)
Pyridine	380(4760)	534(3100)	647(1900)	817(3300)
EtOH	376(4790)	525(3000)	ca. 660(sh)	794(3780)
H_2O	372(2700)	519(1700)	—	767(2400)

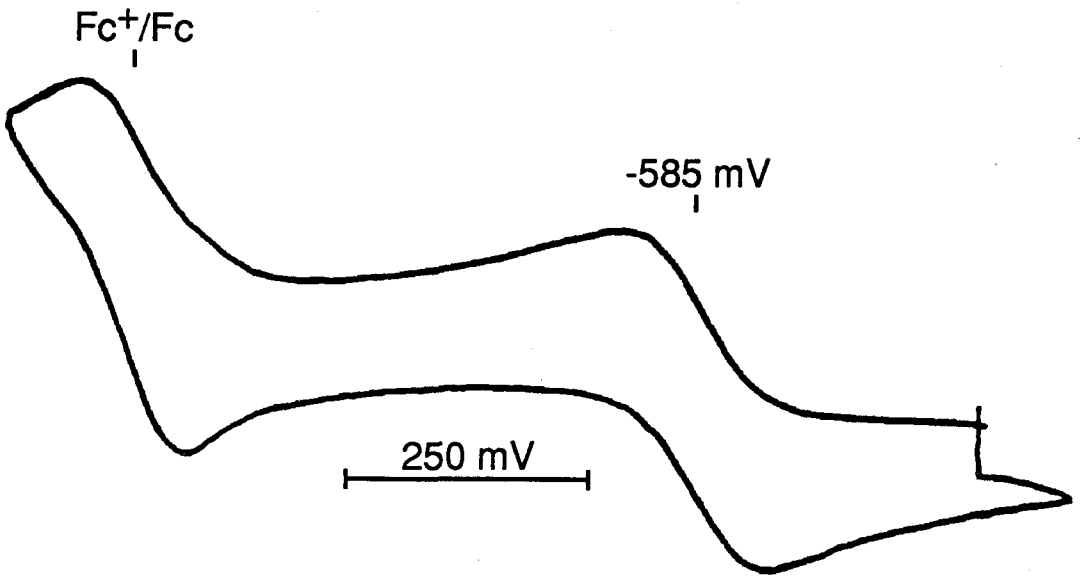

Figure 7.9. Cyclic voltammetry of $[Ni(\eta^4\text{-MAC*})]^{2-}$ (0.1 M $[Bu_4N][ClO_4]$, CH_2Cl_2, 1.100 V sweep width, 200 mV s^{-1}).

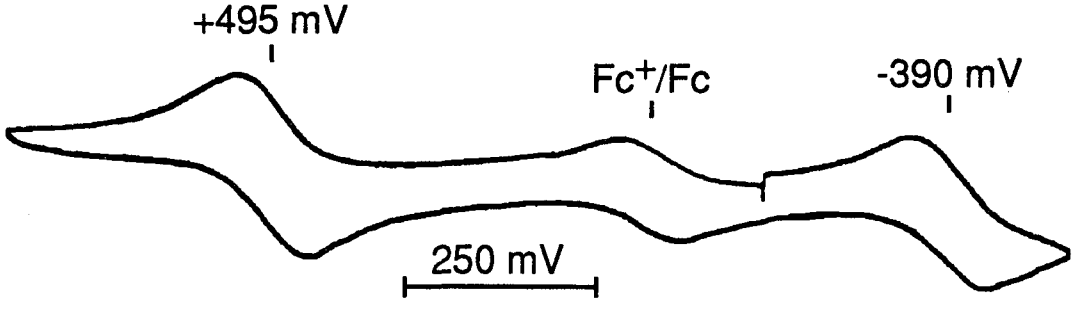

Figure 7.10. Cyclic voltammetry of $[Ni(\eta^4\text{-DEMAMPA-DCB})]^{-}$ (0.1 M $[Bu_4N][ClO_4]$, CH_2Cl_2, 1.400 V sweep width, 200 mV s^{-1}).

The complex, $[Et_4N][Ni(\eta^4\text{-MAC*})]$, is the first planar four-coordinate structure of Nickel(III) with an innocent ligand (Figure 7.11). The amide nitrogens alternate 0.25 Å above and below their mean plane and the Ni atom sits 0.09 Å above this mean plane. The average Ni–N distance is 1.84 Å. The average amide O–C bond distance of 1.22 Å is the same as the ketone O–C distance.

The average amide N–C bond distance is 1.35 Å. The N_1NiN_3 angle is 170.1°, and the N_2NiN_4 angle is 158.6°. In contrast, the octahedral complex shown in Figure 7.12a has a substantially longer average Ni–N distance (1.97 Å), a nearly square array of amine nitrogens (N_1NiN_3=179.0, N_2NiN_4=179.7), and the nickel atom is within 0.004 Å of the amines' mean plane.[5a] In an analogous octahedral complex (Figure 7.12b) the average Ni–N distance was even longer (2.00 Å).[5b] Even for the octahedral nickel(III) complex of 1,4,7-triazacyclononane-N,N′,N″-triacetate, a ligand known to compress metal ions, the average Ni–N distance is 1.93 Å, and the average Ni–O distance is 1.91Å (Figure 7.12c).[5c] The average Ni(III)–N distance is 2.04 Å in a organometallic Ni(III) five-coordinate compound (Figure 7.12d).[5d] The Ni(III)–$N_{(amide)}$ bonds are also shorter than low spin Ni(II)–$N_{(amine)}$ bonds (1.89Å).[26] Thus, the strong donor capacity of $(\eta^4$-MAC*$)^{4-}$ stabilizes nickel(III) in the absence of axial ligands, and this leads to the equatorial compression of the Ni–N framework. Although the complex stacks along the c-axis of the crystal, the Ni–Ni separation of 7.99 Å is 4.77 Å greater than found in stacked dimethylglyoxime complexes (vide supra).[17] $[Et_4N][Ni(\eta^4$-MAC*$)]$ is also noteworthy in having a significantly nonplanar amido-*N* ligand (see Chapter 9).

The bond distances in the aromatic framework of $[(Me)_4N][Ni(\eta^4$-DEMAMPA-DCB$)]$ (Figure 7.13) are consistent with a formal oxidation state of +III for the nickel ion (in Å: N4–C8 1.415(3), C8–C9 1.411(4), C8–C13 1.376(4), C12–C13 1.387(4), C11–C12 1.380(4), C10–C11 1.386(4), C9–C10 1.387(4)). The average Ni–N distance is 1.83 Å, the average amide O–C bond distance is 1.23 Å, and the average amide N–C bond distance is 1.36 Å. The N_1NiN_3 angle is 171.7°, and the N_2NiN_4 angle is 171.8°. It is a remarkably

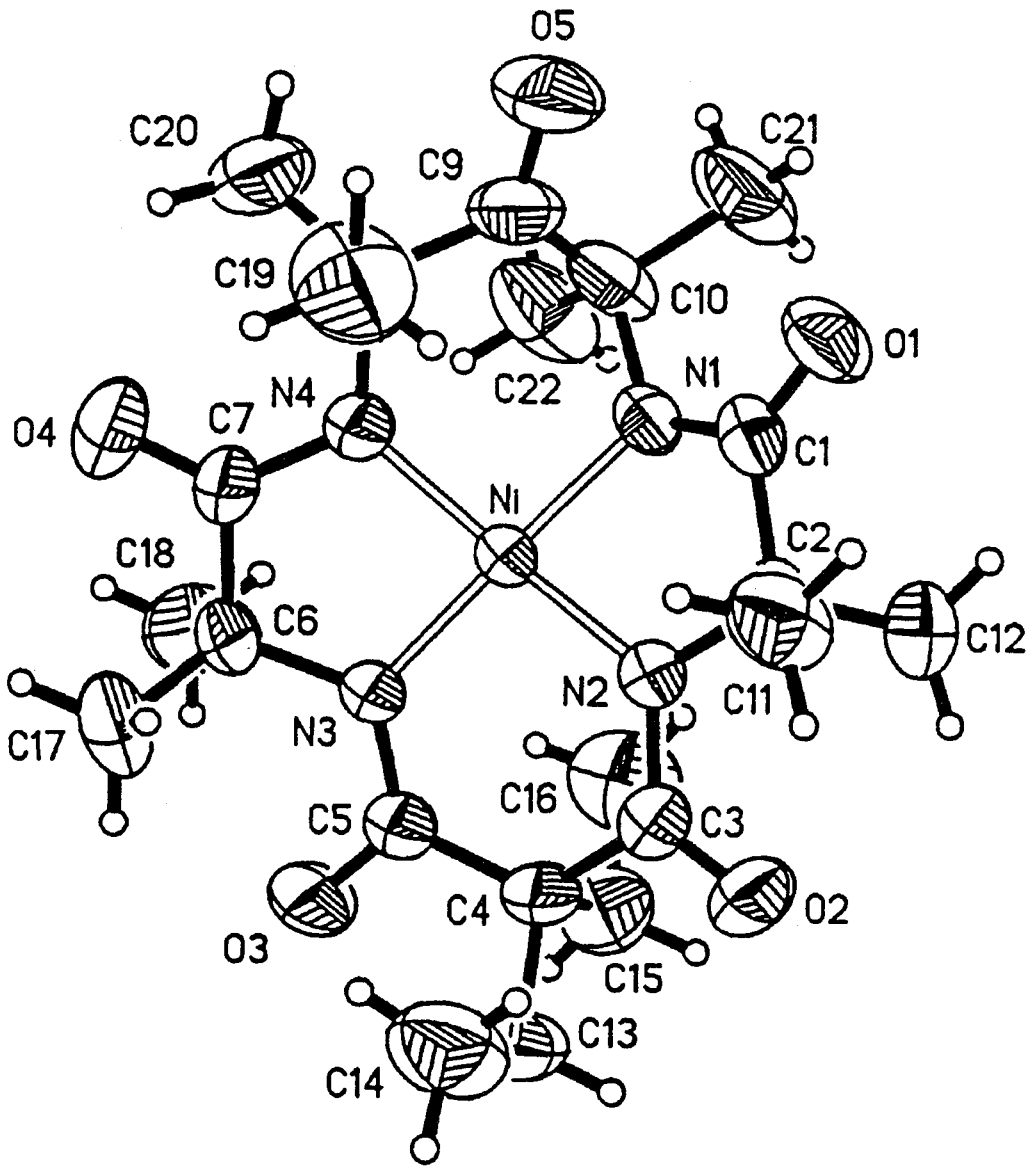

Figure 7.11. Molecular structure of anion of $[Et_4N][Ni(\eta^4\text{-MAC*})]$. ORTEP drawing with all nonhydrogen atoms drawn to encompass 50% of electron density.

Table 7.2. Bond Lengths in $[Ni(\eta^4\text{-MAC*})]^-$			
Atoms	Length (Å)	Atoms	Length (Å)
NiN1	1.849(3)	NiN2	1.825(4)
NiN3	1.848(3)	NiN4	1.849(4)

Table 7.2. Bond Lengths in [Ni(η^4-MAC*)]$^-$ (continued)			
Atoms	Length (Å)	Atoms	Length (Å)
O1C1	1.212(5)	O2C3	1.222(6)
O3C5	1.242(5)	O4C7	1.223(7)
O5C9	1.215(6)	N1C1	1.356(7)
N2C3	1.357(5)	N3C5	1.343(5)
N4C7	1.350(6)	N1C10	1.499(6)
N2C2	1.487(6)	N3C6	1.474(6)
N4C8	1.517(6)	C1C2	1.530(6)
C3C4	1.541(7)	C4C5	1.512(7)
C6C7	1.524(7)	C8C9	1.553(8)
C9C10	1.501(9)	C2C11	1.502(9)
C2C12	1.518(8)	C4C13	1.549(7)
C4C15	1.542(9)	C13C14	1.501(10)
C15C16	1.529(8)	C6C17	1.524(8)
C6C18	1.526(10)	C8C19	1.521(12)
C8C20	1.509(9)	C10C21	1.527(7)
C10C22	1.535(10)		

Table 7.3. Bond Angles in [Ni(η^4-MAC*)]$^-$			
Atoms	Angle (°)	Atoms	Angle (°)
N1NiN2	84.4(1)	N1NiN3	170.1(2)
N1NiN4	94.9(2)	N2NiN3	97.2(1)
N2NiN4	158.6(2)	N3NiN4	87.1(1)
NiN1C1	111.5(3)	NiN1C10	119.6(3)

Table 7.3. Bond Angles in [Ni(η^4-MAC*)]$^-$ (continued)			
Atoms	Angle (°)	Atoms	Angle (°)
NiN2C2	113.1(3)	NiN2C3	127.8(3)
NiN3C5	125.5(3)	NiN3C6	114.2(2)
NiN4C7	114.5(3)	NiN4C8	124.2(3)
C1N1C10	122.4(3)	C2N2C3	118.6(4)
C5N3C6	119.1(3)	C7N4C8	116.5(4)
N1C1O1	127.0(4)	N1C1C2	112.0(4)
O1C1C2	120.9(5)	N2C3O2	122.7(4)
N2C3C4	118.7(4)	O2C3C4	118.3(4)
N3C5O3	122.3(4)	N3C5C4	121.1(4)
O3C5C4	116.6(4)	N4C7O4	126.6(5)
N4C7C6	114.5(4)	O4C7C6	118.9(4)
C8C9C10	122.7(4)	C8C9O5	116.2(6)
C10C9O5	121.0(5)	C1C2C11	109.1(4)
C1C2C12	104.5(4)	N2C2C1	106.0(4)
N2C2C12	113.9(5)	C11C2C12	112.2(5)
C3C4C5	120.0(4)	C3C4C13	106.0(4)
C3C4C15	107.1(4)	C5C4C13	107.8(4)
C5C4C15	107.9(5)	C13C4C15	107.6(4)
C7C6C17	108.7(5)	C7C6C18	106.2(4)
N3C6C7	106.5(3)	N3C6C17	111.4(4)
N3C6C18	112.1(5)	C17C6C18	111.7(4)
N4C8C9	110.1(5)	N4C8C19	108.3(5)
N4C8C20	112.3(5)	C9C8C19	108.8(5)

7.3. Bond Angles in [Ni(η^4-MAC*)]$^-$ (continued)			
Atoms	Angle (°)	Atoms	Angle (°)
C9C8C20	104.3(5)	C19C8C20	112.8(6)
N1C10C9	102.5(4)	N1C10C21	111.6(5)
N1C10C22	108.1(4)	C9C10C21	112.6(5)
C9C10C22	114.6(5)	C21C10C22	107.4(5)
C4C13C14	113.5(5)	C4C15C16	116.5(5)
N2C2C11	110.7(4)		

planar complex and has planar amides. In fact, for the atoms in the macrocyclic or aromatic rings, the largest deviation from the $N_1N_2N_3N_4$ mean plane is 0.18 Å; sixteen of the atoms deviate from this plane by less than 0.10 Å, and the nickel atom sits 0.002 Å below this plane.

Both purple complexes [Ni(η^4-MAC*)]$^-$, and [Ni(η^4-DEMAMPA-DCB)]$^-$ have a low affinity for axial ligands in solution at 20 °C. For [Ni(η^4-MAC*)]$^-$, neat MeCN, pyridine, acetone, 2,5-Me_2THF, THF, CH_2Cl_2, water, and EtOH all give purple solutions (see Table 7.1). In contrast, addition of cyanide results in an immediate color change from purple to yellow.[27] Mole ratio plots indicate a 1:1 adduct with CN^- ($K_{20°} = 3.2(9) \times 10^3$ mol^{-1}); comparison with [Ni(η^4-DEMAMPA-DCB)]$^-$ is not possible because [Bu_4N][CN] reduces it. At 77 K, frozen solutions of [Ni(η^4-MAC*)]$^-$ in water, MeCN, 2,5-Me_2THF, THF, CH_2Cl_2 or acetone remain purple, as do solutions also containing Ph_3P or Et_3N. In contrast, when purple solutions of [Ni(η^4-**1**)]$^-$ in 2,5-Me_2THF containing any one of the potential ligands, ethanol, pyridine, 2,6-lutidine, ammonia, or Me_3P are cooled to 77 K green (EtOH) or yellow (other ligands)

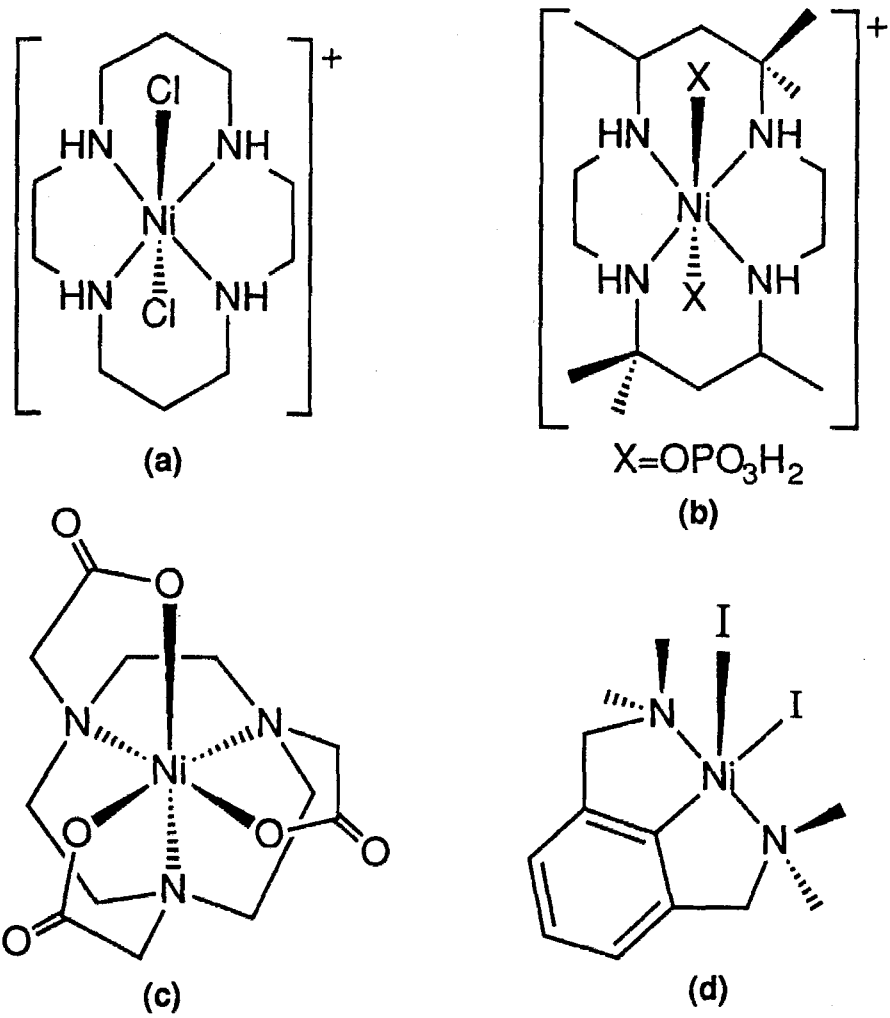

Figure 7.12. (a) The octahedral complex of Ito, et al. [average Ni–N distance 1.97 Å. The complex was prepared by oxidizing the five-coordinate Ni(II) complex with $(NH_4)_2S_2O_8$ in an excess of concentrated HCl. No EPR was reported] (b) The octahedral complex of Zeigerson, et al. [average Ni–N distance 2.00 Å. The compound was prepared electrochemically. No EPR was reported.] (c) The octahedral complex of Hancock, et al. [average Ni–N distance 1.93 Å, average Ni–O distance 1.91 Å. The complex was prepared by oxidizing the Ni(II) species with aqueous nitric acid. No EPR was reported] (d) The five-coordinate organometallic complex of Grove, et al. [average Ni–N distance 2.04 Å. The compound was prepared by oxidizing the four-coordinate Ni(II) iodide complex with either CuI_2 or I_2. EPR was done on the dichloride at -140 °C in a toluene glass—rhombic spectrum with $g_1 = 2.366$, $g_2 = 2.190$, and $g_3 = 2.020$ superhyperfine observed only to *one* Cl 28 G, and no coupling observed to nitrogen.]

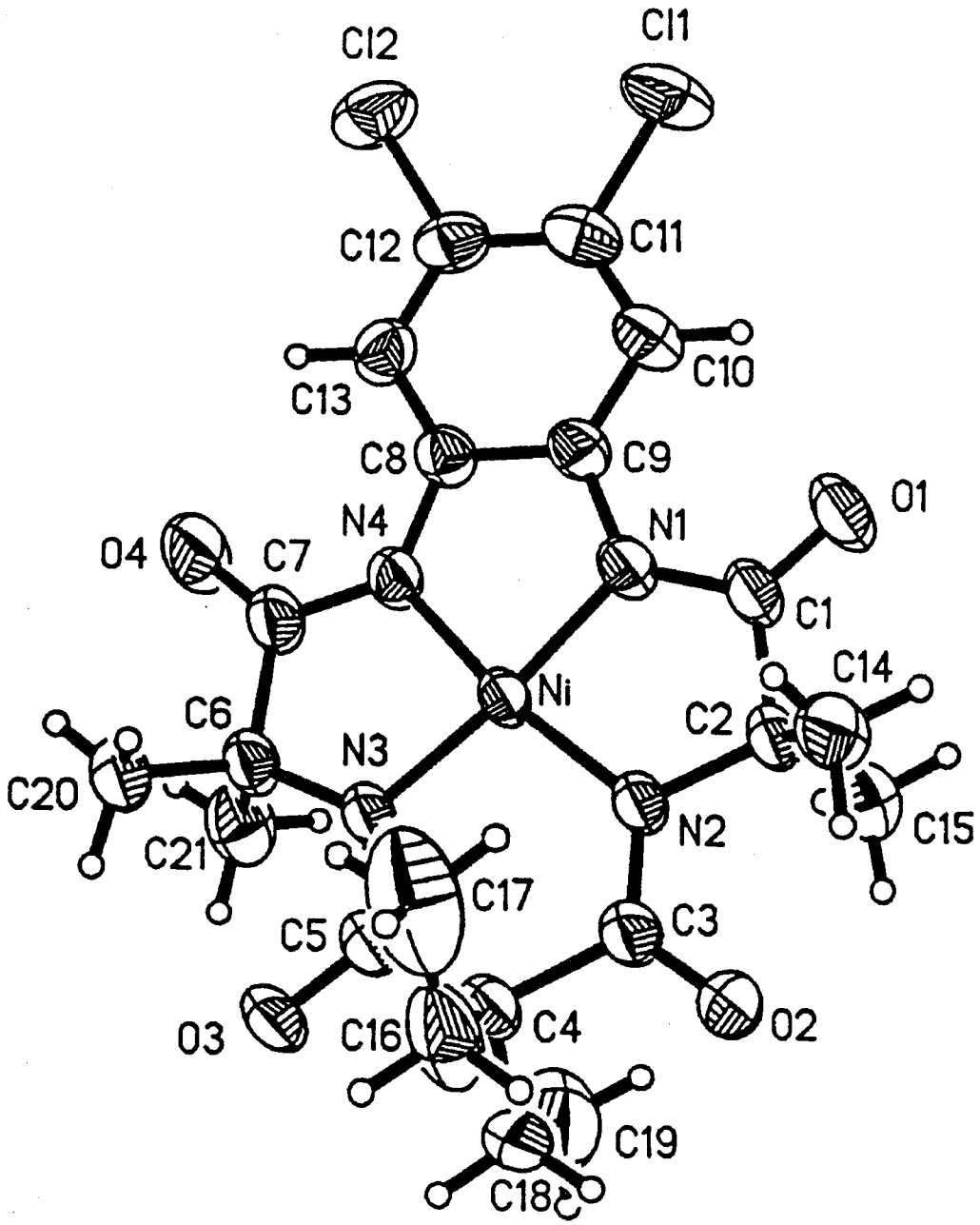

Figure 7.13. Molecular structure of anion of $[Me_4N][Ni(\eta^4\text{-DEMAMPA-DCB})]$. ORTEP drawing with all nonhydrogen atoms drawn to encompass 50% of electron density.

Table 7.4. Bond Lengths in [Ni(η^4-DEMAMPA-DCB)]$^-$			
Atoms	Length (Å)	Atoms	Length (Å)
NiN1	1.816(3)	NiN2	1.842(2)
NiN3	1.831(3)	NiN4	1.812(2)
Cl1C11	1.745(4)	Cl2C12	1.741(3)
O1C1	1.221(4)	O2C3	1.240(3)
O3C5	1.239(4)	O4C7	1.221(4)
N1C1	1.372(3)	N1C9	1.397(4)
N2C3	1.338(4)	N3C5	1.353(4)
N4C7	1.362(4)	N4C8	1.402(4)
N2C2	1.491(4)	N3C6	1.492(3)
C1C2	1.527(5)	C3C4	1.552(5)
C4C5	1.543(4)	C6C7	1.534(5)
C8C9	1.413(4)	C8C13	1.393(4)
C9C10	1.394(5)	C10C11	1.367(5)
C11C12	1.396(5)	C12C13	1.385(5)
C2C14	1.528(4)	C2C15	1.523(5)
C4C16	1.551(6)	C4C18	1.525(6)
C6C20	1.523(4)	C6C21	1.534(5)
C16C17	1.530(8)	C18C19	1.475(7)

Table 7.5. Bond Angles in [Ni(η^4-DEMAMPA-DCB)]$^-$			
Atoms	Angle (°)	Atoms	Angle (°)
N1NiN2	87.2(1)	N2NiN3	101.0(1)
N2NiN4	171.8(1)	N1NiN3	171.7(1)

Table 7.5. Bond Angles in [Ni(η^4-DEMAMPA-DCB)]$^-$ (continued)

Atoms	Angle (°)	Atoms	Angle (°)
N1NiN4	84.8(1)	N3NiN4	87.1(1)
NiN1C1	117.2(2)	NiN1C9	115.8(2)
NiN2C2	114.8(2)	NiN3C5	126.5(2)
NiN3C6	115.0(2)	NiN4C7	117.4(2)
NiN4C8	116.0(2)	NiN2C3	127.2(2)
C1N1C9	126.8(3)	C2N2C3	118.0(2)
C5N3C6	118.4(2)	C7N4C8	126.5(2)
O1C1N1	124.6(3)	O1C1C2	122.2(3)
N1C1C2	113.2(3)	O2C3N2	123.7(3)
O2C3C4	115.5(3)	N2C3C4	120.8(2)
O3C5N3	122.5(2)	O3C5C4	116.2(3)
N3C5C4	121.2(3)	O4C7N4	124.5(4)
O4C7C6	122.2(3)	N4C7C6	113.3(2)
N2C2C1	107.5(2)	N2C2C14	111.9(3)
C1C2C14	106.9(3)	N2C2C15	111.5(3)
C1C2C15	106.8(3)	C14C2C15	112.0(3)
C3C4C5	122.1(3)	C3C4C16	106.3(3)
C5C4C16	106.2(3)	C3C4C18	105.5(3)
C5C4C18	106.4(3)	C16C4C18	110.1(3)
N4C8C9	111.4(2)	N4C8C13	128.2(3)
C9C8C13	120.4(3)	N1C9C8	111.9(3)
N1C9C10	128.2(2)	C8C9C10	119.9(3)
C9C10C11	119.1(3)	Cl1C11C10	118.6(3)

Table 7.5. Bond Angles in [Ni(η^4-DEMAMPA-DCB)]$^-$ (continued)			
Atoms	Angle (°)	Atoms	Angle (°)
Cl1C11C12	119.9(3)	C10C11C12	121.5(4)
Cl2C12C11	121.4(3)	Cl2C12C13	118.1(2)
C11C12C13	120.5(3)	C8C13C12	118.6(3)
C4C16C17	114.9(4)	C4C18C19	114.5(4)
N3C6C7	106.7(2)	N3C6C20	113.8(2)
C7C6C20	107.9(3)	N3C6C21	110.8(3)
C7C6C21	106.2(3)	C20C6C21	110.9(3)

glasses are obtained. The similarity of the purple color in the solutions and the crystalline material, the similarity of the UV-vis spectra of purple solutions in coordinating and noncoordinating solvents, and the changes to yellow or green that occur with certain ligands suggest that the nickel(III) anion is purple when it is four-coordinate and green or yellow when it is higher coordinate.

EPR spectroscopy has been of special significance to the study of enzymatic systems containing nickel(III),[2] and EPR studies of [Ni(η^4-MAC*)]$^-$ lend further support to the color/coordination number relationship enunciated above. The EPR spectrum of [Bu_4N][Ni(η^4-MAC*)] with excess CN^- is rhombic in both frozen CH_2Cl_2 (Figure 7.14) and glassed EtOH (Figure 7.15). Using $^{13}CN^-$ confirms that only one CN^- binds at low temperature (Figure 7.16). Spectra of glasses of 2,5-Me_2THF/CH_2Cl_2 with pyridine are also rhombic and also confirm one py is coordinated, but only g_3 shows superhyperfine interactions (Figure 7.17). Even in neat frozen pyridine, the EPR shows only one

py is coordinated (Figure 7.18). Me_3P slowly reduces [Ni(η^4-MAC*)]$^-$, but an EPR may be obtained of the adducts if the sample is immediately frozen after ligand addition (Figure 7.19). The spectrum would appear to contain the monoadduct as the majority species (g=2.315, 2.248, 2.059; ^{31}P superhyperfine on g_3 of 385 G) with some bisadduct present as well (g=2.121, 2.059, 2.010; ^{31}P superhyperfine on g_3 obscured). The superhyperfine coupling order in these five-coordinate Ni(III) complexes is $A_{31_P} > A_{13_C} > A_{14_N}$; identifiable factors contributing to this difference are the greater s character of the σ ligand donor orbital (sp for CN^- and sp^2 for py) and the relative sizes of the isotropic hyperfine constant, A_0, ^{31}P (10,178 MHz) > ^{13}C (3,110 MHz) > ^{14}N (1,540 MHz).[28] Interestingly, the EPR of [Ni(η^4-DEMAMPA-DCB)]$^-$ in a 2,5-Me_2THF/pyridine glass is *axial* and confirms one py is coordinated (Only g_3 shows superhyperfine interactions. Figure 7.20). The EPR of [Ni(η^4-DEMAMPA-DCB)]$^-$ in an EtOH glass is rhombic (Figure 7.21). The EPR of [Ni(η^4-MAC*)]$^-$ in an EtOH glass shows a mixture of at least three species.

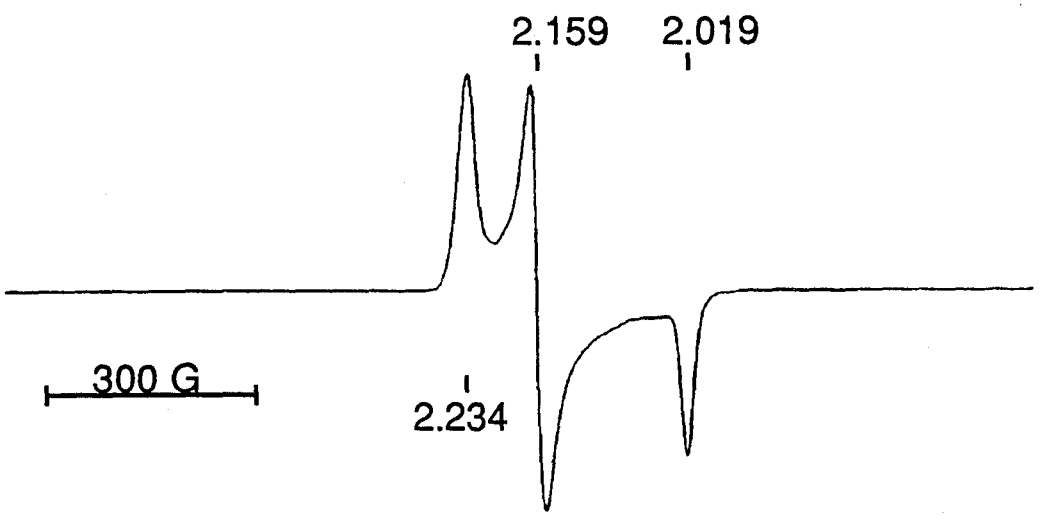

Figure 7.14. EPR spectrum of $[Ni(\eta^4\text{-MAC*})]^-$ with excess $[Bu_4N][CN]$ at 4.2 K, 9.46 GHz, in CH_2Cl_2 (two scan average, 1500 G scan range, 3100 G mid range).

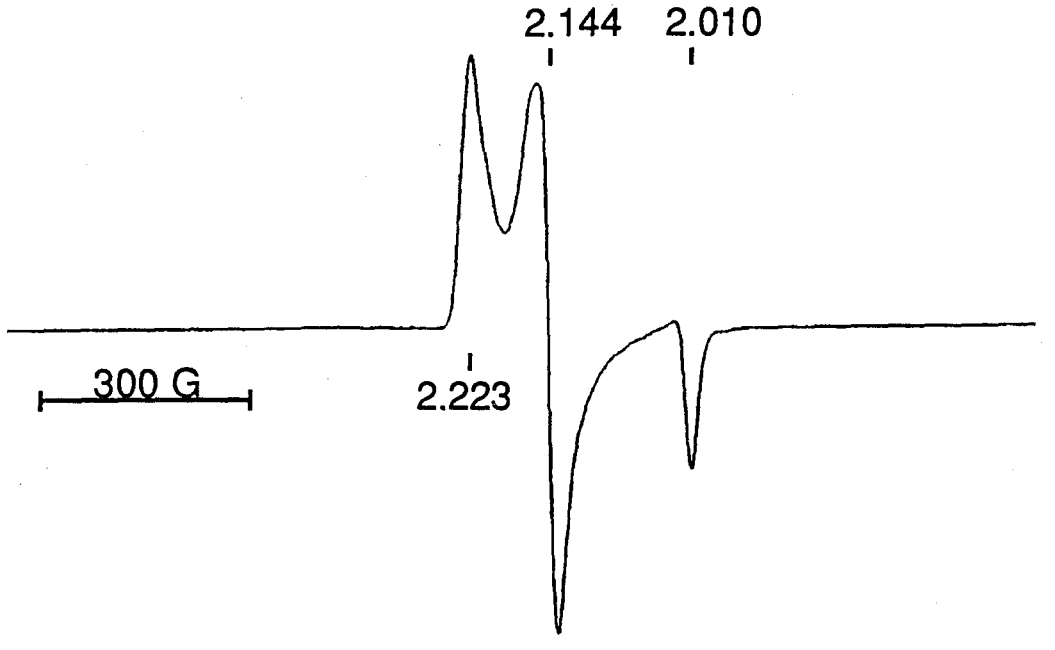

Figure 7.15. EPR spectrum of $[Ni(\eta^4\text{-MAC*})]^-$ with excess KCN at 4.0 K, 9.46 GHz, in EtOH (1500 G scan range, 3100 G mid range).

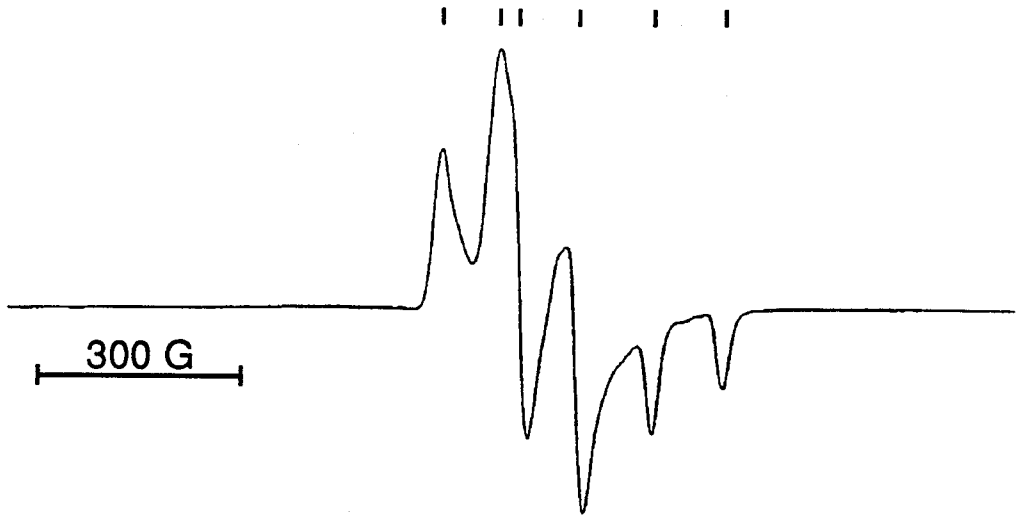

Figure 7.16. EPR spectrum of $[Ni(\eta^4\text{-MAC*})]^-$ with excess $K^{13}CN$ at 4.0 K, 9.46 GHz, in EtOH (1500 G scan range, 3100 G mid range). Cyanide-^{13}C superhyperfine coupling constant (anisotropic) 88 G, 82 G, 102 G.

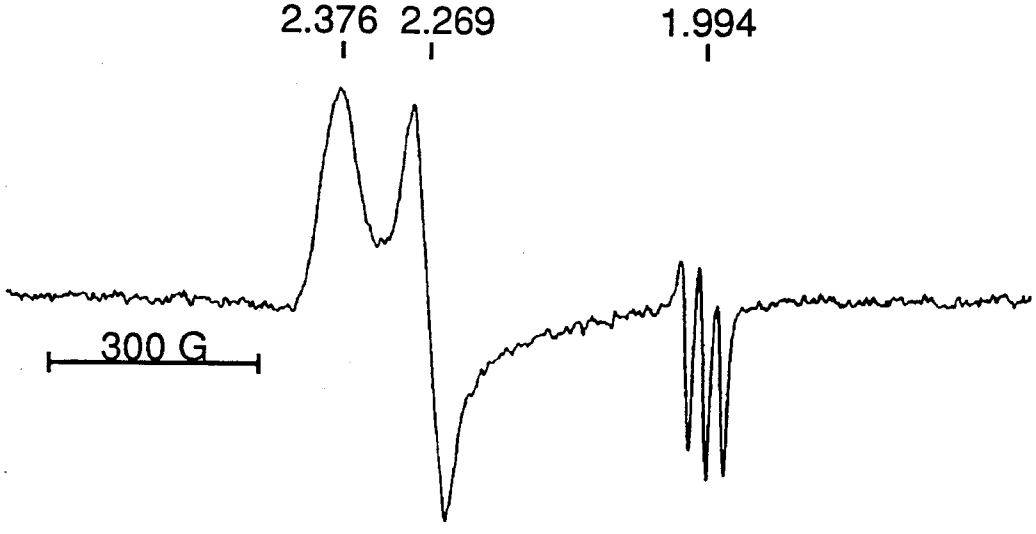

Figure 7.17. EPR spectrum of $[Ni(\eta^4\text{-MAC*})]^-$ at 4.6 K, 9.46 GHz, in 2,5-dimethyltetrahydrofuran/pyridine (1500 G scan range, 3100 G mid range). Pyridine-^{14}N superhyperfine coupling constant (observable only on g_3) 25.5 G.

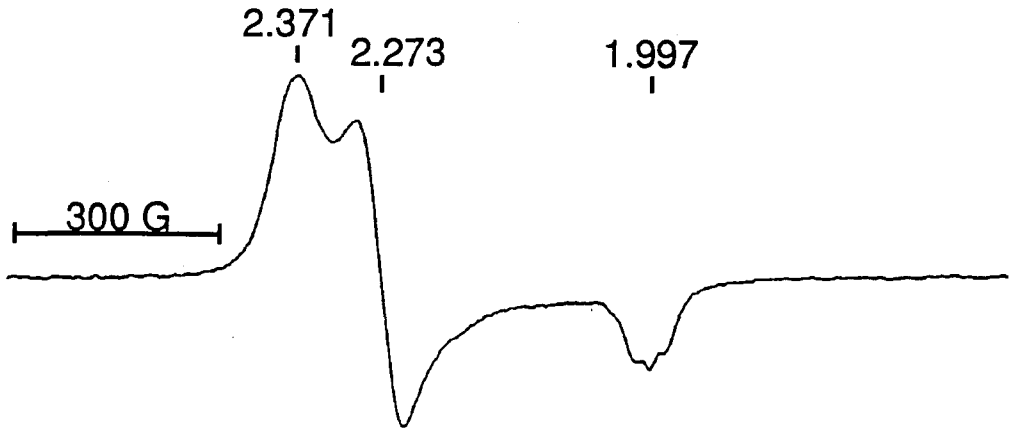

Figure 7.18. EPR spectrum of [Ni(η^4-MAC*)]$^-$ at 143 K, 9.34 GHz, in neat pyridine (1500 G scan range, 3100 G mid range). Pyridine-^{14}N superhyperfine coupling constant (observable only on g_3) 22 G.

EPR has been used to attempt to determine whether the four-coordination found in the solid state for the purple anion, [Ni(η^4-MAC*)]$^-$, is carried into purple solutions. In noncoordinating solvents, water is the ubiquitous potentially coordinating impurity and water has been found to coordinate weakly to nickel(III) complexes of otherwise four-coordinate ligand complements containing amido-*N* donors by Margerum, et al. (Figure 7.22).[2c] The Margerum ligands have smaller donor capacities than the macrocycle presented here, so his complexes should have a higher affinity for axial ligands. In glasses of 2,5-Me_2THF/CH_2Cl_2 or toluene/CH_2Cl_2 at 4.6 K, [Ni(η^4-MAC*)]$^-$ remains purple (all solvents, except 2,5-Me_2THF, Aldrich Sureseal, EPR tubes vacuum dried and charged and sealed under an inert atmosphere). The EPR spectra of these glasses are shown in Figure 7.23. Each spectrum is axial with $g_\perp$ greater than $g_\parallel$. Addition of $H_2{}^{16}O$ or 45% $H_2{}^{17}O$, beyond the point of saturation of the 2,5-Me_2THF/CH_2Cl_2 or toluene/CH_2Cl_2 aprotic solvent mixtures, leads

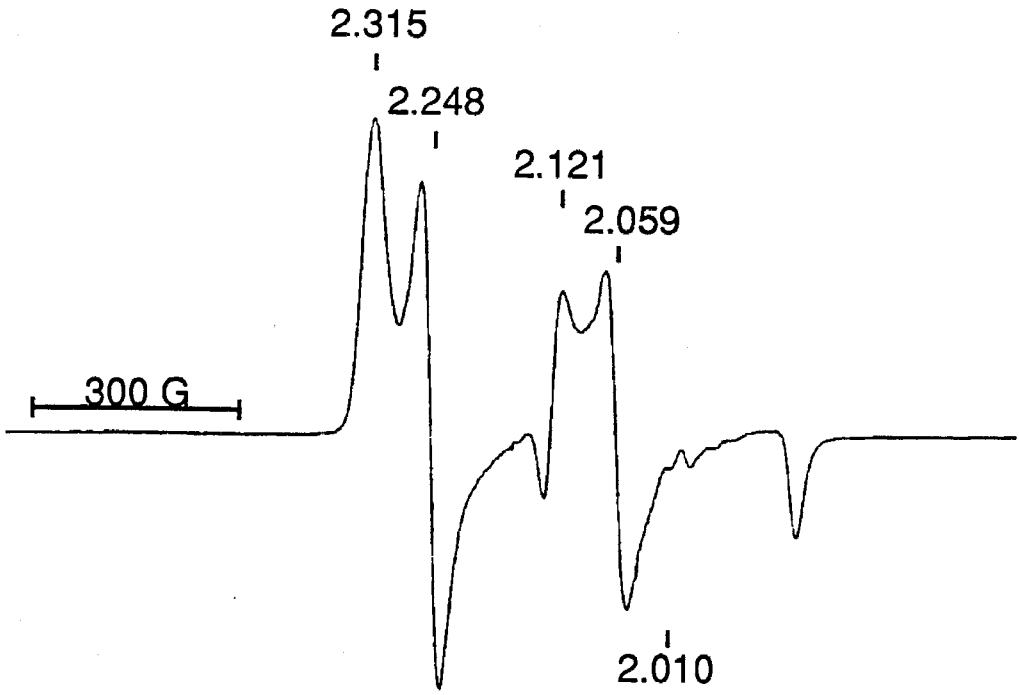

Figure 7.19. EPR spectrum of [Ni(η^4-MAC*)]$^-$ at 4.0 K, 9.46 GHz, in toluene/CH_2Cl_2 + PMe_3 (1500 G scan range, 3100 G mid range). ^{31}P superhyperfine coupling constant (observable only on g_3) 385 G.

to virtually identical EPR spectra for the four glasses at 4.6 K to those found in the absence of deliberately added water (Figure 7.23). The absence of identifiable broadening or splitting in any of the g values does not support the case for axial ligation of water in the purple glasses (the A_0 of ^{17}O (−4,628 MHz[28]) is greater in magnitude than that for ^{13}C).

The $g_\perp$ and $g_\parallel$ resonances of [Ni(η^4-MAC*)]$^-$ show structuring, possibly attributable to hyperfine interactions. The related purple compound, [$(CH_3)_4N$][Ni(η^4-DEMAMPA-DCB)], exhibits rigorously planar coordination (vide supra). The EPR spectra of the $[Bu_4N]^+$ salt in purple 2,5-Me_2THF/CH_2Cl_2 or toluene/CH_2Cl_2 glasses at 4.6 K exhibit $g_\perp > g_\parallel$ and

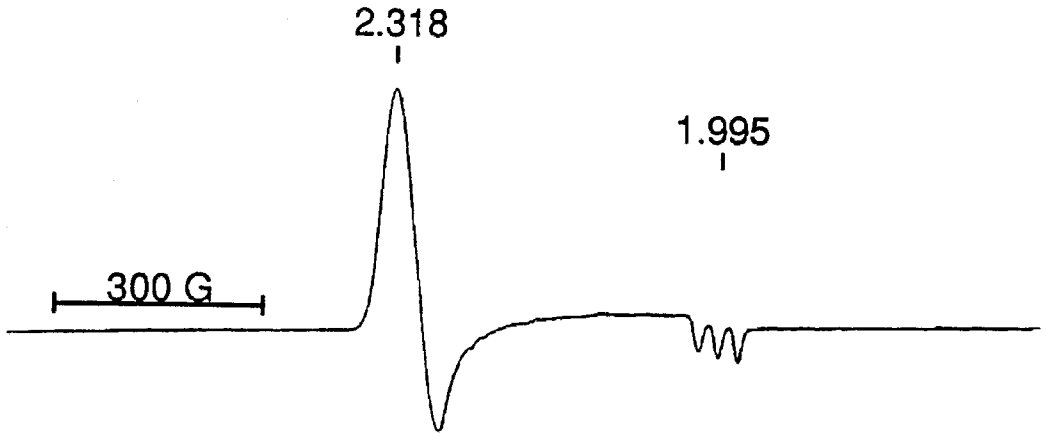

Figure 7.20. EPR spectrum of [Ni(η^4-DEMAMPA-DCB)]$^-$ at 4.0 K, 9.46 GHz, in 2,5-dimethyltetrahydrofuran/pyridine (1500 G scan range, 3100 G mid range). Pyridine-^{14}N superhyperfine coupling constant (observable only on g_3) 28 G.

Figure 7.21. EPR spectrum of [Ni(η^4-DEMAMPA-DCB)]$^-$ at 4.0 K, 9.46 GHz, in EtOH (1500 G scan range, 3100 G mid range).

show less structuring than found for [Ni(η^4-MAC*)]$^-$ (Figure 7.24). Conformational variations at low temperature in the macrocyclic ligand framework are expected to be less prevalent in [Ni(η^4-DEMAMPA-DCB)]$^-$ than in [Ni(η^4-MAC*)]$^-$. The evidence presented here suggests that impurity water is not

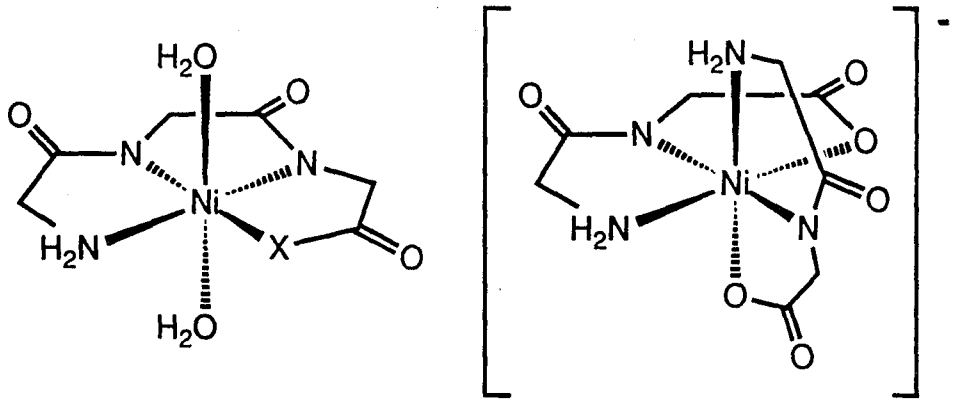

Figure 7.22. Margerum's oligopeptide complexes of Ni(III). Left, general structure of a monopeptide complex: X = O, $[Ni(H_{-2}G_3)(H_2O)_2]$; X = $NCH_2CO_2^-$, $[Ni(H_{-3}G_4)(H_2O)_2]^-$; X = NCH_2CONH_2, $[Ni(H_{-3}G_4a)(H_2O)_2]$. Right, a bis(dipeptide) complex, $[Ni(H_{-1}G_2)_2]^-$.

axially bound to $[Ni(\eta^4\text{-MAC*})]^-$ in noncoordinating solvent glasses that are purple, i.e., that the EPR spectra of these purple glasses are of four-coordinate species.

These observations have wider significance, since an EPR spectrum for Ni(III) with $g_{\|} > g_{\perp}$ has come to be considered as a signature of square planar nickel(III), based on the orbital splitting diagram in Figure 7.25.[2,19] That is, it has been considered that the odd electron would reside in a d_{xy} orbital in square planar complexes. Holm has obtained EPR spectra similar to several of the ones shown here, and attributed them to four-coordinate species in which the odd electron is in a d_{z^2} orbital.[6c] However, it should be noted that his putative four-coordinate Ni(III) species have not been stable enough to isolate as pure solids, and his spectra have been run at low temperatures in DMF. We have noted dramatic temperature effects on axial ligand affinities in our Ni(III) species. It is possible that Holm's group might have axial DMF coordination

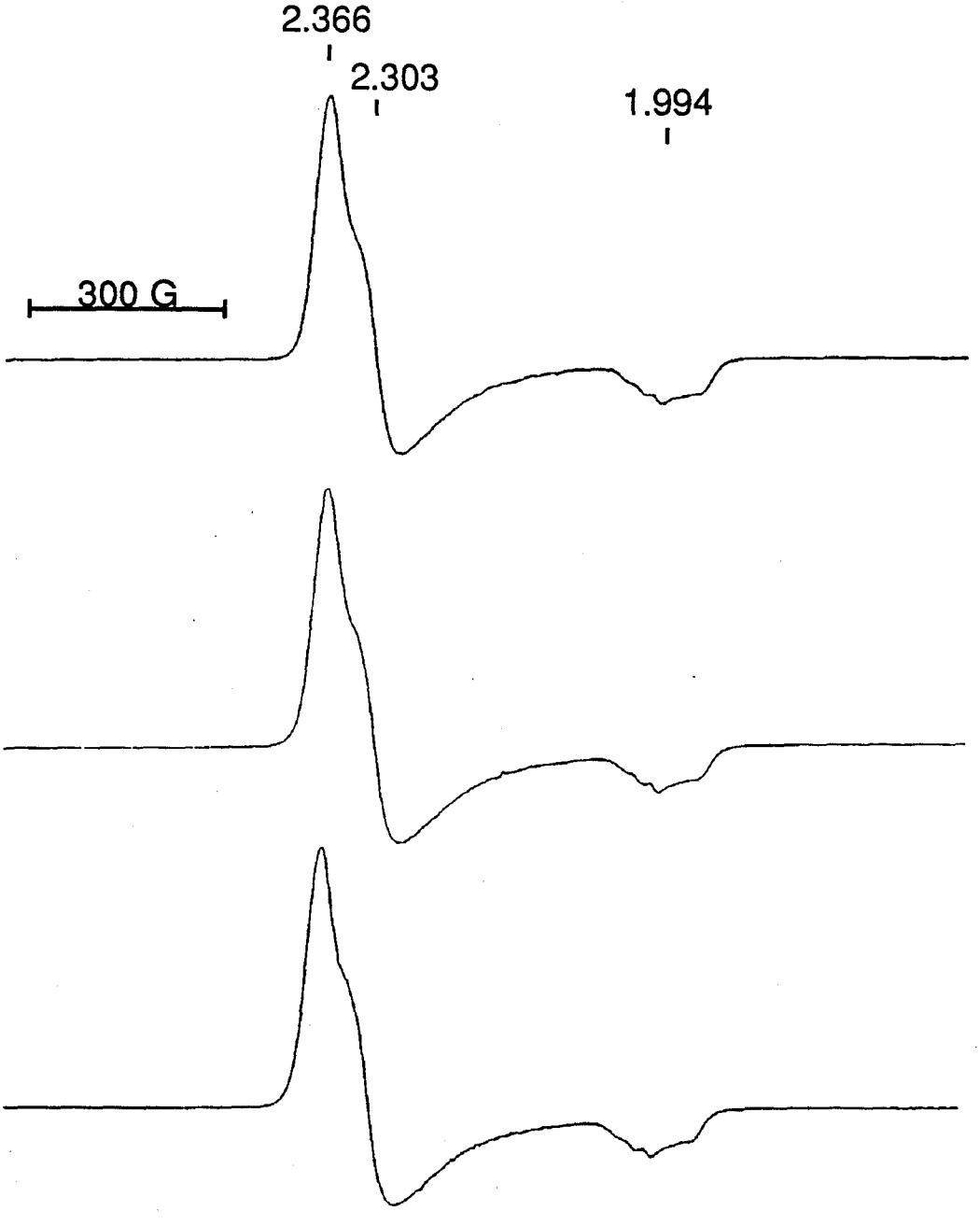

Figure 7.23. EPR spectrum of $[Ni(\eta^4\text{-MAC*})]^-$ without water (top), with water (middle), and with $H_2{}^{17}O$ (bottom) at 4.6 K, 9.46 GHz, in 2,5-dimethyltetrahydrofuran/CH_2Cl_2 (1500 G scan range, 3100 G mid range). Identical spectra are obtained when this set of experiments is conducted in toluene/CH_2Cl_2.

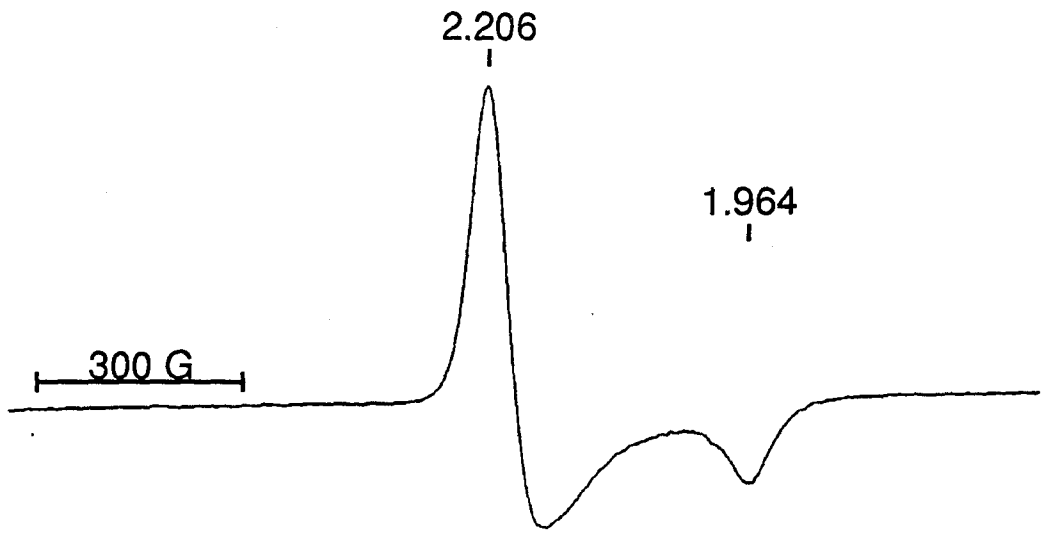

Figure 7.24. EPR spectrum of [Ni(η^4-DEMAMPA-DCB)]$^-$ at 4.5 K, 9.46 GHz, in 2,5-dimethyltetrahydrofuran (1500 G scan range, 3100 G mid range).

at 100 K (^{16}O has no nuclear spin and, thus, will not show superhyperfine interactions.).

Two square planar Ni(III) complexes with $g_\perp > g_\parallel$ have been prepared in this thesis work, and both of these species appear to remain four-coordinate in noncoordinating glasses. It is worth noting in closing that the $\langle g \rangle$ value of 2.20 for [Ni(η^4-MAC*)]$^-$, the first square planar Ni(III) complex of an innocent ligand, is significantly greater than the $\langle g \rangle$ value (2.05–2.08) found in the nickel dithiolene/dithiolate complexes where the formal oxidation state at the metal has been a subject of considerable controversy. It is interesting that although the crystal structure and electrochemical data of [Ni(η^4-DEMAMPA-DCB)]$^-$ are consistent with a formal oxidation state assignment of +III for Ni, the $\langle g \rangle$ value (2.13) is lower than found in [Ni(η^4-MAC*)]$^-$, but still considerably higher than that found for the nickel dithiolene/dithiolate complexes.

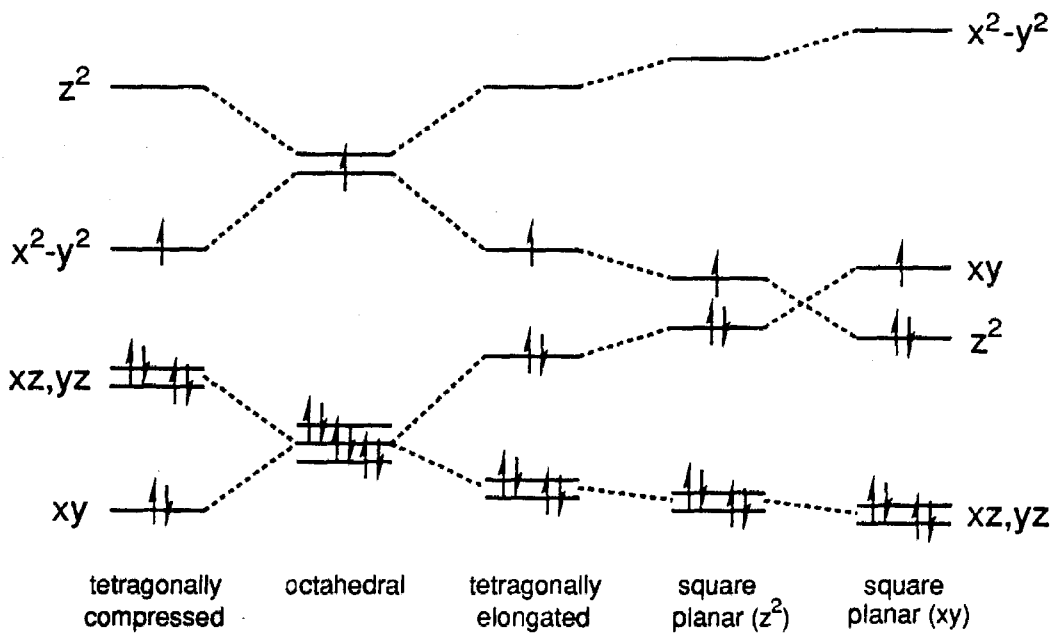

Figure 7.25. Orbital splitting diagram for Ni(III) complexes. An axial spectrum with $g_{\|} > g_{\perp}$ is expected for systems in which the odd electron is in a d_{xy} or a $d_{x^2-y^2}$ orbital. An axial spectrum with $g_{\perp} > g_{\|}$ is expected for systems in which the odd electron is in a d_{z^2} orbital.

Experimental

Materials. All solvents and reagents were reagent grade (Aldrich) except for THF and benzene (Aldrich, Sureseal) and were used as received except as described for electrochemical measurements.

Physical Measurements. ^{1}H NMR were measured at 300 MHz on an IBM NR/300 FT-NMR Spectrometer. ^{1}H NMR data are reported in δ vs. $(CH_3)_4Si$ with the solvent as internal standard. EPR spectra were recorded on a Bruker ER300 Spectrometer. Infrared data were obtained on a Nicolet 5DXB FT-IR Spectrometer. UV-vis data were obtained on a Perkin-Elmer Lambda Array 3840 Spectrophotometer. Crystal structures were solved by Crystalytics Co. of Lincoln, Nebraska.

Electrochemical Data. Cyclic voltammetry was performed on a Princeton Applied Research Model 173/179 potentiostat/digital coulometer equipped with positive feedback IR compensation and a Model 175 universal programmer. Current voltage curves were recorded on a Houston Instruments Model 2000 X-Y recorder.

Sureseal anhydrous CH_2Cl_2 (Aldrich) was used as received. $[Bu_4N][ClO_4]$ (Fluka) was vacuum dried at 80 °C. In all cases experiments were performed under N_2 with a supporting electrolyte concentration of 0.1 M. Cyclic voltammetry was performed in CH_2Cl_2 solutions of $[Bu_4N][ClO_4]$ at a 3 mm Pt disk working electrode with a silver wire quasi-reference electrode and a Pt foil counter electrode. At the conclusion of each experiment, ferrocene (Fc) was added as an internal potential standard. All formal potentials were taken as the average of anodic and cathodic peak potentials and are reported vs. the Fc^+/Fc couple. Peak-to-peak separation of the Fc^+/Fc couple was similar to

that of the Ni couples in all cases. Plots of peak current vs. the square root of scan rate over the range 10–500 mV s^{-1} were made and found to be linear for couples that are stated to be reversible. Bulk electrolysis was performed in CH_2Cl_2 solutions of $[Bu_4N][ClO_4]$ in a standard three-compartment cell at Pt gauze working and counter electrodes with a silver wire quasi-reference electrode.

Synthetic Note. The experimental work reported here for the $(\eta^4$-MAC*$)^{4-}$ system has been published in substantially similar form in *J. Am. Chem. Soc.* and the M.S. thesis of Mr. Thomas R. Nichols.[29]

Li_2[Ni(η^4-MAC*)]. H_4MAC* (100 mg, 0.23 mmol) was dissolved in anhydrous THF (20 mL, 20 °C) under nitrogen in a dry 100 mL three-necked round-bottom flask. A THF solution of lithium bis(trimethylsilyl)amide (1.0 M, 1.0 mL, 4.4 equiv) was syringed into the solution, which was allowed to stir (3–5 min). $(Ph_3P)_2NiBr_2$ (180 mg, 0.24 mmol) was added and the reaction was stirred (5 min). The reaction was quenched with a few drops of water. The solvent was removed (in vacuo) and all of the solids were washed into a 125 mL separatory funnel with CH_2Cl_2 and H_2O. Upon vigorous shaking, pale orange $[Ni(\eta^4$-MAC*$)]^{2-}$ and LiBr moved into the aqueous layer, which was separated and filtered through glass wool to remove suspended organic material. The water was removed *in vacuo* (60 °C), yielding a nearly quantitative amount of Ni(II), based on the final product containing LiBr (2 equiv).

$[Ph_4P]_2$[Ni(η^4-MAC*)]. $Li_2[Ni(\eta^4$-MAC*$)]$ and a large excess of $[Ph_4P]Cl$ were dissolved in a minimum of water. After the solvent was removed (in vacuo, 60 °C), the complex was dissolved in CH_2Cl_2 and dried over anhydrous sodium sulfate. After filtration and removal of solvent (in vacuo, 20 °C),

the compound was recrystallized by diffusion of ethyl ether into an acetonitrile solution (20 °C). The complex co-crystallized with tetraphenylphosphonium chloride, as seen by elemental analysis, and could not be purified.

Li[Ni(η^4-MAC*)]. Li_2[Ni(η^4-MAC*)] was dissolved in 100% EtOH (50 mL). Benzoyl peroxide (50 mg) was added and the mixture was stirred. The solution turned dark purple in a matter of seconds; the mixture was stirred (30 min) to ensure that all of the nickel(II) was oxidized. The solvent was removed (in vacuo, 20 °C); after washing the purple solids with benzene to remove the peroxide, the solids were collected on a sintered glass filter. The yield of Li[Ni(η^4-MAC*)] was high, but the complex could not be satisfactorily purified; the lithium salt was immediately metathesized with tetraalkylammonium or tetraphenylphosphonium halide salts as described below.

[Bu_4N][Ni(η^4-MAC*)]. An aqueous solution of [Bu_4N]Cl was added dropwise to an aqueous solution of Li[Ni(η^4-MAC*)] until all of the complex had precipitated. The purple precipitate was filtered away and washed with a copious amount of water. The compound was dissolved in CH_2Cl_2 and briefly dried over anhydrous sodium sulfate; after filtration the solvent was removed (in vacuo, 20 °C). Small, dark purple crystals were grown by diffusion of pentane into a 1,2-dichloroethane solution. Anal. Calcd for [Bu_4N][Ni(η^4-MAC*)]: C, 62.04; H, 9.59; N, 9.52. Found: C, 62.01; H, 9.75; N, 9.59.

[Et_4N][Ni(η^4-MAC*)]. A slight excess of [Et_4N][F] was added to an EtOH solution of Li[Ni(η^4-MAC*)] and the solvent was immediately removed (in vacuo, 20 °C) to avoid reduction. The Ni(III) complex was dissolved in CH_2Cl_2 and briefly dried over anhydrous Na_2SO_4; after filtration the solvent was removed (in vacuo, 20 °C). Dark purple X-ray quality crystals were grown

by diffusion of pentane into a 1,2-dichloroethane solution. Anal. Calcd for $[Et_4N][Ni(\eta^4\text{-MAC*})]$: C, 57.79; H, 8.73; N, 11.23. Found: C, 57.92; H, 9.00; N, 11.18.

$[Ph_4P][Ni(\eta^4\text{-MAC*})]$. An aqueous solution of $[Ph_4P]Cl$ was added dropwise to an aqueous solution of $Li[Ni(\eta^4\text{-MAC*})]$ until all of the complex had precipitated. The purple precipitate was filtered away and washed with a copious amount of water. Large, dark purple crystals were grown by evaporation of ethanol from an ethanol/water solution (20 °C).

$Li_2[Ni(\eta^4\text{-DEMAMPA-DCB})]$. H_4DEMAMPA-DCB (100 mg, 0.22 mmol) was dissolved in dry, deoxygenated THF (20 mL). $Li[N(SiMe_3)_2]$ (1 mL, 1.0 M in THF, 1 mmol, 4.5 equiv) was syringed into the solution which was allowed to stir (3–5 min). $(Ph_3P)_2NiBr_2$ (170 mg, 0.23 mmol) was added to the resultant pale yellow solution. The reaction was stirred under N_2 (30–60 min). The solvent was removed under reduced pressure and the solids were washed into a separatory funnel with CH_2Cl_2 and H_2O. $Li_2[Ni(\eta^4$-DEMAMPA-DCB)] and LiBr extracted into the aqueous layer, which became bright yellow. The aqueous layer was separated and filtered through glass wool to remove suspended organic material. The organic layer was washed with H_2O until the aqueous washes were colorless. The aqueous layers were filtered and combined and the water was removed under reduced pressure at room temperature. The yield of $Li_2[Ni(\eta^4$-DEMAMPA-DCB)] is nearly quantitative, based on a final product containing LiBr (2 equiv).

$[Et_4N]_2[Ni(\eta^4\text{-DEMAMPA-DCB})]$. $Li_2[Ni(\eta^4$-DEMAMPA-DCB)] was dissolved in a minimum of water. A slight excess of $[Et_4N]F$ was added and the solution was reduced to a minimum volume at reduced pressure (max-

imum bath temperature = 50 °C). CH_2Cl_2 and finely powdered anhydrous Na_2SO_4 were added. As the water was removed by the drying agent, the [Ni(η^4-DEMAMPA-DCB)]$^{2-}$ moved into the CH_2Cl_2. The solution was filtered through a fine glass frit and taken to dryness under reduced pressure. Recrystallization was achieved by vapor diffusion of pentane into a 1,2-dichloroethane solution. [n. b. The compound will not dissolve in CH_2Cl_2 if all the water is pumped off. The $[Et_4N]^+$ salt is quite water soluble and will not extract into CH_2Cl_2 from a saturated aqueous solution.]

$[Ph_4P]_2$[Ni(η^4-DEMAMPA-DCB)]. Li_2[Ni(η^4-DEMAMPA-DCB)] (45 mg, or 60 mg of LiBr contaminated product) was dissolved in water (10 mL). $[Ph_4P]Cl$ (63 mg) was added. $[Ph_4P]_2$[Ni(η^4-DEMAMPA-DCB)] precipitated as a dark yellow oil. The aqueous oil was extracted with CH_2Cl_2 until all of the [Ni(η^4-DEMAMPA-DCB)]$^{2-}$ moved into the organic layer. The combined organic layers were taken to dryness at reduced pressure. The yellow solid was washed with water to remove excess $[Ph_4P]Cl$. The wet solid was then dissolved in CH_2Cl_2 and dried over Na_2SO_4. The solution was filtered and taken to dryness under reduced pressure. Recrystallization was achieved by diffusion of ethyl ether into an acetone solution.

Li[Ni(η^4-DEMAMPA-DCB)]. Li_2[Ni(η^4-DEMAMPA-DCB)] was dissolved in a small amount of 95% EtOH. A small amount of benzoyl peroxide, which is only slightly soluble, was added and the reaction was stirred. The solution turned dark purple in a matter of seconds. After the solution was very dark purple, it was stirred (30 min) to ensure that all the Ni(II) was oxidized. The solution was taken to dryness under reduced pressure (20 °C). The solid was washed with copious amounts of benzene to remove the perox-

ide. Yields are nearly quantitative for Li[Ni(η^4-DEMAMPA-DCB)]. [n.b. Any benzoyl peroxide left in the product makes the Ni(III) Li^+ salt difficult to work with.]

[Ph_4P][Ni(η^4-DEMAMPA-DCB)] and [Bu_4N][Ni(η^4-DEMAMPA-DCB)]. An aqueous solution of [Ph_4P]Cl or [Bu_4N]Cl was slowly added to an aqueous solution of Li[Ni(η^4-DEMAMPA-DCB)]. The purple precipitate was filtered and washed with copious amounts of water. The solid was dissolved in CH_2Cl_2 and briefly dried over Na_2SO_4. The solution was then filtered and taken to dryness under reduced pressure (20 °C). Recrystallization was achieved by diffusion of pentane into a 1,2-dichloroethane solution. Anal. Calcd for [Bu_4N][Ni(η^4-DEMAMPA-DCB)]: C, 57.83; H, 7.87; N, 9.11. Found: C, 57.77; H, 7.83; N, 9.01. UV-vis (CH_2Cl_2) [Bu_4][Ni(η^4-DEMAMPA-DCB)]: 330 nm (8.15×10^3 M^{-1} cm^{-1}), 406 nm (1.68×10^3 M^{-1} cm^{-1}), 418 nm (1.40×10^3 M^{-1} cm^{-1}), 530 nm (1.13×10^3 M^{-1} cm^{-1}), 740 nm (6.15×10^3 M^{-1} cm^{-1}).

[Me_4N][Ni(η^4-DEMAMPA-DCB)]. [Me_4N]Cl was added to an EtOH solution of Li[Ni(η^4-DEMAMPA-DCB)]. The solvent was removed under reduced pressure ($\leq$ 35 °C). The residue was treated with MeCN and filtered. Ethyl ether was added to the filtrate until white solid precipitated (addition of too much ethyl ether precipitates the Ni(III) salt) and the solution was filtered. The solvents were removed under reduced pressure. X-ray quality crystals were grown by vapor diffusion of ethyl ether into an acetonitrile solution. Anal. Calcd for [Me_4N][Ni(η^4-DEMAMPA-DCB)]: C, 50.03; H, 6.05; N, 11.67. Found: C, 50.16; H, 6.04; N, 11.67.

[Et_4N][Ni(η^4-DEMAMPA-DCB)]. One equivalent of [Et_4N][F] was

added to an EtOH solution of Li_2[Ni(η^4-DEMAMPA-DCB)]. Benzoyl peroxide was added along with a few mL of benzene (to solubilize the peroxide). The solution was stirred (10-30 min). The solution was taken to dryness under reduced pressure (20 °C). The residue was thoroughly washed with benzene and filtered. The Ni(III) salt was dissolved in 1,2-dichloroethane, filtered, and crystallized by vapor diffusion of pentane.

Ni(η^4-DEMAMPA-DCB). [Bu_4N][Ni(η^4-DEMAMPA-DCB)] was added to the bulk electrolytic apparatus and the apparatus was then placed in an ice bath. Bulk electrolysis 200 mV above the [Ni(η^4-DEMAMPA-DCB)]$^{0/-}$ couple caused the solution to change from dark purple to dark green. When the coulometer counted less than 10^{-5} C per 10 s, the electrolysis was stopped (the total coulomb count was within 5% of that calculated), the Ni(η^4-DEMAMPA-DCB)/electrolyte solution was transferred to a flask, and the CH_2Cl_2 was removed under reduced pressure. Dry deoxygenated benzene was added to the flask and the [Et_4N][PF_6] was filtered away. Removal of the benzene at reduced pressure left powdery green product. IR (nujol) Ni(η^4-DEMAMPA-DCB): $\bar{\nu}$[cm^{-1}] = 1724, 1672, 1631, 1594.

X-ray Data Collection and Structure Refinement of [Et_4N][Ni(η^4-MAC*)]. Single crystals of [Et_4N][Ni(η^4-MAC*)] at 20± 1°C are monoclinic, space group $P2_1/c\text{-}C_{2h}^5$ (No. 14) with a = 16.173(2) Å, b = 14.538(4) Å, c = 15.977(4) Å, β = 112.81(1)°, V = 3462(1) Å^3, and Z = 4 (d_{calcd} = 1.196 g cm^{-3}; μ_a(CuK$\bar{\alpha}$) = 1.11 mm^{-1}). A total of 5154 independent reflections having 2θ(CuK$\bar{\alpha}$) < 120.0° (the equivalent of 0.65 limiting CuK$\bar{\alpha}$ spheres) were collected on a computer controlled Nicolet autodiffractometer using θ-2θ scans and Nickel-filtered CuK$\bar{\alpha}$ radiation. The structure was solved

using Direct Methods techniques with the Nicolet SHELXTL software package as modified at Crystalytics Company. The resulting structural parameters have been refined to a convergence of R_1(unweighted, based on F) = 0.053 for 2849 independent reflections having $2\theta_{CuK\bar{\alpha}} < 120.0°$ and $I > 3\sigma(I)$ using counter-weighted full-matrix least-squares techniques and a structural model which incorporated anisotropic thermal parameters for all nonhydrogen atoms and isotropic thermal parameters for the hydrogens of the anion. The methyl groups were included in the refinement as idealized sp^3-hybridized rigid rotors and gave final values for the C-C-H angles which ranged from 98° to 121°. The remaining hydrogen atoms were fixed at idealized sp^3-hybridized positions with a C-H bond length of 0.96 Å. The four ethyl groups of the cation appear to be statistically disordered in the lattice with two alternate resolvable orientations. Methylene carbon atoms C_{41}, C_{51}, C_{61}, and C_{71} with N and the methyl carbon atoms represent one orientation for the cation, while C_{42}, C_{52}, C_{62}, and C_{72} with N and the methyl carbon atoms represent the other orientation.

X-ray Data Collection and Structure Refinement of [Et_4N][Ni(η^4-DEMAMPA-DCB)]. Single crystals of [Me_4N][Ni(η^4-DEMAMPA-DCB)] at 20± 1°C are triclinic, space group $P\bar{1}$-C_i^1 (No. 2) with a = 9.319(2) Å, b = 11.176(3) Å, c = 14.716(4) Å, α = 76.46(2)°, β = 76.47(2)°, γ = 88.55(2)°, V = 1448.1(7) Å^3, and Z = 2 (d_{calcd} = 1.377 g cm^{-3}; μ_a(MoK$\bar{\alpha}$) = 0.89 mm^{-1}). A total of 6642 independent reflections having 2θ(MoK$\bar{\alpha}$) < 55.0° (the equivalent of 1.0 limiting CuK$\bar{\alpha}$ spheres) were collected on a computer-controlled Nicolet autodiffractometer using full (0.90°-wide) ω scans and graphite-monochromated MoK$\bar{\alpha}$ radiation. The structure was solved using Direct Methods techniques with the Nicolet SHELXTL software package

as modified at Crystalytics Company. The resulting structural parameters have been refined to a convergence of R_1(unweighted, based on F) = 0.045 for 4743 independent reflections having $2\theta_{MoK\bar{\alpha}} < 55.0°$ and $I > 3\sigma(I)$ using counter-weighted full-matrix least-squares techniques and a structural model which incorporated anisotropic thermal parameters for all hydrogen atoms. The methyl groups were included in the refinement as idealized sp^3-hybridized rigid rotors and gave final values for the N-C-H and C-C-H angles which ranged from 104° to 121°. The remaining hydrogen atoms were fixed at idealized sp^2- or sp^3-hybridized positions with a C-H bond length of 0.96 Å.

References

1. (a) Haines, R. I.; McAuley, A. *Coord. Chem. Rev.* **1981**, *39*, 77–119. (b) Nag, K.; Chakravorty, A. *Coord. Chem. Rev.* **1980**, *33*, 87–147. (c) Lappin, G.; McAuley, A. *Advances in Inorganic Chemistry*, **1988**, *32*, 241–296. (d) Sacconi, L.; Mani, F.; Bencini, A. "Nickel" in *Comprehensive Coordination Chemistry*, Wilkinson, G.; Guillard, R. D.; McCleverty, J. A., Eds.; Pergamon Press: New York, 1987.

2. (a) Cammack, R. in *Advances in Inorganic Chemistry*, **1988**, *32*, 297–333. (b) *Bioinorganic Chemistry of Nickel* Lancaster, J. R. Jr., Ed.; VCH Publishers, Inc.; 1988 New York, N.Y. (c) Margerum, D. W.; Anliker, S. L. In *Bioinorganic Chemistry of Nickel* Lancaster, J. R. Jr., Ed.; VCH Publishers, Inc.; 1988 New York, N.Y., Chapter 2.

3. (a) Yoon, H.; Wagler, T. R.; O'Connor, K. J.; Burrows, C. J. *J. Am. Chem. Soc.* **1990**, *112*, 4568–4570. (b) Kinneary, J. F.; Albert, J. S.; Burrows, C. J. *J. Am. Chem. Soc.* **1988**, *110*, 6124–6129. (c) Yoon, H.; Burrows, C. J. *J. Am. Chem. Soc.* **1988**, *110*, 4087–4089. (d) Kinneary, J. F.; Wagler, T. R.; Burrows, C. J. *Tetrahedron Lett.* **1988**, *29*, 877-880.

4. Mack, D. P.; Dervan, P. B. *J. Am. Chem. Soc.* **1990**, *112*, 4604–4606.

5. (a) Ito, T.; Sugimoto, M.; Toriumi, K.; Ito, H. *Chem. Lett.* **1981**,1477–1478. (b) Zeigerson, E.; Bar, I.; Bernstein, J.; Kirschenbaum, L. J.; Meyerstein, D. *Inorg. Chem.* **1982**, *21*, 73–80. (c) van der Merwe, M. J.; Boeyens, J. C. A.; Hancock, R. D. *Inorg. Chem.* **1983**, *22*, 3489–3490. (d) Grove, D. M.; van Koten, G.; Zoet, R. *J. Am. Chem. Soc.* **1983**, *105*, 1379–1380. (e) Meek, D. W.; Alyea, E. C.; Stalick, J. K.; Ibers, J. A. *J. Am. Chem. Soc.* **1969**, *91*, 4920–4921. (f) Stalick, J. K.; Ibers, J. A. *Inorg. Chem.* **1970**, *9*, 453–458.

6. See for example (a) Cammack, R.; Fernandez, V. M.; Schneider, K. In *Bioinorganic Chemistry of Nickel*; Lancaster, J. R. Jr., Ed.; VCH: New York, 1988; Chapter 8. (b) Krüger, H.-J.; Holm, R. H. *J. Am. Chem. Soc.* **1990**, *112*, 2955–2963. (c) cf Figure 9 of: Krüger, H.-J.; Peng, G.; Holm, R. H. *Inorg. Chem.* **1991**, *30*, 734–742 and references therein.

7. Jensen, K. A. *Z. Anorg. Allg. Chem.* **1936**, *229*, 265–281.

8. Meek, D. W.; Alyea, E. C.; Stalick, J. K.; Ibers, J. A. *J. Am. Chem. Soc.* **1969**, *91*, 4920–4921.

9. Koola, J. D.; Kochi, J. K. *Inorg. Chem.* **1987**, *26*, 908–916.

10. de Castro, B.; Freire, C. *Inorg. Chem.* **1990**, *29*, 5113–5119.

11. (a) Bour, J. J.; Steggerda, J. J. *J. Chem. Soc., Chem. Commun.* **1967**, 85–86. (b) Bour, J. J.; Birker, P. J. M. W. L.; Steggerda, J. J. *Inorg. Chem.* **1971**, *10*, 1202–1205. (c) Bour, J. J.; aan de Brugh-Arts, J. H. M.; Hendriks, H. M. J.; Steggerda, J. J. *Rec. Trav. Chim. Pays-Bas* **1977**, *96*, 125–128.

12. For crystallographically characterized complexes see: (a) Reith, W.; Polborn, K.; Amberger, E. *Angew. Chem., Int. Ed. Engl.* **1988**, *27*, 699–700. (b) Mentzafos, D.; Hountas, A.; Terzis, A. *Acta Crystallogr., Sect. C* **1988**, *44*, 1550. (c) Welch, J. H.; Bereman, R. D.; Singh, P. *Inorg. Chem.* **1988**, *27*, 3680–3682. (d) Kato, R.; Kobayashi, H.; Kim, H.; Kobayashi, A.; Sasaki, Y.; Mori, T.; Inokuchi, H. *Chem. Lett.* **1988**, 865–868. (e) Clemenson, P. I.; Underhill, A. E.; Hursthouse, M. B.; Short, R. L. *J. Chem. Soc., Dalton Trans.* **1988**, 1689–1691. (f) Kim, H.; Kobayashi, A.; Sasaki, Y.; Kato, R.; Kobayashi, H.; Nakamura, T.; Nogami, T.; Shirota, Y. *Bull. Chem. Soc. Jpn.* **1988**, *61*, 2559–2562. (g) Sandman, D. J.; Allen, G. W.; Acampora, L. A.; Stark, J. C.; Jansen, S.; Jones, M. T.; Ashwell, G. J.; Foxman, B. M. *Inorg.*

Chem. **1987**, *26*, 1664–1669. (h) Kramer, G. J.; Groeneveld, L. R.; Joppe, J. L.; Brom, H. B.; De Jongh, L. J.; Reedijk, J. *Synthetic Metals* **1987**, *19*, 745–750. (i) Bousseau, M.; Valade, L.; Legros, J.-P.; Cassoux, P.; Garbauskas, M.; Interrante, L. V. *J. Am. Chem. Soc.* **1986**, *108*, 1908–1916. (j) Johannsen, I.; Bechgaard, K.; Rindorf, G.; Thorup, N.; Jacobsen, C. S.; Mortensen, K. *Synthetic Metals* **1986**, *15*, 333-343. (k) Kato, R.; Kobayashi, H.; Kobayashi, A.; Sasaki, Y. *Bull. Chem. Soc. Jpn.* **1986**, *59*, 627–630. (l) Groeneveld, L. R.; Schuller, B.; Kramer, G. J.; Haasnoot, J. G.; Reedijk, J. *Recl. Trav. Chim. Pays-Bas* **1986**, *105*, 507–509. (m) Vance, C. T.; Bereman, R. D.; Bordner, J.; Hatfield, W. E.; Helms, J. H. *Inorg. Chem.* **1985**, *24*, 2905–2910. (n) Kobayashi, H.; Kato, R.; Kobayashi, A.; Sasaki, Y. *Chem. Lett.* **1985**, 535–538. (o) Kato, R.; Kobayashi, H.; Kobayashi, A.; Sasaki, Y. *Chem. Lett.* **1985**, 131–134. (p) Kisch, H.; Fernández, A.; Wakatsuki, Y.; Yamazaki, H. *Z. Naturforsch., B: Anorg. Chem., Org. Chem.* **1985**, *B40*, 292–297. (q) Kobayashi, H.; Kato, R.; Kobayashi, A.; Sasaki, Y. *Chem. Lett.* **1985**, 191–194. (r) Kuppusamy, P.; Manoharan, P. T.; Mahadevan, C.; Seshasayee, M. *J. Cryst. Spec. Res.* **1985**, *15*, 359–376. (s) Mahadevan, C.; Seshasayee, M.; Kuppusamy, P.; Manoharan, P. T. *J. Cryst. Spec. Res.* **1985**, *15*, 305–316. (t) Mahadevan, C.; Seshasayee, M.; Kuppusamy, P.; Manoharan, P. T. *J. Cryst. Spec. Res.* **1984**, *14*, 179–191. (u) Cotrait, M.; Gaultier, J.; Polycarpe, C.; Giroud, A. M.; Mueller- Westerhoff, U. T. *Acta Crystallogr., Sect. C* **1983**, *C39*, 833–835. (v) Valade, L.; Bousseau, M.; Gleizes, A.; Cassoux, P. *J. Chem. Soc., Chem. Commun.* **1983**, 110–112. (w) Lindqvist, O.; Andersen, L.; Sieler, J.; Steimecke, G.; Hoyer, E. *Acta Chem. Scand.* **1982**, *A36*, 855–856. (x) Brown, R. K.; Bergendahl, T. J.; Wood, J. S.; Waters, J. H. *Inorg. Chim.*

Acta **1983**, *68*, 79–85. (y) Mahadevan, C.; Seshasayee, M.; Murthy, B. V. R.; Kuppusamy, P.; Manoharan, P. T. *Acta Crystallogr., Sect. C* **1983**, *C39*, 1335–1338. (z) Manoharan, P. T.; Noordik, J. H.; de Boer, E.; Keijzers, C. P. *J. Chem. Phys.* **1981**, *74*, 1980–1989. (aa) Kobayashi, A.; Sasaki, Y. *Bull. Chem. Soc. Jpn.* **1977**, *50*, 2650–2656. (bb) Singhabhandhu, A.; Robinson, P. D.; Fang, J. H.; Geiger, W. E., Jr. *Inorg. Chem.* **1975**, *14*, 318–323. (cc) Herman, A.; Wing, R. M. *J. Organomet. Chem.* **1973**, *63*, 441–450. (dd) Wing, R. M.; Schlupp, R. L. *Inorg. Chem.* **1970**, *9*, 471–475. (ee) Schmitt, R. D.; Wing, R. M.; Maki, A. H. *J. Am. Chem. Soc.* **1969**, *91*, 4394–4401.

13. See for example: (a) McCleverty, J. A. *Prog. Inorg. Chem.* **1968**, *10*, 49–221. (b) Davison, A.; Edelstein, N.; Holm, R. H.; Maki, A. H. *Inorg. Chem.* **1963**, *2*, 1227–1232. (c) Shupack, S. I.; Billig, E.; Clark, R. J. H.; Williams, R.; Gray, H. B. *J. Am. Chem. Soc.* **1964**, *86*, 4594–4602. (d) Balch, A. L.; Röhrscheid, F.; Holm, R. H. *J. Am. Chem. Soc.* **1965**, *87*, 2301–2302. (e) Stiefel, E. I.; Waters, J. H.; Billig, E.; Gray, H. B. *J. Am. Chem. Soc.* **1965**, *87*, 3016–3017. (f) Holm, R. H.; Balch, A. L.; Davison, A.; Maki, A. H.; Berry, T. E. *J. Am. Chem. Soc.* **1967**, *89*, 2866–2874. (g) Schmitt, R. D.; Maki, A. H. *J. Am. Chem. Soc.* **1968**, *90*, 2288. (h) Dori, Z.; Eisenberg, R.; Stiefel, E. I.; Gray, H. B. *J. Am. Chem. Soc.* **1970**, *92*, 1506–1511.

14. Drago, R. S.; Baucom, E. I. *Inorg. Chem.* **1972**, *11*, 2064–2069.

15. Schlemper, E. O.; Murmann, R. K. *Inorg. Chem.* **1983**, *22*, 1077–1081.

16. Gordon, G. C.; Peng, S.-M.; Goedken, V. L. *Inorg. Chem.* **1978**, *17*, 3578–3586.

17. (a) Foust, A. S.; Soderberg, R. H. *J. Am. Chem. Soc.* **1967**, *89*, 5507–

5508. (b) Gleizes, A.; Marks, T. J.; Ibers, J. A. *J. Am. Chem. Soc.* **1975**, *97*, 3545–3546. (c) Cowie, M.; Gleizes, A.; Grynkewich, G. W.; Kalina, D. W.; McClure, M. S.; Scaringe, R. P.; Teitelbaum, R. C.; Ruby, S. L.; Ibers, J. A.; Kannewurf, C. R.; Marks, T. J. *J. Am. Chem. Soc.* **1979**, *101*, 2921–2936.

18. Wolberg, A.; Manassen, J. *Inorg. Chem.* **1970**, *9*, 2365–2367.

19. See for example (a) Lovecchio, F. V.; Gore, E. S.; Busch, D. H. *J. Am. Chem. Soc.* **1974**, *96*, 3109–3118. (b) Fox, S.; Wang, Y.; Silver, A.; Millar, M. *J. Am. Chem. Soc.* **1990**, *112*, 3218–3220. (c) Takvoryan, N.; Farmery, K.; Katovic, V.; Lovecchio, F. V.; Gore, E. S.; Anderson, L. B.; Busch, D. H. *J. Am. Chem. Soc.* **1974**, *96*, 731–742.

20. Zimmer, M.; Schulte, G.; Luo, X.-L.; Crabtree, R. H. *Angew. Chem. Int. Ed. Engl.* **1991**, *30*, 193–194.

21. (a) Jarvis, J. A. J.; Mais, R. H. B.; Owston, P. G. *J. Chem. Soc., Sect. A* **1968**, 1473–1486. (b) Garton, G.; Henn, D. E.; Powell, H. M.; Venanzi, L. M. *J. Chem. Soc.* **1963**, 3625–3629. (c) Kilbourn, B. T.; Powell, H. M. *J. Chem. Soc., Sect. A* **1970**, 1688–1693.

22. IR (KBr pellet) $[Et_4N]_2[Ni(\eta^4\text{-DEMAMPA-DCB})]$: $\bar{\nu}[cm^{-1}] = 1610$, 1576, 1544. IR (KBr pellet) $[Ph_4P]_2[Ni(\eta^4\text{-MAC*})]$: $\bar{\nu}[cm^{-1}] = 1697$ (ketone), 1579.

23. UV-vis (CH_2Cl_2) $[Ph_4P]_2[Ni(\eta^4\text{-MAC*})]$: 416 nm (130 M^{-1} cm^{-1}), 496 nm (110 M^{-1} cm^{-1}). UV-vis (CH_2Cl_2) $[Et_4N]_2[Ni(\eta^4\text{-DEMAMPA-DCB})]$: 432 nm ($\approx$200 M^{-1} cm^{-1}).

24. Kimura, E.; Machida, R.; Kodama, M. *J. Am. Chem. Soc.* **1984**, *106*, 5497–5505.

25. IR (nujol) $[Bu_4N][Ni(\eta^4\text{-DEMAMPA-DCB})]$: $\bar{\nu}[cm^{-1}] = 1629$, 1573.

IR (nujol) $[Et_4N][Ni(\eta^4\text{-MAC*})]$: $\bar{\nu}[cm^{-1}] = 1707$ (ketone), 1604, 1576, 1554. IR (nujol) $Ni(\eta^4\text{-DEMAMPA-DCB})$: $\bar{\nu}[cm^{-1}] = 1724$, 1672, 1631, 1594.

26. Thöm, V. J.; Boeyens, J. C. A.; McDougall, G. J. Hancock, R. D. *J. Am. Chem. Soc.* **1984**, *106*, 3198–3207.

27. The electronic spectrum of $[Ni(\eta^4\text{-MAC*})]^-$ with excess CN^- in CH_2Cl_2 is a featureless curve, tailing off into the visible region from just above the UV cutoff of the solvent; there is essentially zero absorbance above 450 nm.

28. Drago, R. S. *Physical Methods in Chemistry*; W. B. Saunders: Philadelphia, 1977; inside cover, "Properties of Selected Nuclei."

29. (a) Collins, T. J.; Nichols, T. R.; Uffelman, E. S. *J. Am. Chem. Soc.* **1991**, *113*, 4708–4709. (b) Nichols, T. R. M.S. Thesis, Carnegie Mellon University, 1991.

Chapter 8

Copper(III) Complexes of Macrocyclic Tetraamido-*N* Ligands

This chapter will very briefly summarize the copper results obtained with the macrocycles of this thesis. This work is ongoing; a crystal structure of $[Me_4N][Cu(\eta^4\text{-DEMAMPA-DCB})]$ is currently being solved.[1] The remarkably robust copper(III) species obtained with the macrocycles encourage us to believe that we may be able to isolate an organometallic Cu(III) species and a high potential neutral copper species. Results from the literature have recently been reviewed[2] and been discussed by Treco.[2b]

Results and Discussion

The insertion of copper into the macrocyclic tetraamides of this thesis is distinctive. Unlike the insertion reactions for the other first row metals, the use of a strong base and a Cu(II) salt in THF has been unsuccessful to date. Ironically, the anhydrous MeCN/proton sponge method which works for copper (see Figure 2.20), has not worked for the other metals to date. In addition, $(\eta^4\text{-MAC*})^{4-}$ has not yet been coordinated to copper using either method.

Unlike all of the other insertions, the copper insertion almost certainly does not proceed via a poly- or perhaps tetra-deprotonated ligand, because Proton Sponge is a much weaker base than $Li[(Me_3Si)_2N]$ or *tert*-butyllithium.[3] Thus, it is speculated that the insertion begins in one of two ways, either the copper acetate reacts with the equilibrium concentration of monodeprotonated macrocycle to form an intermediate whose pKa's 2, 3, and 4 are lowered by the immediate proximity of the divalent copper center, or the copper acetate has a viable equilibrium interaction with the fully protonated complex which lowers pKa 1 and allows the reaction to proceed. Whether copper is initially O- or N-bound to the amide is conjectural. CPK models of the ligand indicate it is rather "stiff," and it is tempting to speculate that the subsequent

binding required (after the initial ligation occurs) happens primarily by dissociative means.[4] Whether H_4MAC* has failed to coordinate so far because it, presumably, has a higher pKa 1 than H_4DEMAMPA-DCB (and derivatives), or because it is stucturally less amenable to the required transition states is a matter of speculation. Although it is assumed that the Cu(II) complex of the ligand is fully formed before oxidation occurs (based primarily on ligand donor strength arguments), this does not have to be the case.

The ^{1}H NMR spectra of the copper complexes at room temperature are diamagnetic and consistent with a C_{2v} square planar d^8 system.[5] The ligand based reactivity of [Cu(η^4-DEMAMPA-B)]$^-$ may be followed by NMR and indicates the necessity of having the DEMAMPA-DCB system available. Exposure of [Cu(η^4-DEMAMPA-B)]$^-$ to Br_2 causes aromatic ring halogenation, but does not lead to decomposition.[6] Exposure of [Cu(η^4-DEMAMPA-DCB)]$^-$ to Br_2 or even Cl_2 causes no reaction. These results further indicate that ligand degradation problems which had afflicted virtually every ligand produced for oxidation systems, including earlier Collins group acyclic ligands, have been eliminated to a significant degree in the macrocyclic systems of this thesis. Remarkably, treatment of aqueous Li[Cu(η^4-DEMAMPA-DCB)]$^-$ with HBF_4 gives a precipitate of a monoprotonated neutral complex, with no decomposition.

Copper chemistry has special significance to the area of inorganic oxidation chemistry, because the Cu(III)/Cu(II) couple is highly sensitive to the σ-donor strength of a square planar ligand complement. Because Cu(II) is a d^9 metal ion and there are only five d orbitals, the highest energy electron is almost inevitably found in an orbital which points directly at the ligand donor atoms

(see Chapter 1 and Figure 1.4). The Cu(III/II) couples for the macrocycles of this thesis (Table 8.1 and Figure 8.1) may be directly compared with previous Cu(III/II) couples obtained in the Collins group (see Table 1.1). It is interesting to note that the Cu(III/II) potential for [Cu(η^4-DEMAMPA-DCB)]$^-$ and [Cu(η^4-HMPA-DCB)]$^-$ differ by only 20 mV. The Cu(III/II) potential for [Cu(η^4-DEMAMPA-DMB)]$^-$ is within 35 mV of that for [Cu(η^4-HMPA-DMP)]$^-$. While it was observed that the acyclic [Cu(η^4-HMPA-DMP)]$^-$ system slowly decomposed in solution,[2b] the macrocyclic species are stable in solution indefinitely. Collins group compounds have the lowest potentials observed for the Cu(III/II) couple, and the Cu(III/II) couples shown for the macrocycles of this thesis are as much as 1.9 V lower than those of some cyclam-type macrocycles.[2a]

Table 8.1. Copper Electrochemistry in MeCN (V vs. Fc^+/Fc)

Complex	$[Cu]^{0/-}$	Cu(III/II)
[Cu(η^4-DEMAMPA-DCB)]$^-$	0.830	−0.815
[Cu(η^4-DEMAMPA-B)]$^-$	0.675*	−0.955*
[Cu(η^4-DEMAMPA-DMB)]$^-$	0.530	−0.965
[Cu(η^4-DEMAMPA-DMOB)]$^-$	0.230	−0.940*
* denotes a couple which is not fully reversible		

Unlike the previous copper complexes of the Collins group acyclic ligands, [Cu(η^4-DEMAMPA-DCB)]$^-$ and its derivatives exhibit high potential *reversible* waves corresponding to oxidation of the copper(III) macrocyclic species (Table 8.1 and Figure 8.2). Even though the oxidations in these compounds are almost certainly predominantly ligand-localized (because of the very high

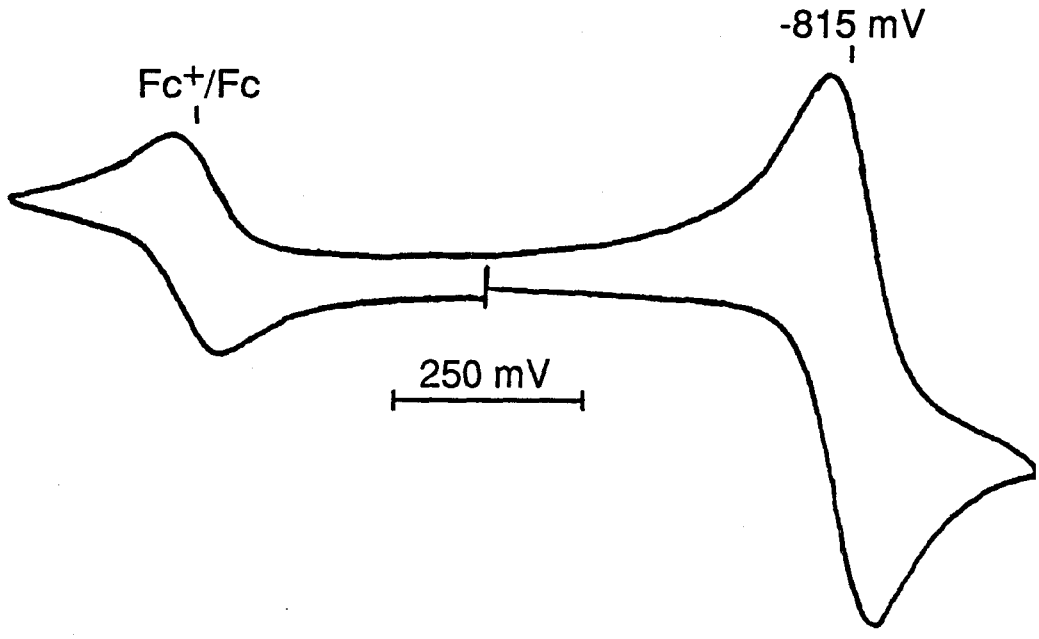

Figure 8.1. Cyclic voltammetry of $[Me_4N][Cu(\eta^4\text{-DEMAMPA-DCB})]$ and ferrocene in MeCN (0.1 M $[Me_4N][ClO_4]$ supporting electrolyte, 1.300 V sweep-width).

formal potentials) further characterization of these species by EPR will be very worthwhile. If these species are isolable, they will be of great interest, since they will be potent neutral electron transfer oxidants, similar to the cobalt complexes discussed in Chapter 6, but even more oxidizing.

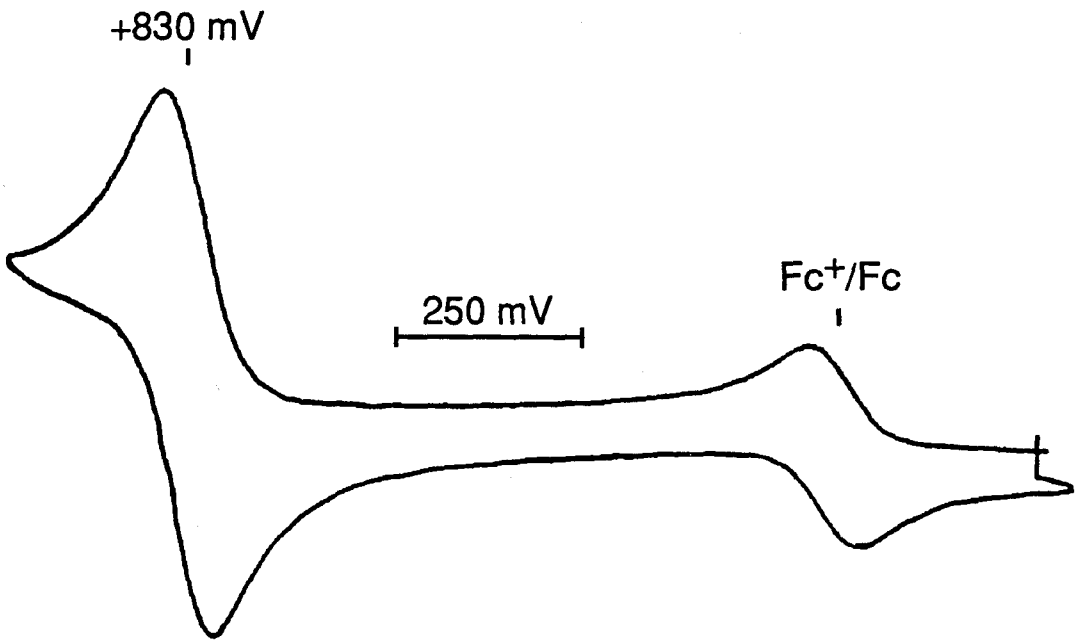

Figure 8.2. Cyclic voltammetry of $[Me_4N][Cu(\eta^4\text{-DEMAMPA-DCB})]$ and ferrocene in MeCN (0.1 M $[Me_4N][ClO_4]$ supporting electrolyte, 1.400 V sweep-width).

Experimental

Materials. All solvents and reagents were reagent grade (Aldrich) and were used as received except as described for electrochemical measurements.

Physical Measurements. ^{1}H NMR were measured at 300 MHz on an IBM NR/300 FT-NMR Spectrometer. ^{1}H NMR data are reported in δ vs. $(CH_3)_4Si$ with the solvent as internal standard. EPR spectra were recorded on a Bruker ER300 Spectrometer. Infrared data were obtained on a Nicolet 5DXB FT-IR Spectrometer.

Electrochemical Data. Cyclic voltammetry was performed on a Princeton Applied Research Model 173/179 potentiostat/digital coulometer equipped with positive feedback IR compensation and a Model 175 universal programmer. Current voltage curves were recorded on a Houston Instruments Model 2000 X-Y recorder.

Sureseal anhydrous MeCN (Aldrich) was used as received. $[Bu_4N][ClO_4]$ (Fluka) was vacuum dried at 80 °C. In all cases experiments were performed under N_2 with a supporting electrolyte concentration of 0.1 M. Cyclic voltammetry was performed in MeCN solutions of $[Bu_4N][ClO_4]$ at a 3 mm Pt disk working electrode with a silver wire quasi-reference electrode and a Pt foil counter electrode. At the conclusion of each experiment, ferrocene (Fc) was added as an internal potential standard. All formal potentials were taken as the average of anodic and cathodic peak potentials and are reported vs. the Fc^+/Fc couple. Peak-to-peak separation of the Fc^+/Fc couple was similar to that of the Cu couples in all cases. Plots of peak current vs. the square root of scan rate over the range 10–500 mV s^{-1} were made and found to be linear for couples that are stated to be reversible.

Synthetic Note. Work with the copper compound is ongoing. The crystal structure of [Me_4N][Cu(η^4-DEMAMPA-DCB)] is currently being determined. Small samples of H_4DEMAMPA-DMOB and H_4DEMAMPA-DMB were obtained from Mr. José Workman and Mr. Michael Bartos, respectively.

[HSponge][Cu(η^4-DEMAMPA-DCB)]. Hydrated Proton Sponge (N,N,N′,N′-tetramethyl-1,8-naphthalenediamine, 26.24 g) was dissolved in dry MeCN (600 mL decanted from 3 Å sieves), and this solution was poured into a screw top Nalgene bottle (1 L) containing 250 mL of 3 Å molecular sieves (dryed 24 h, 150 °C). This stock solution was used after drying was judged complete (48 h). H_4DEMAMPA-DCB (0.246 g, 0.522 mmol) and anhydrous $Cu(OAc)_2$ (0.115 g, 0.633 mmol) were added to a round bottom flask (25 mL) equipped with a reflux condensor and a drying tube. Stock Proton Sponge solution (13.0 mL) was added to the solids. The mixture turned dark red-brown as the solution was heated. The suspension was heated under reflux (8 h). After cooling, the dark red-brown solution was evaporated to dryness under reduced pressure. The solid residue was redissolved in acetone and applied to a silica gel pad (3.8 cm in a 30 mL sintered glass crucible) which was eluted with acetone until all of the red-brown color was gone (a blue residue remained on the silica gel). The acetone solution was taken to dryness under reduced pressure, and the product was redissolved in CH_2Cl_2. The CH_2Cl_2 solution was filtered, and the filtrate was evaporated to dryness under reduced pressure. The solid was washed with a very small amount of $CHCl_3$ and then with copious amounts of pentane. The powder was dried in vacuo (0.372 g, 91.9% yield). Anal. Calcd for [HSponge][Cu(η^4-DEMAMPA-DCB)]·H_2O: C, 55.01; H, 5.94; N, 11.00. Found: C, 55.25; H, 5.69; N, 10.94.

[Me_4N][Cu(η^4-DEMAMPA-DCB)]. [HSponge][Cu(η^4-DEMAMPA-DCB)] (0.211 g) was dissolved in a minimum of EtOH (100%) and solid [Me_4N][OH]·$5H_2O$ was added. The solution was taken to dryness under reduced pressure and the solids were washed with pentane and CH_2Cl_2 and then redissolved in MeCN. This solution was filtered through celite and then taken to dryness under reduced pressure. The solids were dissolved in EtOH, water was added, and the solution was concentrated until all of the solid reprecipitated. The solid was filtered, washed copiously with water, and then redissolved in EtOH (100%). The ethanolic solution was taken to dryness under reduced pressure and the solid was washed with pentane to yield the product as a powder (0.134 g, 78.3%). Anal. Calcd for [Me_4N][Cu(η^4-DEMAMPA-DCB)]·H_2O: C, 49.63; H, 6.00; N, 11.57. Found: C, 49.25; H, 5.89; N, 11.34. ^{1}H NMR (CD_3OD): 8.20 (s, 2H), 3.19 (cation, s, 12H), 1.77 (q, 4H, 8 Hz), 1.73 (s, 12H), 0.80 (t, 6H, 8 Hz). IR (nujol/MeCN) $\bar{\nu}$[cm^{-1}] = 1649, 1620, 1582, 1559. Large dark red-brown crystals suitable for diffraction were grown by vapor diffusion of ethyl ether into an acetonitrile solution.

[Bu_4N][Cu(η^4-DEMAMPA-DCB)]. [HSponge][Cu(η^4-DEMAMPA-DCB)] was dissolved in absolute EtOH and an excess of aqueous solution of [Bu_4N][OH] (40% by weight) was added. The solution was taken to dryness under reduced pressure, the residue was washed copiously with water, dissolved in CH_2Cl_2, and the CH_2Cl_2 solution was dried over Na_2SO_4. The CH_2Cl_2 solution was taken to dryness under reduced pressure and the solid was redissolved in a minimum of 1,2-dichloroethane. Crystalline product was obtained by vapor diffusion of pentane into this solution (yield typically 75%). ^{1}H NMR ($CDCl_3$): 8.22 (s, 2H), 3.01 (cation, t, 8H), 1.75 (q, 4H, 7 Hz), 1.69

(s, 12H), 1.55 (cation, m, 8H), 1.37 (cation, m, 8H), 0.96 (cation, t, 12H), 0.73 (t, 6H, 7 Hz).

Li[Cu(η^4-DEMAMPA-DCB)]. [HSponge][Cu(η^4-DEMAMPA-DCB)] was dissolved in EtOH, LiOH (1.2 equiv) was added, and the mixture was stirred (10 min). The EtOH was removed under reduced pressure, and the solid was washed copiously with CH_2Cl_2 to leave the powdery product.

[Ph_4P][Cu(η^4-DEMAMPA-DCB)]. Li[Cu(η^4-DEMAMPA-DCB)] was dissolved in water and a concentrated aqueous solution of [Ph_4P]Cl was added. The precipitated product was washed thoroughly with water, dissolved in CH_2Cl_2, and the CH_2Cl_2 solution was dried over Na_2SO_4. The CH_2Cl_2 solution was taken to dryness under reduced pressure and the product was redissolved in 1,2-dichloroethane. Crystalline product was obtained by vapor diffusion of pentane into this solution (yield typically 75%).

The analogous macrocyclic derivatives are made using identical procedures:

Li[Cu(η^4-DEMAMPA-B)]. Anal. Calcd for Li[Cu(η^4-DEMAMPA-B)]·$4H_2O$: C, 46.62; H, 6.33; N, 10.36. Found: C, 46.24; H, 5.92; N, 10.25.

[Ph_4P][Cu(η^4-DEMAMPA-B)]. Anal. Calcd for [Ph_4P][Cu(η^4-DEMAMPA-B)]: C, 67.44; H, 5.79; N, 6.99; P, 3.86. Found: C, 67.20; H, 5.69; N, 6.85; P, 3.87.

[Bu_4N][Cu(η^4-DEMAMPA-B)]. ^{1}H NMR ($CDCl_3$): 8.15 + 6.83 (AA′BB′ multiplet, 4H), 3.06 (cation, t, 8H), 1.82 (q, 4H, 8.5 Hz), 1.77 (s, 12H), 1.55 (cation, m, 8H), 1.42 (cation, m, 8H), 1.02 (cation, t, 12H), 0.80 (t, 6H, 8.5 Hz). IR (nujol) $\bar{\nu}$[cm^{-1}] = 1631, 1584, 1571, 1562.

[Bu_4N][Cu(η^4-DEMAMPA-DMB)]. Anal. Calcd for [Bu_4N][Cu(η^4-

DEMAMPA-DMB)]: C, 63.95; H, 9.08; N, 9.56. Found: C, 63.94; H, 9.17; N, 9.63. ^{1}H NMR ($CDCl_3$): 7.97 (s, 2H), 3.12 (cation, t, 8H), 2.15 (s, 6H), 1.82 (q, 4H, 8 Hz), 1.78 (s, 12H), 1.56 (cation, m, 8H), 1.43 (cation, m, 8H), 1.02 (cation, t, 12H), 0.82 (t, 6H, 8 Hz).

[HSponge][Cu(η^4-DEMAMPA-DMOB)]. Anal. Calcd for [HSponge]-[Cu(η^4-DEMAMPA-DMOB)]·1.5H_2O: C, 58.14; H, 6.86; N, 10.99. Found: C, 58.32; H, 6.67; N, 10.93.

[Bu_4N][Cu(η^4-DEMAMPA-DMOB)]. ^{1}H NMR (CD_2Cl_2): 7.80 (s, 2H), 3.68 (s, 6H), 3.00 (cation, t, 8H), 1.63 (q, 4H, 8 Hz), 1.61 (s, 12H), 1.50 (cation, m, 8H), 1.33 (cation, m, 8H), 0.93 (cation, t, 12H), 0.67 (t, 6H, 8 Hz).

References

1. The crystal structure is being solved by Dr. Clifford Rickard of the University of Auckland, New Zealand.

2. (a) Levason, W.; Spicer, M. D. *Coord. Chem. Rev.* **1987**, *76*, 45–120. (b) Treco, B. G. R. T. Ph.D. Thesis, California Institute of Technology, 1988. (c) Margerum, D. W.; Owens, G. D. *Metal Ions in Biological Systems* **1981**, *12*, 75. (d) Anson, F. C.; Collins, T. J.; Richmond, T. G.; Santarsiero, B. D.; Toth, J. E.; Treco, B. G. R. T. *J. Am. Chem. Soc.* **1987**, *109*, 2974–2979.

3. Monoprotonated Proton Sponge cation has a pKa of 12.3. Proton Sponge (N,N,N′,N′-tetramethyl-1,8-naphthalenediamine) derives its significant basicity (seven orders of magnitude greater than aniline and two greater than triethylamine) from the steric clash of the methyls which prevents the nitrogen lone pairs from interacting directly with the aromatic system (the major cause) and from its ability to "chelate" a proton (the secondary cause). See: Alder, R. W.; Bowman, P. S.; Steele, W. R. S.; Winterman, D. R. *J. Chem. Soc., Chem. Commun.* **1968**, 723–724.

4. Lindoy, L. F. "The Chemistry of Macrocyclic Ligand Complexes"; Cambridge University Press: New York, 1989.

5. See the Experimental for ^{1}H NMR data. It is worth noting that the complexes appear to go paramagnetic in CD_2Cl_2 at 230 K. The reason for this is not yet known, but parallels the NMR results for the Ni(II) compounds (see Chapter 7).

6. Bromination eliminates the AA′BB′ splitting observed at 8.15 + 6.83 and leaves a less-split set of aromatic resonances with less integrated intensity relative to the aliphatic signals, which remain unaffected.

Chapter 9

Nonplanar Amides in Complexes of Macrocyclic Tetraamido-*N* Ligands

This chapter discusses the amide nonplanarity found in many of the macrocyclic complexes reported in this thesis. It will be seen that square planar complexes of $(\eta^4$-DEMAMPA-DCB$)^{4-}$ have planar amides and that square pyramidal complexes exhibit amide nonplanarity. It will also be seen that all complexes of $(\eta^4$-MAC*$)^{4-}$ should be expected to have nonplanar amides.

Background

In a ground-breaking series of papers,[1,2] the Collins group demonstrated that the Dunitz nonplanar amide analysis[3] could be applied to inorganic complexes of amido-*N* ligands. Three separate classes of nonplanar amide ligands were synthesized—the first in inorganic chemistry.

A typical representation of bonding in an amide is represented in Figure 9.1.* In this normal picture, there are three significant resonance structures involving sp^2 hybridized C, N, and O atoms. The resonance structure with a double bond between the carbon and nitrogen atoms is the contributor used to explain the barrier to rotation about the C–N bond (10–35 kcal/mol) and the planarity of the amide group.[5] However, with osmium complexes of the CHBA-DCB and HBA-B ligands metal oxidation or coordination of π-acids generated *cis*-α complexes, while ligand substitution by bidentate chelating ligands, such as 2,2′-bipyridyl, led to *cis*-β complexes (See Figure 1.15.). The only way to achieve these geometries with ligands with such limited rotational degrees of freedom was to generate nonplanar amides. Ultimately, three distinct classes of inorganic nonplanar amides have been elucidated by the Collins group to

* Although Wiberg et. al. have severely questioned this picture for simple organic amides, in the absence of theoretical study of transition metal bound amido-*N* ligands, the classical resonance formulation will be used in this discussion.[4]

date:[2]

(i) amides nonplanar due to enhanced thermodynamic stability over the structurally accessible planar form (a class never before observed in chemistry),

(ii) amides nonplanar due to ring strain (a class previously primarily of significance only in organic chemistry),

(iii) amides nonplanar due to steric clash (a class never documented in organic chemistry and rarely documented in inorganic chemistry).

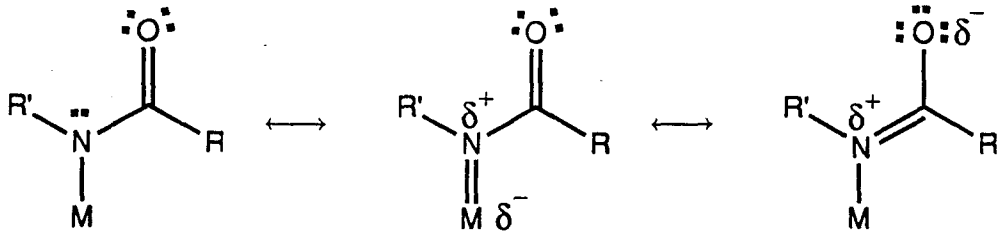

Figure 9.1. Amide resonance structures.

The nonplanarity of amides may be effectively analyzed in terms which Dunitz, et al. derived from crystallographic parameters.[3] In any nonlinear molecule there are $3N - 6$ coordinates needed to specify the relative positions of N atoms and $2N - 3$ of these coordinates may be chosen to lie in a plane. Dunitz realized that, with six atoms associated with the amide group and $N - 3$ remaining coordinates, there must be three terms which describe displacement from the chosen plane. By taking combinations of the torsion angles involved with the six atoms associated with the amide group, Dunitz was able to define the three terms (Figure 9.2). The twist angle τ and the pyramidalization terms χ_C and χ_N are ob-

tained from the primary torsion angle data ω_1, ω_2, and ω_3 as follows:*

$$\tau = (\omega_1 + \omega_2)/2$$

$$\chi_N = (\omega_2 - \omega_3 + \pi) mod 2\pi$$

$$\chi_C = (\omega_1 - \omega_3 + \pi) mod 2\pi$$

The $\bar{\tau}$ term equals the angle between the p orbitals on carbon and nitrogen ($\bar{\tau} = (\tau) mod \pi$).[2a] Although it loses the distinction between *cis* and *trans* amides, $\bar{\tau}$ is easily visualized and can be interpreted as the angle between the idealized positions of the $p\pi$ orbitals on C and N and maximizes at $\pm 90°$. The pyramidalization terms equal $\pm 60°$ for idealized sp^3 hybridized atoms. The signs of the torsion angles and the resultant nonplanar amide terms are chosen to be consistent with IUPAC-IUB recommendations for biochemical nomenclature. Of these amide distortions, χ_N distortions cost the least energy, followed by $\bar{\tau}$ distortions, and distantly followed by χ_C distortions. These trends are revealed by force field calculations[3] and in plots of inorganic structural data compiled by Collins, Keech, and Peake (Figures 9.3 and 9.4). Peake and Keech found that amides of the first class, i.e., amides nonplanar due to enhanced stability over the structurally accessible planar form, were formed exclusively in complexes rendered electron defficient either by oxidation or by coordination of a π-acid. Studies by Keech revealed that, as expected from resonance arguments, the nonplanar amides are better donors to metals than their planar analogues, sometimes lowering redox couples as much as 460 mV (Figure 9.5).

---

* Employing the fourth torsion angle associated with the six atoms leads to redundancy. Since $(\omega_1 + \omega_2) - (\omega_3 + \omega_4) = 0 (mod 2\pi)$, χ_N may also be defined as $\chi_N = (-\omega_1 + \omega_4 + \pi) mod 2\pi$ and χ_C as $\chi_C = (-\omega_2 + \omega_4 + \pi) mod 2\pi$.

It was conclusively shown that the different spatial distribution of the donor atoms had virtually no effect on the redox potentials (Figure 9.6). Thus, by lowering the percentage contribution of the C–N double bond resonance structure to the resonance hybrid, amide nonplanarity localizes negative charge on nitrogen, making the amide a stonger σ and π donor.

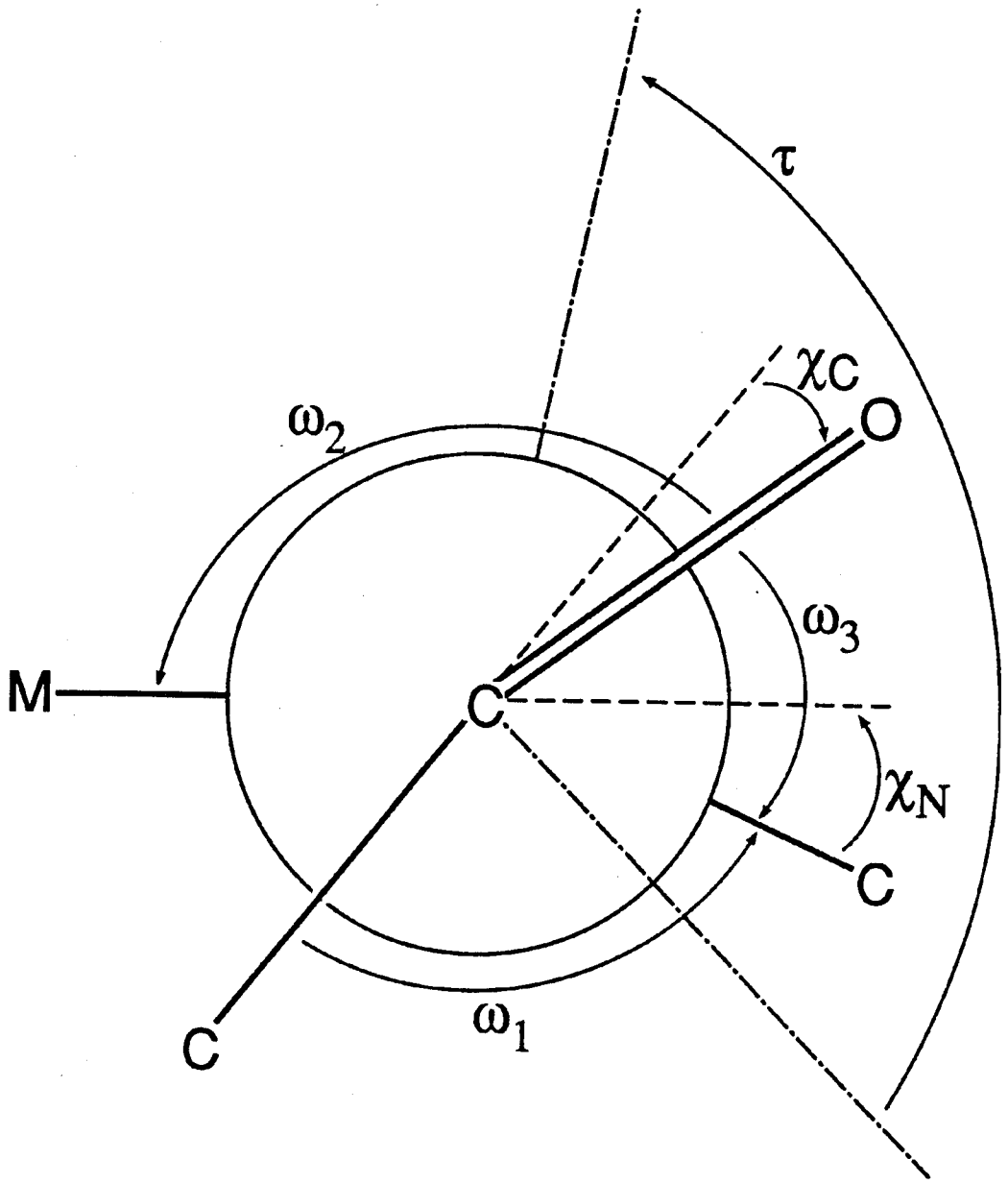

Figure 9.2. The Dunitz amide nonplanarity parameters.

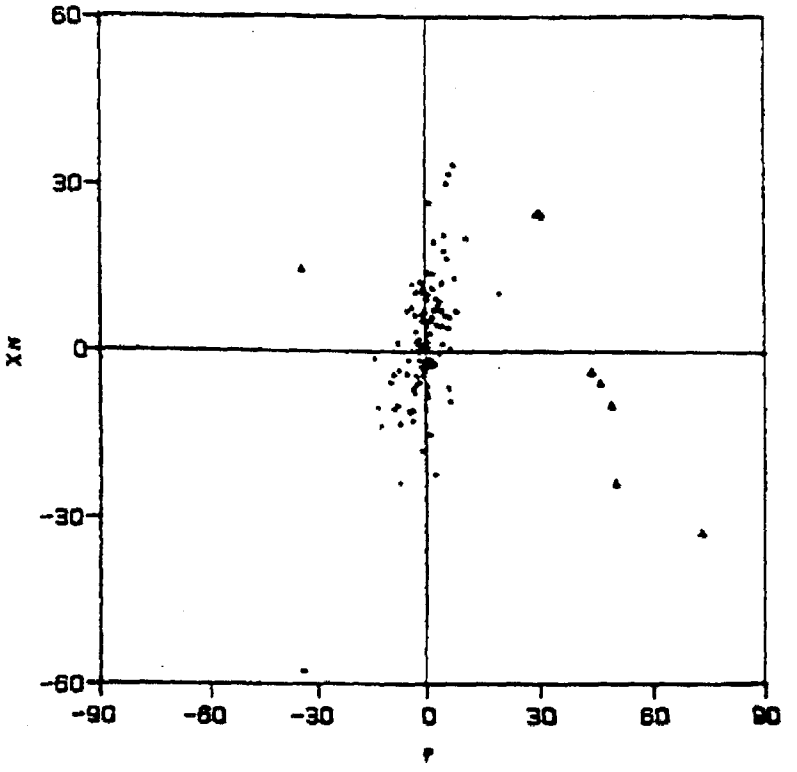

Figure 9.3. Plot of χ_N versus $\bar{\tau}$ for metallated secondary amides. The triangles represent the very distorted amides of Keech and Peake.

Initially it was reasonable to question how important this amide distortion phenomenon was as a general concept in coordination chemistry, since the first results were all obtained with osmium and the all-aromatic ligands. However, Workman's results indicated that the phenomenon can be observed with other ligands and other metals.[6] The complex shown (Figure 9.7) provided the first example of a nonplanar amide of the first class with a first row metal and an all-aliphatic ligand. As was expected, based on the π-acidity of cyanide, the amide *trans* to the cyanide has a small χ_N value and a significant $\bar{\tau}$ value, making the amide both a better σ- and π-donor.

Results and Discussion

Since CPK models of the macrocycles of this thesis demonstrated that

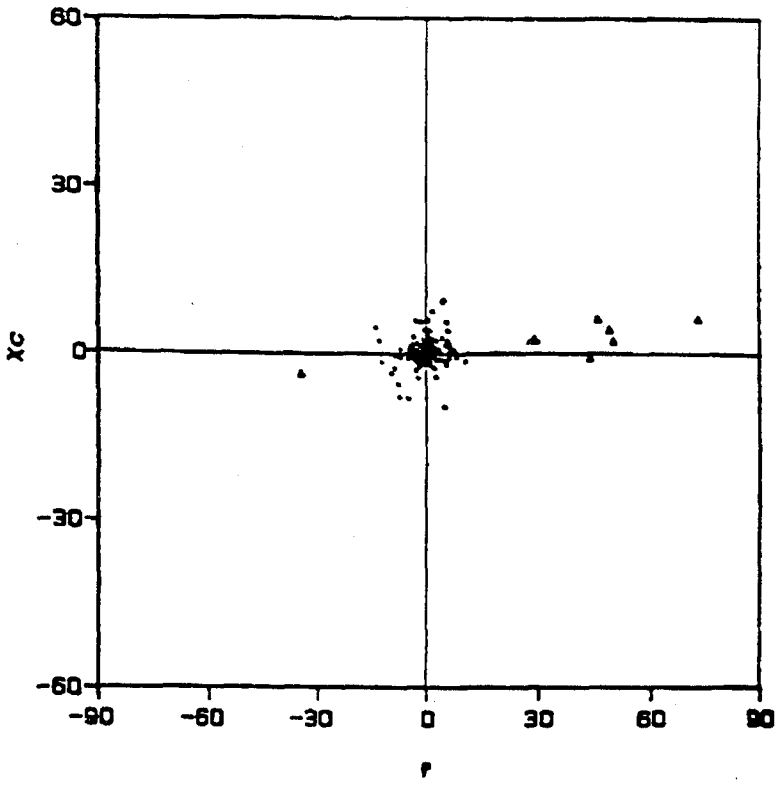

Figure 9.4. Plot of χ_C versus $\bar{\tau}$ for metallated secondary amides. The triangles represent the very distorted amides of Keech and Peake.

complexes would be unable to isomerize to the *cis*-α or *cis*-β geometries, it was anticipated that nonplanar amides would not be observed in these systems. However, comparing the data in Table 9.1 with the scatter plots shown in Figures 9.3 and 9.4 illustrates that many of the macrocyclic systems have very nonplanar amides.[7] Although none of the amides are as nonplanar as those found with the *cis*-α and *cis*-β complexes of CHBA-DCB and HBA-B (e.g., *cis*-α Os(CO)(Ph_3P)(η^4-HBA-B): $\bar{\tau}$=73°, χ_N=−33°), many of the numbers listed in Table 9.1 are significantly outside the cluster of data points found for planar amides.

It was interesting to note that for the CHBA-DCB and HBA-B systems deviations of ω_1 from 0° or 180° often contributed more to the nonplanar $\bar{\tau}$

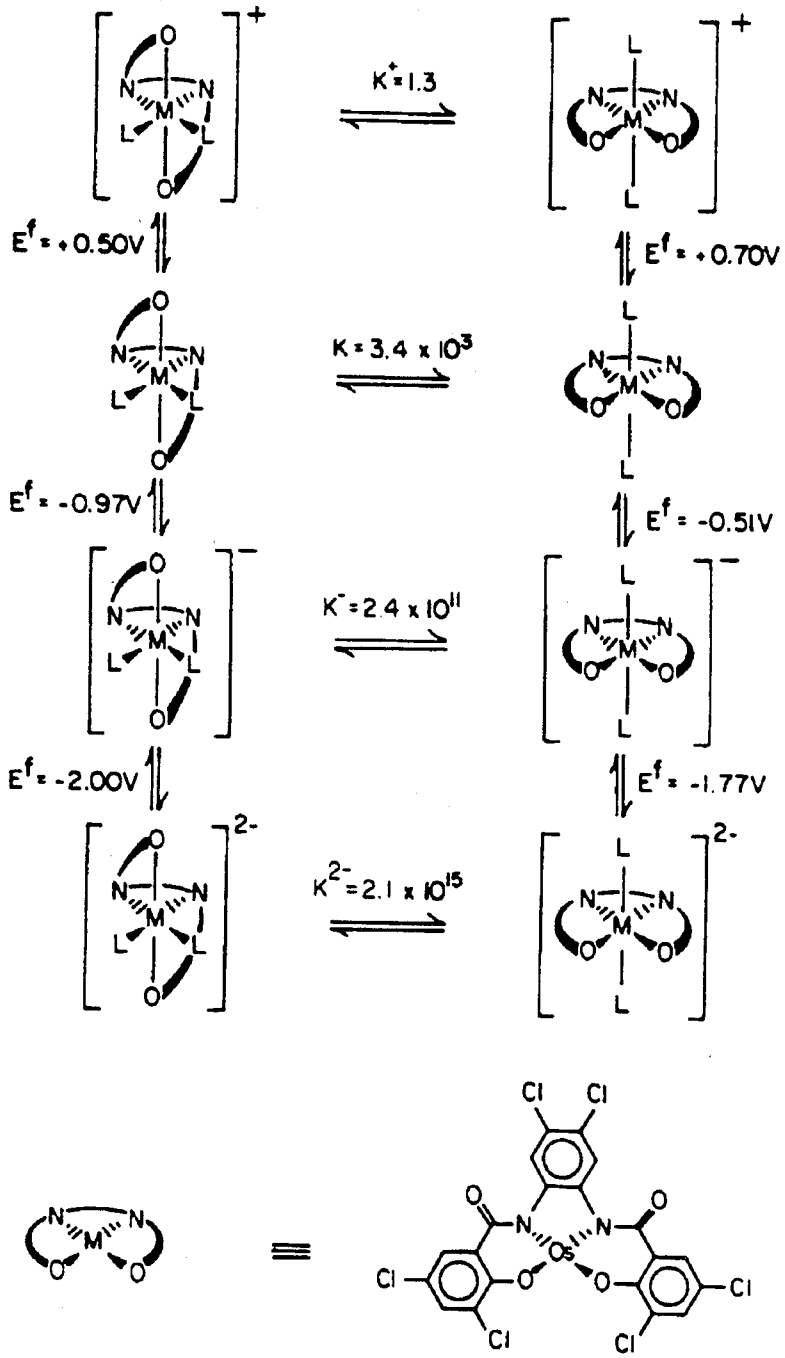

Figure 9.5. Thermodynamic ladder showing the relationship between the redox potentials and equilibrium constants for the *cis*-α and *trans* geometries at different oxidation states.

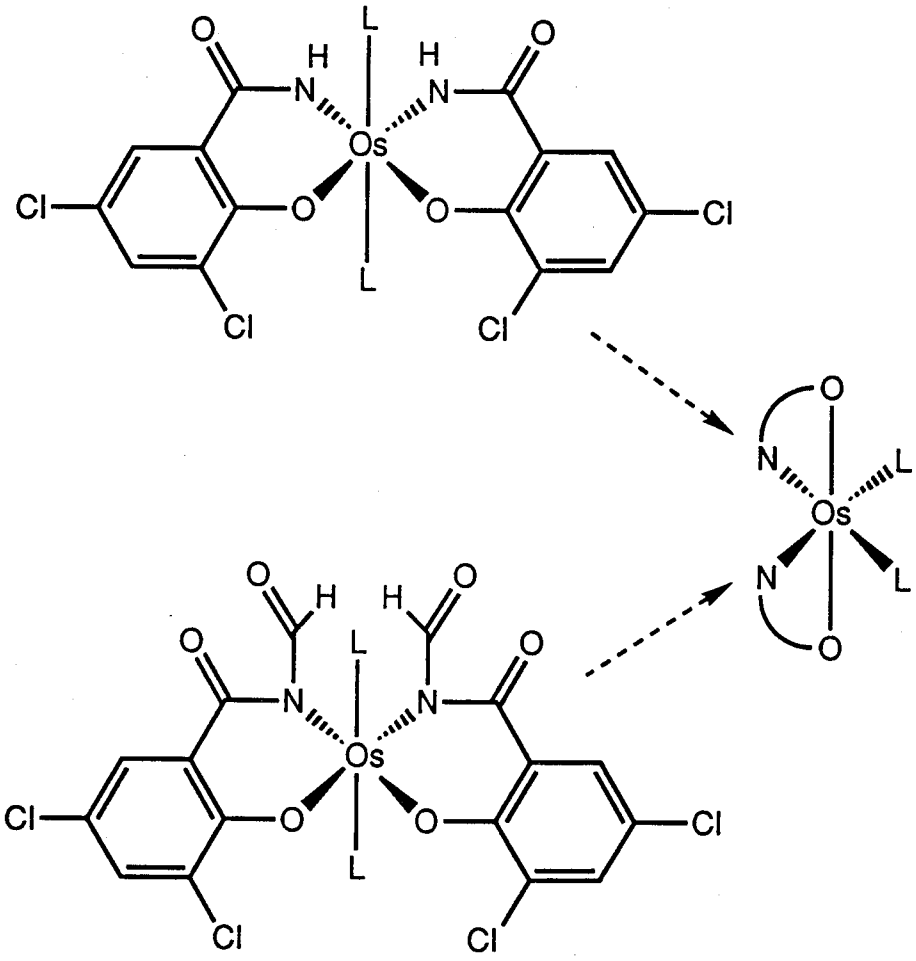

Figure 9.6. The *trans-* and *cis-α* isomers of two different ligands which have planar amides. For the top complex the Os(IV/III) and Os(III/II) couples are -0.70 and -1.99 V; for the corresponding *cis-α* complex the potentials are -0.70 and -1.91 V. For the bottom complex the Os(IV/III) and Os(III/II) couples are -0.39 and -1.88 V; for the corresponding *cis-α* complex the potentials are -0.46 and -1.88 V [referenced to Fc^+/Fc in 0.1 M TBAP in CH_2Cl_2].

values than did deviations of ω_2 from 0° or 180°; i.e., ω_1 was twisted more than ω_2. For nonplanar amides in the macrocycles, however, ω_2 was usually twisted more than ω_1. The reason for this can be seen by referring back to Figure 9.2 and examining Figures 9.8 and 9.9. CPK models of $(\eta^4$-DEMAMPA-DCB$)^{4-}$ indicate that it is a very flat and rigid molecule. If the ligand forms a square pla-

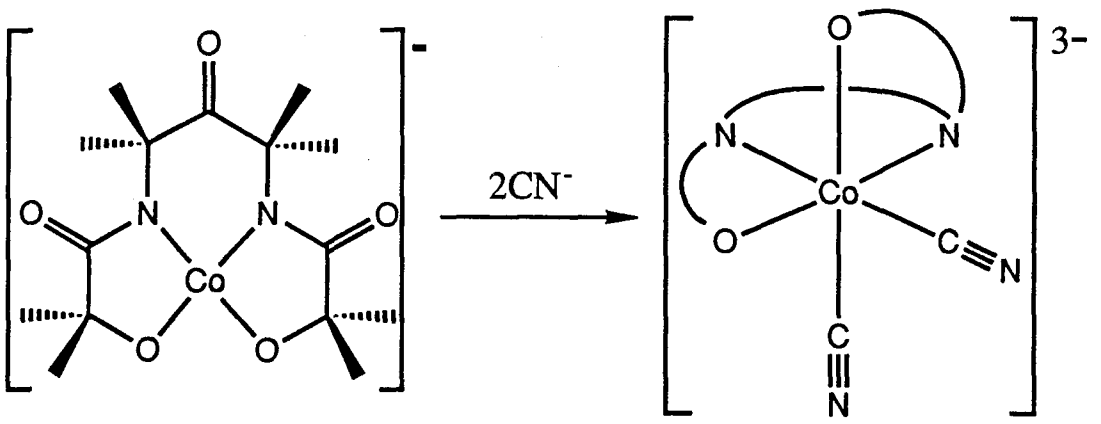

Figure 9.7. Nonplanar amides with an aliphatic ligand and a first row metal.

nar complex with a metal ion of the appropriate size, then the system will stay flat, and no nonplanar amides will result. This is, in fact, the case for [Ni(η^4-DEMAMPA-DCB)]$^-$ (Figure 9.8), [Co(η^4-DEMAMPA-DCB)]$^-$, and Co(η^4-DEMAMPA-DCB). It is predicted that [Cu(η^4-DEMAMPA-DCB)]$^-$ will also exhibit no amide nonplanarity. If, however, the complex has an axial ligand which lifts the metal out of the plane of the macrocycle, and if the macrocycle is inflexible, then ω_2 must be the most altered torsion angle, since it is the only torsion angle that includes an atom which is not part of the ligand. In the structure of [Cr(O)(η^4-DEMAMPA-DCB)]$^-$ (Figure 9.9) and [Mn(O)(η^4-DEMAMPA-DCB)]$^-$, it can be seen that the metal ion is lifted 0.6 Å out of the ligand plane, but the ligand periphery is unable to dome enough to reduce the amide nonplanarity. Even the [FeCl(η^4-DEMAMPA-DCB)]$^-$ system, in which the iron atom is lifted 0.4 Å out of the plane, exhibits a nonplanar amide. Although the manganese atom in the acyclic complex, [Mn(O)(η^4-HMPA-B)]$^-$,[8] is 0.6 Å out of the plane of the ligand, it has no nonplanar amides because the acyclic ligand permits more ligand flexibilty and because rotation occurs

Table 9.1. Dunitz Parameters				
1=MAC*, 2=DEMAMPA-DCB				
Compound	Amide	$\bar{\tau}$ (°)	χ_N (°)	χ_C (°)
$[Cr(O)(\eta^4\text{-}\mathbf{1})]^-$	$N_1C_1O_1$	-17.35	-12.4	-3.5
$[Cr(O)(\eta^4\text{-}\mathbf{1})]^-$	$N_2C_3O_2$	28.45	24.0	0.6
$[Cr(O)(\eta^4\text{-}\mathbf{1})]^-$	$N_3C_5O_3$	16.0	10.9	5.7
$[Cr(O)(\eta^4\text{-}\mathbf{1})]^-$	$N_4C_7O_4$	-7.85	-25.0	0.7
$[Cr(O)(\eta^4\text{-}\mathbf{2})]^-$	$N_1C_1O_1$	-9.21	-3.14	0.76
$[Cr(O)(\eta^4\text{-}\mathbf{2})]^-$	$N_2C_3O_2$	-12.79	-16.74	-2.32
$[Cr(O)(\eta^4\text{-}\mathbf{2})]^-$	$N_3C_5O_3$	14.39	19.54	3.90
$[Cr(O)(\eta^4\text{-}\mathbf{2})]^-$	$N_4C_7O_4$	9.51	3.15	-0.86
$[Mn(O)(\eta^4\text{-}\mathbf{2})]^-$	$N_1C_1O_1$	-6.42	-2.69	0.50
$[Mn(O)(\eta^4\text{-}\mathbf{2})]^-$	$N_2C_3O_2$	-16.97	-23.27	-2.49
$[Mn(O)(\eta^4\text{-}\mathbf{2})]^-$	$N_3C_5O_3$	10.46	16.77	1.61
$[Mn(O)(\eta^4\text{-}\mathbf{2})]^-$	$N_4C_7O_4$	10.68	0.90	0.56
$[Fe(Cl)(\eta^4\text{-}\mathbf{1})]^-$	$N_1C_1O_1$	-16.90	7.30	-3.24
$[Fe(Cl)(\eta^4\text{-}\mathbf{1})]^-$	$N_2C_3O_2$	7.58	-0.33	-1.83
$[Fe(Cl)(\eta^4\text{-}\mathbf{1})]^-$	$N_3C_5O_3$	-6.98	-5.89	1.64
$[Fe(Cl)(\eta^4\text{-}\mathbf{1})]^-$	$N_4C_7O_4$	9.01	-5.48	6.87
$[Fe(Cl)(\eta^4\text{-}\mathbf{2})]^-$	$N_1C_1O_1$	-1.70	4..29	-1.29
$[Fe(Cl)(\eta^4\text{-}\mathbf{2})]^-$	$N_2C_3O_2$	15.79	20.02	3.35
$[Fe(Cl)(\eta^4\text{-}\mathbf{2})]^-$	$N_3C_5O_3$	-3.13	-7.02	-0.13
$[Fe(Cl)(\eta^4\text{-}\mathbf{2})]^-$	$N_4C_7O_4$	-9.09	-4.20	-1.79

Table 9.1. Dunitz Parameters (continued)				
1=MAC*, 2=DEMAMPA-DCB				
Compound	Amide	$\bar{\tau}$ (°)	χ_N (°)	χ_C (°)
[Co(η^4-**1**)]$^-$ anion 1	$N_1C_1O_1$	4.65	16.17	2.49
[Co(η^4-**1**)]$^-$ anion 1	$N_2C_3O_2$	9.96	11.61	0.87
[Co(η^4-**1**)]$^-$ anion 1	$N_3C_5O_3$	6.68	5.46	5.91
[Co(η^4-**1**)]$^-$ anion 1	$N_4C_7O_4$	-22.31	-23.82	-0.60
[Co(η^4-**1**)]$^-$ anion 2	$N_1C_1O_1$	18.64	16.87	4.84
[Co(η^4-**1**)]$^-$ anion 2	$N_2C_3O_2$	4.26	4.18	6.34
[Co(η^4-**1**)]$^-$ anion 2	$N_3C_5O_3$	8.70	11.97	0.22
[Co(η^4-**1**)]$^-$ anion 2	$N_4C_7O_4$	-6.13	13.55	0.39
[Co(η^4-**2**)]$^-$	$N_1C_1O_1$	-4.00	1.49	-1.27
[Co(η^4-**2**)]$^-$	$N_2C_3O_2$	3.62	7.25	1.09
[Co(η^4-**2**)]$^-$	$N_3C_5O_3$	-0.39	0.76	-0.65
[Co(η^4-**2**)]$^-$	$N_4C_7O_4$	2.66	4.36	0.95
Co(η^4-**2**)	$N_1C_1O_1$	-5.63	1.13	0.57
Co(η^4-**2**)	$N_2C_3O_2$	9.18	6.62	4.00
Co(η^4-**2**)	$N_1'C_1'O_1'$	-5.63	1.15	0.57
Co(η^4-**2**)	$N_2'C_3'O_2'$	9.18	6.61	3.99
[Ni(η^4-**1**)]$^-$	$N_1C_1O_1$	17.30	28.57	2.92
[Ni(η^4-**1**)]$^-$	$N_2C_3O_2$	8.86	8.74	5.82
[Ni(η^4-**1**)]$^-$	$N_3C_5O_3$	12.75	13.13	0.44
[Ni(η^4-**1**)]$^-$	$N_4C_7O_4$	-4.24	-23.35	-0.31

Table 9.1. Dunitz Parameters (continued)				
1=MAC*, 2=DEMAMPA-DCB				
Compound	Amide	$\bar{\tau}$ (°)	χ_N (°)	χ_C (°)
[Ni(η^4-**2**)]$^-$	$N_1C_1O_1$	1.04	4.98	-0.62
[Ni(η^4-**2**)]$^-$	$N_2C_3O_2$	-2.86	-0.89	-2.45
[Ni(η^4-**2**)]$^-$	$N_3C_5O_3$	5.77	-170.85	-176.72
[Ni(η^4-**2**)]$^-$	$N_4C_7O_4$	-0.82	3.77	-1.50
H_4MAC*	$N_1C_2O_1$	8.64	-10.10	5.15
H_4MAC*	$N_4C_5O_2$	-2.74	7.57	-6.88
H_4MAC*	$N_8C_7O_3$	-8.56	-3.68	-7.29
H_4MAC*	$N_{11}C_{10}O_4$	12.30	-5.01	5.32
CuCl(η^3-Imine)	$N_2C_2O_1$	0.7	4.4	-3.0
CuCl(η^3-Imine)	$N_4C_6O_2$	-7.6	-2.6	-4.2

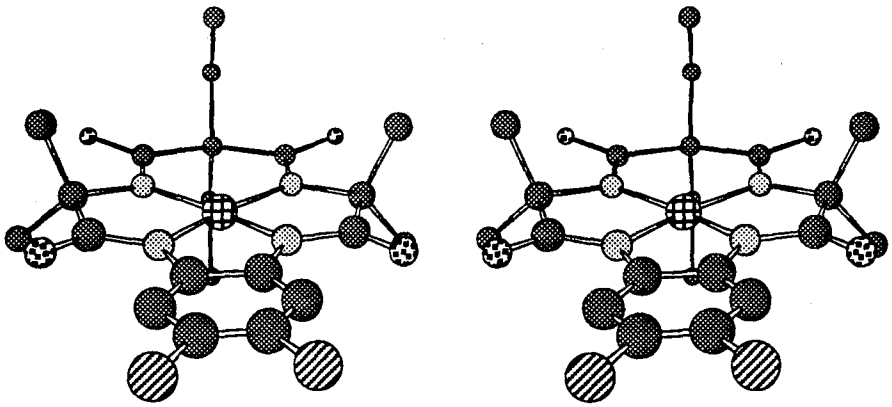

Figure 9.8. Stereo view of [Ni(η^4-DEMAMPA-DCB)]$^-$ emphasizing the planarity of the macrocycle.

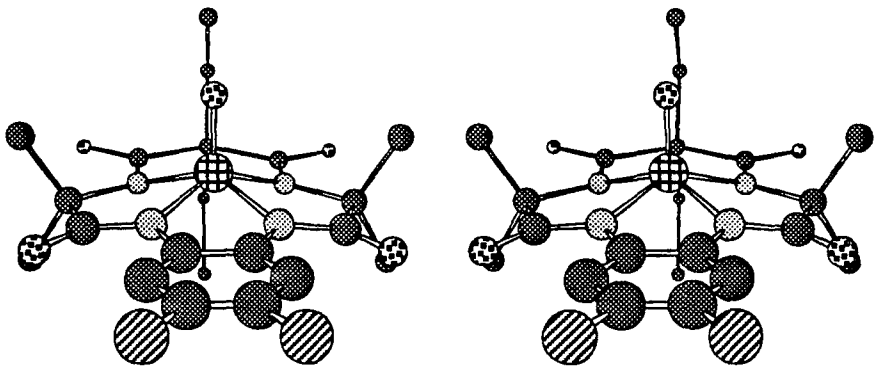

Figure 9.9. Stereo view of [Cr(O)(η^4-DEMAMPA-DCB)]$^-$ emphasizing the amide nonplanarity which results from lifting the metal above the plane of a flat ligand.

about the C–O bonds of the alcoxides.

CPK models of (η^4-MAC*)$^{4-}$ and H_4MAC* are stiff, and somewhat ruffled and twisted in any conformation. The free ligand, H_4MAC*, twists in on itself to form two intramolecular hydrogen bonds and exhibits a nonplanar amide (Figure 9.10). In the copper complex of the non-macrocyclic precursor, CuCl(η^3-Imine), no amide nonplanarity is observed (Figure 9.11). In the

square planar complexes, $[Co(\eta^4\text{-MAC*})]^-$ (Figure 9.12) and $[Ni(\eta^4\text{-MAC*})]^-$, a nonplanar amide is observed. These results have enrichened the class of ring constrained nonplanar amido-*N* ligands. Whereas the other examples in the ring-constrained class arose when an unstrained amide-containing chelate ring was forced into a strained configuration by the geometrical demands of additional ligands, $[Co(\eta^4\text{-MAC*})]^-$ was the first example in which the amido-*N* nonplanarity arose in the absence of ancillary ligand effects. The controlling ring strain term in both the free ligand and the complexes appears to be similar to that of the medium-ring lactams of organic chemistry.

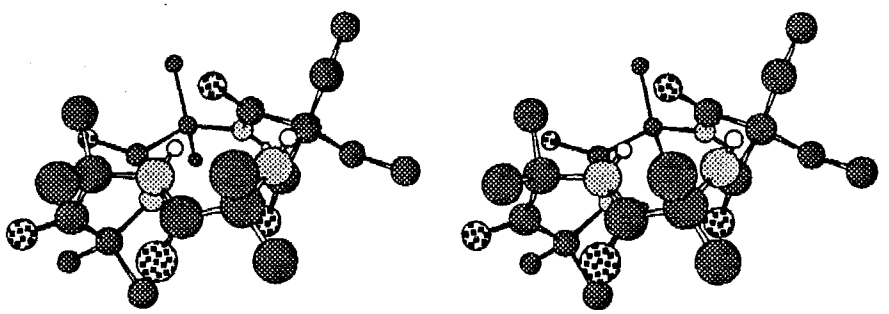

Figure 9.10. Stereo view of H_4MAC* showing the amide nonplanarity, ligand ruffling, and one of the two intramolecular hydrogen-bonds.

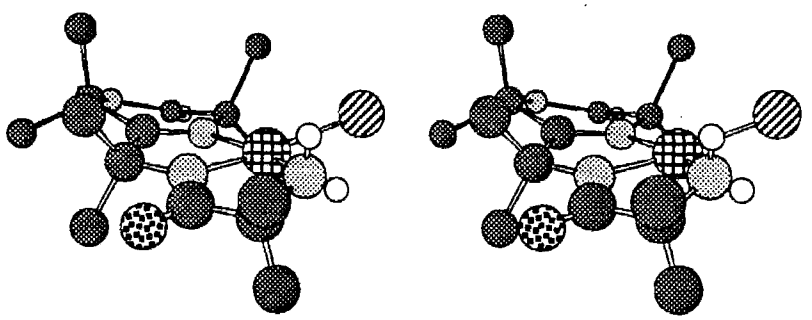

Figure 9.11. Stereo view of $CuCl(\eta^3\text{-Imine})$ showing one of the two planar amides.

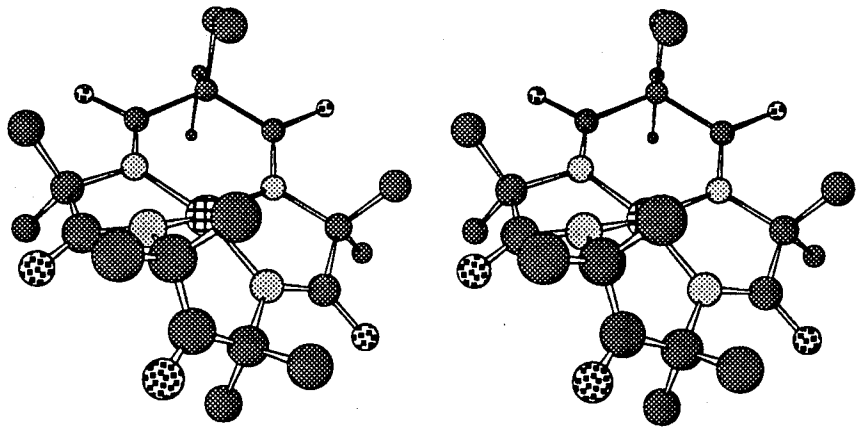

Figure 9.12. Stereo view of $[Co(\eta^4\text{-MAC*})]^-$ showing amide nonplanarity and ligand ruffling in a square planar complex.

The crystal structures of $[Cr(O)(\eta^4\text{-MAC*})]^-$ (Figure 9.13) and $[FeCl(\eta^4\text{-MAC*})]^-$ show the effects of the strain which appears to be inherent in the $(\eta^4\text{-MAC*})^{4-}$ systems and the effects of lifting the metal out of the plane of the macrocycle (vide supra). The $[Cr(O)(\eta^4\text{-MAC*})]^-$ complex is unique in having four amides which have nonplanar values of $\bar{\tau}$, χ_N, or both. As can be seen from the structure (Figure 9.13), the ligand is ruffled and twisted, and the chromium atom has been lifted 0.6 Å above the plane of the nitrogens.

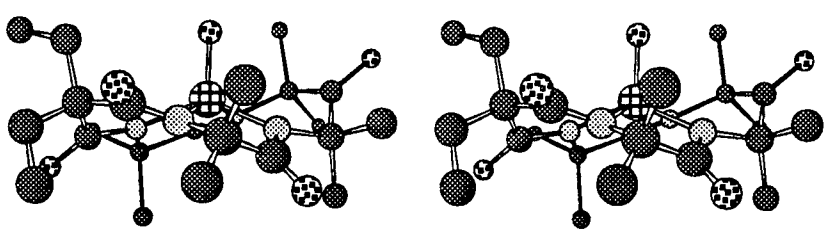

Figure 9.13. Stereo view of $[Cr(O)(\eta^4\text{-MAC*})]^-$ showing amide nonplanarity due both to lifting the metal above the donor atoms and ligand ruffling.

In conclusion, it should be stated that although the Dunitz analysis of previous literature complexes revealed scant amide nonplanarity, the accumu-

lating instances of amide nonplanarity in different systems indicate that the Dunitz analysis should be routinely performed on new structures of amido-*N* complexes.

References

1. (a) Collins, T. J.; Coots, R. J.; Furutani, T. T.; Keech, J. T.; Peake, G. T.; Santarsiero, B. D. *J. Am. Chem. Soc.* **1986**, *108*, 5333-5339. (b) Anson, F. C.; Collins, T. J.; Gipson, S. L.; Keech, J. T.; Krafft, T. E.; Peake, G. T. *J. Am. Chem. Soc.*, **1986**, *108*, 6593–6605. (c) Collins, T. J.; Lai, T.; Peake, G. T. *Inorg. Chem.* **1987**, *26*, 1674–1677. (d) Collins, T. J.; Lee, S. C. Keech, J. T. *J. Am. Chem. Soc. 110*, **1988**, 1162-1167.

2. (a) Keech, J. T. Ph.D. Thesis, California Institute of Technology, 1987. (b) Peake, G. T. Ph.D. Thesis, California Institute of Technology, 1987.

3. (a) Dunitz, J. D.; Winkler, F. K. *J. Mol. Biol.* **1971**, *59*, 169–182. (b) Dunitz, J. D.; Winkler, F. K. *Acta Cryst., Sect. B: Struct. Crystallogr. Cryst. Chem.* **1975**, *B31*, 251–263. (c) Warshel, A.; Levitt, M.; Lifson, S. *J. Mol. Spectrosc.* **1970**, *33*, 84-99.

4. Wiberg, K. B.; Laidig, K. E. *J. Am. Chem. Soc.* **1987**, *109*, 5935–5943.

5. Stewart, W. E.; Siddall, T. H., III *Chem. Rev.* **1970**, *70*, 517–551.

6. Collins T. J.; Workman, J. M. *Angew. Chem. Int. Edn. Engl.* **1989**, *28*, 912–914.

7. (a) Collins, T. J.; Uffelman, E. S. *Angew. Chem. Int. Ed. Engl.* **1989**, *28*, 1509-1511. (b) Collins, T. J.; Powell, R. D.; Slebodnick, C.; Uffelman, E. S. *J. Am. Chem. Soc.* **1990**, *112*, 899–901. (c) Collins, T. J.; Kostka, K. L.; Münck, E.; Uffelman, E. S. *J. Am. Chem. Soc.* **1990**, *112*, 5637–5639. (d) Collins, T. J.; Slebodnick, C.; Uffelman, E. S. *Inorg. Chem.* **1990**, *29*, 3432–3436. (e) Collins, T. J.; Nichols, T. R.; Uffelman, E. S. *J. Am. Chem. Soc.* **1991**, *113*, 4708–4709. (f) Collins, T. J.; Powell, R. D.; Slebodnick, C.; Uffelman, E. S. *J. Am. Chem. Soc.* in press. (g) Collins, T. J.; Kostka, K. L.;

Uffelman, E. S. *Inorg. Chem.* in press.

8. Collins, T. J.; Gordon-Wylie, S. W. *J. Am. Chem. Soc.* **1989**, *111*, 4511–4513.

Appendix A

Crystal Structure of $[Me_4N][Cu(\eta^4\text{-DEMAMPA-DCB})]$

The crystal structure of [Me_4N][Cu(η^4-DEMAMPA-DCB)] was solved by Dr. Clifford Rickard of the University of Auckland, New Zealand.

Cell parameters were obtained from the four circle coordinates of 25 reflections measured on a CAD-4 diffractometer. The data were corrected for Lorentz and polarization effects and absorption correction applied using empirical psi scans. The structure was solved by direct methods and refined by full matrix least squares. After initial isotropic refinement hydrogen atoms were located from difference maps and incorporated in the refinement with fixed thermal parameters. All non-hydrogen atoms were allowed to assume anisotropic motion. Crystal data and refinement details are given below.

The Cu–N distances are quite short, average 1.831 Å, consistent with the formulation as a Cu(III) complex. The whole ring system of the ligand shows a high degree of planarity except for C4 which is displaced 0.23 Å from the mean plane of the rest of the system. Distances are within the normally expected range. There are no close axial approaches to the copper atom, the closest being 3.70 Å to a chlorine of an adjacent molecule.

Single crystals of [Me_4N][Cu(η^4-DEMAMPA-DCB)] at 2± 1°C are triclinic, space group P-1 with a = 11.214(5) Å, b = 9.331(1) Å, c = 14.568(3) Å, α = 103.60(1)°, β = 103.87(3)°, γ = 89.13(2), V = 1436.9 Å^3, and Z = 2 (d_{calcd} = 1.397 g cm^{-3}). A total of 4368 independent reflections were collected on a computer controlled Nonius CAD-4 diffractometer using Mo-kα (λ = 0.71069 Å) radiation. The resulting structural parameters have been refined to a convergence of R = 0.047 for 2911 reflections.

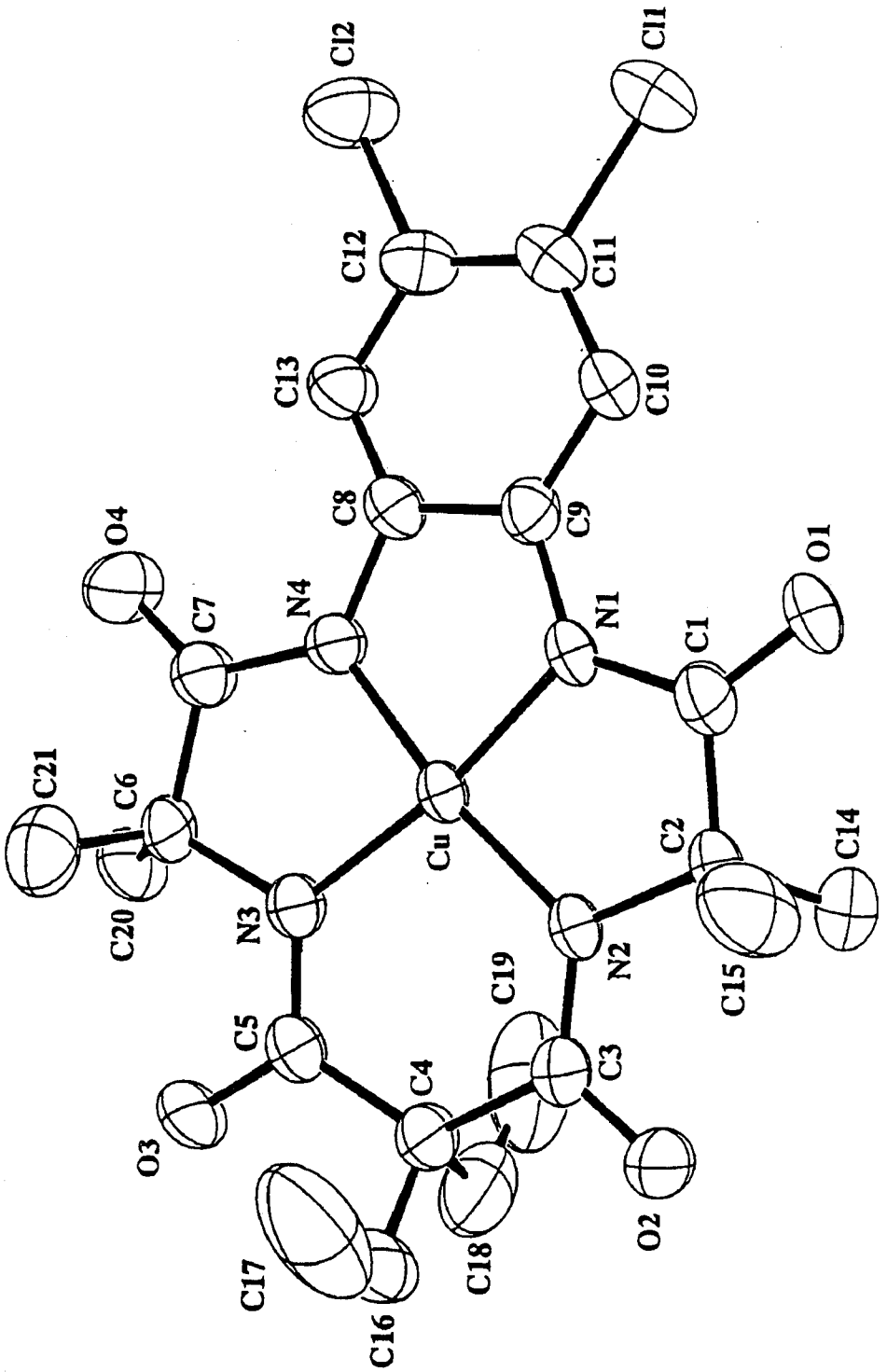

Figure A.1. Molecular structure of the anion of $[Me_4N][Cu(\eta^4\text{-DEMAMPA-DCB})]$, ORTEP drawing.

Table A.1. Bond Lengths in [Cu(η^4-DEMAMPA-DCB)]$^-$			
Atoms	Length (Å)	Atoms	Length (Å)
CuN1	1.820(4)	CuN2	1.839(4)
CuN3	1.849(4)	CuN4	1.817(4)
Cl1C11	1.739(5)	Cl2C12	1.738(5)
O1C1	1.223(6)	O2C3	1.248(6)
O3C5	1.248(6)	O4C7	1.216(6)
N1C1	1.362(6)	N1C9	1.405(6)
N2C3	1.326(6)	N3C5	1.339(6)
N4C7	1.366(6)	N4C8	1.408(6)
N2C2	1.491(6)	N3C6	1.491(6)
C1C2	1.518(7)	C3C4	1.553(7)
C4C5	1.520(7)	C6C7	1.526(7)
C8C9	1.421(7)	C8C13	1.359(7)
C9C10	1.378(7)	C10C11	1.374(8)
C11C12	1.392(8)	C12C13	1.386(7)
C2C14	1.539(9)	C2C15	1.517(10)
C4C16	1.520(11)	C4C18	1.541(12)
C6C20	1.532(8)	C6C21	1.514(9)
C16C17	1.474(14)	C18C19	1.507(14)

Table A.2. Bond Angles in [Cu(η^4-DEMAMPA-DCB)]$^-$			
Atoms	Angle (°)	Atoms	Angle (°)
N1CuN2	87.0(2)	N2CuN3	101.1(2)
N2CuN4	171.8(2)	N1CuN3	171.4(2)

Table A.2. Bond Angles in [Cu(η^4-DEMAMPA-DCB)]$^-$ (continued)

Atoms	Angle (°)	Atoms	Angle (°)
N1CuN4	85.0(2)	N3CuN4	86.9(2)
CuN1C1	117.5(3)	CuN1C9	115.6(3)
CuN2C2	114.3(3)	CuN3C5	125.4(3)
CuN3C6	114.4(3)	CuN4C7	117.1(3)
CuN4C8	116.0(3)	CuN2C3	126.4(3)
C1N1C9	126.6(4)	C2N2C3	119.3(4)
C5N3C6	119.9(4)	C7N4C8	126.5(4)
O1C1N1	124.7(5)	O1C1C2	122.4(5)
N1C1C2	113.0(4)	O2C3N2	122.7(5)
O2C3C4	115.7(5)	N2C3C4	121.5(5)
O3C5N3	121.2(5)	O3C5C4	116.5(5)
N3C5C4	122.2(4)	O4C7N4	123.6(5)
O4C7C6	122.9(5)	N4C7C6	113.6(4)
N2C2C1	108.1(4)	N2C2C14	110.8(5)
C1C2C14	106.7(5)	N2C2C15	111.7(5)
C1C2C15	107.7(5)	C14C2C15	111.6(6)
C3C4C5	121.9(4)	C3C4C16	105.7(5)
C5C4C16	106.0(6)	C3C4C18	106.4(5)
C5C4C18	106.7(6)	C16C4C18	109.8(7)
N4C8C9	111.2(4)	N4C8C13	128.5(5)
C9C8C13	120.2(5)	N1C9C8	112.0(4)
N1C9C10	128.4(5)	C8C9C10	119.5(5)
C9C10C11	120.0(5)	Cl1C11C10	118.7(4)

Table A.2. Bond Angles in [Cu(η^4-DEMAMPA-DCB)]$^-$ (continued)			
Atoms	Angle (°)	Atoms	Angle (°)
Cl1C11C12	121.1(4)	C10C11C12	120.1(5)
Cl2C12C11	120.7(4)	Cl2C12C13	118.8(4)
C11C12C13	120.4(5)	C8C13C12	119.7(5)
C4C16C17	115.2(7)	C4C18C19	115.6(7)
N3C6C7	107.3(4)	N3C6C20	112.7(5)
C7C6C20	107.8(5)	N3C6C21	110.9(5)
C7C6C21	106.5(5)	C20C6C21	111.4(5)

Table A.3. Dunitz Parameters for [Cu(η^4-DEMAMPA-DCB)]$^-$			
Amide	$\bar{\tau}$ (°)	χ_N (°)	χ_C (°)
$N_1C_1O_1$	-0.3	-6.6	0.3
$N_2C_3O_2$	1.45	-0.9	2.0
$N_3C_5O_3$	-2.5	-6.4	-4.0
$N_4C_7O_4$	-0.1	-7.8	0.9